Syntheses and Structural Studies of Polynuclear Copper(II) Complexes of Schiff-Base Macrocycles and Related Ligands

A thesis submitted
in partial fulfilment of the requirements
for the degree of
Doctor of Philosophy in Chemistry
by

Novalina Lingga

University of Canterbury
1996

ACKNOWLEDGEMENTS

I would like to extend my thanks and appreciation to all those (friends & family) who have assisted me in various ways during my nine years of study in New Zealand. Among those are the following special people:

Dr V. M^{c}Kee (The Queen's University of Belfast, Northern Ireland), my Ph.D. supervisor. I am very much indebted to her for guidance, supervision, invaluable suggestions and especially for her patience during the writing of this thesis.

Prof. D.A. House, my Ph.D. co-supervisor. I am grateful for his supervision and suggestions during the last two and a half years of this research.

Prof. W.T. Robinson, Mark Nieuwenhuyzen and Dr Huo Wen are among those who have kindly and patiently helped me to understand X-ray crystallography.

Dr C.J. Harding (Open University, U.K.) has kindly carried out the electron paramagnetic resonance spectroscopic and magnetic susceptibility measurements.

The technical staff in the Chemistry Department of the University of Canterbury, especially Mr. Bruce M. Clark (mass spectrometry laboratory) and Mr. Rewi Thompson and Mr. R. McGregor and Mr. D. MacDonald (glassblowing workshop), Mr. J. Davis (electronic workshop), who all have been very helpful during my study in the University of Canterbury.

The Physical Sciences Library staff, past and present (J.J., J.B., R.P., C.J., M.T., D.C., A.O., J.O.). Thank you all for being very kind and helpful since I first met you.

The Ministry of External Relation and Trade of New Zealand, for the University of Canterbury Overseas Postgraduate Scholarship.

Jan Wikaira. I thank thee for all the help you have given me throughout my four-and-a-half years of postgraduate study and for being such a wonderful person.

On a more personal level, I am very much indebted to my parents, who have provided me the opportunity to study in New Zealand and supported me morally and financially throughout. I would also like to thank my brother Suhendi for his assistance in preparing this thesis.

Last but not the least, a special thanks is due to a special person, Iwan Pekerti, for his love and moral support, especially during the gruelling time in preparing this thesis.

CONTENTS

3.1 Condensation of 1,3-diaminopropane and 2,6-diformyl-4-R-phenol (R = Me or ^{t}Bu)

3.2 Ring-closure reactions of complexes 1 and 4 with 2,5-diformylfuran

3.3 Condensation of 1,3-diamino-2-hydroxy-propane and 4-*t*-butyl-2,6-diformylphenol

ABSTRACT

Two diimine-diamine ligands derived from the [2+1] template condensation of 1,3-diaminopropane with 2,6-diformyl-4-R-phenol [R = Me, $(L^1)^-$; R = ^{t}Bu, $(L^8)^-$], have been isolated as their dicopper(II) hydroxo-bridged complex cations. The ring-closure condensation reaction of the dicopper complex cation of $(L^1)^-$ with 2,5-diformylfuran produced a new asymmetric tetraimine macrocycle, $(L^3)^-$ as the methoxo-, hydroxo- and ethoxo-bridged dicopper(II) complexes. The hydroxo- and ethoxo-bridged dicopper(II) complexes of $(L^3)^-$ were isolated from the recrystallisation of the methoxo-bridged analogue using *N,N*-dimethylformamide, in the absence or presence of ethanol, respectively. The structures of the dicopper(II) acyclic complexes of $(L^1)^-$ and of the ethoxo-bridged complex of $(L^3)^-$ have been determined by X-ray crystallography.

Two hexacopper(II) complexes of a new acyclic Schiff-base ligand, derived from the [3+2] condensation of 1,3-diamino-2-hydroxypropane with 4-*t*-butyl-2,6-diformylphenol, were isolated. Preliminary X-ray crystallographic investigations on these hexacopper(II) complexes revealed a Cu_6 ring templating the ligand such that the primary amine groups are held in an appropriate orientation and separation for ring-closure with a dicarbonyl compound.

Two tetracopper(II) macrocyclic complexes were obtained from the [2+2] template condensation of 1,5-diamino-3-hydroxypentane and 2,6-diformyl-4-methylphenol. One of the complexes was isolated as a tetrafluoroborate complex, while the other as a formate complex. The formate complex, whose crystal structure has been determined, is believed to have been generated by the hydrolysis of *N,N*-dimethylformamide at room temperature, promoted by the tetrafluoroborate complex. The tetrafluoroborate complex underwent dimerisation to give an octacopper(II) complex.

Another tetracopper(II) complex was synthesised by the template condensation of 1,5-diamino-3-hydroxypentane and 2,6-diformyl-4-methylphenol. X-ray structure determination of this complex revealed that it is a dimer of two dinuclear macrocyclic complexes. The two copper(II) ions in one unit of the dimer are bound inside the macrocycle "laterally". In contrast, two copper(II) ions are found to be held "diagonally" within the cavity of another Schiff-base macrocycle, derived from the [2+2] template condensation of 2,6-diformyl-4-methylphenol with triethylenetetramine.

Chapter 1

LITERATURE REVIEW

Introduction

The development of the chemistry of macrocyclic complexes has been driven by the increasing knowledge of the structure-function relationships of metal-containing proteins or enzymes. A number of these enzymes or proteins require two or more metal ions for their activities, implying that their function or catalytic action depends on finely-balanced interactions between the metal ions. For example, the oxygen transport protein, hemocyanin, and the blue copper oxidase enzymes.

Hemocyanin contains at its active site a dicopper unit in which both copper ions are involved in binding oxygen. The blue oxidases (namely, laccase, ascorbate oxidase and ceruloplasmin), contain three copper centres which cooperate in binding and activating dioxygen for reduction to water. The discovery of these dicopper and tricopper units gave rise to interest in the development of synthetic strategies for dicopper or polycopper complexes, which could lead to the development of model complexes for the proteins.

Synthetic model complexes for hemocyanin have been studied for over twenty years. Whereas synthetic and structural studies on copper complexes, with the potential to model the blue oxidase tricopper active site, have received increased attention only since the recent X-ray crystallographic characterisation of the Zucchini ascorbate oxidase. The present work was initiated to investigate a synthetic strategy which could be used to develop macrocyclic model complexes for the tricopper active site of the blue oxidases and to develop routes to polycopper systems.

A brief overview of the structural aspects of proteins containing dicopper or tricopper units is presented in the first part of the literature review chapter (Chapter 1). The emphasis will be on the blue oxidase tricopper site; also discussed are a few structurally characterised copper complexes which have been designed as models for this site. The second part of this chapter contains brief descriptions of the general synthetic methods employed throughout this work. Macrocyclic ligands and complexes related to those prepared in this work will be presented in the third part of Chapter 1, with emphasis on the structural aspects of the ligands and complexes.

Chapter 2 gives experimental details concerning the synthesis and characterisation of the complexes and their precursors. Infrared and mass spectra of most of the copper complexes synthesised are included in the appendices.

The first section of the third chapter contains a more detailed description of the synthetic approach adopted in the major part of this study. The main results of this work are presented and discussed in the remaining sections of Chapter 3.

1.1 Tricopper site in blue oxidases

Definition of copper types in copper proteins

Copper sites in copper-containing proteins were initially grouped into three types based mainly on their spectroscopic properties. These types are designated type 1, type 2 and type 3.[1, 2] However, as will be shown below, recent developments in the structural characterisation of copper protein active sites requires new types of copper sites to be defined.

The type 1 copper(II) is characterised by the following features:[1, 2]

1) an intense band ($\varepsilon \sim 5000\ M^{-1}\ cm^{-1}$) around 600 nm in the electronic spectrum, instead of weak ligand-field transitions expected for "normal" tetragonal copper(II) in inorganic copper complexes;
2) a small parallel hyperfine splitting ($A_{\parallel} < 63 \times 10^{-4}\ cm^{-1}$) for a $d_{x^2-y^2}$ ground state ($g_{\parallel} > g_{\perp} > 2.0023$) in the electron paramagnetic resonance (EPR) spectrum;
3) a high reduction potential.[1]

These properties were explained by the X-ray crystal structure of plastocyanin[1], a type 1 copper protein, which revealed a copper ion in a distorted tetrahedral geometry with an N_2S_2 ligand donor set including a coordinated thiolate sulfur from a cysteine residue. The structure of this site results in a low energy ligand-to-metal charge transfer transition which corresponds to the 600 nm band, and stabilises the Cu(I) oxidation state with respect to Cu(II).

The type 2 copper exhibits features similar to those of normal copper(II) complexes, [1-3] namely:

1) an EPR spectrum with $g_{\parallel} > g_{\perp} > 2.0023$ and a hyperfine splitting constant ($A_{\parallel}$) of greater than $140 \times 10^{-4}\ cm^{-1}$;
2) weak ligand field absorption features in the electronic spectrum.

The type 3 copper is a binuclear site. Hemocyanin, an oxygen transport protein found in arthropods and molluscs,[6, 7] contains such type 3 copper site and is capable of reversibly binding dioxygen. The *oxy-* (oxygen-bound, oxidised) form of this protein shows two intense absorption features in the electronic spectrum: a band at about 600

nm ($\varepsilon \sim 1000\ M^{-1}\ cm^{-1}$) and another at about 350 nm ($\varepsilon \sim 20\,000\ M^{-1}\ cm^{-1}$).[1, 2] Despite the copper atoms being in the +II oxidation state, the oxy form shows no EPR signals (EPR silent or non-detectable). Magnetic susceptibility studies show that this diamagnetism results from a strong ($-2J > 550\ cm^{-1}$) antiferromagnetic coupling between the two copper(II) ions.[2]

The large antiferromagnetic coupling in the type 3 copper site requires an orbital overlap between the two Cu(II) ions. In the case of hemocyanin, EXAFS studies[4, 5] indicate that the copper atoms are *ca.* 3.6 Å apart, hence a superexchange pathway through a bridging ligand must be involved. X-ray crystallographic study on the *deoxy*- (oxygen-free, reduced) form of hemocyanin has shown that each copper has three histidine ligands but no bridging ligand.[1 and refs. herein] Hence the superexchange pathway must be formed on oxygen binding and oxidation of the site.

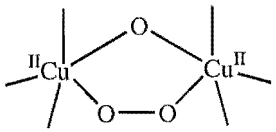

(a)

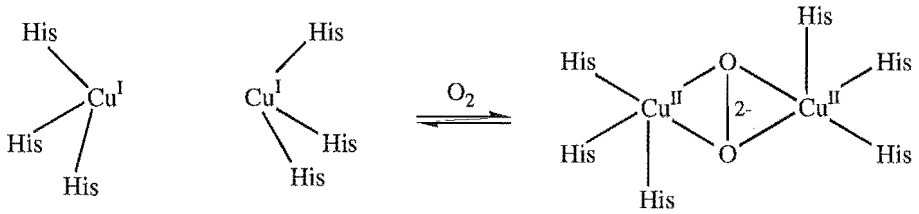

(b)

Figure 1.1. (a) Early structural model for oxyHc; (b) Chemical structure of oxyhemocyanin as revealed by recent X-ray crystallographic study of oxyhemocyanin (His = histidine residue).

Resonance Raman studies on hemocyanin[8, 9] suggest that dioxygen is bound as a symmetrically bridging peroxide. These chemical, magnetic and spectroscpic data initially led to the proposed structure for oxyhemocyanin shown in **Figure 1.1a**. However, recent X-ray crystallographic study on oxyhemocyanin[10] shows that the peroxide binds to the dicopper site of oxyhemocyanin in what is termed the 'side-on' or $\eta^2{:}\eta^2$ bridging geometry (**Figure 1.1b**).

Recent X-ray crystallographic structure determination at 2.8 Å resolution of oxidised cytochrome c oxidase[11, 12] revealed a binuclear copper centre at the CuA site, which initially was believed to be a mononuclear centre. These copper atoms are bridged by two sulfur atoms from two cysteine residues, thus forming a [2Cu-2S] centre (**Figure 1.2**). EPR spectroscopic studies showed that this site could be described as a mixed-valent [$Cu^{1.5+}\cdots Cu^{1.5+}$] site, where an electron is delocalised between the two copper atoms. A histidine nitrogen and a methionine sulfur complete the tetrahedral coordination around one of the copper atoms. Another histidine nitrogen and the peptide carbonyl of a glutamate residue are bound to the second copper atom, also in a tetrahedral geometry.

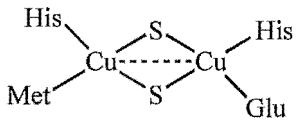

Figure 1.2. CuA binuclear site of cytochrome c oxidase.

Another copper site which does not fit into the general classification is the trinuclear copper site of the blue copper oxidases,[13] laccase, ascorbate oxidase and ceruloplasmin. These enzymes catalyse the 4-electron reduction of dioxygen to water and contain four to eight copper atoms per molecule and were considered to contain distinct type 1, type 2 and type 3 copper sites per molecule.[14] However, recent spectroscopic studies on laccase[7, 15-22] and X-ray crystallographic structure determination of ascorbate oxidase[13, 23a] and ceruloplasmin[23b], have demonstrated that the type 2 and type 3 sites in these enzymes are physically close together and act as a single trinuclear unit during the catalytic reduction of dioxygen. The results of these studies are summarised below.

Structures of the tricopper sites in blue oxidases

The structure of oxidised ascorbate oxidase at 1.9 Å resolution[13, 23a] reveals four copper atoms per sub-unit, bound as one mononuclear and one trinuclear species. The tricopper cluster is triangularly arranged (**Figure 1.3**). Two of these copper atoms (Cu1 and Cu2) are bridged by an oxygen ligand (presumed to be either OH^- or O^{2-}) at 3.71 Å. Three histidine residues also coordinate to each of these copper atoms forming a distorted tetrahedral geometry around each copper.

The third copper ion (Cu3) is three-coordinate, bound to two histidine residues and an oxygen ligand (OH^- or H_2O). This copper atom is 3.84 Å and 3.68 Å away from Cu1 and Cu2, respectively. The copper-nitrogen distances are within the range of 1.98-2.2 Å, while the copper-oxygen distance is about 2.0 Å.

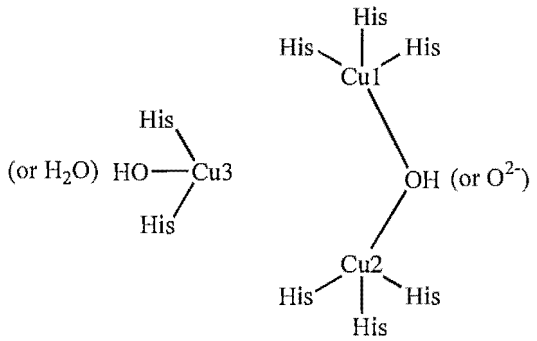

Figure 1.3. Schematic representation of the ascorbate oxidase tricopper active site.

A trinuclear copper site in laccase was established mainly by spectroscopic studies on *Rhus Vernicifera* laccase.[7, 15, 18-22] First it was demonstrated that the "type 2" and "type 3" Cu(II) centres of laccase strongly interact electronically, thus acting as a single trinuclear copper active site.[7] A derivative of laccase (T2D laccase) which is depleted in the "type 2" copper, does not readily reduce dioxygen; whereas another derivative of laccase, which has its trinuclear site intact (T1Hg* laccase), was shown to reduce dioxygen readily to an oxygen intermediate. This indicates that tricopper site is the minimum structural unit required for the dioxygen reactivity of laccase.[18-20] Spectroscopic investigations on azide-binding to laccase and *Zucchini* ascorbate

* A derivative of laccase which has its type 1 copper substituted for Hg^{2+}, a spectroscopically "innocent" ion, to remove the intense absorption features due to the type 1 copper in the spectrum of the enzyme. Thereby allowing the features due to the "type 2" and "type 3" to be studied.

oxidase[17] have demonstrated that at least one azide ion binds, in a μ-1,3 mode, to the "type 2" and one of the "type 3" Cu(II) of these enzymes. This suggests a bridged-binding coordination mode of dioxygen by laccase or ascorbate oxidase during the catalytic reduction of dioxygen.

Based on these spectroscopic investigations, it is proposed[21, 22] that the 4-electron reduction of dioxygen to water proceeds through two 2-electron transfer steps producing the oxygen intermediates illustrated in **Figure 1.4**. The intermediate **A** is produced when dioxygen binds to the trinuclear copper cluster as a hydroperoxide in a μ-1,1 mode. Loss of a further two electrons would then give the intermediate **B**.

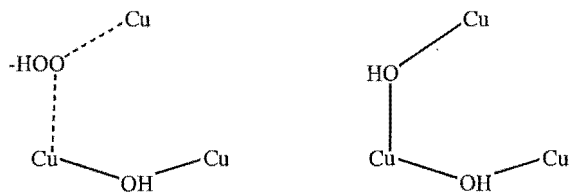

Figure 1.4. Proposed intermediates in the reduction of oxygen by laccase.

Several pieces of evidence lead to the conclusion that ceruloplasmin also contains a tricopper site. The first is comparison of the amino acid sequence analysis of ceruloplasmin with the structure of ascorbate oxidase which indicates similarities in the amino acid sequences between the two enzymes.[24] EPR and electronic spectroscopic studies on the reaction of dioxygen with ceruloplasmin,[25] indicate a dependence on the state of the "type 2" and "type 3" copper centres of the enzyme activity. The most convincing evidence was provided by a recent X-ray crystal structure determination of ceruloplasmin at 3.1 Å resolution,[23b] which reveals a cluster of three copper atoms in this enzyme.

Model complexes for the tricopper sites

Model complexes for metalloprotein active sites may be classified into two types:[26] structural and functional models. A structural model reproduces some of the structural features and/or the spectroscopic properties of the biosite in question. In contrast, a functional model mimics the function of the biosite, but need not mimic the structure very accurately.

Complexes that are specifically designed to model the trinuclear copper site in blue oxidases are not many. However, a number of triangular trinuclear copper complexes have been synthesised and characterised[27-36] prior to the structural characterisation of the trinuclear biosite. A common feature of many of these complexes is a μ_3-OH^- bridging group present in the centre of the three copper ions (**Figure 1.5**). This ligand is largely responsible for maintaining the triangular structure of the tricopper unit.

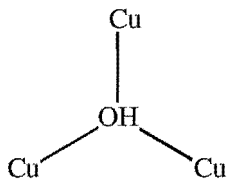

Figure 1.5. Cu_3OH trinuclear copper centre in some synthetic model complexes.

Recently, the synthesis and structure of the triangular copper complex $[Cu_3(Me_3[9]aneN_3)(im)_3]^{3+}$ (**Figure 1.6**) was reported.[37] The complex contains a triangular array of three copper(II) ions at 5.92 Å separation. In contrast to many other tricopper complexes, no μ_3-bridging group is present in the centre of the three copper ions. An imidazolate anion bridges each pair of copper atoms. In contrast to the tricopper site of ascorbate oxidase, the copper(II) ions have identical coordination environments; each is coordinated to a cyclic amine ligand and to two bridging imidazolate anions in a distorted square-pyramidal geometry.

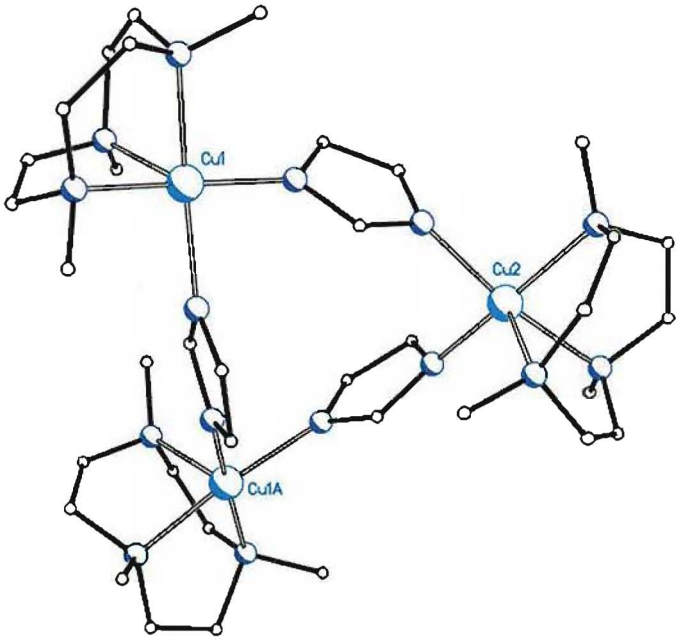

Figure 1.6. Xray structure of $[Cu_3(Me_3[9]aneN_3)(im)_3]^{3+}$

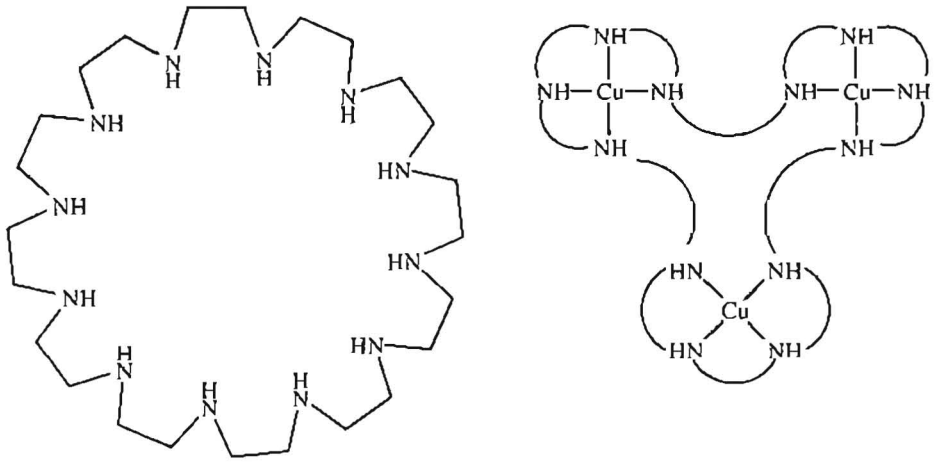

$[36]aneN_{12}$

Figure 1.7

Tricopper complexes of the polyaza macrocycles $[33]aneN_{11}$ and $[36]aneN_{12}$ have been isolated with formula $Cu_3([33]aneN_{11})(ClO_4)_6.2H_2O$ and $Cu_3([36]aneN_{12})(ClO_4)_6.3H_2O$.[37] The X-ray structures for these complexes have not been obtained. However, two possible structures are proposed: one with the copper ions in a linear array, and one with the copper ions in a triangular array as shown in **Figure 1.7**.

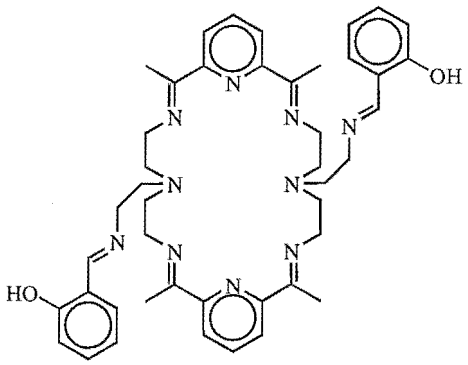

MC1

Figure 1.8. Chemical structure of the 'pendant-armed' macrocycle **MC1**.

M^{c}Kee pointed out[26] that "[in] principle, a suitably designed large macrocyclic ligand would define a cavity within which three copper atoms could be bound in a fixed geometrical relationship without requiring a μ_3-bridging unit. If the copper coordination sites are designed to be inequivalent, it should be possible to bridge only one pair of metal ions."

Fenton et al.[39a, 39b] designed and synthesised the macrocyclic ligand (**MC1**) (**Figure 1.8**), which is among the few that are specifically designed to form a tricopper model complex for ascorbate oxidase. The ligand is expected to bind one copper ion in each pyridinediimine unit and a third copper ion using its pendant arms. In effect, the tricopper complex would have a pair of copper ions in identical environments and one copper ion in a different coordination site, similar to the features of the tricopper site of blue oxidase.

The crystal structure of the tricopper macrocyclic complex (**Figure 1.9**) $[Cu_3(\mathbf{MC1})(OH)(H_2O)]^{3+}$ revealed a triangular array of copper ions as expected. Two of these copper atoms are 3.6 Å apart and are bridged by a hydroxo ion, resembling the type 3 copper pair of the trinuclear biosite. The third copper is 4.9 Å and 5.9 Å away from each atom of the bridged copper pair.

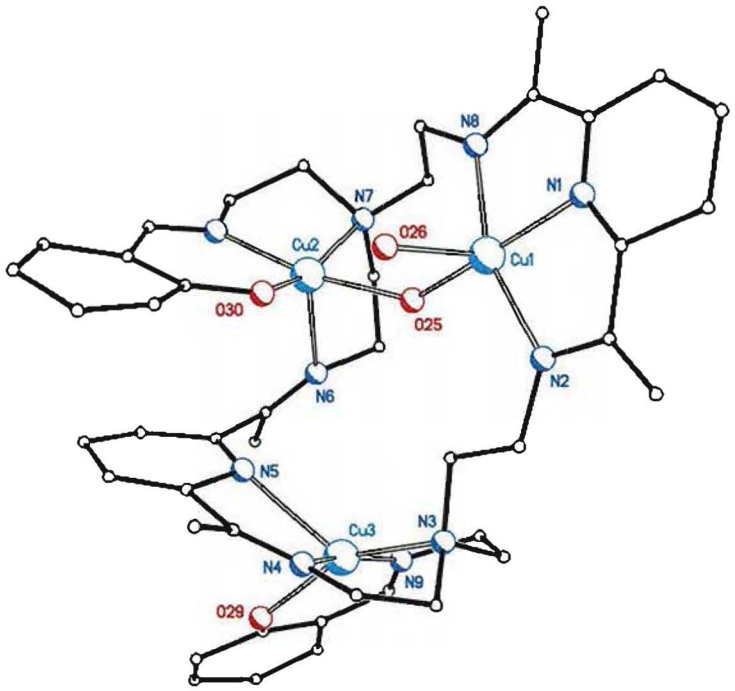

(a)

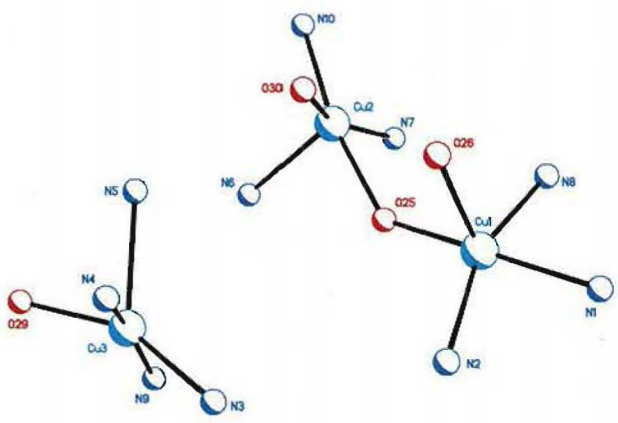

(b)

Figure 1.9. Structures of $[Cu_3(\mathbf{MC1})(OH)(H_2O)]^{3+}$ and the tricopper core.

1.2 Template synthesis of Schiff-base macrocycles

The syntheses of macrocyclic ligands[40, 41] may be categorised into two groups, those which employ metal ions and those which do not. The former is usually termed 'template synthesis', while the latter 'direct synthesis'. Since the reactions carried out in this work belong to the first category, the second method will not be discussed further.

In template synthesis, two important effects are recognised which are due to the metal ion.[40, 41] The first of these is the 'kinetic template effect', where the metal ion directs the reaction course to a cyclic rather than polymeric product. The second is the 'thermodynamic template effect', where the metal ion stabilises the macrocyclic ligand as its metal complex.[40] Both effects would increase the yield of the macrocyclic product, and in most cases cannot be distinguished since they are both operative in the reaction.

The template method is usually employed in the syntheses of Schiff-base macrocycles because the metal-free macrocycles are often unstable with respect to two things. The first is towards hydrolysis of the imine linkages; coordination of the imine nitrogen to a metal-ion usually results in the stabilisation of the macrocycle. Second, the macrocyclic ligand may be destabilised relative to some non-cyclic polyimine products. This in turn maybe due to the loss in internal entropy on ring closure or to ring strain.

In some cases Schiff-base macrocycles may be isolated in the absence of a metal ion template.[42] This may be possible when the macrocyclic product has a relatively low solubility with respect to any non-macrocyclic species present, or when there is a special stabilisation of the macrocyclic product arising from the presence of intramolecular hydrogen bonds.

The size of the metal ion may be used to direct the condensation between a dicarbonyl compound and a diamine compound towards [1+1] or [2+2]* macrocyclic

---

* [1+1] condensation (or [2+2] condensation) is the cyclic condensation between one (or two) molecule of dicarbonyl compound and one (or two) molecule of diamine compound. The macrocycle formed from this condensation is termed [1+1] or [2+2] macrocycle.

product.[41, 43] As illustrated by the system shown in **Figure 1.10**, the size of the metal ion template determines the nature of the cyclic products generated. The [1+1] hexadentate macrocycle is generated when the cations calcium, strontium, barium and lead are the template ions. Magnesium, which is a smaller cation, is ineffective in generating the hexadentate macrocycle, but is able to generate the related pentadentate macrocycle.

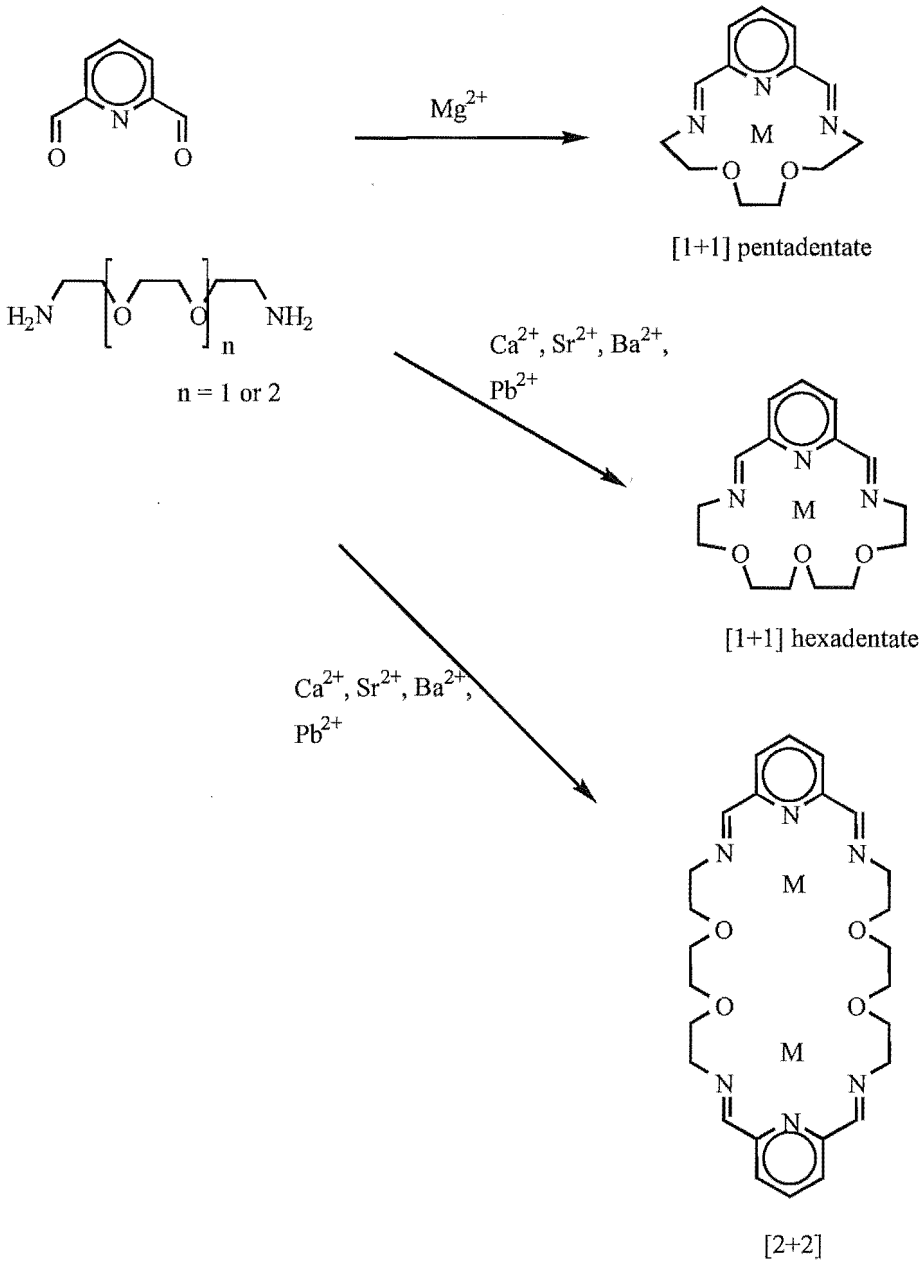

Figure 1.10. A system which illustrates the effect of metal ion size in determining the products generated.

However, the pentadentate [1+1] macrocycle is formed only when magnesium is employed as the template ion. The larger [2+2] macrocycle is generated from the same components when the larger cations are used.

Whether the condensation reaction between a dicarbonyl compound and a diamine compound leads to a [1+1], [2+2] or [n+n] macrocycle depends on the nature of the template metal ion and the length of the diamine.[42-46] Although [1+1] and [2+2] Schiff-base macrocycles are the more common ones, [3+3][47-49] and [4+4][50, 51] condensations have been reported.

The possible reaction pathways leading to the [1+1] and [2+2] products are outlined in **Figure 1.11**,[42, 43] assuming the initial product of the reaction between the dicarbonyl (1) and the diamine (2) is to be the monoimine complex (3).

The [1+1] macrocycle will only be formed if the diamine (2) has a sufficient chain length to span the two carbonyl groups of (1). If the metal ion is large relative to the size of the macrocyclic cavity of the [1+1] macrocycle, a [2+2] condensation may occur. The electronic nature of the metal ion and the conformation of the ligand in (3) may also influence the subsequent course of reaction in ways that are difficult to probe.[43] The structure of the intermediate (3) may be such that the NH_2 and C=O groups are not in the necessary steric relationship for ring-closure.

From the intermediate (3) there are several possible routes leading to the [2+2] macrocyclic complex (5), four of them are indicated in the diagram. In route 1, the intermediate (3) may condense with a molecule of dicarbonyl (1) to form a new dicarbonyl compound (6), which then may react with a molecule of diamine (2) to form the macrocyclic product (5). In route 2, the condensation sequence is reversed, and a diamine compound (7) is formed as the intermediate. Two molecules of (3) may undergo a bimolecular self-condensation (route 3), or alternatively, two molecules of the diamine-diimine compound (7) may also undergo self-condensation (route 4) leading to an overall amine exchange or *transamination*.[43]

In general, the template synthesis of Schiff-base macrocycle proceeds directly to the cyclic product with no isolation of an intermediate. However, the isolation of any intermediates of type (6) or (7), followed by a subsequent ring-closure reaction with a

diamine or dicarbonyl compound different from (2) or (1), would provide a route to asymmetric [2+2] Schiff-base macrocycles.[42] This route may be termed the stepwise template method.

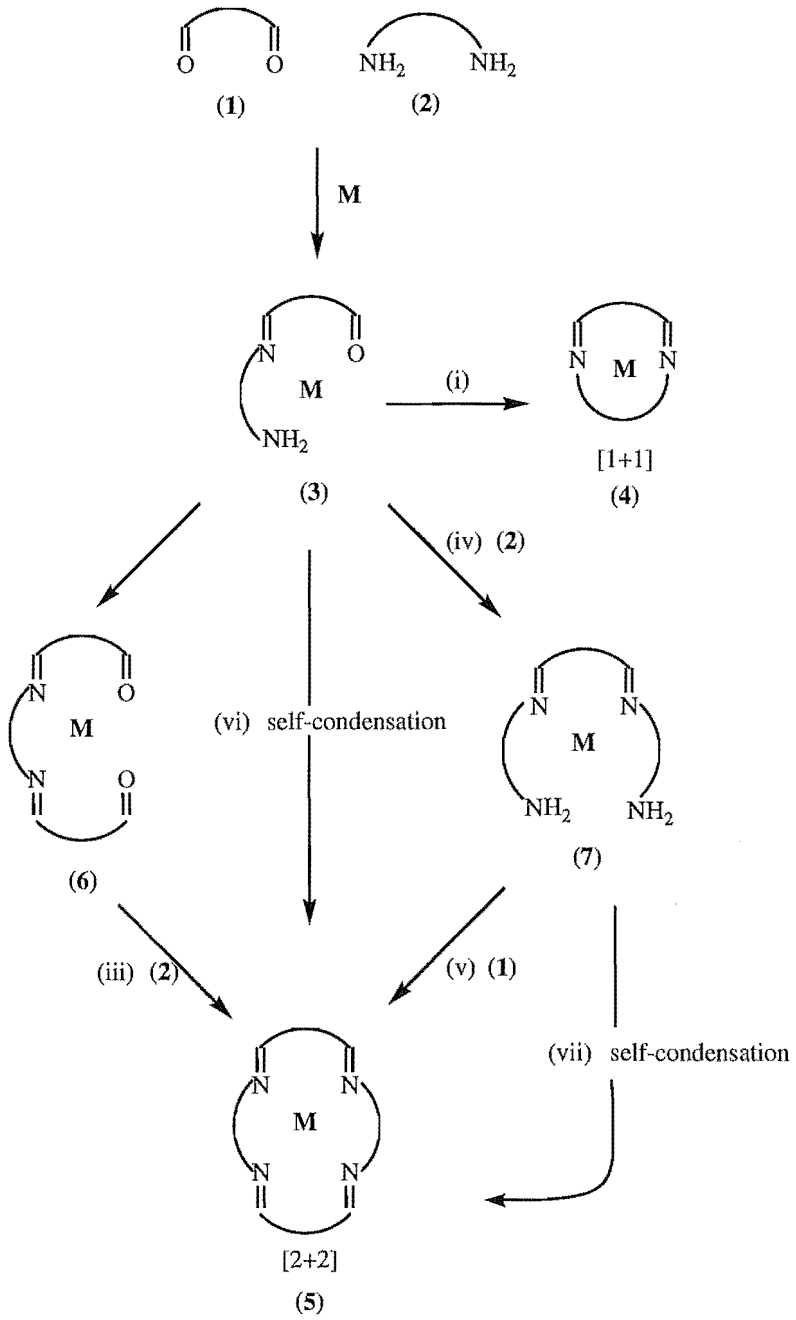

Figure 1.11. Schematic representation of the possible reaction pathways for the template condensation leading to [1+1] or [2+2] Schiff-base macrocycles.

Stepwise template synthesis

Open-chain ligands of type (6) and their mononuclear copper(II) or nickel(II) complexes (**Figure 1.12a**) have been isolated either in the un-complexed form[52, 53] or as the mononuclear copper(II) complex.[54] The free ligands **AC2a**, **AC2b**, and **AC2d** can be converted to their mononuclear copper(II) and nickel(II) complexes by treating them with the appropriate metal salt. These acyclic complexes are intermediates in the stepwise template syntheses of some macrocycles of type **MC2** (**Figure 1.12b**). The resulting macrocycles are obtained as their mononuclear complexes which can then yield dinuclear[53, 55-57] or trinuclear[58] complexes by treating them with an appropriate metal salt.

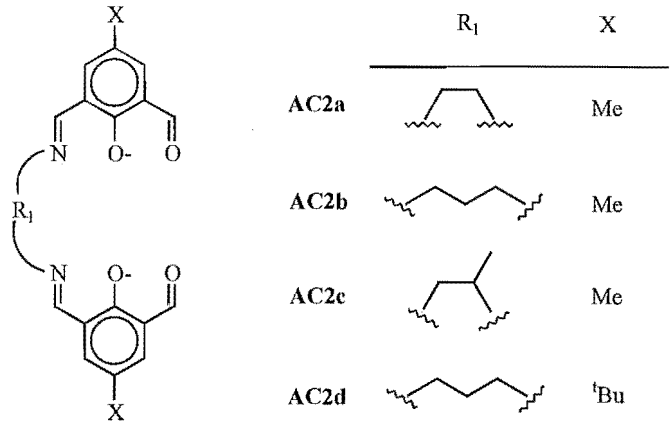

(a)

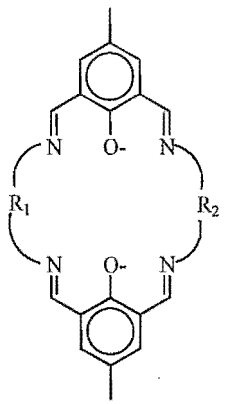

MC2

(b) $R_1 \neq R_2$

Figure 1.12.

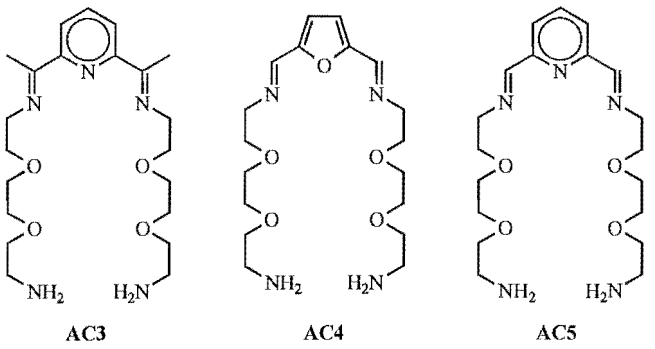

(a)

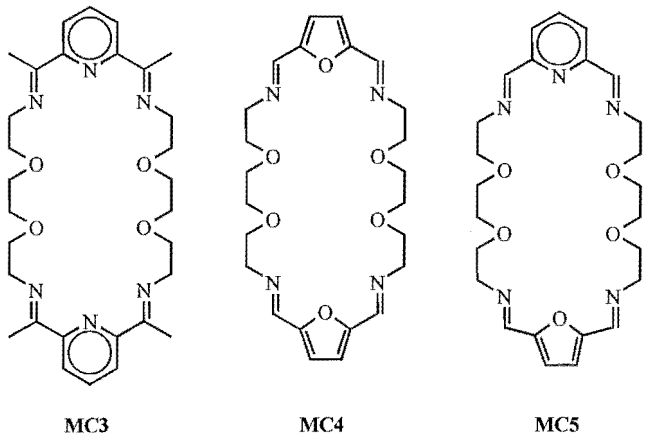

(b)

Figure 1.13.

On the other hand, Nelson and co-workers[43, 59] have isolated some open-chain ligands of type (7) (**Figures1.13a** and **1.14a**) as their mononuclear complexes. The ligand **AC3** was isolated as its barium and strontium complexes, while **AC4** and **AC5** were isolated as their barium complexes. **AC6** could be obtained as its Ba(II), Sr(II), Ca(II) or Mg(II) complexes. These ligands have been shown to be intermediates to the formation of the corresponding [2+2] macrocycles shown in **Figures 1.13b** and **1.14b**.

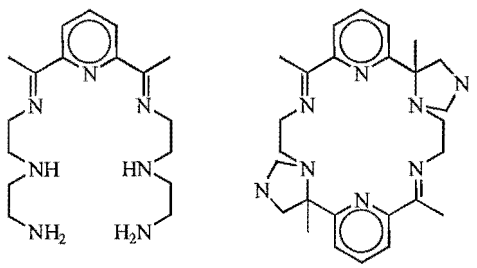

Figure 1.14.

The complexes (Ba**MC3**)$^{2+}$, (Ba**MC4**)$^{2+}$ and (Ba**MC5**)$^{2+}$ could be generated at room temperature simply by treating (Ba**AC3**)$^{2+}$ with one equivalent of 2,6-diacetylpyridine or (Ba**AC4**)$^{2+}$ and (Ba**AC5**)$^{2+}$ with 2,5-diformylfuran. Interestingly, (Ba**MC3**)$^{2+}$ could also be obtained from dry or normal methanol at room temperature *without* treating it with another equivalent of 2,6-diacetylpyridine or other dicarbonyl compound.[43] Nelson et al. proposed that in the case of (Ba**MC3**)$^{2+}$, the ring-closure proceeds by way of transamination mechanism involving two molecules of (Ba**AC3**)$^{2+}$ (route 4 of the reaction pathways described above). Intra- and intermolecular nucleophilic attack by an uncoordinated NH_2 group at a coordinated C=N group are also involved.

In the course of studying the ring-closure reaction of (Ba**AC3**)$^{2+}$, Nelson et al. observed that when the diamine 3.6-dioxaoctane-1,8-diamine (DOD) is added to a solution of (Ba**AC3**)$^{2+}$, the formation of the macrocycle **MC3** is completely suppressed. Even when the ratio of DOD to (Ba**AC3**)$^{2+}$ is 1:1. Excess Ba^{2+} ion was also found to suppress ring-closure of (Ba**AC3**)$^{2+}$ to a certain extent. This was suggested to be due to an equilibrium between the mononuclear barium complex of **AC3** and the corresponding binuclear barium complex. In the binuclear complex, the terminal primary amine of the ligand is coordinated to the metal ion, thus making them less available for nucleophilic attack.

In other words, the strength of interaction between the metal ion with the NH_2 groups of the ligand may determine whether ring-closure will occur or not. Support for this came from the fact that the strontium complex of **AC3** does not undergo ring-closure either in the absence or presence of an added DOD. Strontium, owing to its higher charge density, may bond more effectively to the NH_2 groups of **AC3** than barium.

In contrast to its behaviour in methanol, the complex (Ba**AC3**)$^{2+}$ does not undergo ring-closure in acetonitrile solution. This shows that the nature of the solvent - aside from the nature of the metal ion - is another factor that may determine whether ring-closure reaction will occur or not.

The complexes $(MAC6)^{2+}$ were generated from the reaction of the alkali earth metal salt, 2,6-diacetylpyridine and diethylenetriamine (dien) in 1:1:1 molar ratio at room temperature.[59] The yields of these complexes were significantly increased when an excess of dien was used. These complexes are intermediates in the formation of the macrocyclic complexes of **MC6**.

The macrocyclic complexes of **MC6** could be obtained by carrying out the 1:1:1 reaction in refluxing methanol. However, the formation of these complexes is suppressed in the presence of an excess diamine even when a high reaction temperature is employed. The macrocyclic complexes of **MC6** could also be obtained by treating the Ba(II), Sr(II) or Ca(II), but not Mg(II), complex of **AC6** with an extra equivalent of 2,6-diacetylpyridine. The reaction could be carried out either at 65 °C or 20 °C, although the use of lower reaction temperature requires a much longer reaction time.[59]

As in the case of $(BaAC3)^{2+}$, the complexes $(M(MC6))^{2+}$ (M = Ba(II), Sr(II) or Ca(II)) may be obtained from $(MAC6)^{2+}$, in the *absence* of an extra dicarbonyl compound, either by heating in methanol or by standing at ambient temperature. This ring-closure was observed in dried solvent, without reduction in the yield of the macrocyclic complex, indicating that the formation of **MC6** could not have resulted from a partial hydrolysis of the **AC6** complexes.

Nelson et al.[60] also isolated two acyclic ligands of a slightly different type from the ones discussed above (**Figure 1.15a**). Both ligands are condensation products of two molecules of 2,6-diacetylpyridine (DAP) and three molecules of ethylenediamine (en). As with the other acyclic ligands, the ligand **AC7** was obtained at room temperature using barium as the template metal and a five-fold molar excess of ethylenediamine over 2,6-diacetylpyridine.

AC7 may be regarded as being derived from the ligand **AC8** by addition of the two terminal NH_2 groups across adjacent imine bonds, resulting in the formation of two five-membered imidazolidine rings. The isolation in good yield of $(BaMC7)^{2+}$ by heating $(BaAC7)^{2+}$ in dry ethanol or methanol demonstrated that **AC7** is an intermediate to the formation of the macrocyclic ligand **MC7**.

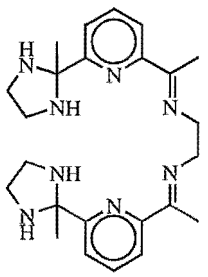

AC7

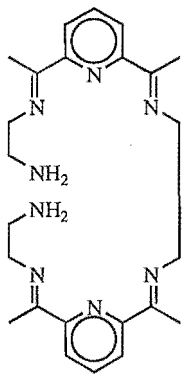

AC8

(a)

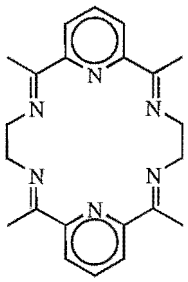

MC7

(b)

Figure 1.15.

The barium complex of **AC7** was also demonstrated to also be an intermediate to the formation of the dinuclear complex $[Cu_2(\mathbf{AC8})(ClO_4)_4]$. The complex was obtained by treating the barium complex of **AC7** with an excess of copper perchlorate (a transmetallation reaction) at room temperature. In contrast to the barium complex of **AC7**, the dicopper(II) complex does not undergo a ring-closure reaction on heating its solutions, either in the presence or absence of an added 2,6-diacetylpyridine.

The formation of the [2+3] acyclic ligand **AC7** compared with the formation of the [1+2] ligands **AC3** - **AC6** suggests that for an intermediate to be sufficiently stable to be isolated, the ligand needs to have a certain number of available donor atoms. A [1+2] acyclic Schiff-base ligand from dap and en would only have five donor atoms, which probably is too few to satisfy the coordination number of the large Ba^{2+} ion.[60]

The stepwise template method is also employed in the synthesis of dinucleating Schiff-base macrocycles **MC9**, **MC10**, and **MC11** (**Figures 1.16**, **1.17**, **1.18**) through the isolation of the open-chain ligands **AC9**, **AC10**, and **AC11**, respectively. The

acyclic ligand **AC9**[61] is isolated as its dinuclear Cu(II) complex and this complex will be discussed later in **Chapter 3**. In contrast, **AC10**[62] and **AC11**[63] are prepared as their hydrochloride salts, free of metal ions. The ring-closure reactions of these ligands were, however, carried out by template method, using Pb(II) and Ni(II) as the template metal ions for **MC10** and **MC11**, respectively.

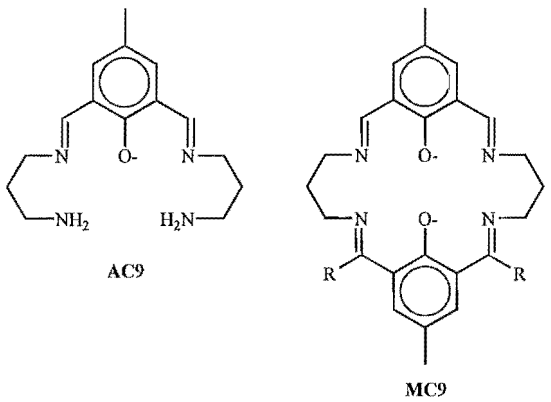

Figure 1.16.

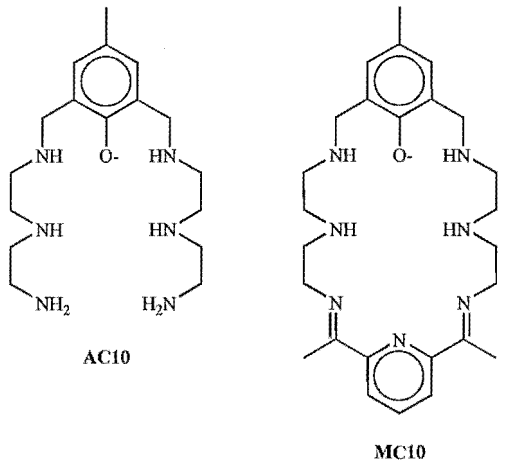

Figure 1.17.

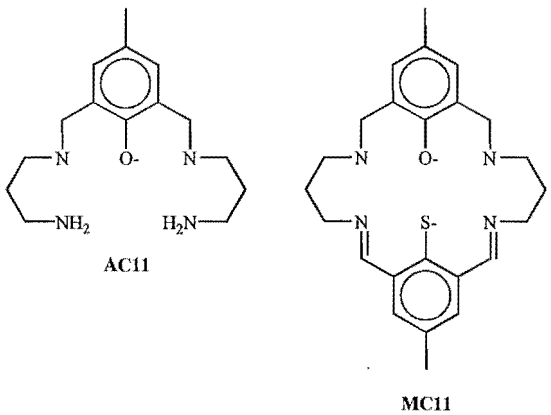

Figure 1.18.

1.3 Polynucleating Schiff-base macrocycles

Polynucleating macrocycles have the potential to organise more than two transition metal ions and hence to yield complexes where the metal centres are in close proximity to each other. The close proximity of several transition metal centres may give rise to metal···metal interactions which leads to unusual physical and chemical properties of the complexes. In addition, such polynuclear metal complexes may be able to bind small ions or molecules to the metal centres; the coordination of these substrates may activate them for further reactions.

The following discussion focuses on the various factors that may render a [2+2] Schiff-base macrocycle polynucleating.

Macrocyclic cavity size is one important factor in determining the number of metal ions (of a particular type and size) that can be accomodated by a macrocycle. For example, the macrocycle **MC12** (**Figure 1.19**) has a longer saturated chains than **MC13**, hence a larger cavity. Whereas the **MC13** can only bind two copper(II) ions per macrocycle,[64] **MC12** is able to bind up to four copper(II) ions per macrocycle as shown by the crystal structure of the complex $[Cu_4(\mathbf{MC12})(\mu\text{-}OH)_2(^{i}PrOH)_2(MeCN)_2]^{4+}$ (**Figure 1.20**).[65, 66]

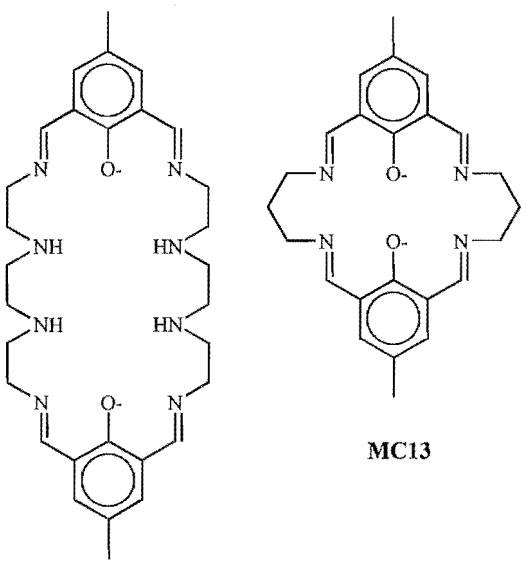

MC12 **MC13**

Figure 1.19.

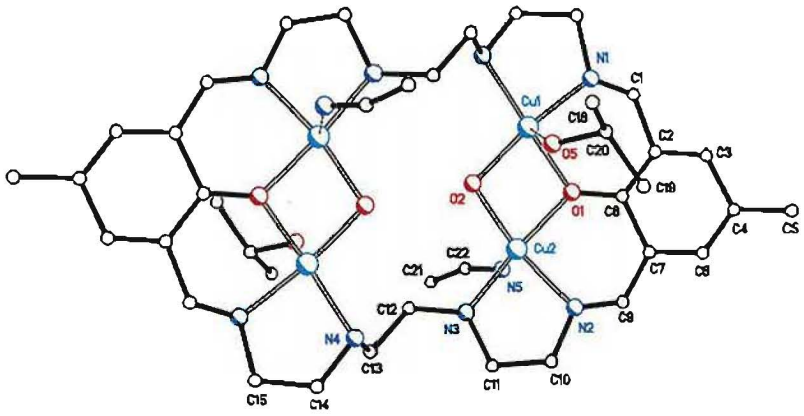

Figure 1.20. Structure of $[Cu_4(\mathbf{MC12})(\mu\text{-}OH)_2(^i PrOH)_2(MeCN)_2]^{4+}$.

The structure of the complex $[Cu_4(\mathbf{MC12})(\mu\text{-}OH)_2(^i PrOH)_2(MeCN)_2]^{4+}$ illustrates that for a macrocycle to be able to accomodate several metal ions, a sufficient number of donor atoms which are appropriately disposed are required. In the macrocycle **MC12** the donors are grouped into four N_2O sets, each of which has an appropriate arrangement for coordinating one copper(II) ion.

A phenol group has long been recognised to be able to form bonds to two transition metal ions simultaneously when deprotonated.[67] Robson and Pilkington utilised this property of a phenol group to synthesise a Schiff-base macrocycle[64], **MC13**, which is capable of securing two transition metal ions in close proximity. Phenol groups are also utilised in the Schiff-base macroycle **MC12** along with a large enough cavity size (ie. long macrocyclic side chains) to produce the tetranuclear complex $[Cu_4(\mathbf{MC12})(\mu\text{-}OH)_2(^i PrOH)_2(MeCN)_2]^{4+}$, where the phenol groups are deprotonated and each bridging two copper(II) ions.

Also illustrated by the complex $[Cu_4(\mathbf{MC12})(\mu\text{-}OH)_2(^i PrOH)_2(MeCN)_2]^{4+}$, is the presence of "external", non-macrocyclic ligands such as OH^- ions, isopropanol and acetonitrile molecules, to complete the coordination spheres of the metal ions. In doing so, these small molecules and ions probably serve to hold the tetranuclear structure.

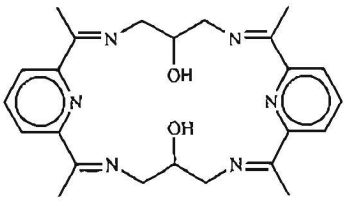

MC14

(a)

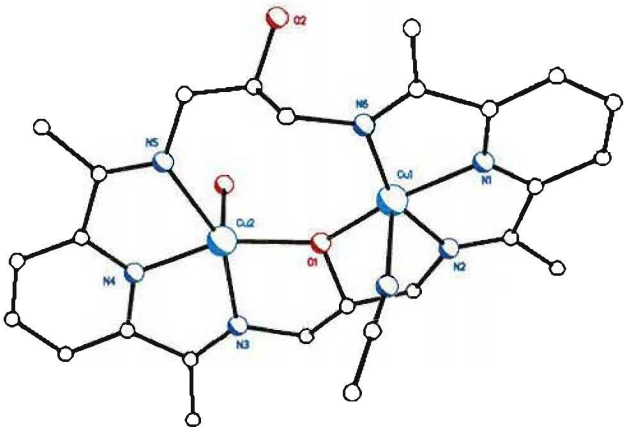

(b)

Figure 1.21. (a) Chemical structure of the macrocycle **MC14**; (b) the structure of the complex $[Cu_2(\mathbf{MC14})(CH_3CN)(H_2O)]^{3+}$ showing a mono-μ-alkoxo bridge between the copper ions.

Alcohol group(s) may also be incorporated into a macrocyclic Schiff-base ligand as pendant donor(s). An alcohol group may also function as a bridging donor when deprotonated, in a similar way to a deprotonated phenol group. Hence a deprotonated alcohol group in a Schiff-base macrocycle could also increase the nuclearity of the complex formed by partitioning the macrocycle. For example, the macrocyclic ligand **MC14**[68, 69] which, as shown in **Figure 1.21a**, contains two pendant alcohol groups that divides the macrocyclic cavity into two compartments. Each of these N_3O_2 compartments has a size comparable to the size of a first row transition metal ion.

A dicopper(II) complex of the macrocycle **MC14** has been synthesised and structurally characterised by X-ray crystallography. The structure of this complex is shown in **Figure 1.21b**. The two copper(II) ions in this complex are indeed held in the two compartments of the macrocycle. However, only one of the alcohol groups is

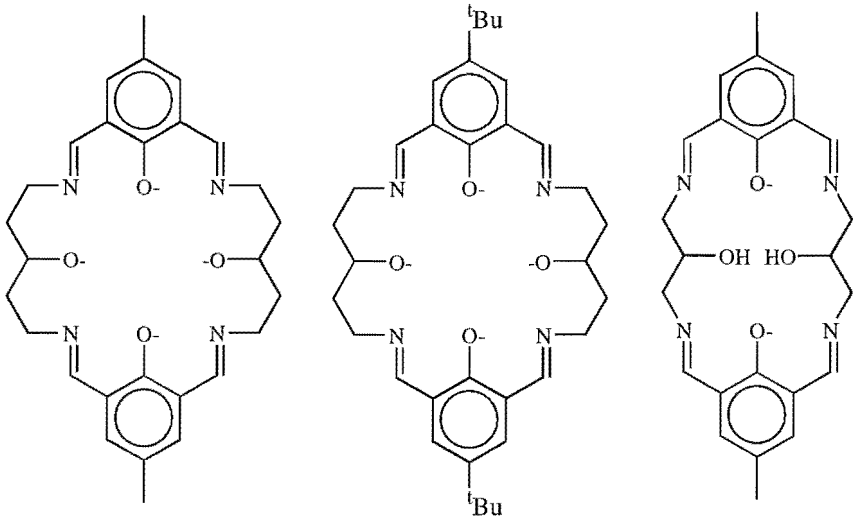

MC15 **MC16** **MC17**

Figure 1.22.

deprotonated and bridging two copper(II) ions. The second alcohol group remains protonated and un-coordinated.

If a [2+2] Schiff-base macrocycle has a large enough cavity and suitably arranged pendant, bridging donors incorporated into the ring, then intuitively the macrocycle would be expected to be partitioned into four, leading to a tetranucleating [2+2] macrocycle. M^{c}Kee et al.[70-76] applied this strategy to prepare tetranucleating [2+2] Schiff-base macrocycles from a diformylphenol and an alcohol component.

The tetranucleating ability of this type of macrocycle is determined by the length of the alcohol-containing saturated chains of the macrocycles. The Schiff-base macrocycles **MC15** and **MC16** (**Figure 1.22**) each have four metal binding sites by virtue of the pendant phenol and alcohol donors. Both macrocycle have been shown[70-73] to form tetranuclear complexes with the transition metal ions Cu(II)[70, 71], Mn(II)[72], Co(II), Ni(II) and with Zn(II)[73], as illustrated by the crystal structures of two tetracopper(II) complexes of **MC16** (**Figure 1.23**).

It is interesting to note that the complex $[Cu_4(\mu\text{-}N_3)_2(\mathbf{MC16})(N_3)_2]$ was prepared[70a] from the complex $[Cu_4(\mathbf{MC16})(\mu_4\text{-}OH)(H_2O)_2]^{3+}$ by treating the latter complex with azide. This demonstrates that the central OH^- ligand may be replaced by other species, pointing to the possibility of activation of the OH^- due to its unusual coordination geometry.

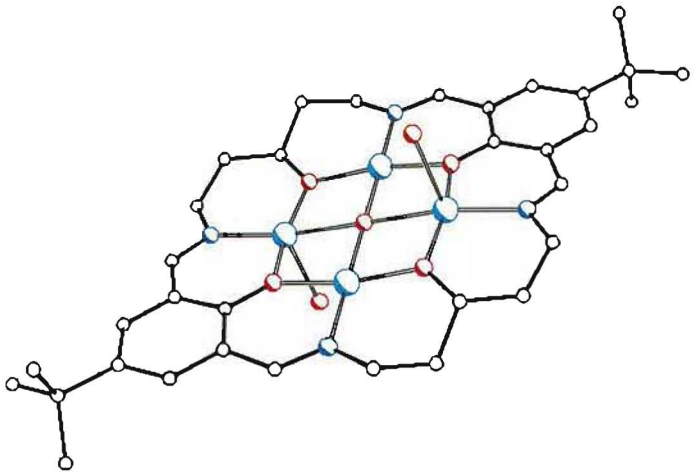

(a)

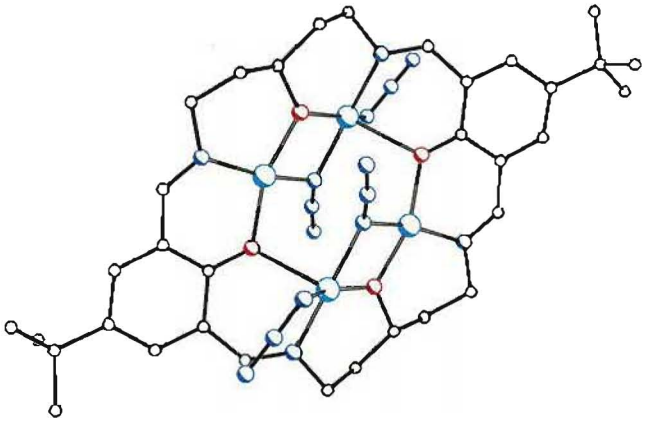

(b)

Figure 1.23. The crystal structures of (a) the complex $[Cu_4(\mathbf{MC16})(\mu_4\text{-}OH)(H_2O)_2]^{3+}$; (b) the complex $[Cu_4(\mu\text{-}N_3)_2(\mathbf{MC16})(N_3)_2]$.

On the other hand, the macrocyclic Schiff-base ligand **MC17** (**Figure 1.22**), prepared using 1,3-diamino-2-hydroxypropane (a three-carbon-chain), turned out to form only dinuclear complexes with Cu(II), Ni(II)[74, 75] and Pb(II)[76], although the macrocycle itself has four metal binding sites.

The dependence of the tetranucleating ability of this type of macrocycles on the length of the saturated chains could imply that the tetranucleating ability of these macrocycles is determined by the chelate rings formed by the alcohol-containing chains upon binding the metal ions, and by the size of the macrocyclic cavity. Whereas the macrocycle **MC15** and **MC16** each form 6-membered chelate rings upon binding four

metal ions, the saturated chains in **MC17** would have formed 5-membered chelate rings if the macrocycle had coordinated four metal ions in its cavity. The strain involved in the formation of four 5-membered chelate rings in one macrocyclic cavity, combined with the smaller cavity size, are probably the factors that do not allow the macrocycle **MC16** to form tetranuclear complexes.

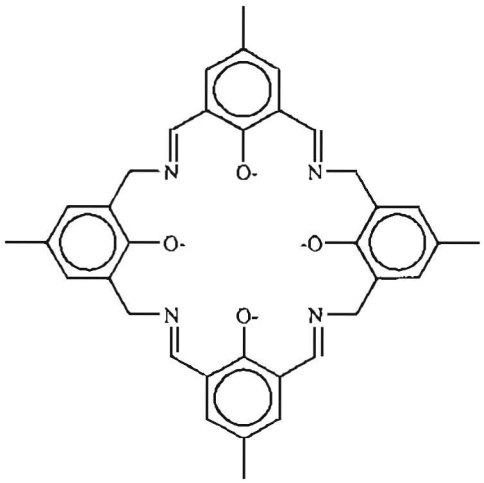

MC18

(a)

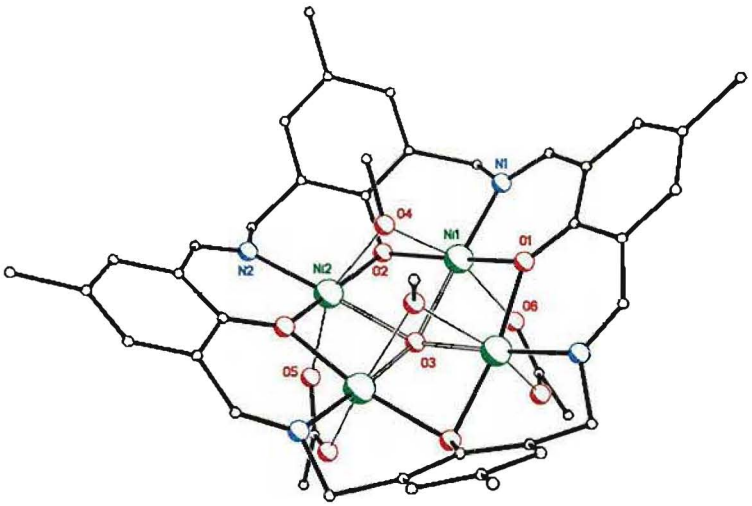

Figure 1.24. (a) The chemical structure of the ligand **MC17**; (b) crystal structure of $[Ni_4(\mathbf{MC17})(\mu_4\text{-}OH)(\mu\text{-}OMe)_2(\mu\text{-}CH_3COO)_2]^+$. The hydrogen bridge between the bridging methoxo groups is not shown.

Another strategy to prepare a tetranucleating [2+2] macrocycle is to incorporate four phenol groups into the macrocycle, instead of two phenol and two alcohol groups. This is illustrated by the macrocycle **MC18**,[77-81] (**Figure 1.24a**) which was prepared by using 2,6-bis(aminomethyl)-4-methylphenol as the diamine component instead of an amino-alcohol compound. This macrocycle has been shown to be capable of binding four Ni(II) or Zn(II) ions, where all four phenol groups are deprotonated and each bridging a pair of metal ions (see for example **Figure 1.24b**).

Chapter 2

EXPERIMENTAL

2.1 Physical Measurements

Infrared spectra were recorded from 450 cm^{-1} to 4000 cm^{-1} on Perkin Elmer 1600 Fourier-transform infrared spectrophotometer as KBr pellets or as nujol mull. The spectra for the complexes are given in **Appendix B**. Elemental analysis was carried out by the microanalytical laboratory, University of Otago, Dunedin. Magnetic susceptibility measurements and electron paramagnetic resonance spectra were obtained through the courtesy of Dr C. J. Harding from the Open University, Milton Keynes, U.K. NMR spectra were obtained using Varian Unity 300 spectrometer, at the operating frequencies of 300 MHz (^{1}H NMR) and 75 MHz (^{13}C NMR). Fast-atom bombardment mass spectra were obtained using Kratos MS80 RFA mass spectrometer operating at 4 kV, with FAB gun 2N11NF (IonTech) and Xe gas at 8 kV. The spectra for selected complexes are given in **Appendix C**.

2.2 Solvents, metal salts and organic reagents

Solvents for preparative chemistry were chemically pure grade and were used without further purification unless stated otherwise. Chemicals which were not prepared in this work were analaR or reagent grade and were used without further purification. 1,3-Diamino-2-hydroxypropane, 2,6-bis(hydroxymethyl)-4-methylphenol and 2,5-bis(hydroxymethyl)furan were purchased from Aldrich. Some of the 4-*t*-Butyl-

2,6-diformylphenol and 2,5-diformylfuran used in this work were received from J. Wikaira and V. M^{c}Kee.

Copper(II) tetrafluoroborate hexahydrate was prepared from copper(II) carbonate and 40% fluoroboric acid. Copper(II) carbonate was added to 50 ml of the acid with stirring until unreacted copper(II) carbonate was obtained. The excess copper(II) carbonate was removed by filtration. The filtrate was concentrated on a hot plate and allowed to cool to room temperature. The product was collected and dried by vacuum filtration and kept in a desiccator.

2,6-Diformyl-4-methylphenol (DFMP)

The acid and its sodium salt were both prepared in this work.

2,6-Diformyl-4-methylphenol was prepared[82] by the method of Gagné et al., outlined in **Scheme 2.1**.

p-Cresol (54.6 g, 0.51 mol) was added to a solution of sodium hydroxide (25 g, 0.62 mol) in water (100 ml). Following a full development of golden colour (standing for *ca.* 3 h), 37% formaldehyde (107.5 g, 3.6 mol) was added. The solution was stirred overnight at ambient temperature, giving a thick, pale yellow suspension. Vacuum filtration gave a white solid and yellow filtrate. The solid was washed with saturated aqueous sodium chloride solution (2 x 100 ml) and dried (the solid turned pale yellow on standing).

The crude 2,6-bis(hydroxymethyl)-4-methylphenol (*ca.* 200 g) was transferred to a 3-neck round-bottom flask fitted with an overhead stirrer. Water (325 ml) and 33% NaOH(aq) solution (32.5 ml) were added and the mixture was stirred for 30 min. *p*-Toluenesulfonylchloride (tosyl chloride) (123.5 g, 0.6 mol) in toluene (500 ml) was added to this thick suspension and stirring was continued for 40 h. After this time an aqueous layer and an emulsion were obtained. The mixture was cooled in an ice-bath and stirred. Two aliquots of toluene (50 ml and 75 ml) was added to this cold mixture with 10 min interval. The mixture was stirred for a further 1 h, at which point solid started to form. A third aliquot of toluene (25 ml) was added and the suspension was

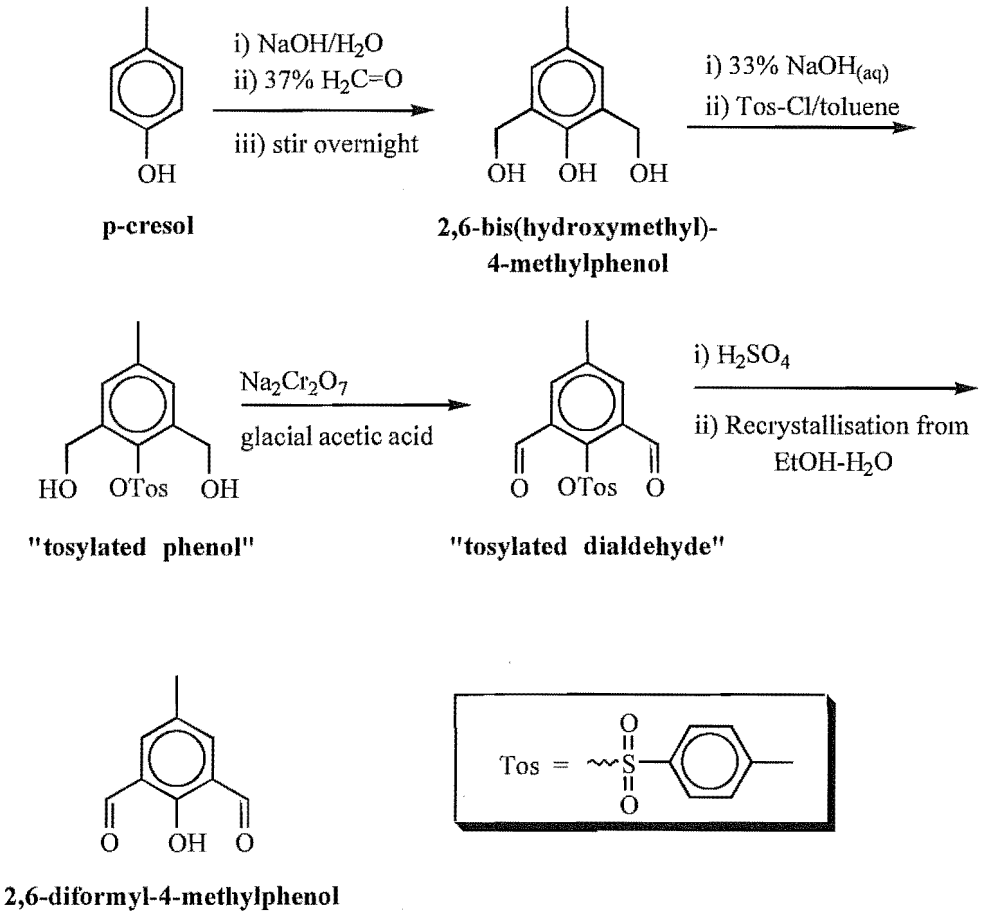

Figure 2.1. Method of preparation of 2,6-diformyl-4-methylphenol.

stirred for another 15 min. The tosylated phenol was collected by vacuum filtration, washed with toluene, and dried under reduced pressure until completely dry. Yield: 109.5 g, 0.34 mol.

The tosylated phenol was oxidized to the tosylated dialdehyde using acetic acid (14 mol/mol of tosylated phenol) and sodium dichromate (1 mol/mol of tosylated phenol). Approximately one-fourth of the total (286.3 g) glacial acetic acid was added to the tosylated phenol in a 3-neck, 3 l round-bottom flask. An overhead stirrer, a reflux condenser and a 100 ml addition funnel were fitted to the flask.

The mixture was then refluxed (110 °C-116 °C) with stirring for *ca.* 20 min. The remaining acetic acid was added to the dichromate (101.3 g) in a high-sided beaker, the mixture was stirred and warmed until the dichromate was completely dissolved. The dichromate/acid solution was added dropwise (over *ca.* 1 h) to the stirred tosylated phenol at reflux. After the addition was complete, the dark green solution was stirred at

reflux for a further 10 min. The solution was then allowed to cool slowly to room temperature (*ca.* 3 h). The crystals that had formed were collected by vacuum filtration and washed with water until most of the green colour had gone. Also formed was green, sticky solid which was harder to filter. This solid was soaked in water overnight before filtering it. The tosylated dialdehyde was dried under reduced pressure for 3 h. Yield: 73 g, 0.23 mol.

The dry tosylated dialdehyde was added slowly to concentrated sulfuric acid (250 ml) in a 2 l beaker and the solution was stirred for 1 h to dissolve all of the solid. The solution was cooled in an ice bath and an ice-water slurry was added to the acid solution until the total volume reached *ca.* 950 ml. Pale brown solid was formed in the mixture. After all the ice had melted, the precipitate was collected by vacuum filtration, washed with water until the filtrate ran clear and dried in air for 2 d. Yield: 38.3 g, 0.23 mol.

Recrystallisation:

Approximately 190 ml of ethanol was heated to boiling in a 500 ml conical flask. The crude DFMP (35.4 g) was added in small portions with stirring and heating. The hot solution was removed from heat and then filtered to remove some undissolved solid. Ethanol was added to the golden brown filtrate until the total volume reached 400 ml, then water was added dropwise to the solution until the solution turned cloudy (used *ca.* 30 ml of water). The solution was re-heated until clear and then allowed to cool to ambient temperature (*ca.* 3 h). Needle-like brown crystals formed and were collected by vacuum filtration. A second crop was obtained by adding water to the filtrate until it turned cloudy, concentrating the solution on a hot plate to *ca.* 400 ml, and cooling the solution to room temperature (3 h). Yield: 18.86 g, 0.11 mol, 53.3% (based on crude product). Overall yield (based on *p*-cresol): 24.0%. Mpt. 131-132 °C (Lit. 129-130 °C)[82].

Selected infrared absorptions:

ν(C-H): 3027 (s, w), 2922 (s, w), 2870 (s, m), ν(C=O): 1682 (s, s), ν(C-O_{phenol}): 1216 (s, s) cm^{-1}.

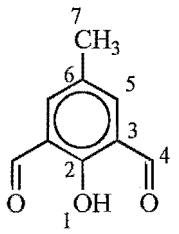

NMR spectrum ($CDCl_3$):

^1H H1 11.46(s); H4 10.22(s); H5 7.77(s); H7 2.39(s) ppm.

Sodium salt of 2,6-diformyl-4-methylphenol was prepared according to a published method.[83]

Selected infrared absorptions:

ν(C-H): 2975 (s, w), 2920 (s, w), 2876 (s, w), 2715 (s, m), ν(C=O): 1670 (s, s), ν(C-O_{phenol}): 1228 (s, s) cm^{-1}.

Microanalysis:

Found: C 57.98%; H 3.60%.

Calculated: C 58.07%; H 3.79% ($C_9H_7O_3Na$)

4-*t*-Butyl-2,6-diformylphenol (TDFP)

4-*tert*-Butyl-2,6-diformylphenol was prepared in two steps as shown in **Figure 2.2**. The first step is that of Drago et al. and Hendrickson et al.[84] while the second step is that of Taniguchi.[85]

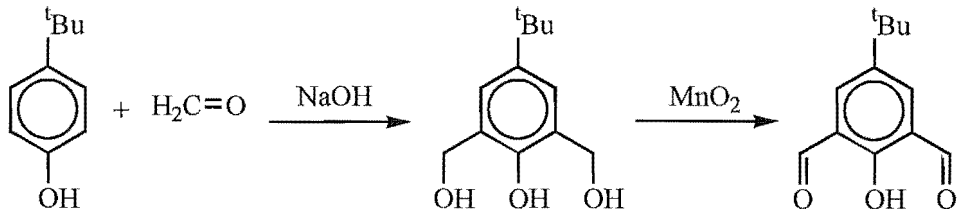

Figure 2.2 Preparation of 4-*t*-butyl-2,6-diformylphenol.

4-tert-Butyl-2,6-bis(hydroxymethyl)phenol. Sodium hydroxide (0.838 mol) was dissolved in water (800 ml) in a 2 L three-neck round bottom flask. *p-tert*-Butylphenol (0.667 mol) was added to the sodium hydroxide solution and the mixture was stirred with a mechanical stirrer and heated gently until all solid had dissolved. The pale orange solution was cooled to room temperature before 37% (w/v) formaldehyde solution (115 ml, 1.42 mol) was added to the stirred solution. The solution was stirred for 6 d, resulting in a yellow suspension. Concentrated hydrochloric acid (74 ml) was added slowly to the suspension. The suspension gradually changed to a reddish brown solution, a yellow suspension, then to a mixture of orange-brown oil and white aqueous suspension. The aqueous layer was decanted and the organic phase was washed with 3 x 50 ml distilled water. Distilled water (330 ml) and chloroform (470 ml) were added to the oil and the mixture was shaken to obtain an emulsion which was then allowed to separate into two layers. The chloroform layer was isolated and dried over anhydrous $MgSO_4$ (70 g) overnight.

Rotary-evaporation of the chloroform solution resulted in a golden brown oil (not a white solid as reported by Drago et al.). Cooling in an ice-bath produced no solid either. The product was obtained as follows. The oil was dissolved in 200 ml chloroform in a beaker and the solution was cooled in a methanol-liquid nitrogen bath (obtained by pouring liquid nitrogen into a methanol in a container) while scratching the surface of the beaker to induce precipitation. Almost immediately the product was precipitated. The product was collected by vacuum filtration and washed with 2 x 50 ml of cold chloroform until it was white and crumbly then it was dried under vacuum overnight. Yield 61.2 g, 0.3 mol, 50%. Mpt. 73-74 °C.

Microanalysis:

Found	C 68.60%; H 8.74%.
Calculated	C 68.55%; H 8.63% ($C_{12}H_{18}O_3$)

EI mass spectrum:

$^{m}/_{e} = 210$ $[C_{12}H_{18}O_3]^{+}$.

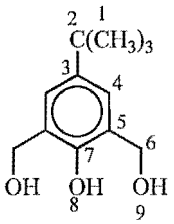

NMR spectra ($CDCl_3$):

^1H	H1 1.30, H4 7.05, H6 4.70, H8 8.10, H9 3.10 ppm.
^{13}C	31.5, 34.0, 63.8, 124.9, 125.4, 142.6, 152.3 ppm.

4-tert-Butyl-2,6-diformylphenol.[85] Manganese dioxide used for this oxidation step was obtained by heating manganese(II) carbonate at 250 °C overnight. The 2,6-bis(hydroxymethyl)-4-*tert*-butylphenol (5 g, 0.024 mol) was dissolved in 300 ml chloroform in a 500 ml conical flask. Active MnO_2 (47 g) was added to the stirred solution and the suspension was stirred at room temperature for 2-3 days. The MnO_2 was then removed by vacuum filtration using a fine sintered glass funnel and washed thoroughly with 4 x 50 ml chloroform. The filtrate and washings were combined and rotary-evaporated to dryness giving yellow solid which was dried in vacuum.

Yield 2.65 g, 0.013 mol, 54% (based on 4-*tert*-butyl-2,6-bis(hydroxymethyl)phenol).

Overall yield: 27% (based on 4-*tert*-butylphenol).

Mpt. 99-100 °C (Lit. 105 °C).[85]

Selected infrared absorptions:

ν(C-H): 3038 (s, w), 2965 (s, s), 2867 (s, m), ν(C=O): 1688 (s, s),

$\nu(C\text{-}O_{phenol})$: 1222 (s, s) cm^{-1}.

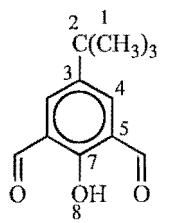

NMR spectra ($CDCl_3$):

^1H	H1 1.4, H4 8.0, H6 10.3, H8 11.5 ppm.
^{13}C	31.0, 34.2, 122.6, 134.6, 143.0, 161.6, 192.5 ppm.

Sodium salt of 4-t-butyl-2,6-diformylphenol was prepared by a method similar to the published method.[83]

Selected infrared absorptions:

ν(C-H): 2960 (s, s), 2902 (s, m), 2867 (s, m), 2725 (s, m),

ν(C=O): 1682 (s, s) , $\nu(C\text{-}O_{phenol})$: 1233 (s, s) cm^{-1}.

Microanalysis:

Found: C 57.98%; H 3.60%.

Calculated: C 58.07%; H 3.79% ($C_9H_7O_3Na$)

2,5-Diformylfuran (DFF)

2,5-Diformylfuran was prepared by the oxidation of 2,5-bis(hydroxymethyl) furan using manganese(IV) dioxide [86, 87a] (**Figure 2.3**).

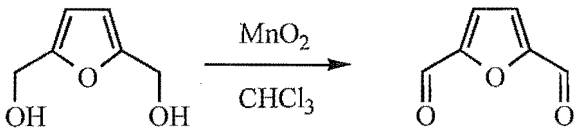

Figure 2.3 Preparation of 2,5-diformylfuran.

Manganese dioxide. MnO_2 was prepared by a modification[86] of the method published by Mancera et al.[88] Approximately 200 g of $MnSO_4 \cdot H_2O$ was added to 400 ml of boiling water in a 5 l conical flask. Saturated aqueous $KMnO_4$ solution (*ca.* 180 g in 5 l) was added dropwise to the boiling manganese(II) sulfate solution over *ca.* 5 h. The resulting black suspension was filtered off and the precipitate was washed thoroughly (stirred in a beaker) with *ca.* 4 l of hot water. The MnO_2 was filtered off again and dried at 130 °C. After *ca.* 4 h of drying, some white solid - presumably K_2SO_4 - was noticed among the black MnO_2. The MnO_2 was washed again with 4 l hot water and then dried at 130 °C for 60 h. Yield 204 g.

2,5-Diformylfuran. 2,5-Bis(hydroxymethyl)furan (19 g, 0.15 mol) was added to a mechanically stirred suspension of freshly prepared manganese dioxide (132 g, 1.5 mol) in 1.5 l chloroform in a 3-neck 2 l round bottom flask. The mixture was stirred under

reflux for 5 - 6 h and then filtered. The MnO_2 was washed with 5 x 300 ml of diethylether. Filtrate and washing was combined and evaporated to dryness under reduced pressure to give 2,5-diformylfuran as a yellow solid. The crude product was recrystallized from 3:2 mixture of cold benzene:pet ether. Yield 6.0 g, 0.048 mol, 32 %. Mpt. 110 - 111 °C. (Lit. 110 °C).[87b]

Selected infrared absorptions:

ν(C-H): 3141 (s, m), 3103 (s, m), 2878 (s, w), ν(C=O): 1680 (b, s) cm^{-1}.

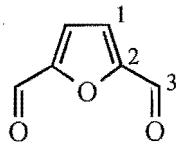

NMR spectra ($CDCl_3$):

^1H	H1 7.4, H3 9.9 ppm.
^{13}C	C1 119.3, C2 154.1, C3 179.2 ppm.

1,5-Diamino-3-hydroxypentane (1,5-DAHP)

1,5-Diamino-3-hydroxypentane was prepared by a modification[86] of the method of Owen[89] and Murase.[90] The synthesis is outlined in **Figure 2.4** and described below. *1,5-Dichloropentan-3-one.* 3-chloropropionyl chloride was either purchased from Aldrich or prepared as follows. 3-Chloropropionic acid (98% purity, 100 g, 0.92 mol) was refluxed in chemically pure $SOCl_2$ (270 ml) for *ca.* 20 h. The excess $SOCl_2$ was distilled off (70-80 °C) leaving 3-chloropropionyl chloride as a colourless liquid. Yield: 75.5 g, 0.59 mol, 60.4%.

1,5-Dichloropentan-3-one was prepared by the Friedel-Crafts acylation[89] of ethylene. 3-Chloropropionyl chloride (133 g, 1.05 mol) was added dropwise over 1 h into a mechanically stirred, cooled (ice bath) suspension of $AlCl_3$ (147.2 g, 1.1 mol) in dichloromethane (110 ml). HCl gas was evolved during addition. The reaction mixture was allowed to warm to room temperature and ethylene gas (dried over KOH) was bubbled into the mixture for *ca.* 6 h. During addition of ethylene the reaction mixture

was tested for starting material as follows: A small aliquot of the mixture was taken and an approximately equal volume of water was added to it. The mixture was dried by adding anhydrous $MgSO_4$, then the dichloromethane layer was separated and evaporated. The oil left was tested by infrared spectroscopy. The disappearance of the absorption at 1790 cm^{-1} and the presence of an absorption at 1720 cm^{-1} indicates that the reaction was complete.

The mixture was poured slowly and carefully into a mixture of dichloromethane (100 ml), ice (300 g) and concentrated HCl (~12 M, 40 ml) contained in a high-sided 4 l beaker placed in an ice-salt bath. The temperature was maintained below 15 °C by

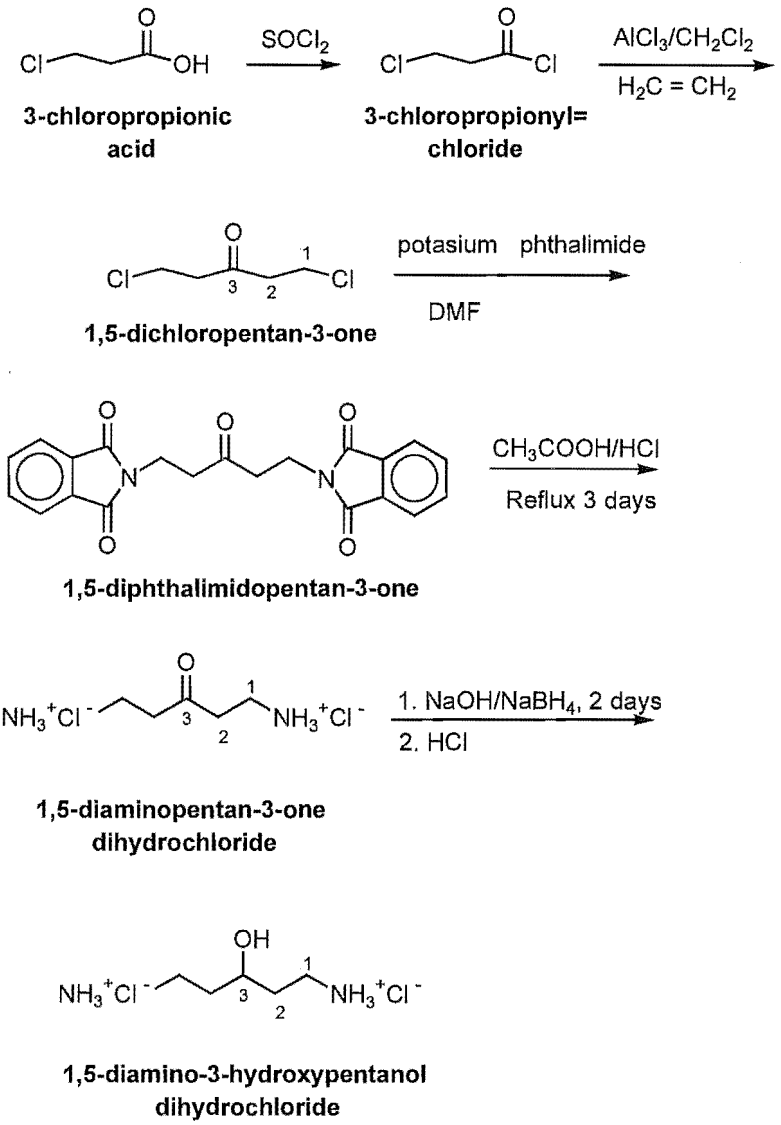

Figure 2.4. Outline of the preparation of 1,5-diamino-3-hydroxypentane. Numbers on atom relate to NMR signal assignment.

adding some ice when necessary. The emulsion was allowed to separate overnight in a separating funnel. The dichloromethane layer was isolated from the cloudy aqueous layer and the aqueous layer was extracted by 30 ml aliquots of dichloromethane until it was clear.

The combined dichloromethane phase was washed with distilled water (3 x 400 ml), separated then dried over anhydrous $MgSO_4$ overnight. Rotary-evaporation of the dichloromethane gave the crude 1,5-dichloropentan-3-one as a dark brown oil. Yield 153.6 g, 0.99 mol, 94.6% (based on 3-chloropropionyl chloride).

Selected infrared absorptions:

ν(C-H): 2972 (s, m), ν(C=O): 1720 (s, s) cm^{-1}.

NMR spectra ($CDCl_3$):

^1H H1 2.94(t); H2 3.76(t) ppm.

1,5-diphthalimidopentan-3-one.[90] Crude 1,5-dichloropentan-3-one (153.6 g, 1.0 mol) was added dropwise over 1 h into a vigorously stirred suspension of potassium phthalimide (337.23 g, 1.82 mol) in DMF that has been dried over molecular sieves. When addition was complete, the suspension was heated carefully to 80-85 °C (mixture became thicker as temperature rose above 80 °C, and thinner as temperature dropped below 80 °C) and stirred well for ~6 h then allowed to stand overnight. The pale yellow solid was collected by vacuum filtration and washed with: (i) chloroform until white precipitate and pale yellow filtrate were obtained; (ii) distilled water (3 x 200 ml), (iii) acetone until a white solid was obtained. More crops were obtained from the DMF, the chloroform and acetone filtrates. These were washed according to the above sequence. Yield 287.56 g, 0.764 mol, 77% (based on crude 1,5-dichloropentan-3-one). Mpt. 226-227 °C.

1,5-Diaminopentan-3-one dihydrochloride. Crude 1,5-diphthalimido-pentan-3-one (70 g, 0.19 mol) was refluxed (110-140 °C) with glacial acetic acid (175 ml) and concentrated hydrochloric acid (113 ml) in a heating mantle. Five 13 ml portions of concentrated HCl were added at ~10 h intervals over 3 d. The reaction mixture changed

during this addition from a white suspension to a brown suspension to a clear yellow solution. Cooling to room temperature gave the creamy-coloured phthalic acid, which was filtered off and washed with 2 x 20 ml of water. The combined filtrate and washings were rotary-evaporated to near dryness (50 °C, 1 h). Approximately 400 ml of water was added to the pale yellow residue and the suspension was filtered to remove the undissolved solid. The filtrate was again rotary-evaporated to *ca.* 50 ml and *ca.* 700 ml of ethanol was added to the suspension. The resulting white crystalline product was vacuum-filtered and dried. A second crop was obtained from the filtrate on standing. Yield 28.86 g, 0.15 mol, 79%.

Selected infrared absorptions:

ν(C=O): 1716 cm^{-1}.

NMR spectra (D_2O):

^1H	H1 3.2(m), H2 3.0(m) ppm.
^{13}C	C1 38.6, C2 34.1, C3 208.3 ppm.

1,5-Diamino-3-hydroxypentane dihydrochloride. NaOH (11.7 g, 0.294 mol) and NaBH4 (5.56 g, 0.147 mol) were dissolved in water (200 ml) in a 1 l beaker. The solution was cooled in an ice bath and crude 1,5-diaminopentan-3-one dihydrochloride (28 g, 0.147 mol) was added in portions, maintaining the temperature of the mixture below 20 °C and stirring between additions. After the addition was complete, the mixture was stirred at room temperature for 2 d. Dilute HCl was added in portions to the solution (maintaining the temperature below 27 °C) to bring the pH of the solution to ~1. During addition a small amount of black precipitate was formed, which dissolved again as the pH reached ~1. The colourless solution was rotary-evaporated to near dryness. Methanol (250 ml) was added to the white residue and the mixture was rotary-evaporated to dryness. This process was repeated five times to remove the boric acid as its methylester. After the final cycle, the solid was refluxed in methanol (70 ml) for *ca.* 30 min. The insoluble sodium chloride was filtered off and the filtrate was rotary-evaporated to *ca.* 70 ml. This solution was added dropwise into 500 ml diethylether in a

1 l beaker with stirring. The ether was decanted, leaving the pale yellow product. The product was washed in 300 ml ether, dried and placed in a desiccator. Yield: 24.39 g, 0.128 mol, 87 % (based on 1,5-diamino-pentan-3-one hydrochloride). Overall yield: 12.2% (based on 3-chloropropionylchloride). Mpt. 157-158 °C. Lit. 158-169 °C.[90]

Selected infrared absorptions:

ν(OH): 3348 cm^{-1}, $\nu(NH_2)$: 3020 cm^{-1}.

N-Acetyl diethylenetriamine

The method used to prepare *N*-acetyl diethylenetriamine is that of Brooker[91] and is a modification of the published method for the acetylation of ethylenediamine.[92, 93] Ethylacetate (95% purity, 0.3 mol) was added dropwise over 3 h to diethylenetriamine (98 ml, 0.90 mol) with stirring. The mixture was stirred for 4 d at room temperature. The unreacted diethylenetriamine and ethanol by-product were distilled under vacuum (77 °C) for 3 h, leaving the product behind as a yellow oil. Yield 34.8 g, 0.24 mol, 80%.

Selected infrared absorptions:

$\nu(NH_2)$: 3283, 3068, ν(C=O): 1656, $\delta(NH_2)$: 1558 cm^{-1}.

NMR spectrum ($CDCl_3$):

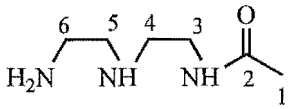

^1H	H1 1.98 (s), H3/H4/H5 2.7-2.8 (multiplets), H6 3.3 ppm.
^{13}C	C1 23.1, C2 170.3, C3 39.1, C4 41.5, C5 48.4, C6 51.8 ppm.

2.3 Complexes

The Schiff-base ligands prepared in this work are shown in **Figure 2.5**. Infrared and fast-atom-bombardment mass spectra for the complexes are given in **Appendices B** and **C**.

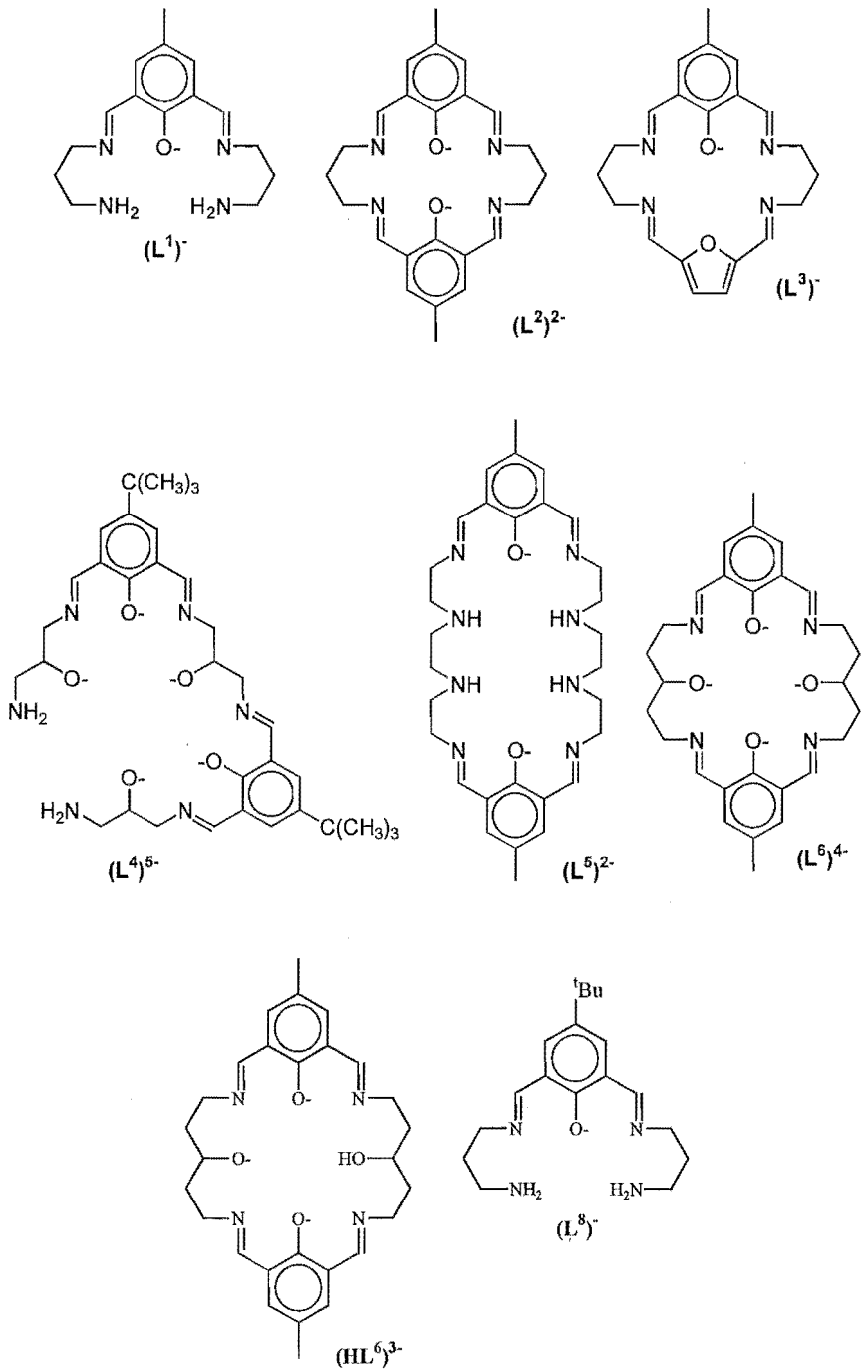

Figure 2.5. The ligands prepared in this work.

Complex 1 - $[Cu_2L^1(\mu\text{-}OH)(H_2O)](ClO_4)_2 \cdot nH_2O$ (n = 0 or 1)

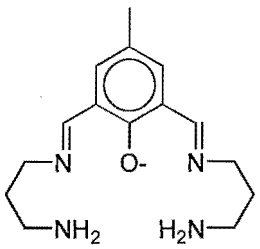

$(L^1)^-$

The complex was prepared by two methods.

Method 1.[61] 2,6-Diformyl-4-methylphenol (1.64 g, 10 mmol) was ground to a paste with NaOH (0.4 g, 10 mmol) and a small amount of water. This paste was added into 1 l of boiling water and stirred to give a yellow solution. In a separate container, $Cu(ClO_4)_2 \cdot 6H_2O$ (9.3 g, 25 mmol) was mixed with 1,3-diaminopropane (2.2 g, 30 mmol) and 50 ml water. The resulting blue solution was added to the hot yellow solution and the mixture was boiled for 1 h. Hot filtration of this mixture gave a brown compound (complex **3**), formulated on the basis of infrared and microanalytical data as $[Cu_2H_2L^2(ClO_4)_4(H_2O)]$, and a deep blue filtrate. The filtrate was allowed to stand at room temperature for 2 d, concentrated to *ca.* 125 ml on a hot plate and filtered hot. The deep blue filtrate was allowed to stand at room temperature for 1 d during which time **1** formed as dark blue crystals, which subsequently were collected and dried. Yield: 0.78 g, 1.2 mmol, 12 %.

A single crystal suitable for X-ray crystal structure determination was obtained from the reaction mixture. The formula $[Cu_2L^1(OH)(H_2O)](ClO_4)_2 \cdot H_2O$ is obtained from X-ray structure analysis, while the microanalytical data suggest the formula $Cu_2L^1(OH)(ClO_4)_2(H_2O)$ for the product. The difference is believed to be due to a loss of the water of crystallisation during microanalysis.

Selected infrared absorptions:

ν(OH): 3555 (s, m), 3448 (b, m), $\nu(NH_2)$: 3313, 3260 (s, m),

ν(C=N): 1641 (s, s), $\delta(NH_2)$: 1622 (s, m) , $\nu(C\text{-}O_{phenol})$: 1564 (s, s),

$\nu(ClO_4)$: 1091 (b, s) cm^{-1}.

Microanalysis:

Found C 28.58%; H 4.20%; N 9.02%.

Calculated C 28.31%; H 4.12%; N 8.80% ($[Cu_2L^1(OH)(H_2O)](ClO_4)_2$ or $C_{15}H_{26}N_4O_{11}Cu_2Cl_2$).

Method 2. $Cu(ClO_4)_2 \cdot 6H_2O$ (1.112 g, 3.0 mmol) was dissolved in 3 ml methanol and then mixed with 1,3-diaminopropane (355.8 mg, 4.8 mmol) in 4 ml of methanol. The resulting violet solution was added to a methanolic solution of 2,6-diformyl-4-methylphenol (246.2 mg, 1.5 mmol, in 100 ml) and the mixture was stirred at room temperature for 1 d giving a blue solution. The solution was concentrated by rotary-evaporation to *ca.* one-third of the initial volume and the solution was allowed to stand for 1 d at ambient temperature. Equal volume of ethanol was added to the methanol solution and the combined solution was concentrated by rotary-evaporation. The solution was allowed to stand for 3 d, and **1** formed as dark blue crystals, which were subsequently collected by vacuum filtration and dried. Yield 590 mg, 0.92 mmol (assuming the formula $C_{15}H_{26}O_{11}N_4Cu_2Cl_2$), 61 % (based on 2,6-diformyl-4-methylphenol).

Selected infrared absorptions:

ν(OH): 3550 (s, m), 3492 (b, m), $\nu(NH_2)$: 3318, 3265 (s, m),

ν(C=N): 1638 (s, s), ν(C-O): 1564 (s, s), $\nu(ClO_4)$: 1092 (b, s) cm^{-1}.

Microanalysis

Found C 28.42%; H 4.17%; N 8.64%.

Calculated C 28.31%; H 4.12%; N 8.80% ($[Cu_2L^1(OH)(ClO_4)_2(H_2O)]$ or $C_{15}H_{26}O_{11}N_4Cu_2Cl_2$).

FAB-MS:

Observed $^m/_e = 401, 417$.

Expected $[Cu_2L^1]^+$ (401), $[Cu_2L^1(OH)\text{-}H]^+$ (417).

Complex 4 - $[Cu_2L^1(\mu\text{-}OH)](BF_4)_2 \cdot H_2O$

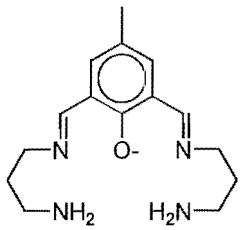

$(L^1)^-$

$Cu(BF_4)_2 \cdot 6H_2O$ in methanol (1.747 g, 5.06 mmol in 20 ml) was mixed with a methanolic solution of 1,3-diaminopropane (524.1 mg, 7.07 mmol in 10 ml). The resulting violet solution was added to a methanolic solution of 2,6-diformyl-4-methylphenol (328.4 mg, 2.00 mmol in 180 ml) and the mixture was stirred at room temperature for 2 d giving a blue solution. The methanol was removed by rotary-evaporation and the solid residue was dissolved in warm (water bath, 40 °C) ethanol-methanol (20 ml:10 ml). Standing the solution in a closed container for 4 d gave **4** as dark blue crystals which were collected by vacuum filtration and dried. A second crop was obtained by a similar method with less amount of solvent. Yield 974.0 mg, 1.59 mmol, 78 % (based on 2,6-diformyl-4-methylphenol).

Selected infrared absorptions:

ν(OH): 3601 (s, m), $\nu(NH_2)$: 3332 (s, m), 3285 (s, m), ν(C=N): 1639 (s, s), $\delta(NH_2)$: 1623 (s, m), 1606 (s, m), $\nu(C\text{-}O_{phenol})$: 1566 (s, s), $\nu(BF_4)$: 1083 (b, s) cm^{-1}.

Microanalysis:

Found C 29.55%; H 4.17%; N 9.41%.

Calculated C 29.48%; H 4.29%; N 9.17% ($[Cu_2L^1(OH)(BF_4)_2(H_2O)]$ or $C_{15}H_{26}N_4O_3Cu_2B_2F_8$).

FAB-MS:

Observed $^m/_e = 401$.

Expected $[Cu_2L^1]^+$ (401).

Complex 5 - $[Cu_2L^2(H_2O)_2](BF_4)_2$

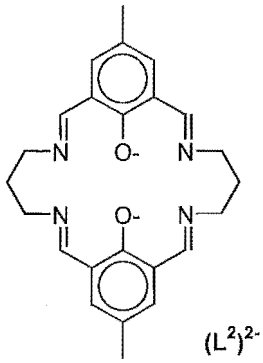

This complex could be obtained by either one of the following methods.

Method 1: An aqueous solution of 1,3-diaminopropane (1.353 g, 18.3 mmol, in 15 ml) was added to an aqueous solution of $Cu(BF_4)_2 \cdot 6H_2O$ (1.428 g, 4.1 mmol, in 5 ml). A blue suspension (presumably containing copper(II) hydroxide) was formed during addition which redissolved to give a violet solution. This solution was then added to a stirred solution of 2,6-diformyl-4-methylphenol (330.7 mg, 2.0 mmol) in methanol (100 ml). The dark green mixture was stirred overnight, allowed to stand for 1 d and then concentrated by rotary-evaporation (40 °C) to *ca.* 40 ml. Complex **5** formed as a green precipitate and was subsequently collected, washed with water and dried under vacuum overnight. Yield 457.8 mg, 0.62 mmol, 31%. This compound was recrystallised by evaporation of the methanol solution to give crystals suitable for single crystal X-ray structure analysis.

Method 2*:* A solution of copper(II) tetrafluoroborate hexahydrate (867 mg, 2.5 mmol) in 10 ml methanol was added to a methanolic solution of 1,3-diaminopropane (261 mg, 3.5 mmol, in 5 ml) giving a violet solution. This solution was added to a stirred solution of 2,6-diformyl-4-methylphenol (164.2 mg, 1.0 mmol) in 100 ml methanol. 2-3 ml of 99 % triethylamine (*ca.* 28.8 mmol) was added next. The solution turned blue after stirring for *ca.* 15 min. The solution was then concentrated by rotary-evaporation to *ca.* 5 ml, allowed to cool to room temperature and mixed with 5 ml of ethanol. The mixture was allowed to stand in a closed container for 4 d, during which time complex **5**

separated as green crystals. The compound was collected and air-dried. Yield 126.5 mg, 0.17 mmol, 17 %.

Selected infrared absorptions:

ν(OH): 3579 (s, m), 3508 (s, m), ν(C=N): 1638 (s, s),

ν(C-O_{phenol}): 1568 (s, s), $\nu(BF_4)$: 1084 (b, s) cm^{-1}.

Microanalysis:

Found	C 39.18%; H 3.92%; N 7.59%.
Calculated	C 39.00%; H 3.82%; N 7.58% ($[Cu_2L^2(H_2O)_2](BF_4)_2$ or $C_{24}H_{30}N_4O_4Cu_2B_2F_8$).

Complex 6 - $Cu_2L^8(\mu\text{-}OH)(ClO_4)_2(H_2O)$

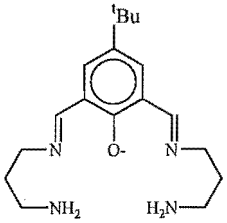

$(L^8)^-$

4-*t*-Butyl-2,6-diformylphenol, (515 mg, 2.50 mmol) was dissolved in 250 ml of methanol and boiled to give a yellow solution. $Cu(ClO_4)_2 \cdot 6H_2O$ (1.89 g, 5.1 mmol) was dissolved in 5 ml of methanol and treated with a solution of 1,3-diaminopropane (566 mg, 7.6 mmol) in 5 ml of methanol, giving first a blue suspension, then a violet solution. The violet solution was added to the stirred 4-*t*-butyl-2,6-diformylphenol solution . The resulting dark green solution was concentrated to *ca.* 150 ml by heating for *ca.* 1 h. Evaporation of this methanol solution at ambient temperature only gave a dark blue paste. Complex **6** was isolated as a solid by the following method.

The blue paste was redissolved in methanol, filtered and rotary-evaporated to near dryness. The residue was redissolved in ethanol, the solution was concentrated to *ca.* 10 ml by rotary-evaporation and treated with a solution of sodium acetate (about 20 mg) in 7 ml of ethanol. The mixture was warmed for *ca.* 5 min and allowed to stand at ambient temperature. Complex **6** was formed as an amorphous precipitate, collected by vacuum filtration, and air-dried. Yield 339.7 mg, 0.50 mmol, 20% (based on 4-*t*-butyl-2,6-diformylphenol).

Selected infrared absorptions:

ν(O-H): 3441 (b, m), $\nu(NH_2)$: 3318, 3261 (s, m), ν(C=N): 1639 (s, s), $\delta(NH_2)$: 1597 (s, m), $\nu(C\text{-}O_{phenol})$: 1566 (s, s), $\nu(ClO_4)$: 1098 (b, s) cm^{-1}.

Microanalysis:

Found	C 31.88%; H 4.81%; N 8.24%.
Calculated	C 31.87%; H 4.75%; N 8.26% ($Cu_2L^8(OH)(ClO_4)_2(H_2O)$ or $C_{18}H_{32}N_4O_{11}Cu_2Cl_2$).

Complex 7 - $[Cu_2L^8(\mu\text{-}OH)](BF_4)_2 \cdot 4H_2O$

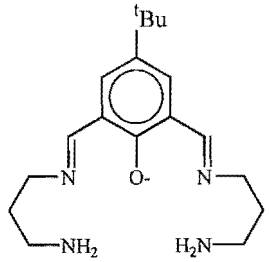

$(L^8)^-$

4-*t*-Butyl-2,6-diformylphenol (208.3 mg, 1.01 mmol) and NaOH (40.4 mg, 1.01 mmol) were dissolved in a water-methanol mixture (100 ml:200 ml). The solution was boiled until a clear yellow solution was obtained. $NaOH_{(aq)}$ (2.9 mg/ml) was added dropwise to the mixture until the solution was slightly basic.

A solution of 1,3-diaminopropane (235.0 mg, 3.17 mmol) in 5 ml of water was mixed with a 10 ml aqueous solution of $Cu(BF_4)_2 \cdot 6H_2O$ (873.5 mg, 2.53 mmol), giving a violet blue solution and pale blue precipitate (presumably $Cu(OH)_2$). More aqueous solution of 1,3-diaminopropane (84.5 mg, 1.14 mmol, in 15 ml) was added to the suspension until a clear solution was obtained. This solution was added to the stirred, boiling solution of 4-*t*-butyl-2,6-diformylphenol/NaOH. The blue green mixture was then boiled for *ca.* 45 min, to give a deep blue solution. This solution was vacuum filtered while hot to remove some undissolved residue and the filtrate was concentrated by heating to a volume of *ca.* 50 ml. Some brownish residue was removed by another filtration and the deep blue filtrate was allowed to evaporate from a beaker covered with a watch glass over *ca.* 12 d. Complex **7** formed as dark blue needles suitable for X-ray crystal structure analysis. Yield 291 mg, 0.42 mmol, 42% (based on 4-*t*-butyl-2,6-diformylphenol).

The crystal structure shows four water of crystallisation, while microanalytical data suggest three water molecules of crystallisation. The discrepancy is probably due to the loss of one water of crystallisation during microanalysis.

Selected infrared absorptions:

ν(OH): 3418 (b, s), ν(C=N): 1640 (s, s), ν(C-O_{phenol}): 1560 (s, s), $\nu(BF_4)$: 1053 (b, s) cm^{-1}.

Microanalysis:

Found	C 31.19%; H 5.43%; N 8.22%.
Calculated	C 31.37%; H 5.27%; N 8.13%
	($[Cu_2L^8(\mu\text{-}OH)](BF_4)_2 \cdot 3H_2O$ or $C_{18}H_{36}N_4O_5Cu_2B_2F_8$).

Complex 8 - $[Cu_2L^3(NCS)_2(\mu\text{-}OCH_3)(H_2O)(CH_3OH)]$, complex 9 - $[Cu_2L^3(NCS)_2(\mu\text{-}OCH_2CH_3)]$, complex 10 - $[Cu_2L^3(NCS)_2(\mu\text{-}OH)]$

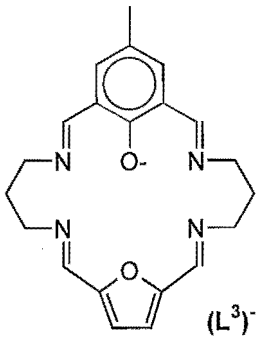

A methanolic solution of 2,5-diformylfuran (74.4 mg, 0.6 mmol, in 4 ml) was filtered into a hot methanolic solution of the complex $[Cu_2L^1(OH)](BF_4)_2 \cdot H_2O$ (226.6 mg, 0.36 mmol, in 6 ml). The mixture was boiled and stirred for *ca.* 1 h or until the colour of the solution changed from blue to green, after which the solution was removed from heat. NH_4NCS in methanol (60.3 mg, 0.79 mmol, in 5 ml) was then added to the hot solution. A green precipitate (**8**), formulated as $Cu_2L^3(CH_3O)(NCS)_2(H_2O)(CH_3OH)$ on the basis of infrared and microanalytical data, formed almost immediately. The suspension was allowed to stand for several hours (overnight) at ambient temperature before filtering this precipitate. Yield 210 mg, 0.3 mmol, 83%.

Emerald green crystals (**9**) and a bright green powder (**10**) could be obtained by diffusing diethylether vapour into a DMF solution of the unrecrystallised compound. The crystals were suitable for single-crystal X-ray structure analysis which gave the formulation $[Cu_2L^3(\mu\text{-}OCH_2CH_3)(NCS)_2]$ for this complex. The powder is formulated as $[Cu_2L^3(\mu\text{-}OH)(NCS)_2]$ based mainly on infrared and microanalytical data, and the crystal structure of $[Cu_2L^3(\mu\text{-}OCH_2CH_3)(NCS)_2]$.

Selected infrared absorptions:

Complex **8**

ν(OH): 3446 (b, m), ν(**NCS**): 2089 (s, s), ν(C=N) 1640,

$\nu(C\text{-}O_{phenol})$: 1560 (s, s), ν(**NCS**): 766 (s, m) cm^{-1}.

Complex **9**

ν(OH): 3440 (b, m), ν(**NCS**): 2094 (s, s), 2077 (s, s), ν(C=N): 1641 (s, s),

$\nu(C\text{-}O_{phenol})$ 1564 (s, s), ν(**NCS**): 766 (s, m) cm^{-1}.

Complex **10**

ν(OH): 3640 (s, m), 3450 (b, m), ν(**NCS**): 2081 (s, s), ν(C=N): 1641 (s, s),

$\nu(C\text{-}O_{phenol})$: 1559 (s, s), ν(**NCS**): 768 (s, m) cm^{-1}.

Microanalysis:

Complex **8**

Found C 43.66%; H 4.50%; N 12.18%.

Calculated C 43.66%; H 4.69%; N 12.22% ($C_{24}H_{32}N_6O_5Cu_2S_2$)

Complex **9**

Found C 46.02%; H 4.13%; N 13.11%.

Calculated C 46.07%; H 4.33%; N 12.89% ($C_{25}H_{28}N_6O_3Cu_2S_2$).

Complex **10**

Found C 44.22%; H 4.11%; N 13.21%.

Calculated C 44.29%; H 3.88%; N 13.48% ($C_{23}H_{24}N_6O_3Cu_2S_2$).

FAB-MS (complexes 8, 9 and 10):

Observed 427, 489.

Expected $[CuHL^3]^+$ (427), $[Cu_2L^3]^+$ (489).

Complex 11 - $\{[Cu_6L^4(\mu\text{-}OH)_4](BF_4)_2 \cdot nH_2O\}^+$, complex 12 - $[Cu_6L^4(\mu\text{-}OH)_4(H_2O)](NO_3)_3 \cdot nH_2O$, complex 12A - $[Cu_6L^4(\mu\text{-}OH)_4](NO_3)_x \cdot nH_2O$

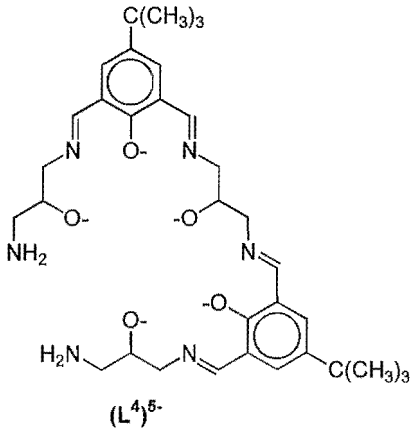

A solution of $Cu(BF_4)_2 \cdot 6H_2O$ (887.4 mg, 2.6 mmol) in 10 ml of water was mixed with an aqueous solution of 1,3-diamino-2-hydroxypropane (274.7 mg, 3.1 mmol, in 10 ml) giving a violet solution. This solution was added to a stirred, boiling (70-80 °C) mixture of 4-t-butyl-2,6-diformylphenol (206.2 mg, 1.0 mmol) and NaOH (1.0 mmol) in 50 ml MeOH and 30 ml H_2O. The mixture was boiled for 20-25 min, changing its colour from green to blue as the temperature rose to 80 °C. Some yellow-brown residue that formed during the heating was removed by hot filtration. The filtrate was concentrated on the hot plate for *ca.* 50 min until the volume was *ca.* 50 ml and filtered to remove some green residue. The deep blue filtrate was allowed to stand and evaporate at ambient temperature for 3 d, during which time **11** separated as dark blue crystals, were subsequently collected and air-dried. Yield 311 mg.

Complex **11** could be recrystallised by evaporating its methanol solution or as follows: approximately 50 mg of the complex was dissolved in 5-7 ml of methanol, treated with an aqueous solution of $NaBF_4$ (*ca.* 200 mg in 5-7 ml) and allowed to evaporate at ambient temperature for *ca.* 2 weeks.

Complex **12** was obtained from complex **11** as dark blue crystals when $NaNO_3$ was substituted for $NaBF_4$ using the above recrystallisation procedure. A single-crystal suitable for X-ray structure determination was obtained this way.

Complex **12A** was obtained as complex **11**, except that copper(II) nitrate trihydrate was used in place of copper(II) tetrafluoroborate. Yield 25 mg. Crystals of this complex were too small for X-ray diffraction data collection.

Preliminary X-ray crystal structure analyses for complexes **11** and **12** showed $[Cu_6L^4(\mu_2\text{-}OH)_4](BF_4)_2$ unit and $[Cu_6L^4(\mu_2\text{-}OH)_4](NO_3)_3$ unit, respectively. The structures of the cations of both complexes are severely disordered (see Chapter 3), which makes the nature and number of anions for both complexes are difficult to determined, thus preventing a single formulation of the complexes to be deduced from the microanalytical and spectroscopic data.

Selected infrared absorptions:

Complex **11**

ν(OH): 3579 (s, m, observed only when the matrix was nujol), 3424 (b, s), $\nu(NH_2)$: 3355 (a shoulder when matrix was KBr, but a sharp peak of medium intensity when matrix was nujol), ν(C=N): 1652 (s, s), $\nu(C\text{-}O_{phenol})$: 1556 (s, s), $\nu(C\text{-}O_{alcohol})$: 1083 (s, s), $\nu(BF_4)$: 1053 (b, s) cm^{-1}.

Complex **12**

ν(OH): 3420 (b, s), $\nu(NH_2)$: 3200-3300 (shoulders), ν(C=N): 1653 (s, s), $\nu(C\text{-}O_{phenol})$: 1554 (s, s), $\nu(NO_3)$: 1384 (s, s), 1353 (b, s) cm^{-1}.

Microanalysis:

Complex **11**

Found	C 28.54%; H 3.65%; N 5.72%.
Calculated	C 28.25%; H 3.59%; N 5.99%
	$([Cu_6L^4(OH)(BF_4)_4(OH)_2(H_2O)])$ or
Calculated	C 28.82%; H 3.81%; N 6.11%
	$([Cu_6L^4(OH)(BF_4)_3F_3(H_2O)_3])$ or
Calculated	C 28.29%; H 3.67%; N 6.00%
	$([Cu_6L^4(OH)(HOBF_3)(BF_4)_3(OH)_2(H_2O)])$ or

Calculated C 28.57%; H 3.41%; N 6.06%

($[Cu_6L^4(OH)(BF_4)_4F(OH)]$)

Complex **12**

Found C 29.29%; H 3.67%; N 8.92%.

Calculated C 29.43%; H 3.89%; N 9.36%

($[Cu_6L^4(OH)(NO_3)_3(OH)_2(BF_4)(H_2O)_2]$) or

Calculated C 29.36%; H 3.88%; N 9.34%

($[Cu_6L^4(OH)(NO_3)_3F_2(BF_3)(H_2O)_3]$) or

Calculated C 29.38%; H 3.81%; N 9.35%

($[Cu_6L^4(OH)(NO_3)_3F_2(HOBF_3)(H_2O)_2]$) or

Calculated C 29.15%; H 3.86%; N 9.27%

($[Cu_6L^4(OH)(NO_3)_3(OH)_2(ClO_4)(H_2O)_2]$)

FAB-MS:

Complex **11**:

Observed 1017, 1051.

Expected $[Cu_6L^4(OH)_2]^+$ (1017), $[Cu_6L^4(OH)_4]^+$ (1051).

Complex **12**:

Observed 1017, 1051.

Expected $[Cu_6L^4(OH)_2]^+$ (1017), $[Cu_6L^4(OH)_4]^+$ (1051).

Complex 13 - $Cu_4L^6(OH)(BF_4)_3(H_2O)_2$

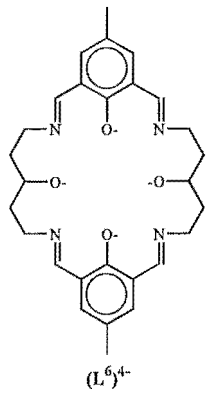

$(L^6)^{4-}$

Method 1: 1,5-diamino-3-hydroxypentane dihydrochloride (1,5-DAHP·2HCl) (460.8 mg, 2.4 mmol) was treated with an 8.03 mg/ml solution of KOH in dry ethanol (33.5 ml, 269.1 mg, 4.8 mmol). The insoluble KCl was removed by vacuum filtration and washed with dry ethanol. The filtrate containing 1,5-DAHP was treated with a solution of $Cu(BF_4)_2 \cdot 6H_2O$ (837 mg, 2.42 mmol) in 10 ml of methanol. The resulting blue solution was added to a warmed and stirred solution of 2,6-diformyl-4-methylphenol (132 mg, 0.8 mmol) in 40 ml of methanol. The green solution was stirred overnight at room temperature and allowed to stand for 3 d at ambient temperature for crystallisation. Complex **13** formed as a green precipitate, was collected by vacuum filtration and air-dried. Yield 244 mg, 0.23 mmol, 29% (based on 2,6-diformyl-4-methylphenol).

Method 2: A solution of 1,5-DAHP (2.4 mmol) in dry methanol was obtained by a method similar to that described in method 1 above. This solution was treated with a solution of $Cu(BF_4)_2 \cdot 6H_2O$ (825 mg, 2.4 mmol) in 10 ml of water. The resulting blue suspension was added to a stirred solution of 2,6-diformyl-4-methylphenol (131.4 mg, 0.8 mmol) in 40 ml of methanol at room temperature. The suspension gradually turned to a green solution after 10 min, which subsequently was stirred overnight. Following this, the solution was concentrated by rotary-evaporation at 35 °C to *ca.* 20 ml, warmed in a heating mantle for *ca.* 10 min and allowed to cool to room temperature. Complex

13 formed as a green powder, was vacuum filtered, washed with ethanol and air-dried. Yield 284.6 mg, 0.27 mmol, 34% (based on 2,6-diformyl-4-methylphenol).

Selected infrared absorptions:

ν(OH): 3423 (b, m), ν(C=N): 1643 (s, s),

ν(C-O_{phenol}): 1575 (s, s), ν(BF_4): 1059 (b, s) cm^{-1}.

Microanalysis:

Complex **13**

Found	C 31.99%; H 3.39%; N 5.67%.
Calculated	C 31.84%; H 3.53%; N 5.30% ($Cu_4L^6(OH)(BF_4)_3(H_2O)_2$ or $C_{28}H_{37}N_4O_7Cu_4B_3F_{12}$).

Complex 14 - $[\{Cu_4L^6(\mu_5\text{-}O)(BF_4)\}_2(BF_4)_2\cdot 2H_2O]$, complex 15 - $[Cu_4L^6(\mu_4\text{-}OH)(\mu\text{-}HCOO)(OH)Cl]\cdot 6H_2O$; complex 16 - $[\{Cu_4(HL^6)(\mu_3\text{-}OH)\}_2]$

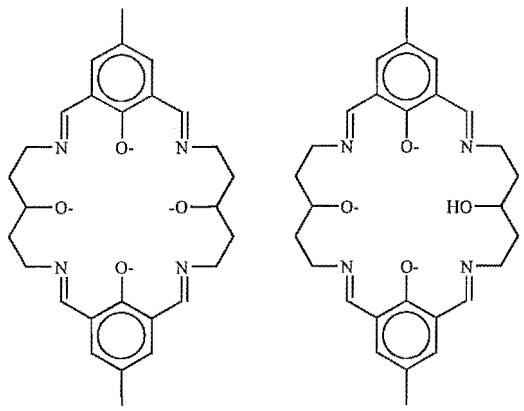

Complex **14** was obtained as green crystals of X-ray quality by diethylether vapour diffusion into the DMF solution of complex **13**. While a slow evaporation (over a period of several months) of the DMF solution of complex **13** yielded complex **15** well-formed green crystals also of X-ray quality.

Complex **16** was obtained as a by-product of the preparation of complex **13** using the second method as follows: the filtrate from collection of **13** was concentrated by rotary-evaporation, vacuum filtered, and allowed to stand at ambient temperature for crystallisation. In *ca.* 16 d more green precipitate was formed and removed by gravity filtration and the filtrate was allowed to evaporate slowly. Complex **16** formed as a few dark green blocks, which appeared almost colourless under polarised light (dichroic). There was insufficient amount of **16** to obtain the infrared or microanalytical data. However, the crystal quality was good enough to obtain an X-ray diffraction data set, which allowed us to determine the connectivity of the macrocycle and tentatively assign the formula $[\{Cu_2HL^6(\mu\text{-}OH)\}_2]$ to this compound. Unfortunately, due to the weakly diffracting crystal we were unable to obtain a fully refined model.

Selected infrared absorptions:

Complex **14**

ν(OH): 3439 (b, m), ν(C=N): 1646 (s, s),

ν(C-O_{phenol}): 1576 (s, s), $\nu(BF_4)$: 1064 (b, s) cm^{-1}.

Complex **15**

ν(O-H): 3482 (b, m), ν(C=N): 1647 (s, s), 1632 (s, s),

ν(C-O_{phenol}): 1587 (s, s), 1570 (s, s) cm^{-1}. No band due to the asymmetric stretch of BF_4 anion is present.

Microanalysis:

Complex **14**

Found C 35.12%; H 3.41%; N 5.93%.

Calculated C 35.39%; H 3.61%; N 5.90%

$([\{Cu_4L^6(\mu_5\text{-}O)\}_2(BF_4)_2](BF_4)_2\cdot 2H_2O$ or $C_{56}H_{68}N_8O_{12}Cu_8B_4F_{16})$.

Complex **15**

Found C 35.60%; H 4.32%; N 6.06%.

Calculated C 35.42%; H 5.02%; N 5.70%

$[Cu_4L^6(\mu_4\text{-}OH)(\mu\text{-}HCOO)(OH)Cl]\cdot 7H_2O$ or $C_{29}H_{49}N_4O_{15}Cu_4Cl$.

FAB-MS:

Complex **15**

Observed 616, 758.

Expected $[Cu_2H_2L^6]^+$ (616), $[Cu_4HL^6(OH)]^+$ (758).

Complex 17 - $[Cu_2L^5](BF_4)_2 \cdot H_2O$

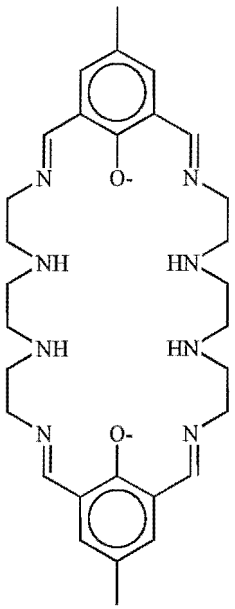

$(L^5)^{2-}$

A solution of $Cu(BF_4)_2 \cdot 6H_2O$ in methanol-ethanol (1:1) (517.9 mg. 1.5 mmol, in 10 ml) and a solution of triethylenetetramine in the same solvent (307.1 mg, 2.1 mmol, in 5 ml) were mixed to give a violet solution. This solution was added to a refluxing solution of 2,6-diformyl-4-methylphenol (98.52 mg, 0.6 mmol) in the same solvent (45 ml). The mixture was refluxed for 1 hr, then allowed to stand at ambient temperature for 7 d in a covered flask for crystallisation. Needle-like crystals, suitable for X-ray crystallography, were collected by vacuum filtration. Yield: 153 mg, 0.18 mmol, 29.5 % (based on 2,6-diformyl-4-methylphenol).

Selected infrared absorptions:

ν(OH): 3440 (b, m), $\nu(NH_2)$: 3308 (s, m), 3273 (s, m), 3207 (s, m),

ν(C=N): 1641 (s, s), $\nu(C\text{-}O_{phenol})$: 1545 (s, s), $\nu(BF_4)$: 1084 (b, s) cm^{-1}.

Microanalysis:

Found	C 41.32%; H 4.92%; N 12.80%.
Calculated	C 41.66%; H 5.12%; N 12.95% ($[Cu_2L^5](BF_4)_2 \cdot H_2O$ or $C_{30}H_{44}N_8O_3Cu_2B_2F_8$).

2.4 Data collection parameters and crystal data

The data sets were collected on a Siemens P4 four-circle diffractometer using graphite-monochromated Mo-Kα radiation (λ = 0.71073 Å). The unit cell parameters were determined by least-squares refinement of 12-30 accurately centered reflections in the range $5 < 2\theta < 42°$. Crystal stability was monitored by recording three check reflections every 97 reflections and no significant variations were observed in any structure. The data sets were corrected for Lorentz and polarisation effects. Empirical or semi-empirical absorption corrections, based on ψ-scan data, were applied. Hydrogen atoms were inserted in idealised positions using a riding model. Neutral scattering factors were taken from Ibers and Hamilton.[94] All structures except that of $[Cu_2L^1(\mu\text{-}OH)(H_2O)](ClO_4)_2 \cdot H_2O$, were refined on F^2 using full-matrix least-squares refinement; the function minimised being $\Sigma[w(F_o^2\text{-}F_c^2)^2]$, where $w = [\sigma^2(F_o^2) + (aP)^2 + bP]^{-1}$ and $P = (\text{Max}\ (F_o^2, 0) + 2F_c^2)/3$. These structures were solved using the program SHELXS-86[95a] and refined using SHELXL-92[95b] or SHELXL-93.[95c] The structure of $[Cu_2L^1(\mu\text{-}OH)(H_2O)](ClO_4)_2 \cdot H_2O$ was refined on F using the program SHELXTL[95d] version 4.2. The function minimised for this structure is $[\Sigma\{w \cdot |F_o\text{-}F_c|^2\}]^{1/2}$, where $w = [\sigma^2(F) + |g| \cdot F^2]^{-1}$.

Complex 1 - $[Cu_2L^1(\mu\text{-}OH)(H_2O)](ClO_4)_2 \cdot H_2O$

Crystal data

Crystal description	needle
Crystal colour	blue
Crystal size	0.42 x 0.40 x 0.13 mm
Empirical formula	$C_{15}H_{26}Cl_2Cu_2N_4O_{12}$
Formula weight	652.38
Crystal system	Orthorhombic
Space group	Pbca
Unit cell dimensions	a = 9.323(3) Å $\alpha = 90°$.
	b = 17.864(5) Å $\beta = 90°$.
	c = 29.069(8) Å $\gamma = 90°$.
Volume, Z	4841(3) $Å^3$, 8
F(000)	2656
Absorption coefficient	2.045 mm^{-1}
Max. and min. transmission	1.000 and 0.664
Density (calculated)	1.790 mg/m^3

Data collection parameters

Temperature	293(2) K
Theta range for data collection	2.28 to 25.00°
Limiting indices	$0 \le h \le 11, 0 \le k \le 21, 0 \le l \le 34$
Reflections collected	4252
Independent reflections	4252 [R(int) = 0.0000]

Refinement details

Data / restraints / parameters	4252 / 0 / 316
Goodness-of-fit on F^2	1.056
Final R indices [$F_o > 4\sigma(F_o)$]	R1 = 0.0626, wR2 = 0.1650
R indices (all data)	R1 = 0.0849, wR2 = 0.1868
Largest diff. peak and hole	1.922 and -1.317 $e.Å^{-3}$

Complex 4 - $[Cu_2L^1(\mu\text{-}OH)](BF_4)_2 \cdot H_2O$

Crystal data

Crystal description	needle
Crystal colour	dark blue
Crystal size	0.88 x 0.52 x 0.30 mm
Empirical formula	$C_{15}H_{26}B_2Cu_2F_8N_4O_3$
Formula weight	611.10
Crystal system	Monoclinic
Space group	$P2_1/n$
Unit cell dimensions	a = 7.339(2) Å $\alpha = 90°$
	b = 21.585(5) Å $\beta = 94.92(2)°$
	c = 14.064(3) Å $\gamma = 90°$
Volume, Z	2219.7(9) $Å^3$, 4
F(000)	1232
Absorption coefficient	2.009 mm^{-1}
Max. and min. transmission	0.987 and 0.571
Density (calculated)	1.829 mg/m^3

Data collection parameters

Temperature	130(2) K
Theta range for data collection	2.38 to 27.50°
Limiting indices	$0 \le h \le 9, 0 \le k \le 28, -18 \le l \le 18$
Reflections collected	5482
Independent reflections	5095 [R(int) = 0.0403]

Refinement details

Data / restraints / parameters	5094 / 0 / 308
Goodness-of-fit on F^2	1.047
Final R indices [$F_o > 4\sigma(F_o)$]	R1 = 0.0585, wR2 = 0.1214
R indices (all data)	R1 = 0.1126, wR2 = 0.1455
Largest diff. peak and hole	1.676 and -.550 $e.Å^{-3}$

Complex 5 - $[Cu_2L^2(H_2O)_2](BF_4)_2$

Crystal data

Crystal description	needle
Crystal colour	green
Crystal size	0.60 x 0.50 x 0.20 mm
Empirical formula	$C_{24}H_{30}B_2Cu_2F_8N_4O_4$
Formula weight	739.22
Crystal system	Monoclinic
Space group	$P2_1/c$
Unit cell dimensions	a = 16.491(3) Å $\alpha = 90°$
	b = 12.323(1) Å $\beta = 105.37(1)°$
	c = 14.529(3) Å $\gamma = 90°$
Volume, Z	2847.0(8) $Å^3$, 4
F(000)	1496
Absorption coefficient	1.586 mm^{-1}
Max. and min. transmission	0.964 and 0.721
Density (calculated)	1.725 mg/m^3

Data collection parameters

Temperature	293(2) K
Theta range for data collection	2.09 to 25.00°
Limiting indices	$-19 \leq h \leq 19, -14 \leq k \leq 1, -1 \leq l \leq 17$
Reflections collected	5580
Independent reflections	4972 [R(int) = 0.0279]

Refinement details

Data / restraints / parameters	4968 / 0 / 398
Goodness-of-fit on F^2	1.092
Final R indices [$F_o > 4\sigma(F_o)$]	R1 = 0.0404, wR2 = 0.1034
R indices (all data)	R1 = 0.0500, wR2 = 0.1143
Extinction coefficient	0.0102(7)
Largest diff. peak and hole	.629 and -.620 $e.Å^{-3}$

Complex 7 - $[Cu_2L^8(\mu\text{-}OH)](BF_4)_2 \cdot 4H_2O$

Crystal data

Crystal description	needle
Crystal colour	dark blue
Crystal size	0.90 x 0.70 x 0.50 mm
Empirical formula	$C_{18}H_{36}B_2Cu_2F_8N_4O_5$
Formula weight	689.21
Crystal system	Orthorhombic
Space group	Pbcn
Unit cell dimensions	a = 28.872(5) Å $\alpha = 90°$
	b = 16.286(3) Å $\beta = 90°$
	c = 11.800(2) Å $\gamma = 90°$
Volume, Z	5549(2) $Å^3$, 8
F(000)	2816
Absorption coefficient	1.623 mm^{-1}
Max. and min. transmission	0.886 and 0.499
Density (calculated)	1.650 mg/m^3

Data collection parameters

Temperature	143(2) K
Theta range for data collection	2.25 to 25.00°
Limiting indices	$0 \leq h \leq 34$, $0 \leq k \leq 19$, $-14 \leq l \leq 0$
Reflections collected	4874
Independent reflections	4874 [R(int) = 0.0000]

Refinement details

Data / restraints / parameters	4874 / 0 / 207
Goodness-of-fit on F^2	1.033
Final R indices [$F_o > 4\sigma(F_o)$]	R1 = 0.0871, wR2 = 0.2155
R indices (all data)	R1 = 0.1363, wR2 = 0.2571
Largest diff. peak and hole	2.083 and -1.011 $e.Å^{-3}$

Complex 9 - $[Cu_2L^3(\mu\text{-}OCH_2CH_3)(NCS)_2]$

Crystal data

Crystal description	block
Crystal colour	green
Crystal size	0.37 x 0.35 x 0.14 mm
Empirical formula	$C_{23}H_{23}Cu_2N_6O_3S_2$
Formula weight	622.67
Crystal system	Monoclinic
Space group	$P2_1/c$
Unit cell dimensions	$a = 9.113(2)$ Å $\quad \alpha = 90°$
	$b = 21.440(4)$ Å $\quad \beta = 91.19(3)°$
	$c = 14.102(3)$ Å $\quad \gamma = 90°$
Volume, Z	2754.7(10) $Å^3$, 4
F(000)	1268
Absorption coefficient	1.731 mm^{-1}
Max. and min. transmission	0.851 and 0.655
Density (calculated)	1.501 mg/m^3

Data collection parameters

Temperature	130(2) K
Theta range for data collection	2.24 to 24.97°
Limiting indices	$0 \le h \le 10$, $0 \le k \le 25$, $-16 \le l \le 16$
Reflections collected	5156
Independent reflections	4833 [R(int) = 0.0471]

Refinement details

Data / restraints / parameters	4832 / 0 / 345
Goodness-of-fit on F^2	1.050
Final R indices [$F_o > 4\sigma(F_o)$]	R1 = 0.0494, wR2 = 0.0915
R indices (all data)	R1 = 0.0845, wR2 = 0.1047
Largest diff. peak and hole	.764 and -.538 $e.Å^{-3}$

Complex 11 - $[Cu_6L^4(\mu\text{-}OH)_4](BF_4)_2 \cdot nH_2O$*

Crystal data

Crystal colour	dark blue
Crystal size	0.60 x 0.50 x 0.45 mm
Crystal system	Monoclinic
Space group	$P2_1/c$
Unit cell dimensions	a = 16.775(7) Å $\alpha = 90°$
	b = 15.624(5) Å $\beta = 100.62(3)°$
	c = 18.912(4) Å $\gamma = 90°$
Volume, Z	4872(3) $Å^3$, 8
F(000)	2768
Absorption coefficient	1.886 mm^{-1}
Max. and min. transmission	0.419 and 0.109
Density (calculated)	1.863 mg/m^3

Data collection parameters

Temperature	150(2) K
Theta range for data collection	1.80 to 25.12°
Limiting indices	$0 \le h \le 19$, $0 \le k \le 17$, $-21 \le l \le 21$
Reflections collected	8415
Independent reflections	8101 [R(int) = 0.1679]

Refinement details

Data / restraints / parameters	8101 / 42 / 555
Goodness-of-fit on F^2	2.207
Final R indices [$F_o > 4\sigma(F_o)$]	R1 = 0.1587, wR2 = 0.3606
R indices (all data)	R1 = 0.1907, wR2 = 0.3720
Largest diff. peak and hole	2.974 and -1.921 $e.Å^{-3}$

* The structure is severely disordered and not fully-refined as described in Chapter 3 Section 3. The formula given here is that of the major component of the structure.

Complex 12 - $Cu_6L^4(\mu\text{-}OH)_4](NO_3)_3 \cdot nH_2O$*

Crystal data

Crystal description	block	
Crystal colour	dark blue	
Crystal size	0.80 x 0.58 x 0.42 mm	
Crystal system	Monoclinic	
Space group	$P2_1/c$	
Unit cell dimensions	a = 11.345(3) Å	$\alpha = 90°$
	b = 33.239(6) Å	$\beta = 101.32(2)°$
	c = 12.648(2) Å	$\gamma = 90°$
Volume, Z	4677(2) $Å^3$, 4	
F(000)	2692	
Absorption coefficient	3.247 mm^{-1}	
Max. and min. transmission	1.000 and 0.764	
Density (calculated)	1.853 mg/m^3	

Data collection parameters

Temperature	143(2) K
Theta range for data collection	1.23 to 22.50°
Limiting indices	$-12 \le h \le 2$, $0 \le k \le 35$, $-13 \le l \le 13$
Reflections collected	11155
Independent reflections	6116 [R(int) = 0.0396]

Refinement details

Data / restraints / parameters	6108 / 0 / 531
Goodness-of-fit on F^2	1.083
Final R indices [$F_o > 4\sigma(F_o)$]	R1 = 0.0697, wR2 = 0.1844
R indices (all data)	R1 = 0.0943, wR2 = 0.2167
Largest diff. peak and hole	1.767 and -0.986 e.$Å^{-3}$

* see footnote for complex 11 on the previous page.

Complex 14 - $[\{Cu_4L^6(\mu_5\text{-}O)(BF_4)\}_2]\cdot 2H_2O$

Crystal data

Crystal description	block	
Crystal colour	green	
Crystal size	0.55 x 0.36 x 0.16 mm	
Empirical formula	$C_{28}H_{32}B_2Cu_4F_8N_4O_5$	
Formula weight	932.36	
Crystal system	Monoclinic	
Space group	P-1	
Unit cell dimensions	a = 11.272(5) Å	$\alpha = 103.14(2)°$
	b =12.548(4) Å	$\beta = 113.36(2)°$
	c =13.329(2) Å	$\gamma = 99.66(3)°$
Volume, Z	1613.7(9) $Å^3$, 2	
F(000)	932	
Absorption coefficient	2.693 mm^{-1}	
Max. and min. transmission	1.000 and 0.762	
Density (calculated)	1.919 mg/m^3	

Data collection parameters

Temperature	130(2) K
Theta range for data collection	2.01 to 23.25°
Limiting indices	$0 \le h \le 11$, $-13 \le k \le 12$, $-14 \le l \le 13$
Reflections collected	4280
Independent reflections	4013 [R(int) = 0.0179]

Refinement details

Data / restraints / parameters	4013 / 62 / 519
Goodness-of-fit on F^2	0.992
Final R indices [$F_o > 4\sigma(F_o)$]	R1 = 0.0379, wR2 = 0.0783
R indices (all data)	R1 = 0.0604, wR2 = 0.0891
Largest diff. peak and hole	.742 and -.559 $e.Å^{-3}$

Complex 15 - $[Cu_4L^6(\mu_4\text{-}OH)(\mu\text{-}HCOO)(OH)Cl]$

Crystal data

Crystal description	block	
Crystal colour	emerald green	
Crystal size	0.48 x 0.32 x 0.20 mm	
Empirical formula	$C_{29}H_{32}ClCu_4N_4O_{14}$	
Formula weight	950.20	
Crystal system	Monoclinic	
Space group	C2/m	
Unit cell dimensions	a = 7.944(2)Å	$\alpha = 90°$
	b = 20.288(4)Å	$\beta = 94.570(10)°$
	c = 11.223(2) Å	$\gamma = 90°$
Volume, Z	1803.0(7) $Å^3$, 2	
F(000)	958	
Absorption coefficient	2.472 mm^{-1}	
Max. and min. transmission	0.949 and 0.726	
Density (calculated)	1.750 mg/m^3	

Data collection parameters

Temperature	130(2) K
Theta range for data collection	1.82 to 25.00°
Limiting indices	$-9 \le h \le 9, 0 \le k \le 24, -13 \le l \le 13$
Reflections collected	3274
Independent reflections	1643 [R(int) = 0.0261]

Refinement details

Data / restraints / parameters	1643 / 2 / 136
Goodness-of-fit on F^2	1.062
Final R indices [$F_o > 4\sigma(F_o)$]	R1 = 0.0473, wR2 = 0.1269
R indices (all data)	R1 = 0.0628, wR2 = 0.1365
Largest diff. peak and hole	1.115 and -.452 $e.Å^{-3}$

Complex 16 - $[\{Cu_2HL^6(\mu_3\text{-}OH)\}_2]$

Crystal data

Crystal description	block
Crystal colour	dark green (colourless under polarised light)
Crystal size	0.72 x 0.40 x 0.20 mm
Empirical formula	$C_{28}H_{32}BCu_2F_4N_4O_5$
Formula weight	718.47
Crystal system	Monoclinic
Space group	$P2_1/n$
Unit cell dimensions	a = 11.144(6) Å $\alpha = 90°$
	b = 24.116(10) Å $\beta = 111.56(2)°$
	c = 13.286(3) Å $\gamma = 90°$
Volume, Z	3321(2) $Å^3$, 4
F(000)	1468
Absorption coefficient	1.344 mm^{-1}
Max. and min. transmission	0.912 and 0.665
Density (calculated)	1.437 mg/m^3

Data collection parameters

Temperature	130(2) K
Theta range for data collection	1.85 to 22.49°
Limiting indices	$-11 \leq h \leq 0$, $0 \leq k \leq 25$, $-12 \leq l \leq 13$
Reflections collected	3841
Independent reflections	3822 [R(int) = 0.0358]

Refinement details

Data / restraints / parameters	3814 / 0 / 197
Goodness-of-fit on F^2	1.063
Final R indices [$F_o > 4\sigma(F_o)$]	R1 = 0.1522, wR2 = 0.3742
R indices (all data)	R1 = 0.2809, wR2 = 0.4891
Largest diff. peak and hole	1.387 and -.784 $e.Å^{-3}$

Complex 17 - $[Cu_2L^5](BF_4)_2 \cdot H_2O$

Crystal data

Crystal description	needle
Crystal colour	dark green
Crystal size	0.7 x 0.6 x 0.3 mm
Empirical formula	$C_{30}H_{44}B_2Cu_2F_8N_8O_3$
Formula weight	865.43
Crystal system	Monoclinic
Space group	C2/c
Unit cell dimensions	a = 41.602(8) Å $\alpha = 90°$
	b = 7.0020(10) Å $\beta = 112.950(10)°$
	c = 26.728(5) Å $\gamma = 90°$
Volume, Z	7170(2) $Å^3$, 8
F(000)	3552
Absorption coefficient	1.273 mm^{-1}
Max. and min. transmission	0.967 and 0.687
Density (calculated)	1.604 mg/m^3

Data collection parameters

Temperature	130(2) K
Theta range for data collection	2.13 to 24.90°
Limiting indices	$-47 \leq h \leq 43$, $0 \leq k \leq 8$, $0 \leq l \leq 29$
Reflections collected	5700
Independent reflections	5543 [R(int) = 0.0151]

Refinement details

Data / restraints / parameters	5543 / 62 / 522
Goodness-of-fit on F^2	1.055
Final R indices [$F_o > 4\sigma(F_o)$]	R1 = 0.0528, wR2 = 0.1147
R indices (all data)	R1 = 0.0841, wR2 = 0.1274
Largest diff. peak and hole	1.047 and -.467 $e.Å^{-3}$

Chapter 3

RESULTS AND DISCUSSION

Introduction to Chapter 3

Synthetic approach

The synthetic approach adopted to prepare the complexes in this work is outlined in **Figure 3.1** and is aimed at preparing asymmetric Schiff-base macrocycles. The first step in this approach is to prepare an acyclic Schiff-base ligand from two molecules of a di-primaryamine and one molecule of a diformylphenol compound by using the template method (with Cu(II) as the template). The second step is the template cyclocondensation of the acyclic intermediate, using a dicarbonyl compound containing no pendant phenol (or other pendant bridging donor).

2,6-Diformyl-4-methylphenol (DFMP) and its related compound, 4-*t*-butyl-2,6-diformylphenol (TDFP), were the diformylphenol components, while the diamine compounds shown in **Figure 3.1** were employed as the di-primaryamine components.

This approach is based on one of the mechanisms outlined by Nelson for the formation of symmetric [2+2] Schiff-base macrocycles[42, 43] (see also **Chapter 1**). Nelson et al. have also prepared asymmetric Schiff-base macrocycles by using the stepwise route through the di-primaryamine acyclic intermediate. However, in this case pyridine-dicarbonyl compounds were employed as the building blocks for the "head units" of the macrocycle, and alkaline earth cations as the metal templates.

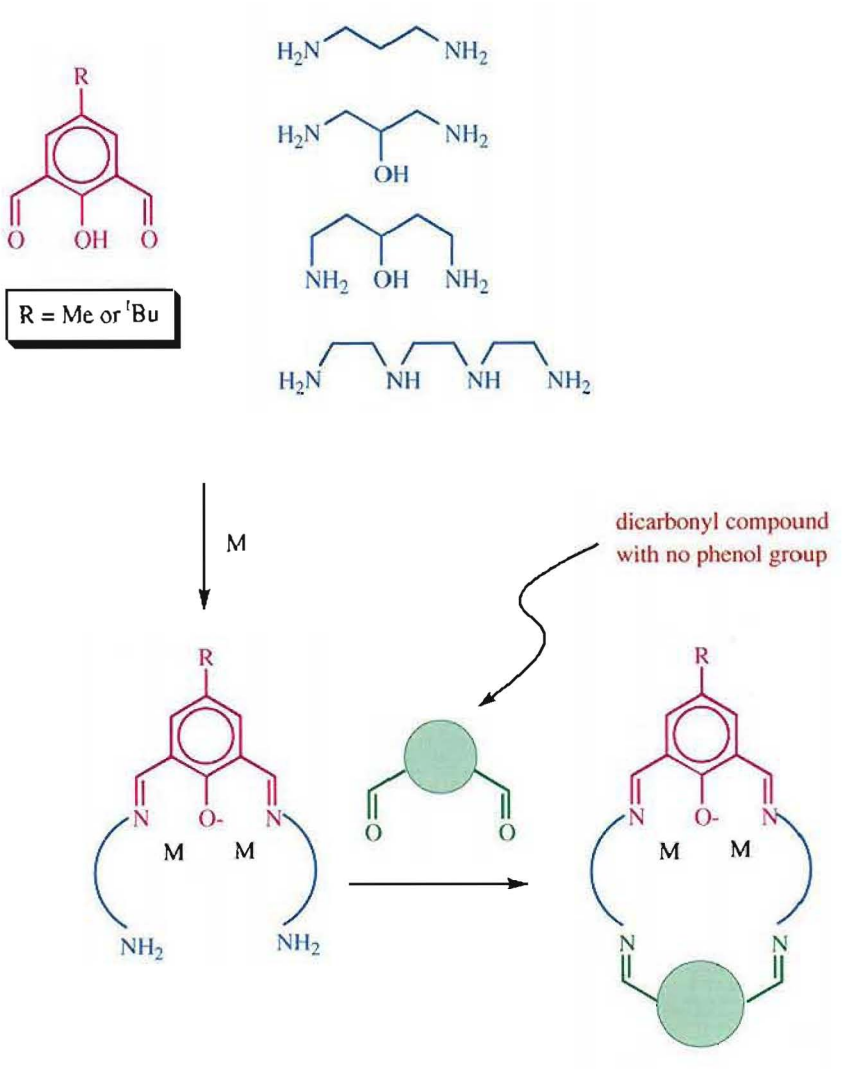

Figure 3.1. The synthetic approach adopted in this work to prepare asymmetric Schiff-base macrocycles based on diformylphenol.

Mandal and Nag[61] prepared some asymmetric Schiff-base macrocycles using the same route through an acyclic di-primaryamine Schiff-base intermediate, based on phenol-containing dicarbonyl compounds as the building blocks for both "head units" of the asymmetric macrocycles and copper(II) as the template metal. The phenol-containing compounds employed by Mandal and Nag are 2,6-diformyl-4-methylphenol (DFMP) and its derivatives, which have alkyl or phenyl substituents on the carbonyl carbon atoms. Several acyclic di-primaryamine Schiff-base intermediates of this system have been prepared using several di-primaryamine compounds,[61, 96] but only the one which is derived from DFMP and 1,3-diaminopropane has been reported to be an intermediate to some [2+2] asymmetric Schiff-base macrocycles.

Brooker and Croucher[62, 63, 91] adopted another variation of this synthetic approach for the preparation of asymmetric [2+2] macrocycles. In this alternative approach, the acyclic precursor to the asymmetric macrocycle was prepared by condensing two molecules of protected-diamine and one molecule of diformylphenol in the absence of a metal template. The diamine is protected by acetylating one of the NH_2 functions.[91] The acyclic precursor was subsequently isolated as the hydrochloride salt of a reduced ligand instead of as the metal complex of the Schiff-base analogue. The asymmetric macrocycles were then generated by template condensation using "head unit" components which are not diformylphenol compounds. *N*-Acetyl diethylenetriamine was one of the diamines protected by acylation. It was employed to prepare the reduced analogue of the acyclic ligand **AC1** (**Figure 3.2**).[91]

The protected diamine was prepared in this work to synthesise the Schiff-base ligand **AC1**. However, due to time constraints, the synthesis of the free Schiff-base ligand has not been attempted.

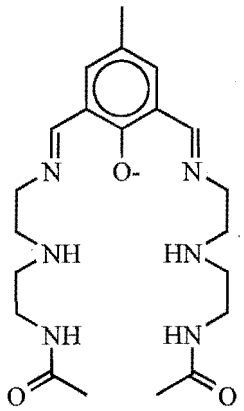

AC1

Figure 3.2

Experimental conditions

The experimental conditions employed to prepare the acyclic ligands in this work are based on the methods of Nelson et al.[43, 59, 60] and of Mandal and Nag.[61, 96] Mild conditions[43, 59] (room temperature) were necessary to obtain the open-chain ligands in the systems illustrated in **Figure 3.3**, as ring closure could be induced in some of the ligands merely on heating solutions of the acyclic complexes. The open-chain ligands result from the condensation of one molecule of the dicarbonyl compound and two molecule of the diamine compound.

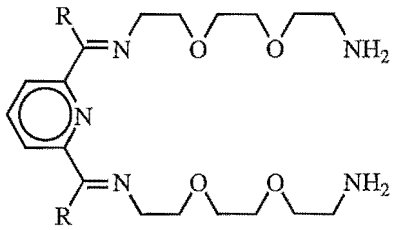

Figure 3.3

In those systems, an excess of diamine over the dicarbonyl was observed to increase the yield of the acyclic complexes and suppress the formation of the corresponding macrocyclic complexes (ring-closure), even at an elevated temperature.[59] Nelson et al. proposed a mechanism, called the *transamination* mechanism[43] to explain the ring-closure reaction in the absence of an added dicarbonyl compound (i.e. merely by heating the solutions of the acyclic complexes).

The transamination mechanism is illustrated by the system shown in **Figure 3.4**. The mechanism involves two nucleophilic attacks at an imino-carbon atom by an NH_2 group. The first is an *inter*molecular nucleophilic attack at one imino carbon of one molecule of (1) by a second molecule of (1), producing the intermediate (2). This step is followed by the loss of one molecule of diamine to give the intermediate (3). The second nucleophilic attack is *intra*molecular, involving an NH_2 group and an imino carbon atom of (3), producing the macrocyclic complex (4). The whole process is a bimolecular self-condensation reaction of the open-chain complex (1), one of the routes towards the formation of the [2+2] Schiff-base macrocycles (see **Chapter 1**).

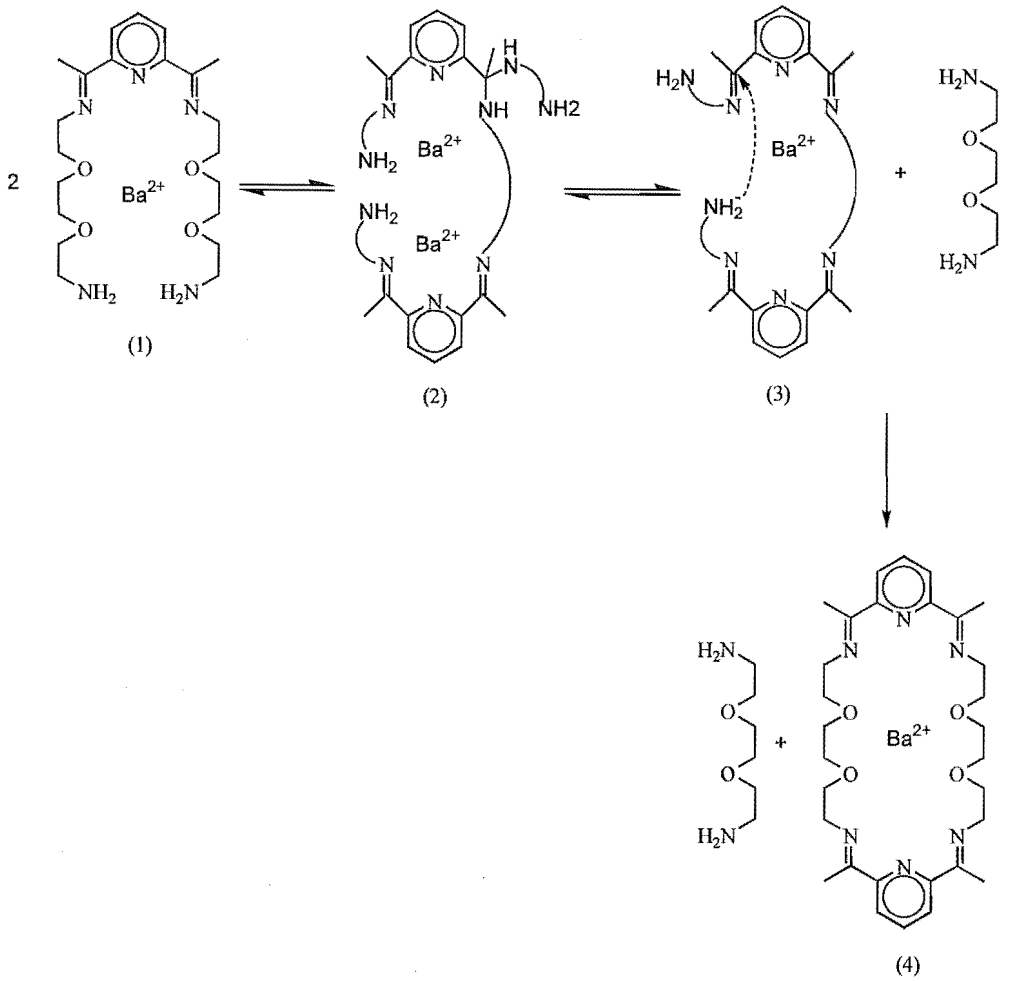

Figure 3.4

The ring closure is suppressed in the presence of a substantial concentration of an NH_2-containing compound, because the free (or not strongly-coordinated) NH_2 groups in any species other than the open-chain complex are available for nucleophilic attack at the imino carbon atoms of (1).[43] This reaction competes with the formation of the intermediate (2), thus also competing with the ring-closure reaction. Nelson et al.[43] have obtained some support for the imine-amine exchange (transamination) mechanism from some systems involving 2,6-diacetylpyridine (DAP).

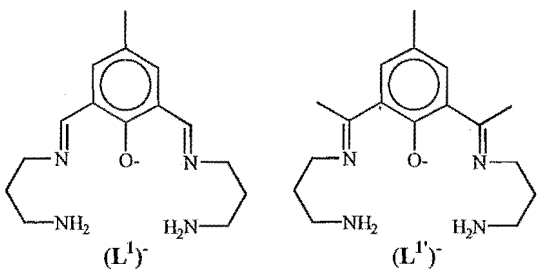

Figure 3.5

This excess of diamine strategy was also employed in the preparations of the acyclic dicopper(II) complexes of the ligands $(L^1)^-$,[61] $(L^{1'})^-$[96] (**Figure 3.5**) and other ligands derived from DFMP and a di-primaryamine compound.[61] A 3-fold excess of diamine over the phenol compound was employed, and the same stoichiometric ratio was also employed in most of the preparations in this work. Interestingly, however, the preparation of $(L^1)^-$ was carried out in dilute aqueous solution at 100 °C, in contrast to the preparations of the related [2+2] macrocyclic dicopper(II) complexes which are usually carried out in refluxing methanol. This indicates that the dicopper(II) complex of $(L^1)^-$ is very stable, despite the ligand being a Schiff-base.

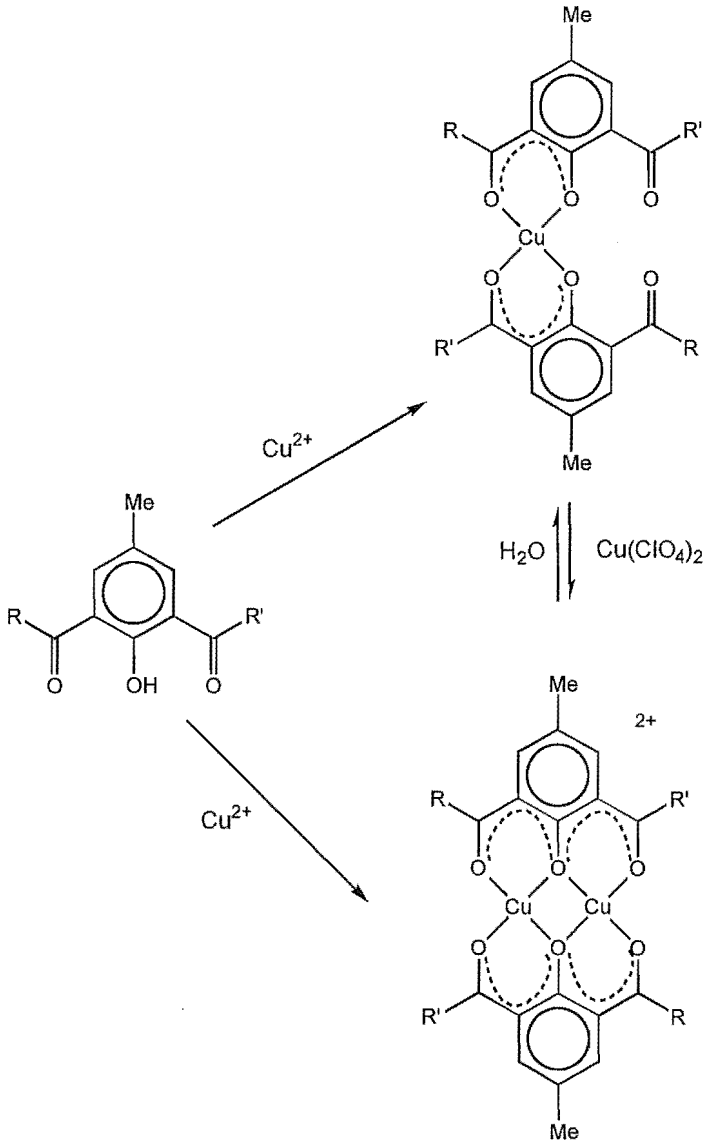

Figure 3.6. Reaction of a diformylphenol compound with a Cu(II) salt could form a mononuclear or dinuclear copper(II) complex.

The presence of water appears to be essential to the formation of the dicopper(II) hydroxo-bridged complexes, since water was also used in the preparations and recrystallisations of two dicopper(II) hydroxo-bridged complexes of the Schiff-base ligands derived from the condensation of DFMP with N,N-dimethylethylenediamine or with N,N-diethylethylenediamine.[97]

2,6-Diformyl-4-methylphenol or its derivatives could react with a copper(II) salt[98] to form a mononuclear or a dinuclear complex as illustrated in **Figure 3.6**. Such species would be expected to form a symmetrical [2+2] Schiff-base macrocycle rather easily upon condensation with a di-primaryamine compound, since the dicarbonyl compounds would have "templated" around the copper(II) ions in the appropriate arrangement for the formation of a [2+2] Schiff-base macrocycle. As the formation of a symmetrical [2+2] macrocycle was undesirable in the course of this work, the diamine compound was always mixed with the copper(II) salt prior to condensation with the diformylphenol compound. That is, mixing of the copper(II) salt with the diformylphenol compound was avoided.

Interpretation of the infrared spectra of the complexes

The formation of Schiff-base complexes is indicated by the presence of an intense band in the 1640-1655 cm^{-1} region, due to the C=N stretching vibration and a strong band at *ca.* 1550 cm^{-1}, assigned to the stretching vibration of the C-O group of the phenol moeity.[98] The phenol C-O vibration in the complexes absorbs at a higher frequency than the normal alcohol C-O frequency (1200-1000 cm^{-1})* due to the

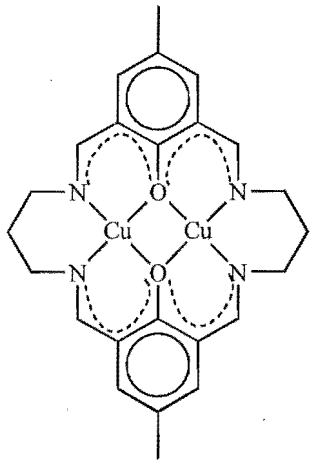

Figure 3.7.

conjugation in the chelate ring (**Figure 3.7**) which results in the phenol C-O bond attaining a partial double-bond character.

The formation of a macrocyclic complex is indicated by the absence of the C=O stretch of the diformylphenol (1688-1660 cm^{-1}) and of the NH_2 stretch (3300-3200 cm^{-1}), replaced by the C=N stretch (see above).

The formation of the acyclic diimine-diamine complexes is indicated by the presence of the imine band (see above) and a sharp doublet between 3260 and 3330 cm^{-1}, due to the symmetric and asymmetric stretching of NH_2 groups.

---

* The phenol C-O band of 2,6-diformyl-4-methylphenol appears at 1216 cm^{-1} and that of 4-*t*-butyl-2,6-diformylphenol at 1220 cm^{-1}.

3.1 Condensation of 1,3-diaminopropane and 2,6-diformyl-4-R-phenol (R = Me or ^{t}Bu)

Synthesis

The complexes obtained from the template condensation of 2,6-diformyl-4-R-phenol (R = Me or ^{t}Bu) and 1,3-diaminopropane are listed in **Table 3.1.1**; those for which the structures have been determined crystallographically are indicated. The chemical structures of the ligands are shown in **Figure 3.1.1**. Some infrared absorption bands of the complexes and the microanalytical data are given in **Tables 3.1.2** and **3.1.3** respectively.

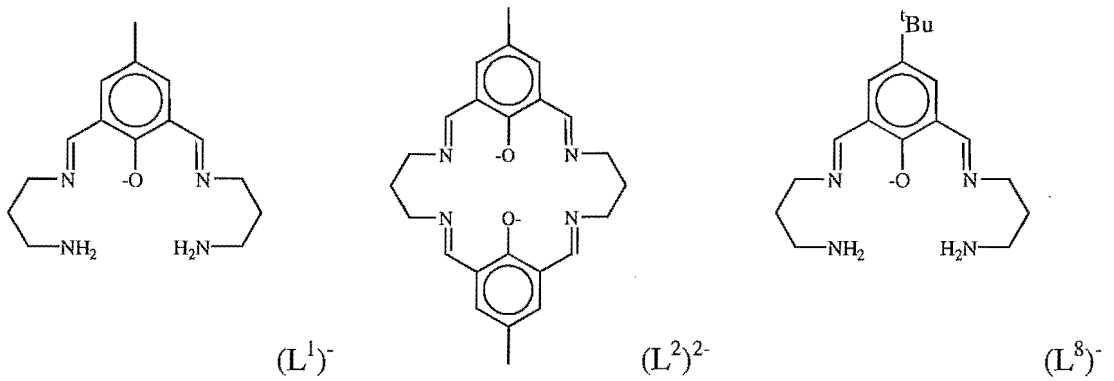

$(L^1)^-$ $(L^2)^{2-}$ $(L^8)^-$

Figure 3.1.1

Table 3.1.1. Complexes **1-7**, synthesised from the condensation of 1,3-diaminopropane with 2,6-diformyl-4-methylphenol (ligands L^1 and L^2) or 4-*t*-butyl-2,6-diformylphenol (ligand L^8).

Complex	Formula	X-ray structure
1*	$[Cu_2L^1(\mu\text{-}OH)(H_2O)](ClO_4)_2{\cdot}H_2O$	yes
2	$Cu_2L^2(ClO_4)_2(H_2O)_2$	
3	$Cu_2H_2L^2(ClO_4)_4(H_2O)$	
4	$[Cu_2L^1(\mu\text{-}OH)](BF_4)_2{\cdot}H_2O$	yes
5	$[Cu_2L^2(H_2O)_2](BF_4)_2$	yes
6	$Cu_2L^8(OH)(ClO_4)_2(H_2O)$	
7	$[Cu_2L^8(\mu\text{-}OH)](BF_4)_2{\cdot}4H_2O$	yes

* This formula is the one obtained from X-ray crystal structure analysis.

Table 3.1.2. Infrared spectral data (cm^{-1}) for the dinuclear copper(II) complexes **1-7** (s = sharp, b = broad; intensity: S = strong, M = medium, W = weak.)

Complex	hydroxo	aquo	ν(NH)	ν(C=N)	δ(NH)	ν(C–O)
1	3555 M, s	3492 M, b	3318 M, s 3265 M, s	1638 S, s	1622 M, s 1605 W, s	1564 S, s
2		3482 M, b		1640 S, s		1568 S, s
3		3472 M, b		1638 S, s		1567 M, s
4	3601 M, s	3427 M, b	3332 M, s 3285 M, s	1641 S, s	1623 M, s 1606 W, s	1565 S, s
5		3577 M, s 3508 M, s		1637 S, s		1568 S, s
6		3432 M, b	3319 M, s 3261 M, s	1639 S, s	1622 M, s 1594 W, s	1564 M, s
7	3587 M, s (nujol)	3331 S, b (KBr)	3316 M, s (nujol)	1639 S, s	1622 M, s ~1595 W, s	1558 M, s

Table 3.1.3. Microanalytical data for the dinuclear copper(II) complexes **1-7**. Calculated figures are given in parentheses.

Complex	Mass percent		
	C	H	N
1*	28.42 (28.31)	4.17 (4.12)	8.64 (8.80)
2	37.98 (37.71)	4.16 (3.96)	7.29 (7.33)
3	30.25 (30.43)	3.58 (3.19)	5.79 (5.91)
4	29.55 (29.48)	4.17 (4.29)	9.41 (9.17)
5	39.18 (39.00)	3.92 (3.82)	7.59 (7.58)
6	31.88 (31.87)	4.81 (4.75)	8.24 (8.26)
7	30.97 (30.57)	5.43 (5.42)	8.22 (7.92)

* The microanalytical data are consistent with the formula $[Cu_2L^1(\mu\text{-}OH)(H_2O)](ClO_4)_2$; the discrepancy with the formula obtained from X-ray crystal structure analysis is probably due to the loss of the lattice water during elemental analysis.

The dicopper acyclic complex **1** was initially prepared[61] by converting 2,6-diformyl-4-methylphenol (DFMP) to its sodium salt (denoted by NaDFMP from here on) in a paste form and dissolving the paste in a large quantity of boiling water to obtain an aqueous solution of DFMP in its deprotonated form. This solution was then treated with the copper(II) perchlorate and 1,3-diaminopropane mixture. The crude yield of complex **1**, obtained by this method, was only between 12 - 17% (cf. 80%[61]). The macrocyclic complexes **2** and **3** were obtained as by-products. Complex **3** was precipitated almost immediately on mixing the copper-amine solution with the NaDFMP solution.

Complex **2** was obtained when a 4.7-fold excess of 1,3-diaminopropane was used, apparently contrary to the hypothesis that excess amine suppresses the formation of the macrocyclic ligand. In this case, the formation of the macrocyclic ligand is probably promoted by a high pH of the reaction mixture, caused by the presence of an excess of 1,3-diaminopropane. This hypothesis is supported by the isolation of complex **5** as described below.

Since DFMP will be readily deprotonated and able to bind two metal ions in the presence of a metal ion,[65, 70] the preparation of complex **1** was later carried out in methanol, at room temperature with the intention of increasing the yield of the complex and avoiding the use of large volume and high reaction temperature. It was discovered that complex **1** could indeed be obtained in a higher yield (~60%) using this method. In addition, neither complex **2** nor complex **3** was obtained as a by-product. Consequently, the subsequent experiments were based on this room temperature method, employing 2,6-diformyl-4-methylphenol or 4-*t*-butyl-2,6-diformylphenol as their methanol solution. Complex **4** was obtained in a good yield (~60 %) by using this method, substituting copper(II) tetrafluoroborate for copper(II) perchlorate.

The macrocyclic complex **5** was obtained at room temperature from when the template condensation of 1,3-diaminopropane and DFMP was carried out either by using a 9:1 molar ratio of diamine to phenol, or by using a 3:1 ratio in the presence of an added base (triethylamine).

Infrared spectra

The sharp peak at 3555 cm^{-1} in the infrared spectrum of complex **1** is assigned to the stretching vibration of a non hydrogen-bonded hydroxo group,[61, 97] while the sharp bands at 3318 and 3265 cm^{-1} are assigned to the asymmetric and symmetric stretching vibrations of the primary-amine functions. Two sharp bands of weak to medium intensity at *ca.* 1622 - 1595 cm^{-1} in the spectra of **1** are absent in the spectra of the $(L^2)^{2-}$ complexes or any macrocyclic complexes prepared in this work. This observation and similar observations involving other related complexes,[43, 59-61] led to the assignment of these vibrations to the bending vibrations of the NH_2 groups.

The presence of perchlorate counterions was indicated by the strong and broad absorption at *ca.* 1100 cm^{-1} combined with the sharp band of medium intensity at *ca.* 622 cm^{-1}.[99]

The infrared and microanalytical data for complex **2** suggest that it is a dicopper(II) complex of the macrocycle $(L^2)^{2-}$. On the other hand, the infrared data for complex **3** do not give a more detailed information other than: i) complex **3** contains at least one Schiff-base linkage; ii) perchlorate ion is present as a counterion in the complex. The perchlorate may be coordinated to copper because the perchlorate band at ~1098 cm^{-1} shows some splitting.[99] The best agreement between the calculated and experimental data is obtained for the formulation shown in **Table 3.1.1**. X-ray crystallography is one technique that could be employed to establish the structure of the ligand in this complex; however, single-crystals of complex **3** have not been obtained.

The infrared spectra of complexes **4**, **6** and **7** are very similar to that of complex **1**. Except that in the spectra of complexes **6** and **7** the C-H vibrations are more intense than those in the spectra of **1** or **4**, due to the presence of a t-butyl group in complexes **6** and **7**. The similarity among the infrared spectra of the acyclic complexes, especially in the 1600 - 1595 cm^{-1} region, and the X-ray structures of **1**, **4** and **7**, lend further support to the assignment of the two sharp bands between 1600 - 1595 cm^{-1} to the bending vibrations of the NH_2 groups.

The infrared spectrum of complex **5** (see **Appendix B**) is quite distinct from those of complex **1** or **4**. The absence of two sharp bands around 3300 cm^{-1} indicates that it is a macrocyclic Schiff-base complex, and not an acyclic diimine-diamine complex. However, the presence of two sharp bands of medium intensities at 3577 and 3508 cm^{-1} in the infrared spectrum of complex **5** was intriguing. Sharp infrared bands in this region usually indicate the presence of non-hydrogen-bonded OH group. However, the X-ray crystallographic analysis of this complex (see later) revealed that this is not the case.

Structures of the acyclic complexes (1, 4, 7)

Structure of $[Cu_2L^1(\mu\text{-}OH)](ClO_4)_2 \cdot 2H_2O$ (1)

The structure of complex **1** confirms the formation of the acyclic diimine-diamine ligand $(L^1)^-$ and is illustrated in **Figure 3.1.2** together with the atom numbering scheme. Selected interatomic distances and bond angles are given in **Table 3.1.4**. The asymmetric unit comprises a dicopper(II) complex cation, two perchlorate counterions and two water molecules. In the cation, the copper(II) ions are separated by 3.022(1) Å and bridged by the deprotonated phenol group (O1) of the acyclic ligand $(L^1)^-$ and by a hydroxo ion (O2). The cation has a non-crystallographic mirror plane passing through the deprotonated phenol and hydroxo groups (O1 and O2).

The equatorial ligands for each copper(II) ion in **1** comprise one imine and one amine of the same 'arm' of the ligand, as well as the bridging oxygen atoms of the phenoxo and alkoxo groups. One of the perchlorate ions (that involving Cl(1)) weakly coordinates to both copper ions at the axial sites, although the interaction between O13 and Cu1 is much weaker than that between O14 and Cu2. One of the oxygen atoms of the second perchlorate (O23) occupies the second axial site of Cu1, while one of the water molecules (O3) is coordinated to the copper atom Cu2.

The equatorially coordinated donor atoms of each copper show some tetrahedral distortion from their least-squares plane, especially those around Cu2 [mean deviation = 0.123(2) Å] compared to those around Cu1 [mean deviation = 0.039(3) Å]. The two copper(II) ions are displaced from their N_2O_2 coordination plane to a different extent. Cu1 is displaced by 0.072(3) Å towards O23 and Cu2 is displaced by 0.175(2) Å towards the coordinated water ligand (O3). The difference is related to the strength of axial interaction of the copper ions with the axial ligands; the stronger the interaction with the axial ligand, the further that copper ion is displaced towards the ligand from its equatorial coordination plane.

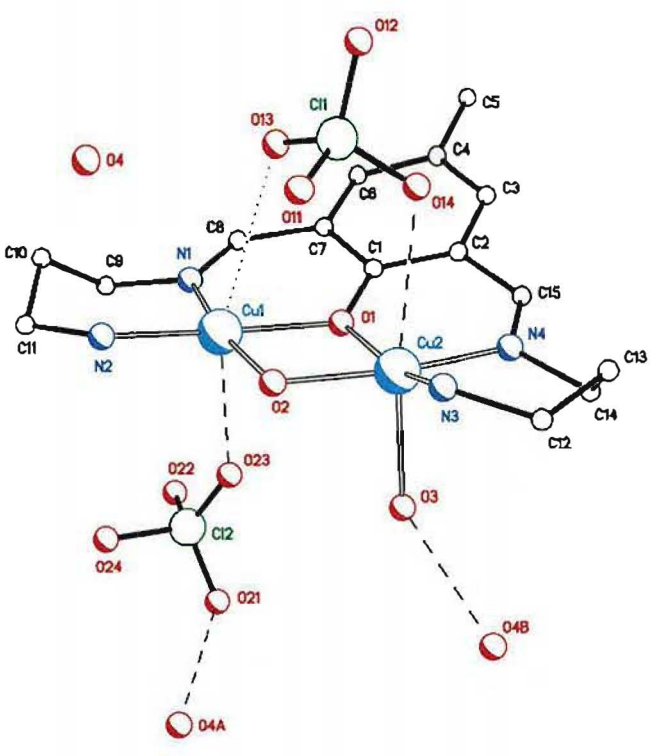

Figure 3.1.2. Perspective view of the complex $[Cu_2L^1(\mu\text{-}OH)H_2O](ClO_4)_2{\cdot}H_2O$ (**1**). The letters A and B indicate atoms from different molecules; the transformations are given in **Table 3.1.4**.

The cation is approximately planar with the saturated carbon atoms of the two side 'arms' (amino-imino fragments) showing the largest deviations from planarity. The aromatic ring of the cation is inclined by 26.6° towards the N_4O_2 copper coordination plane. The two N_2O_2 copper coordination planes are not coplanar: the least-squares planes of the two sets of donor atoms are inclined by 12.6(3)°, hinging at the phenoxo and hydroxo oxygen atoms. The 6-membered chelate rings involving the side 'arms' have approximate boat conformations; the copper and the central carbon atom of each chelate rings are displaced above and below the least-squares plane passing through the N-C···C-N fragment. The hydroxo-bridge (O2) is displaced "below" the Cu1-O1-Cu2 plane by only 0.07 Å (the coordinated water O3 is also "below" this plane). The two primary-amine nitrogen atoms of the ligand are separated by 5.60 Å.

Table 3.1.4. Interatomic distances (Å) and bond angles (°) relevant to copper coordination in complex **1**, $[Cu_2L^1(\mu\text{-}OH)(H_2O)](ClO_4)_2 \cdot H_2O$.

Cu1···Cu2	3.022(1)	Cu2-O1	1.994(4)
Cu1-O1	1.976(4)	Cu2-O2	1.939(4)
Cu1-O2	1.921(4)	Cu2-N3	2.032(5)
Cu1-N1	1.951(5)	Cu2-N4	1.946(5)
Cu1-N2	1.995(5)	Cu2-O3	2.304(5)
Cu1···O23	2.513(8)	Cu2···O14	2.808(5)
Cu1···O13	3.130(6)	O21···O4A	2.904(8)
N2···N3	5.600(6)	O3···O4B	2.824(8)
Cu1-O1-Cu2	99.1(2)	Cu1-O2-Cu2	103.0(2)
N1-Cu1-O1	91.1(2)	O2-Cu2-N3	93.6(2)
N1-Cu1-N2	97.7(2)	N4-Cu2-O1	91.0(2)
O2-Cu1-N2	91.6(2)	N4-Cu2-N3	96.0(2)
O2-Cu1-O1	79.3(2)	O1-Cu2-O2	78.5(2)
N1-Cu1-O23	94.9(3)	O2-Cu2-O3	92.3(2)
N2-Cu1-O23	100.2(3)	O1-Cu2-O3	93.6(2)
O1-Cu1-O23	85.6(3)	N4-Cu2-O3	89.7(2)
O2-Cu1-O23	85.9(3)	N3-Cu2-O3	103.6(2)

Transformation: A = 1+x, y, z; B = 1+x, y, z

The coordinated and the lattice water molecules (O3 and O4 respectively) are involved in intermolecular hydrogen bonding. O3 is hydrogen-bonded to a lattice water in a different asymmetric unit [O4B under transformation: 1+x, y, z, O3···O4B = 2.824(8) Å]. On the other hand, a lattice water molecule [O4 under transformation: -x, 1-y, -z, O4A] is hydrogen bonded to the perchlorate oxygen O21 [O21···O4A = 2.904(8) Å]. These intermolecular hydrogen bonds, along with the interactions of the water and perchlorate groups with the copper(II) ions, form two "cation-water-water-anion-cation" links which pair every two molecules in the crystal (**Figure 3.1.3**).

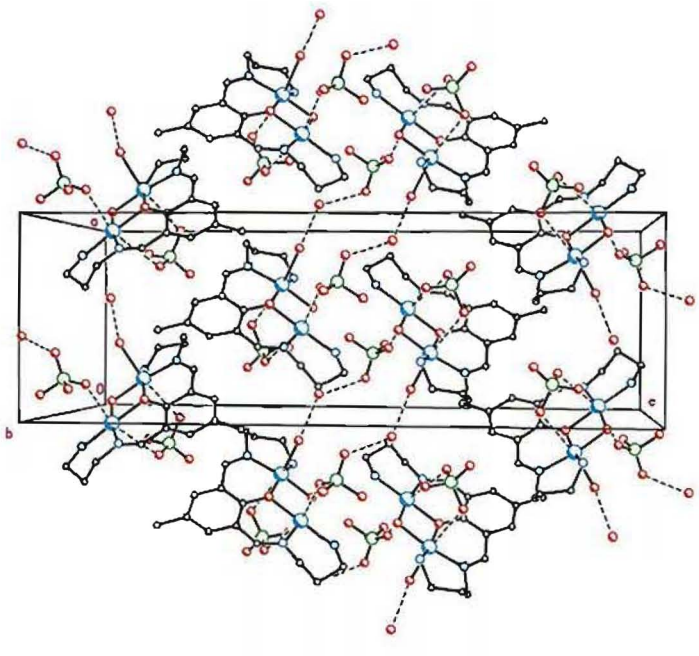

Figure 3.1.3. Molecular packing in complex **1**.

Structure of $[Cu_2L^1(\mu\text{-}OH)](BF_4)_2 \cdot H_2O$ (4)

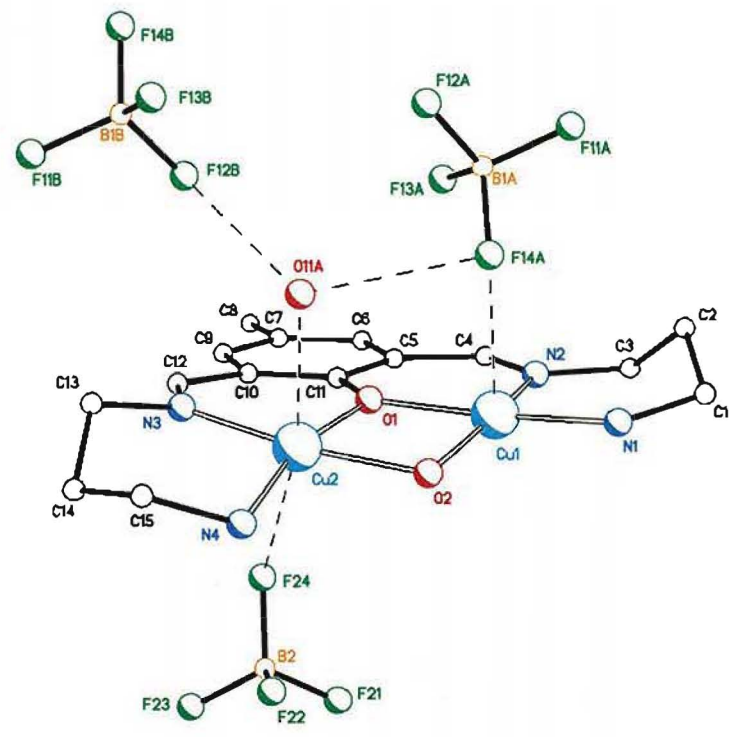

Figure 3.1.4. Perspective view of the complex $[Cu_2L^1(\mu\text{-}OH)](BF_4)_2 \cdot H_2O$ (**4**).

Table 3.1.5. Interatomic distances (Å) and bond angles (°) relevant to copper coordination in complex **4**, $[Cu_2L^1(\mu\text{-}OH)](BF_4)_2 \cdot H_2O$.

Cu1···Cu2	3.060(1)	Cu2-O2	1.929(3)
Cu1-O2	1.909(3)	Cu2-O1	1.989(3)
Cu1-O1	1.963(3)	Cu2-N3	1.958(4)
Cu1-N1	1.978(4)	Cu2-N4	1.989(4)
Cu1-N2	1.955(4)	Cu2···F24	2.733(4)
Cu1···F14A	2.650(3)	Cu2···O11A	2.471(4)
Cu1-O1-Cu2	105.5(2)	Cu1-O2-Cu2	105.8(2)
O2-Cu1-O1	76.6(1)	O2-Cu2-O1	75.5(1)
O2-Cu1-N1	93.9(2)	O2-Cu2-N4	94.4(2)
N2-Cu1-O1	92.4(2)	N3-Cu2-O1	92.5(2)
N2-Cu1-N1	98.4(2)	N3-Cu2-N4	97.7(2)

Transformations: A = -x, -y, -z; B = 1+x, y, z

The structure of complex **4**, $[Cu_2L^1(\mu\text{-}OH)](BF_4)_2 \cdot H_2O$, illustrated in **Figure 3.1.4**, confirms that the ligand $(L^1)^-$ can also be formed when tetrafluroborate is substituted for perchlorate. Selected interatomic distances and bond angles are given in **Table 3.1.5**. A dicopper(II) cation, two tetrafluroborate counterions and a water molecules are present in the asymmetric unit. In the dication, the copper(II) ions are separated by 3.060(1) Å and bridged by the deprotonated phenol group (O1) of the acyclic ligand $(L^1)^-$ and by a hydroxo ion (O2). In contrast to the cation of complex **1**, the dication in complex **4** has an approximate C_2 axis (**Figure 3.1.4**) passing through the phenoxo and hydroxo groups.

Each copper(II) ion in complex **4** is coordinated equatorially to one imine and one amine of the same 'arm' of the ligand, as well as to the oxygen bridging ligands. A fluorine atom (F24) of one of the tetrafluroborate ions forms a weak axial bond with one of the copper ions (Cu2). The second axial site of Cu2 is occupied by the lattice water from a different molecule (O11A; transformation: -x, -y, -z). Cu1 has only one axial interaction: that with a fluorine atom (F14A) of the second tetrafluroborate ion from a different molecule (transformation: -x, -y, -z). The coordination environment of Cu1 can be described as pseudo-square-pyramidal, while that of Cu2 as pseudo-tetragonal.

The N_2O_2 donor atoms of each copper show some tetrahedral distortion from their least-squares plane, especially those around Cu1 [mean deviation = 0.140(2) Å] compared to those around Cu2 [mean deviation = 0.076(2) Å]. Cu1 lies on the least-squares plane of its equatorial ligands; while Cu2 is displaced by 0.070(2) Å towards the coordinated water (O11A), which interacts more strongly with Cu2 than the axial fluorine (F24).

The cation in **4** is also approximately planar, except for the saturated carbon atoms of the two side 'arms' (amino-imino fragments) which shows the largest deviation from planarity above and below the least-squares plane of the complex. The inclination of the aromatic ring of the cation towards the N_4O_2 copper coordination plane is 10.8°. The two N_2O_2 copper coordination planes are not coplanar, instead their least-squares planes are inclined by 12.4(2)°, forming a hinge at the bridging oxygen donors. The hydroxo group deviates from the plane defined by the two copper atoms and the

phenoxo oxygen (O1) by *ca.* 0.2 Å towards the tetrafluoroborate ion involving B2. The two primary amine groups of the ligand in complex **4** are separated by 5.67 Å.

The 6-membered chelate rings involving the side 'arms' have approximate chair conformations with the ring involving Cu2 being closer to the chair conformation than that involving Cu1 [Cu1 is *ca.* 0.02 Å, Cu2 is *ca.* 0.50 Å out of the respective mean plane of the N-C···C-N fragment]. These two chelate rings are 'twisted' with respect to each other; the least-squares planes passing through the N-C···C-N fragments make a dihedral angle of *ca.* 30°.

The lattice water molecule is involved in intermolecular hydrogen-bonding with a fluorine atom of one tetrafluoroborate ion (that involving B1), as well as in coordination to one of the copper(II) ions (**Figure 3.1.4**) [O11A···F12B = 2.93 Å; O11A···F14A = 2.83 Å]. These result in the formation of intermolecular linkages similar to those observed in complex **1** (**Figure 3.1.5**). The linkage in **4** is shorter, however, being of the type "cation-water-anion-cation". Nevertheless two of such linkages join two molecules of complex **4** in the crystal, as observed in complex **1**.

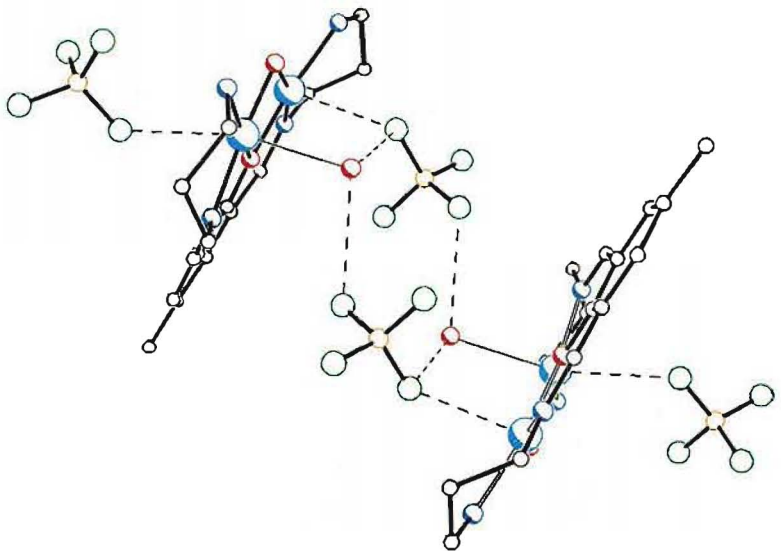

Figure 3.1.5. The intermolecular links in the complex $[Cu_2L^1(\mu\text{-}OH)](BF_4)_2\cdot H_2O$ (**4**).

Structure of $[Cu_2L^8(\mu\text{-}OH)](BF_4)_2 \cdot 4H_2O$ (7)

The structure of complex **7** confirms the formation of the acyclic diimine-diamine ligand $(L^8)^-$, derived from TDFP and 1,3-diaminopropane, and is illustrated in **Figure 3.1.6** with the atom numbering scheme. Selected interatomic distances and bond angles are given in **Table 3.1.6**. The asymmetric unit comprises a dicopper(II) cation, two perchlorate counterions and two water molecules. In the dication, the copper(II) ions are separated by 3.029(2) Å and bridged by the deprotonated phenol group (O1) of the acyclic ligand $(L^1)^-$ and by a hydroxo ion (O2). The dication has an approximate mirror plane passing through the deprotonated phenol and hydroxo groups (O1 and O2).

Each copper(II) ion in **7** is coordinated equatorially to one imine and one amine of the ligand of the same linkage, and to the bridging oxygen atoms of the phenoxo and alkoxo groups. One of the tetrafluoroborate ions (the one involving B2) weakly coordinates to the axial site of Cu1. The second axial site of Cu1 is occupied by one of the water molecules [Cu1···O22 = 2.686(4) Å]. A water molecule (O11) is axially coordinating to the copper ion Cu2, while another water molecule occupies the second axial position of Cu2 more remotely. The equatorially coordinated donor atoms about each copper show some tetrahedral distortion from their least-squares plane. Cu2 is displaced by 0.18(2) Å from its N_2O_2 coordination plane while Cu1 is not displaced significantly.

The cation is approximately planar with the central carbon atoms of the two side 'arms' (amino-imino saturated fragments) showing the largest deviations from planarity. The aromatic ring of the cation is inclined by 14° towards the N_4O_2 copper coordination plane. The two N_2O_2 planes are inclined by *ca.* 2°, hinging at the phenoxo and hydroxo oxygen atoms. The 6-membered chelate rings involving the side 'arms' have twisted chair conformations; the copper and the central carbon atom of each chelate rings are displaced above and below the least-squares plane passing

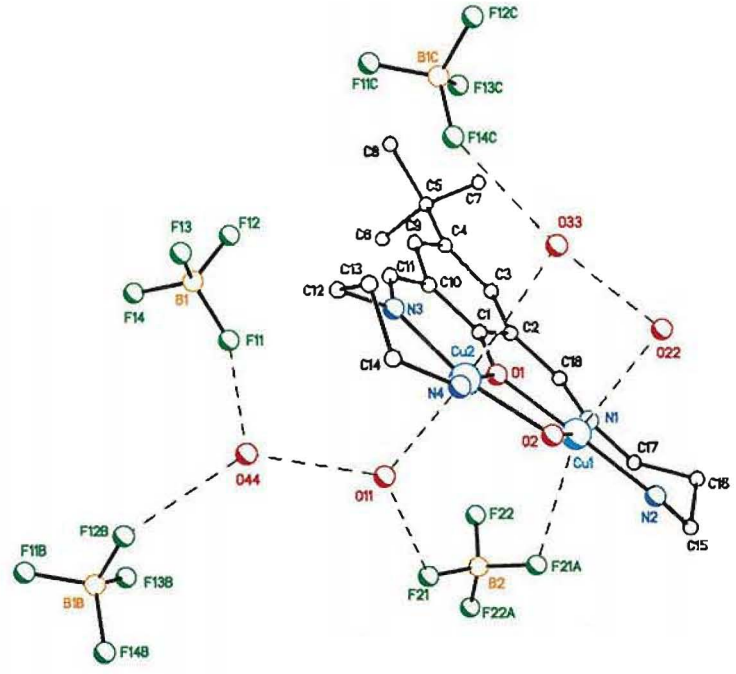

Figure 3.1.6. A perspective view of $[Cu_2L^8(\mu\text{-}OH)](BF_4)_2{\cdot}4H_2O$ (**7**).

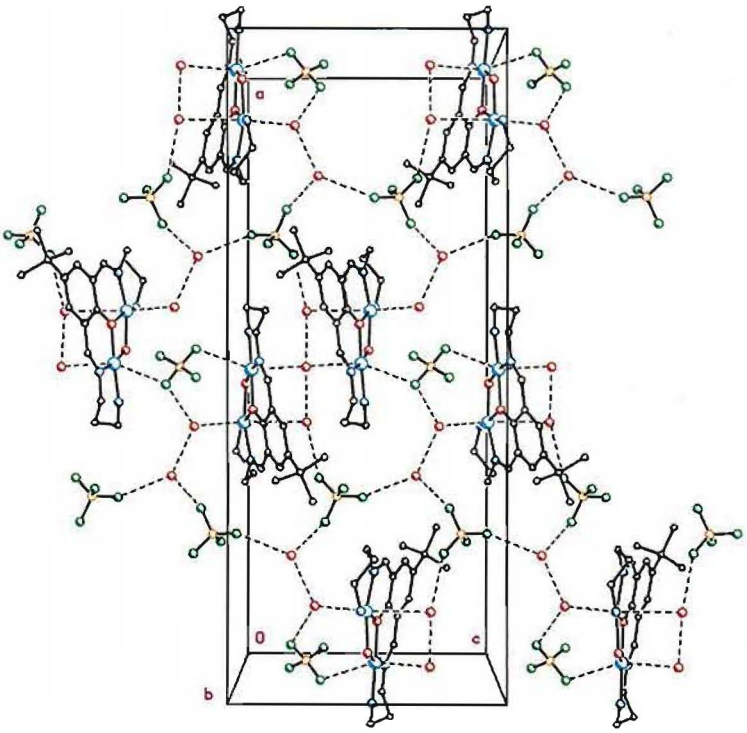

Figure 3.1.7. Hydrogen bonds in $[Cu_2L^8(\mu\text{-}OH)](BF_4)_2{\cdot}4H_2O$.

Table 3.1.6. Interatomic distances and bond angles relevant to copper coordination in $[Cu_2L^8(\mu\text{-}OH)](BF_4)_2 \cdot 4H_2O$.

Cu1···Cu2	3.029(2)		
Cu1-O1	1.958(7)	Cu2-O1	1.978(8)
Cu1-O2	1.94(3)	Cu2-O2	1.96(3)
Cu1-N1	1.941(9)	Cu2-N3	1.950(9)
Cu1-N2	1.998(9)	Cu2-N4	1.99(1)
Cu1···F21A	2.34(2)	Cu2···O11	2.45(1)
Cu1···O22	2.686(4)	Cu2···O33	3.061(2)
Cu1-O1-Cu2	100.6(3)	Cu1-O2-Cu2	102(1)
N1-Cu1-O1	92.0(4)	N3-Cu2-O1	92.9(4)
O1-Cu1-O2	79.1(8)	O1-Cu2-O2	78.2(8)
N1-Cu1-N2	100.4(4)	N3-Cu2-N4	99.1(4)
O2-Cu1-N2	88.4(8)	O2-Cu2-N4	88(1)

Transformation: A = 1-x, y, 0.5+z

through the N-C···C-N fragment. The two nitrogen atoms of the primary amine groups of $(L^8)^-$ are separated by 5.45 Å in this complex.

Hydrogen bonds in complex **7** are more extensive than those in complexes **1** or **4**, due to the presence of four water molecules in the crystal (see **Figure 3.1.6**; distances are presented in **Table 3.1.7**). These interactions are important in the crystal packing, as shown in **Figures 3.1.7** and **3.1.8**. The molecules are linked into individual layers, each extending in the direction of the a axis, by hydrogen bonds and coordination interactions. These layers are packed parallel to each other along the c axis. No hydrogen bonds are present between any two layers.

Table 3.1.7. Hydrogen bonding distances (Å) in $[Cu_2L^8(\mu\text{-}OH)](BF_4)_2 \cdot 4H_2O$ (**7**)

O11···F21	3.03	O33···F14C	2.88
O11···O44	2.69	O44···F11	2.76
O22···O33	2.99	O44···F12B	2.80

Transformation: B = 0.5-x, 0.5-y, -0.5+z; C = 0.5-x, 0.5-y, 0.5+z

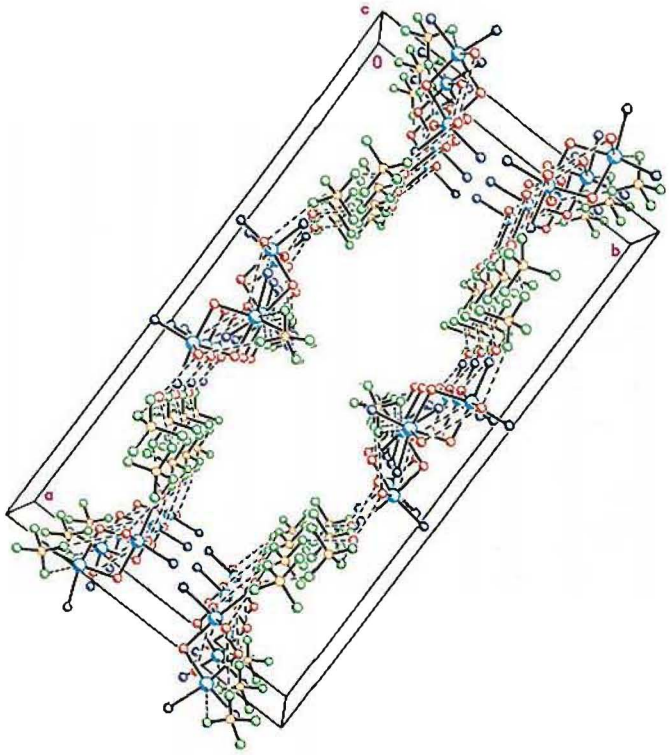

Figure 3.1.8. Molecular packing diagram of $[Cu_2L^8(\mu\text{-}OH)](BF_4)_2{\cdot}4H_2O$ showing the packing of the complex into layers. The carbon atoms are omitted for clarity.

Table 3.1.8. Copper-copper distances in the complexes **1**, **4**, and **7**.

Complex	Formula	Cu···Cu (Å)
1	$[Cu_2L^1(\mu\text{-}OH)(H_2O)](ClO_4)_2{\cdot}H_2O$	3.022(1)
4	$[Cu_2L^1(\mu\text{-}OH)](BF_4)_2{\cdot}H_2O$	3.060(1)
7	$[Cu_2L^8(\mu\text{-}OH)](BF_4)_2{\cdot}4H_2O$	3.029(2)
Ref 96	$[Cu_2(L^{1'})(\mu\text{-}OH)(ClO_4)_2]{\cdot}H_2O$	2.957(2)

The copper-copper distances in complexes **1**, **4** and **7** correlate with the interactions between the dicopper moiety and the counterions in the complex. The Cu···Cu distances in **1**, **4** and **7** are presented in **Table 3.1.8**. The Cu···Cu separation in complex **1** is shorter than that in the complex **4** even though the ligand is the same (ie. $(L^1)^-$). In complex **1**, one of the perchlorate counterions is bidentate, bridging the two copper ions axially. On the other hand, the BF_4^- ions in complex **4**, although interacting axially with the copper ions, are only monodentate. Support for this hypothesis is given

by the crystal structure[96] of a dicopper(II) complex of $(L^{1'})^-$ (**Figure 3.1.9**). In this complex, two perchlorate ions are bridging the two copper(II) ions axially and the two copper ions in this complex is 2.957(2) Å, even shorter than the Cu···Cu separation in complex **1**.

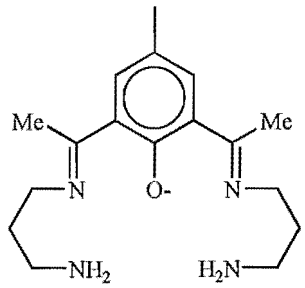

$(L^{1'})^-$

Figure 3.1.9.

The structures of complexes **1**,**4** and **7** all show that the primary amine groups of the acyclic ligands $(L^1)^-$ and $(L^8)^-$ are in the necessary spatial relationship for ring-closure condensation with another molecule of dicarbonyl (at NH_2 ···NH_2 separation between 5.45 - 5.67 Å). This is supported by the ring-closure condensations of complex **1** with some derivatives of DFMP,[61] and by the isolation and structural characterisation of complex **9** (discussed in section **3.2**), a dicopper(II) complex of an asymmetric tetraimine macrocycle derived from the ring-closure condensation of complexes **1** and **4** with 2,5-diformylfuran.

Structure of the macrocyclic complex $[Cu_2L^2(H_2O)_2](BF_4)_2$ (5)

This tetrafluoroborate complex of the macrocycle $(L^2)^{2-}$ has not been structurally characterised previously and the structure is presented here. The crystal structure of **5** consists of two crystallographically independent dicopper complexes (**Figure 3.1.10**: molecules **I** and **II**), each possessing a centre of symmetry between the copper ions. Two water molecules and two tetrafluoroborate counterions are associated with each dicopper macrocyclic cation. The macrocycle, derived from DFMP and 1,3-diaminopropane, has both its phenol groups deprotonated. Selected interatomic distances and angles are given in **Table 3.1.9**.

Each copper ion in molecule **I** is coordinated equatorially to four macrocyclic donor atoms (two symmetry-related phenoxo oxygens and two imine nitrogens from one side-chain) and axially, at a longer distance, to a water molecule (O11). A tetrafluoroborate fluorine (F14) occupies the second axial position of the copper coordination sphere at even a longer distance than the water molecule. So the copper coordination environment may be described as an approximate octahedron.

The two copper atoms are 3.124(1) Å apart and bridged by the phenoxo oxygen atoms of macrocycle with Cu-O-Cu angles of 103.37(9)°. The N_2O_2 donor atoms of each copper show only a slight tetrahedral distortion from planarity [mean deviation 0.02 Å] and Cu1 deviates from the N_2O_2 mean plane by 0.085(1) Å towards the coordinated water molecule. The two N_2O_2 donor sets themselves are coplanar with the phenoxo oxygen atoms deviating above and below this plane by *ca.* 0.04 Å.

The least-squares planes of the two aromatic rings are parallel, *ca.* 0.4 Å apart, and inclined by 11.4° "above" and "below" the plane of the imine nitrogen atoms of the macrocycle. The 6-membered chelate rings involving the saturated side-chains have approximate chair conformations. The central carbon atom of the saturated chain is displaced from the N-C···C-N fragment "above" the plane of the macrocyclic ring (the coordinated water molecule is "below" the ring) and the copper atom is displaced in the opposite direction.

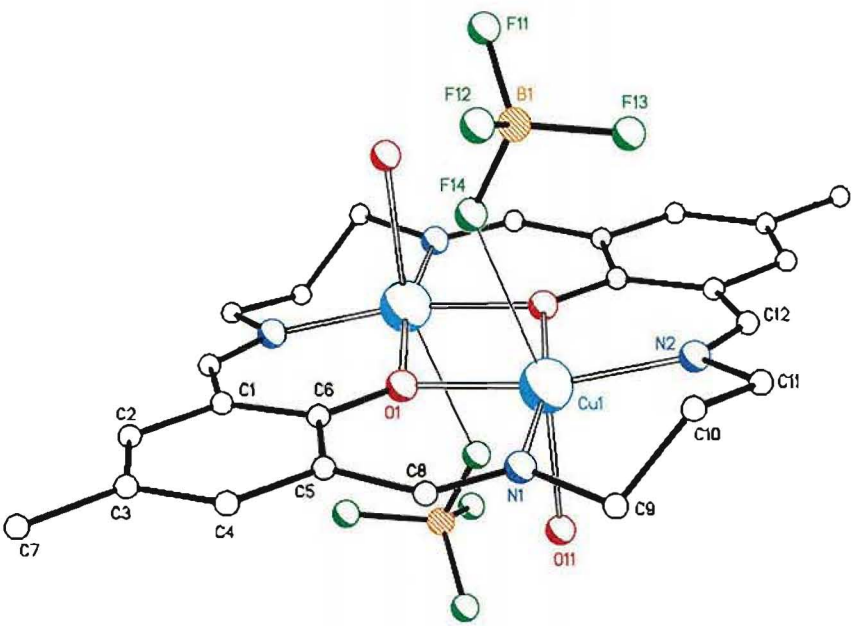

(a) Molecule **I**

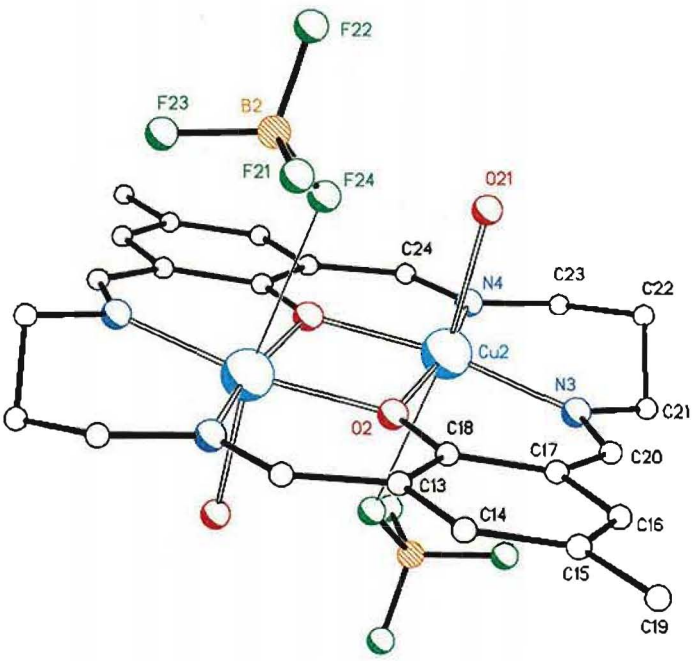

(b) Molecule **II**

Figure 3.1.10. Perspective view of the two crystallographically independent molecules of $[Cu_2L^2(H_2O)_2](BF_4)_2$ (**5**).

Table 3.1.9. Interatomic distances and bond angles relevant to copper coordination in $[Cu_2L^2(H_2O)_2](BF_4)_2$.

Cu1···Cu1A	3.124(1)	Cu2···Cu2A	3.130(1)
Cu1-N1	1.965(2)	Cu2-N3	1.978(3)
Cu1-N2	1.988(2)	Cu2-N4	1.978(3)
Cu1-O1	1.995(2)	Cu2-O2	1.999(2)
Cu1-O1A	1.987(2)	Cu2-O2A	1.987(2)
Cu1-O11	2.330(2)	Cu2-O21	2.395(2)
Cu1···F14	2.700(2)	Cu2···F24A	2.959(2)
Cu1-O1-Cu1A	103.37(9)	Cu2-O2-Cu2A	103.48(9)
N1-Cu1-N2	97.35(1)	N4-Cu2-N3	96.89(1)
N1-Cu1-O1	92.99(9)	N3-Cu2-O2	92.86(10)
O(1A)-Cu1-N2	92.63(9)	N4-Cu2-O21	98.44(10)
O(1A)-Cu1-O1	76.62(9)	O2A-Cu2-O21	90.43(8)
N1-Cu1-O11	91.13(9)	N4-Cu2-O2A	93.22(10)
N2-Cu1-O11	99.20(9)	O2A-Cu2-O2	76.50(9)
O1-Cu1-O11	87.06(8)	N3-Cu2-O21	93.62(9)
O(1A)-Cu1-O11	91.41(8)	O2-Cu2-O21	87.31(8)

Transformation: A = 1-x, 1-y, -z

The copper ions in molecule **II** is each coordinated equatorially to the two symmetry-related phenoxo oxygens and two imine nitrogens from one side-chain of the macrocycle, and axially to a water molecule (O21). A tetrafluoroborate fluorine from a different unit cell (F24A under transformation 1-x, 1-y, -z) occupies the second axial position of the copper coordination sphere at a longer distance than the water molecule. Again, the coordination geometry of the copper atoms in **II** may be regarded as approximately octahedral. The copper ions are separated by 3.130(1) Å, and bridged by the phenoxo oxygen atoms of macrocycle with Cu-O-Cu angles of 103.48(9)°.

The N_2O_2 donor atoms of each copper are less tetrahedrally distorted than those in **I** [mean deviation = 0.008 Å]. The copper ion deviates from the N_2O_2 mean plane by 0.095(1) Å towards the coordinated water molecule. The two N_2O_2 sets are coplanar with the phenoxo oxygen atoms deviating above and below the this plane by *ca.* 0.01 Å. In this molecule, the carbon atoms of the aromatic ring are not coplanar [mean deviation

= 0.008 Å] and the phenoxo oxygen (O2) deviates from this mean plane by 0.02 Å, further than the same oxygen in molecule **I**.

The macrocyclic cation again has a "stepped" conformation; the least-squares planes of the two aromatic rings are parallel (*ca.* 0.5 Å apart) and are inclined by 11.2° "above" and "below" the plane of the imine nitrogen atoms of the macrocycle. The 6-membered chelate rings involving the saturated side-chains also have approximate chair conformations. In contrast to molecule **I**, the central carbon atom of the saturated chain (C22) is positioned on the same side of the macrocyclic plane as the coordinated water molecule.

The two molecules are almost parallel to each other: the least-squares planes through the imine nitrogens of molecules **I** and **II** are inclined by 16.49(7)° (**Figure 3.1.11**) and separated by *ca.* 3.5 Å, while the N_4O_2 coordination planes are inclined by 16.3°. Molecules **I** and **II** are laterally very offset and rotated by almost 90° with respect to each other (**Figure 3.1.12**) so that the only overlap occurs between one of the 4-methylphenyl moieties of each molecule. These π regions are almost parallel to each other (dihedral angle of *ca.* 2.9°) and separated by approximately 3.5 Å, indicating some attractive π-π interactions.[100]

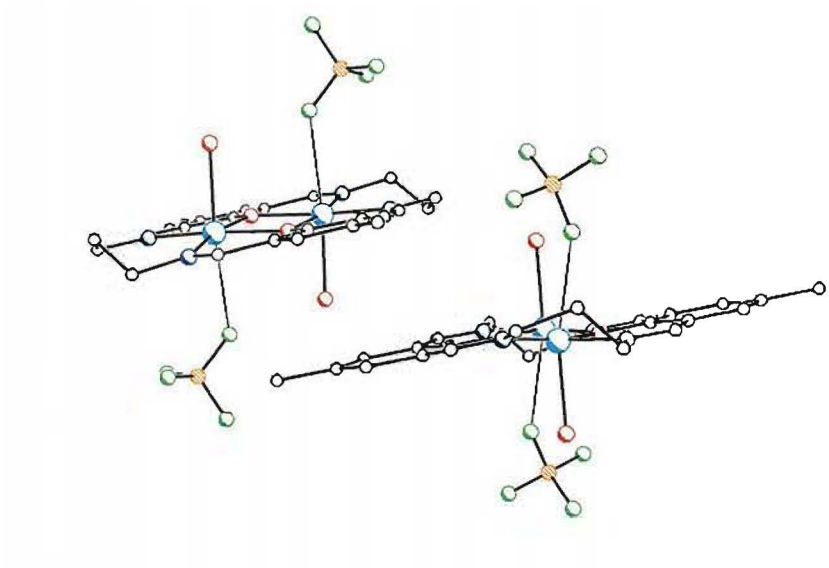

Figure 3.1.11. The two crystallographically independent molecules of $[Cu_2L^2(H_2O)_2](BF_4)_2$ viewed along the mean plane of the nitrogen atoms of molecule **I** (the bottom one)

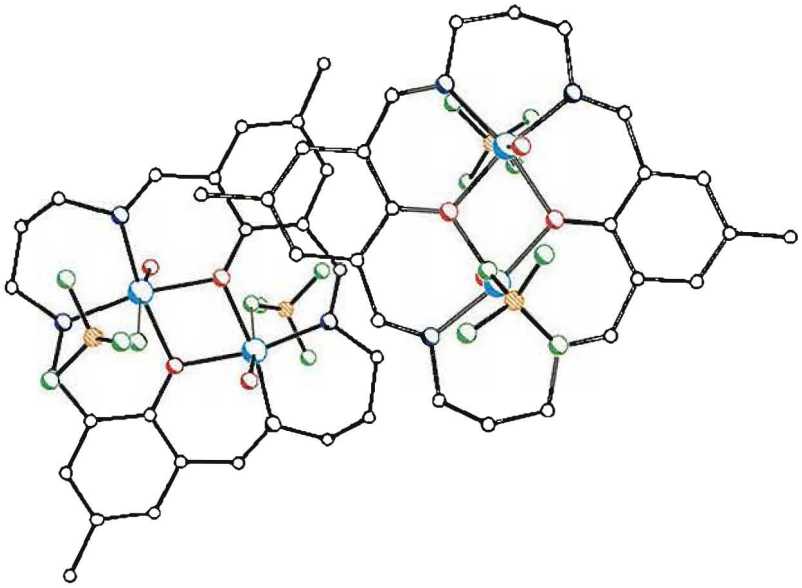

Figure 3.1.12. The two crystallographically independent molecules of $[Cu_2L^2(H_2O)_2](BF_4)_2$ viewed perpendicular to the mean plane of the nitrogen atoms of molecule **I** (the one on the right).

Two sets of intermolecular hydrogen bonding networks (**Figures 3.1.13** and **3.1.14**) are present, involving the two crystallographically distinct water molecules (O11 and O21) and tetrafluroborate ions (those involving B1 and B2). The hydrogen bond distances are given in **Table 3.1.10**. In either molecule **I** or molecule **II**, the coordinated water molecule (O11 or O21, respectively) is hydrogen-bonded to two fluorine atoms from two different molecules. These hydrogen bonding networks result in the formation of molecular layers in the crystal. The layers involving molecule **I** pack alternately with those involving molecule **II**; these are shown separately in **Figures 3.1.15** and **3.1.16** for clarity. The independent layers are held together by the π-π interactions mentioned earlier.

Table 3.1.10. Hydrogen bond distances (Å) in complex **5**.

O11···F13A	2.800(3)	O21···F24	2.830(3)
O11···F14B	2.788(3)	O21···F23C	2.787(3)

Transformations: A = x, 1.5-y, -0.5+z; B = -x, 1-y, -; C = 1-x, 0.5+y, 0.5-z.

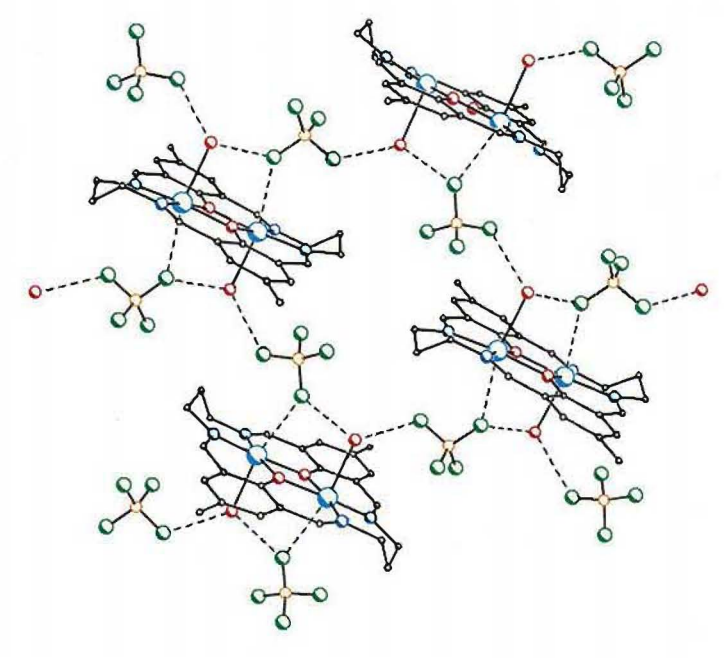

Figure 3.1.13. Hydrogen bonds involving molecule **I**.

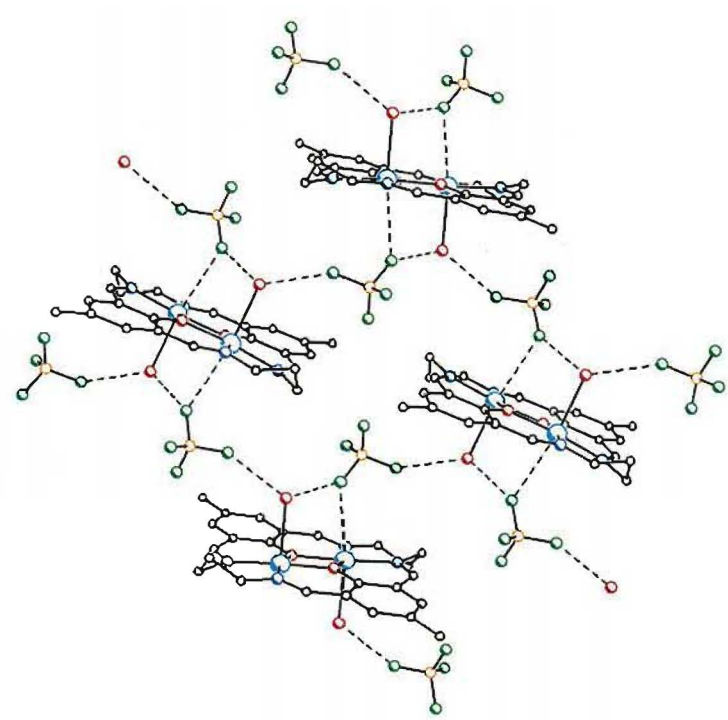

Figure 3.1.14. Hydrogen bonds involving molecule **II**.

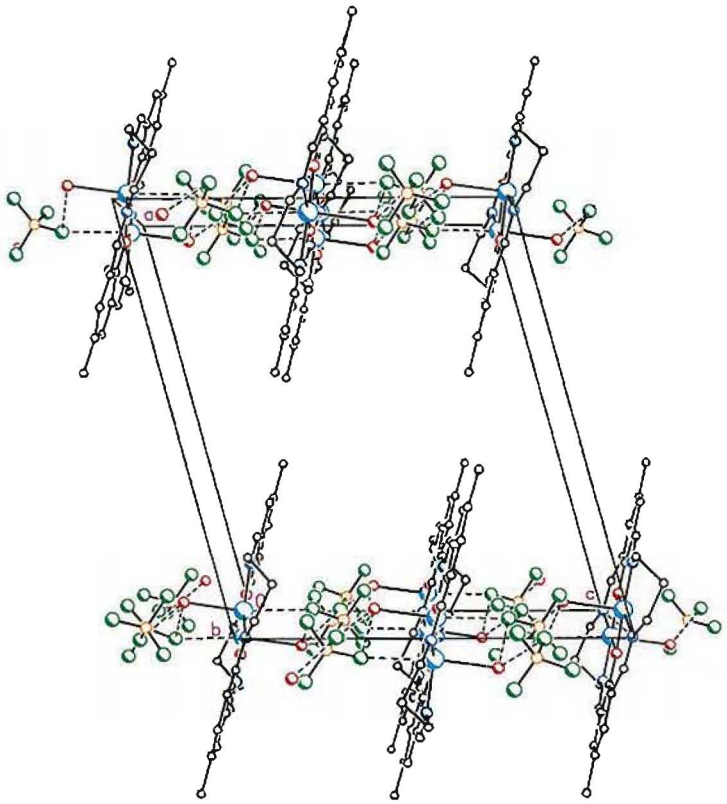

Figure 3.1.15. Molecular packing diagram for molecule **I**.

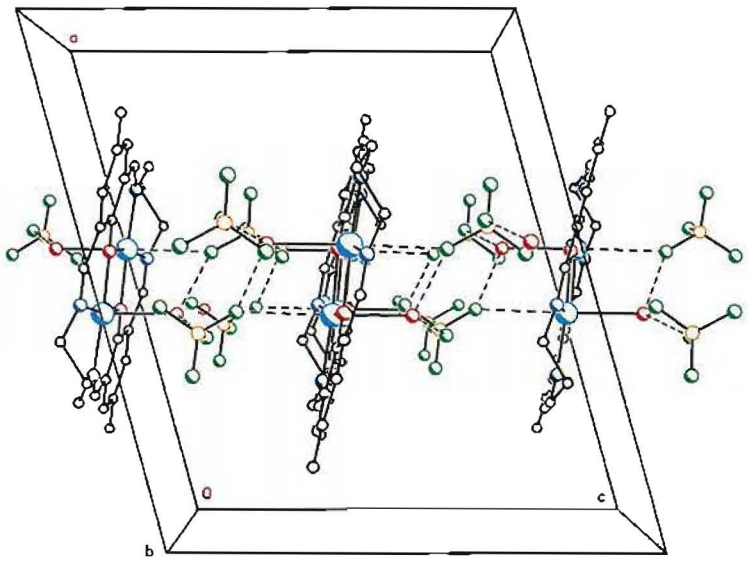

Figure 3.1.16. Molecular packing diagram for molecule **II**.

The structure of a dicopper(II) complex of the macrocycle $(L^2)^{2-}$ was reported by Hoskins et al.[101a] (denoted here as complex **5a**) and is similar to that of **5**. Both complexes **5** and **5a** contain the $[Cu_2L^2]^{2+}$ moiety. In addition, the two copper ions in **5a** are also equatorially coordinated by the macrocyclic ligand and bridged by two phenolate oxygen atoms at a Cu···Cu separation of 3.133(1) Å [cf. 3.124(1) and 3.130(1) Å in complex **5**]. However, two coordinated chloride ions occupy the axial position of each copper ion in **5a**, "above" and "below" the macrocyclic plane.

A dinuclear zinc(II) complex of $(L^2)^{2-}$ has also been synthesised and structurally characterised.[101b] The crystal structure of this zinc(II) complex consists of two crystallographically independent molecules, each containing a centre of symmetry. The N_4O_2 donor set of the macrocycle in each molecule forms the equatorial coordination of the zinc(II) atoms. A water molecule coordinates axially to each zinc(II) ion. However, the coordination sphere of the metal ion is completed by a perchlorate ion, instead of a tetrafluoroborate ion.

3.2 Ring-closure reactions of complexes 1 and 4 with 2,5-diformylfuran

Synthesis

As mentioned in the beginning of this chapter, one main aim of this work is to convert acyclic diimine-diamine type complexes to asymmetric [2+2] Schiff-base macrocyclic complexes containing a phenol "head unit" and a non-phenol "head unit". Accordingly, ring-closure condensations were attempted using complexes **1** and **4***, which contain a common dicopper(II) hydroxo-bridged acyclic complex $[Cu_2L^1(\mu\text{-}OH)]^{2+}$, and several dicarbonyl compounds (see **Figure 3.2.1**). When glyoxal (1) or 2,6-diacetylpyridine (2) was used in the ring-closure reactions, only a mixture of compounds were obtained and recrystallisation attempts to purify the products have so far failed. These reactions will not be discussed further.

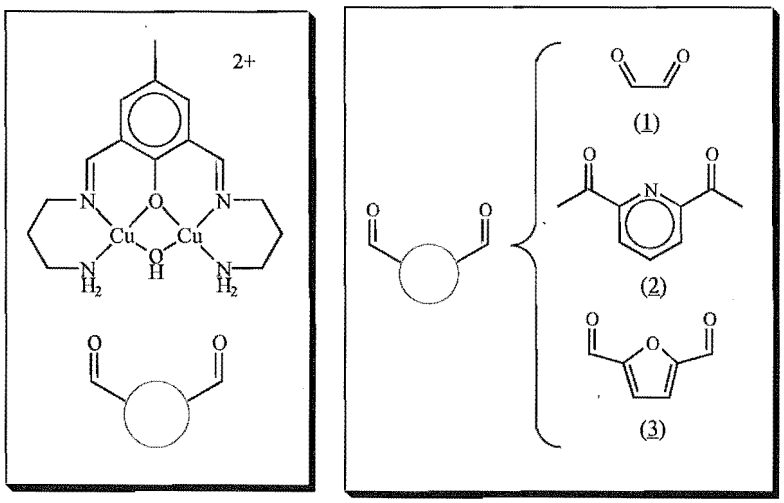

Figure 3.2.1. (1) = glyoxal, (2) = 2,6-diacetylpyridine, (3) = 2,5-diformylfuran.

On the other hand, the template condensation of **1** or **4** with 2,5-diformylfuran, followed by addition of an excess NH_4NCS, yielded three similar, but distinct complexes of the ligand $(L^3)^-$ (see **Figure 3.2.2** for the chemical structure of $(L^3)^-$ and **Table 3.2.1** for the formulae of the complexes). Complex **8** was obtained directly from

---

* Complex **1**: $[Cu_2L^1(\mu\text{-}OH)(H_2O)](ClO_4)_2.H_2O$; complex **4**: $[Cu_2L^1(\mu\text{-}OH)](BF_4)_2.H_2O$.

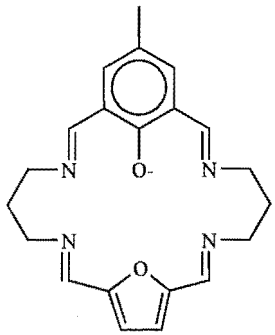

$(L^3)^-$

Figure 3.2.2.

Table 3.2.1. Microanalytical data for complexes **8** - **10**. Calculated values are given in parentheses.

Complex	Formula	Mass percent			X-ray structure
		C	H	N	
8	$Cu_2L^3(\mu\text{-}OCH_3)(NCS)_2(CH_3OH)(H_2O)$	43.66 (43.66)	4.50 (4.69)	12.18 (12.22)	
9	$Cu_2L^3(NCS)_2(\mu\text{-}OCH_2CH_3)$	46.02 (46.07)	4.13 (4.33)	13.11 (12.89)	yes
10	$Cu_2L^3(\mu\text{-}OH)(NCS)_2$	44.29 (44.22)	3.88 (4.11)	13.48 (13.21)	

the reaction mixture as a green precipitate. Complexes **9** and **10** were obtained as emerald green crystals and a bright green powder, respectively, by diethylether diffusion into a DMF solution of **8**. In some cases, complexes **9** and **10** were obtained simultaneously from one diffusion experiment.

The positive ion fast-atom-bombardment (FAB) mass spectra verified that these complexes are similar. Two common peaks are present in the region of interest at $^m/_e$ = 427 and 489, corresponding to the species $[CuHL^3]^+$ and $[Cu_2L^3]^+$, respectively. On the other hand, the infrared spectra indicate that there are distinct differences between the complexes (discussed later); this is supported by their microanalytical data (**Table 3.2.1**). The structure of complex **9** has been established by X-ray single-crystal structure analysis and will be presented next.

Crystal structure of complex 9

The X-ray crystal structure of complex **9** (**Figure 3.2.3**) verifies the structure of the asymmetric macrocycle $(L^3)^-$ and demonstrates that the dicopper(II) complex $[Cu_2L^1(\mu\text{-}OH)]^{2+}$ could undergo a ring-closure condensation with 2,5-diformylfuran (DFF). The macrocycle in complex **9** holds the two copper(II) atoms at 3.087(1) Å apart. The phenoxo oxygen of the macrocycle (O1) bridges the copper pair with a Cu-O-Cu angle of 100.4°. The oxygen of an ethoxide ion (O31) acts as a second monoatomic bridge between the two copper ions, with a Cu-O-Cu angle of 107.9(2)°. Two N-bonded thiocyanate ions complete the asymmetric unit, each coordinating to one copper ion. The coordination environments of the two copper ions in **9** are distinctly different as shown in **Figure 3.2.3b**. Selected interatomic distances and bond lengths are given in **Table 3.2.2**.

The equatorial coordination plane of Cu1 comprises an imine nitrogen from the phenol-diimine fragment (N1) and the phenoxo oxygen (O1) of the macrocycle, the ethoxide oxygen (O31), and an N-bonded thiocyanate ion (N41). These donor atoms are tetrahedrally distorted from their mean plane, with adjacent atoms deviating above and below the least-squares plane [mean deviation = 0.123(2) Å]. Cu1 is displaced from the mean plane of the N_2O_2 donor set by 0.226(2) Å towards an imine nitrogen from the furan-diimine moeity (N4), which interacts only weakly with Cu1 [N4-Cu1 = 2.49 Å].

The coordination geometry around Cu2 may be described as an irregular trigonal bipyramid. The equatorial plane comprises the phenoxo oxygen (O1) and an imine nitrogen from the furan-diimine fragment of the macrocycle (N3), and a second N-bonded thiocyanate ion (N51). An imine nitrogen from the phenol-diimine moiety (N2), and the ethoxide bridge occupy the two axial positions of Cu2. Although the imine nitrogen N2 occupies the axial position of Cu2 coordination sphere, the copper bond to this imine nitrogen is significantly shorter than the bond to the imine nitrogen N3 which occupies the equatorial position.

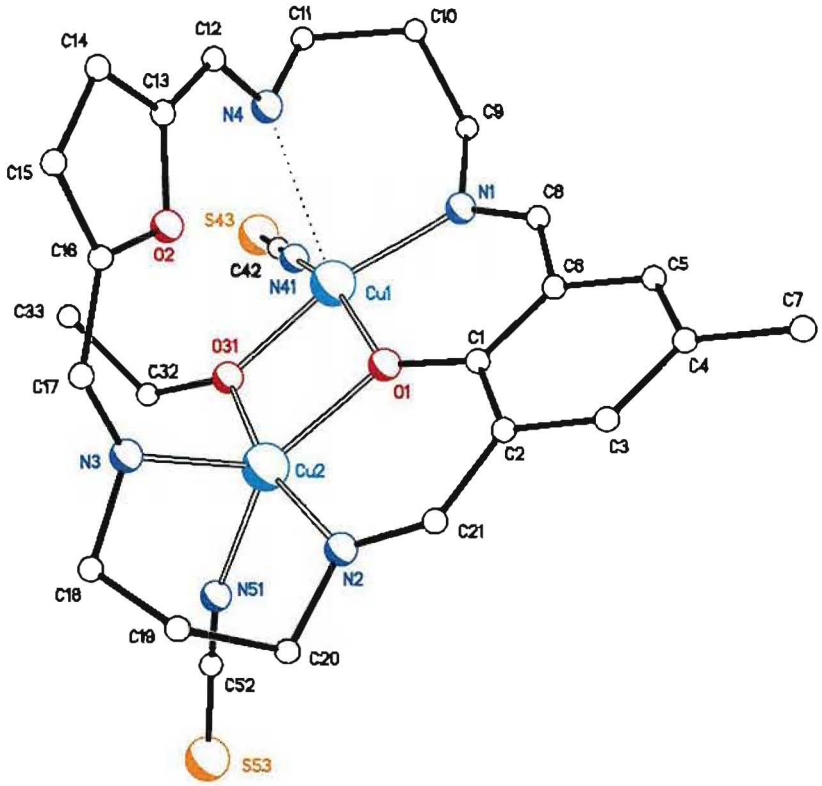

(a)

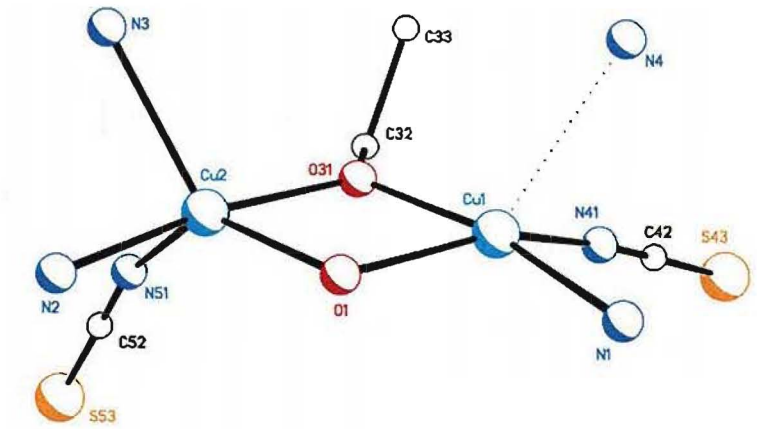

(b)

Figure 3.2.3. (a) A perspective view of the complex $[Cu_2L^3(\mu\text{-}OCH_2CH_3)(NCS)_2]$ (**9**) with the atom numbering scheme; (b) The coordination sphere of the copper ions in **9**.

Table 3.2.2. Interatomic distances (Å) and bond angles (°) relevant to the copper(II) coordination in $[Cu_2L^3(\mu\text{-}OCH_2CH_3)(NCS)_2]$.

Cu1...Cu2	3.087(1)		
Cu1-O1	2.005(3)	Cu2-O1	2.013(3)
Cu1-N1	1.983(4)	Cu2-N2	1.982(4)
Cu1-N41	1.965(4)	Cu2-N51	2.033(4)
Cu1-O31	1.912(3)	Cu2-O31	1.904(3)
Cu1...N4	2.492(4)	Cu2-N3	2.233(4)
Cu1-O1-Cu2	100.4(1)	Cu2-O31-Cu1	107.9(2)
O1-Cu1-N1	90.9(1)	O1-Cu2-N51	135.8(2)
O1-Cu1-O31	75.8(1)	O1-Cu2-N3	125.1(1)
N1-Cu1-N41	96.2(2)	N3-Cu2-N51	96.2(2)
O31-Cu1-N41	95.0(2)	O1-Cu2-N2	90.8(2)
N4-Cu1-O31	107.5(1)	N2-Cu2-N3	85.1(2)
N4-Cu1-N41	86.3(2)	N2-Cu2-N51	94.2(2)
N1-Cu1-N4	81.3(2)	N3-Cu2-O31	103.8(2)
O1-Cu1-N4	115.3(1)	N51-Cu2-O31	94.9(2)
		O1-Cu2-O31	75.8(1)

The bonds between the copper(II) ions and the phenoxo oxygen are significantly longer than the bonds between the copper(II) ions and the ethoxide ion, which is consistent with the larger Cu-O(ethoxide)-Cu angle compared to the Cu-O(phenoxo)-Cu angle.

The macrocycle folds at the flexible saturated side-chains, so the least-squares plane through the phenyl ring is inclined by 88.4(1)° towards that of the furan ring. The folding of the macrocycle is probably due to the mismatch between the size of the macrocyclic cavity and the dimension of the $Cu_2(\mu\text{-}OEt)$ core.

The Cu_2O_2 unit is almost coplanar with the phenyl ring (the least-squares plane of the Cu_2O_2 unit is inclined by 3.8° towards that of the phenyl ring). The two thiocyanate ions, which are approximately linear (∠ N-C-S *ca.* 179°), coordinate to the copper(II) ions from the "outer" face of the folded macrocyclic unit. One of the thiocyanate ions (that involving N51) coordinates to the copper with a more bent geometry than the other [∠ Cu2-N51-C(52) = 164.3(4)°; Cu1-N41-C(42) = 176.1(4)°].

The ethoxide bridge also binds to the copper(II) ions from the "outer" face of the macrocyclic unit with the terminal methyl group bending towards the furan-diimine moiety with a normal tetrahedral C-C-O angle of 109.4(5)°.

The geometry about the phenoxo oxygen (O1) is planar, consistent with the proposed[98] conjugation in the chelate rings involving the phenol-diimine moiety. However, the angles at O1 deviate from the trigonal angle of 120° [Cu1-O1-Cu2 = 100.4(1)°; Cu1-O1-C(1) = 130.4(3)°; Cu2-O1-C(1) = 129.1(3)°; sum = 359.9(2)°], and O1 is not coplanar with the phenyl ring, being displaced from the least-squares plane of the phenyl ring by *ca.* 0.1 Å. This, and the observation that the Cu_2O_2 unit is not coplanar with the phenol-diimine moiety, are due to the geometries at both copper(II) ions which require the imine-Cu-phenoxo angles to be close to 90°.

The three-coordinate ethoxide oxygen has an angular geometry, with the ethoxide oxygen atom deviating by 0.1 Å from the Cu1-Cu2-C32 least-squares plane towards the furan ring. This is expected for an oxygen atom which is not involved in any conjugation. This also suggests that the lone electron pair of the oxygen atom is directed towards the furan ring.

The six-membered chelate ring involving the second saturated side-chain of the macrocycle and Cu2, adopts a pseudo-chair conformation. The atoms of the N-C···C-N fragment each deviates by *ca.* 0.03 Å from their least-squares plane, while the central carbon atom of the saturated chain, C19, and Cu2 are displaced "above" and "below" this least-squares plane by 0.68 Å and 1.19 Å, respectively if the thiocyanate ions are considered to lie "below" this least-squares plane (**Figure 3.2.4**). The distance between the two imine nitrogen atoms of the furan moiety, the sites of ring-closure, is 5.45 Å, which is 0.22 Å shorter than the distance between the two NH_2 groups of the precursor ligand $(L^1)^-$ in complex **4**.

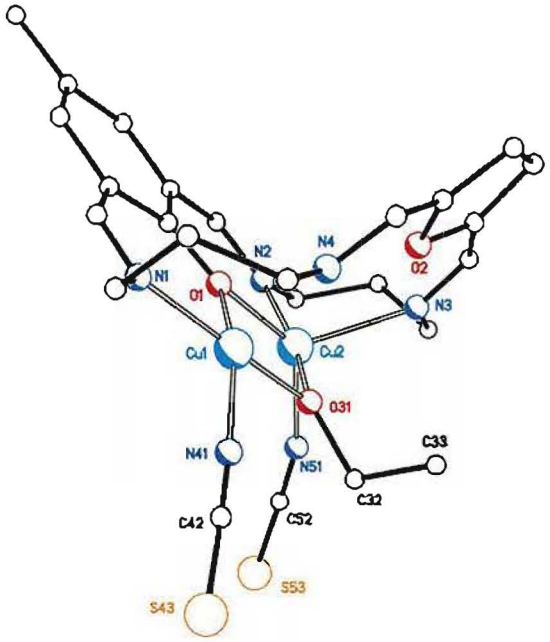

Figure 3.2.4. A perspective view of the complex $[Cu_2L^3(\mu\text{-}OCH_2CH_3)(NCS)_2]$ (**9**) showing the folded conformation of the macrocycle.

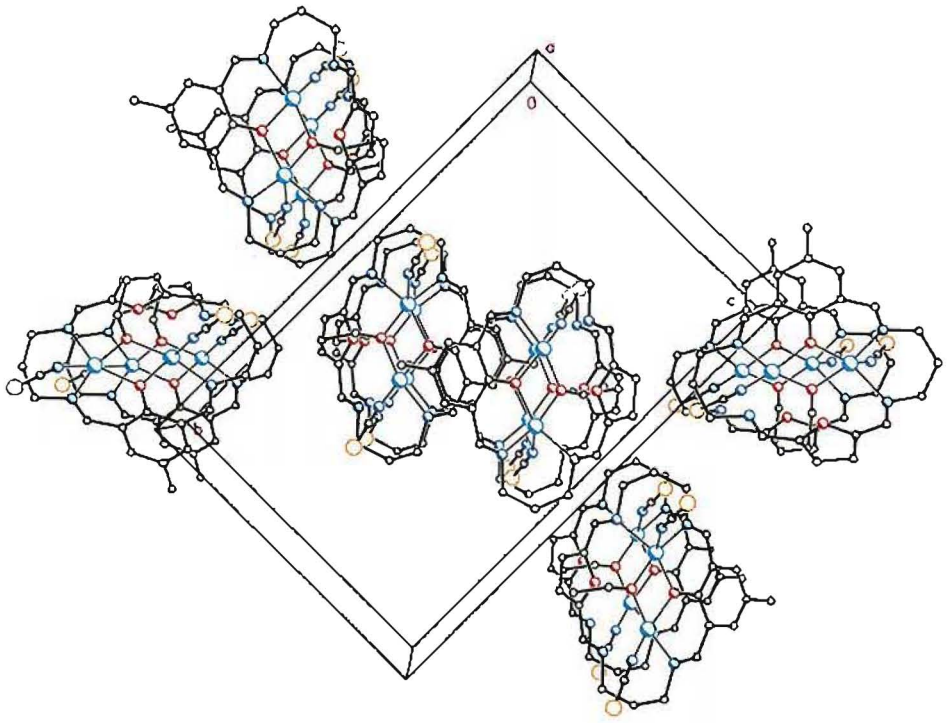

Figure 3.2.5. Molecular packing in the crystal of complex **9**.

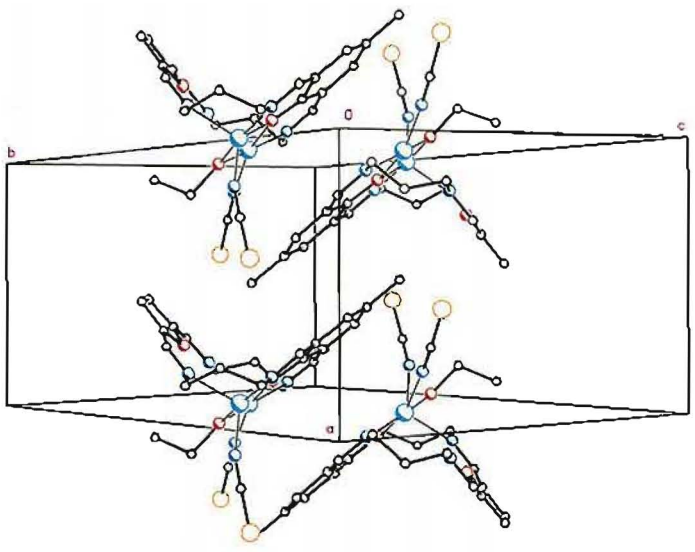

Figure 3.2.6. Packing of molecules **9** in one column.

In the crystal, the molecules of **9** are packed in columns which propagate along the crystallographic *a* axis (**Figures 3.2.5** and **3.2.6**). Within a column the phenol-diimine units interact through the "inner" and "outer" faces of the folded molecules (**Figures 3.2.7a** and **3.2.8a**, respectively) by way of π-π interactions. For the "inner" interaction, the phenyl rings are *ca.* 3.4 Å apart and very offset with respect to each other (**Figure 3.2.7b**) as expected for π-π stacking.[100] On the other hand, the "outer" interaction is between the π-systems of the phenol-diimine units (resulting from the conjugation in the chelate rings involving the deprotonated phenol group), where the phenyl rings of the two adjacent molecules are *ca.* 3.5 Å apart and do not overlap (**Figure 3.2.8b**).

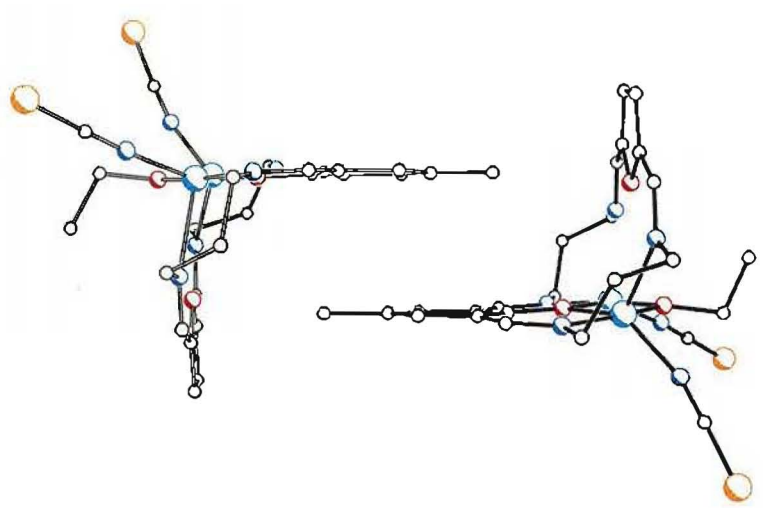

(a)

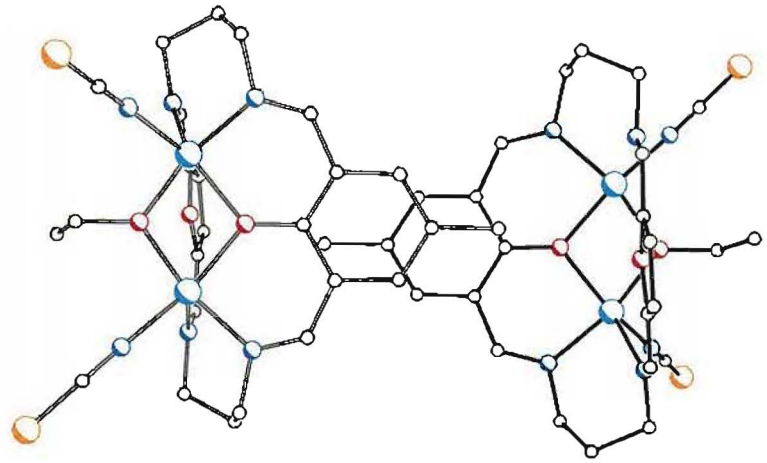

(b)

Figure 3.2.7. π-π interactions of molecules of $[Cu_2L^3(\mu\text{-}OCH_2CH_3)(NCS)_2]$ (**9**) through the "inner" faces: (a) viewed approximately along the mean plane of the phenol moiety; (b) viewed perpendicular to the mean plane of the 6-membered ring of the molecule in white bonds.

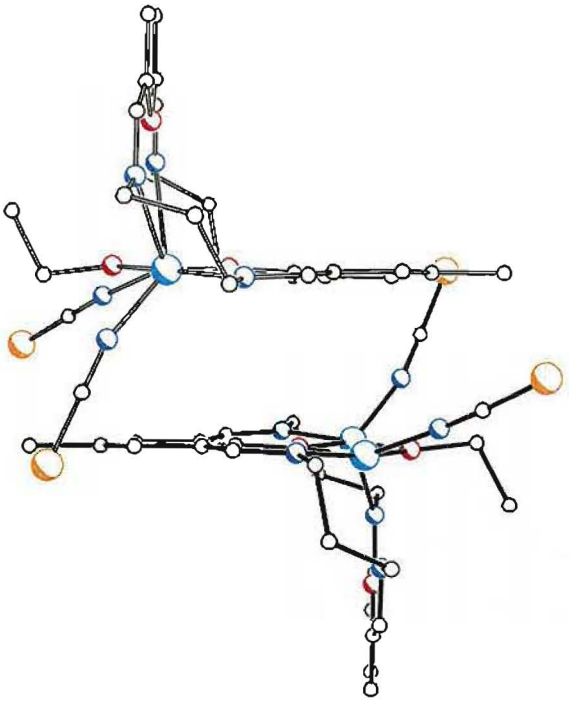

(a)

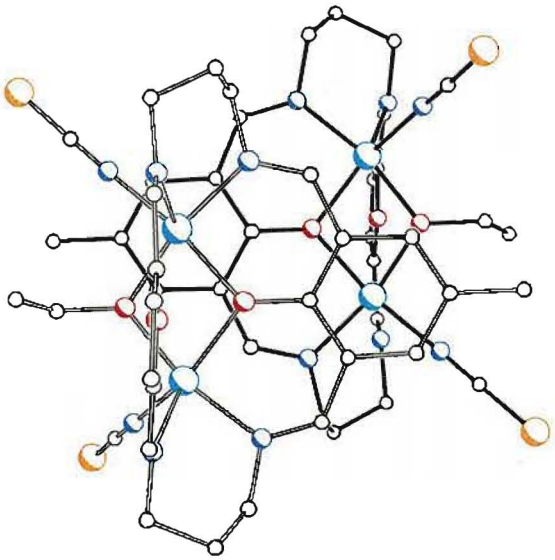

(b)

Figure 3.2.8. π-π interactions of molecules of $[Cu_2L^3(\mu\text{-}OCH_2CH_3)(NCS)_2]$ (**9**) through the "outer" faces: (a) viewed approximately along the mean plane of the phenol moiety; (b) viewed perpendicular to the mean plane of the 6-membered ring of the molecule in white bonds.

Origin of the ethoxide bridge in complex 9

The presence of an ethoxide ion in the structure of the complex $Cu_2L^3(NCS)_2(\mu\text{-}OCH_2CH_3)$ (**9**) was unexpected for the following reason. The ethoxide ion must have originated from ethanol. However, complex **9** was obtained from the recrystallisation of complex **8** by diethylether diffusion into DMF, while complex **8** itself was obtained from methanol. So the source of ethanol had to be determined.

If ethanol was somehow present as an impurity during the preparation of complex **8**, the excess amount of methanol (solvent) would ensure methoxide to bridge the copper(II) ions in preference to ethoxide, since methoxide is a better electron donor than ethoxide. This means that complex **9** could not possibly be formed - that is, the ethoxide ion could not bridge the copper(II) ions - during the ring-closure reaction. Consequently, the ethoxide bridge must have become incorporated during the recrystallisation process of complex **8**.

The two possible sources of ethanol, hence of the ethoxide ion, in the recrystallisation process were the DMF used to dissolve complex **8**, and the diethylether diffused into the DMF solution. The chemically pure grade DMF used in this work does not normally contain ethanol as an impurity. However, the particular batch of DMF employed to obtain complex **9** had been placed over molecular sieves, which were normally used to dry methanol or ethanol prior to distillation.

The sieves were usually dried in an oven at *ca.* 130° for a few days prior to re-use. Nevertheless, it was possible that the DMF had been placed over a particular batch of molecular sieves that were not completely free of ethanol. Subsequently, the ^1H nmr spectrum of the DMF batch that was suspected to contain ethanol, was obtained. However, the spectrum does not show any peaks expected for ethanol, indicating that the DMF contains no or very little amount of ethanol, and that DMF was not a likely source of the ethanol.

The diethylether employed in many of the recrystallisation experiments was of technical grade purity, thus containing a relatively high percentage of ethanol compared with the amount of complex normally used in an individual recrystallisation experiment.

Hence the ether is very likely to be the source of ethanol from which the ethoxide bridge in **9** originated. To test this hypothesis, the recrystallisation of complex **8** was carried out using diethylether that had been purified. Crystals of complex **9** was not formed, instead a bright green powder, very similar in appearance to complex **10**, was obtained.

Infrared spectra and deduction of the structures of complexes 8 and 10

In the following discussion, the chemical structures of complexes **8** and **10** will be deduced by using their microanalytical data (**Table 3.2.1**) and infrared spectra, combined with the known structure of complex **9**. The infrared spectra of complexes **8** - **10** are illustrated in **Figures 3.2.9a - c** for comparison. The full size spectra may be found in **Appendix B**. Some absorption bands in the infrared spectra of complexes **8** - **10** are listed in **Table 3.2.3**.

Table 3.2.3. Infrared spectral data (cm^{-1}) for the dinuclear copper(II) complexes (s = sharp, b = broad; intensity: S = strong, M = medium, W = weak.)

Complex	hydroxo	aquo	ν(NCS)	ν(C=N)	ν(C···O)
8		3446 M, b	2089 S, s 766 M, s	1640 S, s	1560 S, s
9		3445 M, b	2096 S, s 2076 S, s 765 M, s	1641 S, s	1564 S, s
10	3641 M, s	3450 W, b	2081 S, s 768 M, s	1641 S, s	1559 S, s

The infrared spectra of complexes **8** - **10** all show:

a) the absence of the NH_2 stretching absorptions at ca. 3300 cm^{-1} region and of the ClO_4^- or BF_4^- absorptions in the 1050-1100 cm^{-1} region,

b) an increased intensity of the imine band relative to the phenol C-O band (compared with the spectra of complexes **1** and **4**, the acyclic precursors),

c) the presence of an NCS^- stretch at *ca.* 2090 cm^{-1}, corresponding to N-bonded thiocyanate.

These observations are consistent with the formation of a macrocyclic Schiff-base complex with NCS^- as the counterion. However, the infrared spectra of the three complexes also show some differences, which indicate that they are distinct complexes. The chemical structure for **9** and the proposed structures for complexes **8** and **10** are shown in **Figure 3.2.10**.

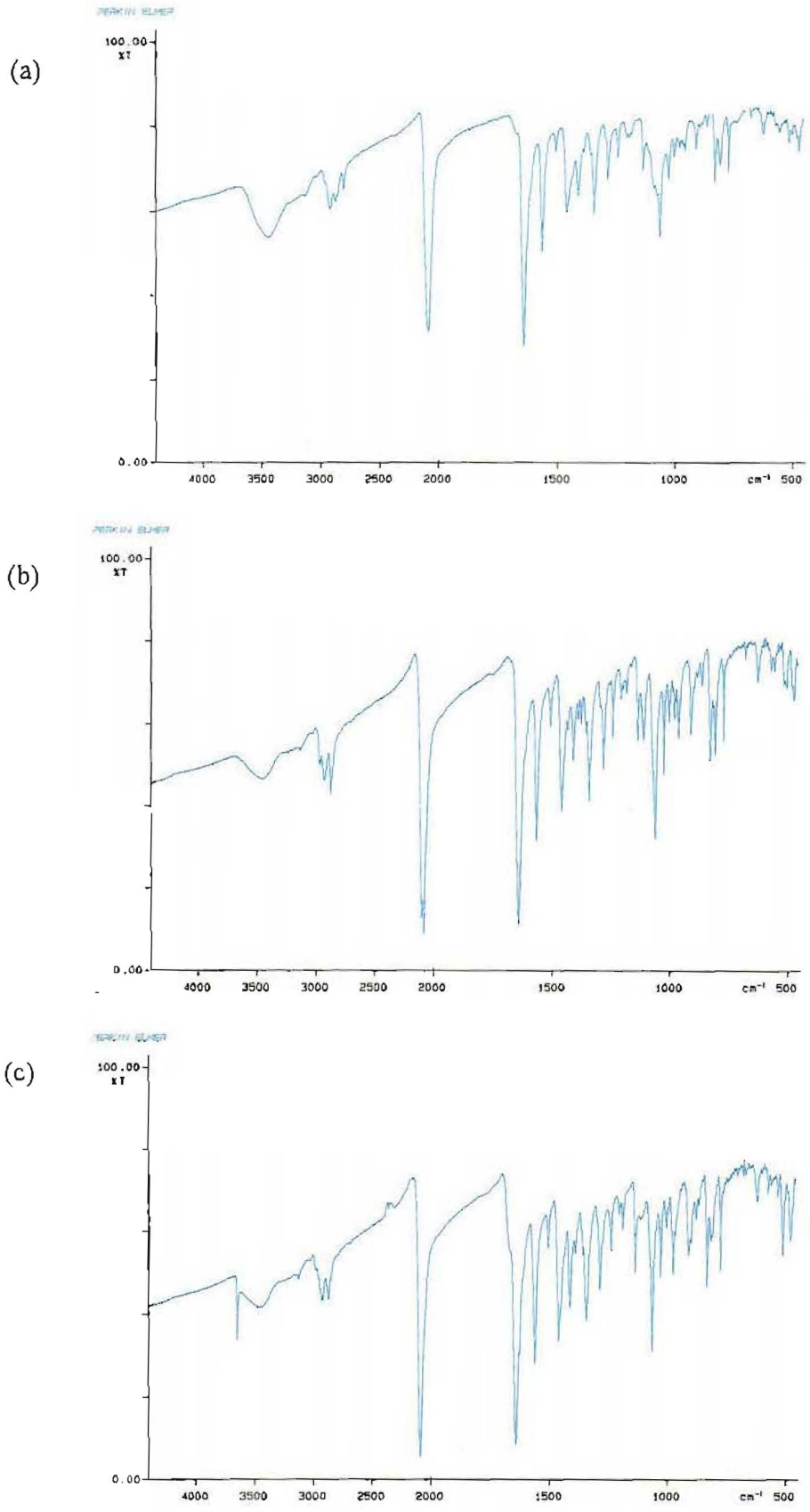

Figure 3.2.9. Infrared spectra of (a) $Cu_2L^3(\mu\text{-}OCH_3)(NCS)_2(H_2O)(CH_3OH)$ (**8**), (b) $[Cu_2L^3(\mu\text{-}OCH_2CH_3)(NCS)_2]$ (**9**), (c) $[Cu_2L^3(\mu\text{-}OH)(NCS)_2]$ (**10**).

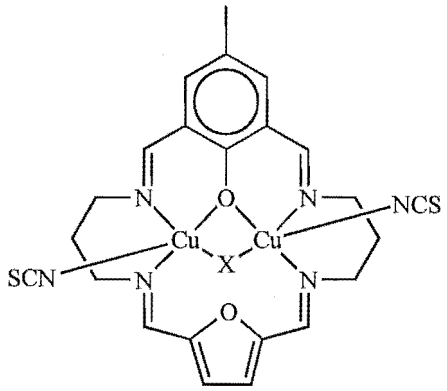

Complex **8** X = OH^- or CH_3O^-

Complex **9** X = $CH_3CH_2O^-$

Complex **10** X = OH^-

Figure 3.2.10. The chemical structure of complex **9** and the proposed chemical structures of complexes **8** and **10**.

A split NCS band in the 2070 - 2096 cm^{-1} region is observed in the infrared spectrum of complex **9**, consistent with its X-ray crystal structure, which shows two NCS^- anions in two different environments. In contrast, the NCS bands at *ca.* 2080 cm^{-1} in the spectra of complexes **8** and **10** are not split, suggesting that the thiocyanate coordination environments in each of these complexes are similar, and hence these complexes are more symmetrical than complex **9**.

It is also interesting to note that the NCS band of complex **8** could be observed at *ca.* 2077 cm^{-1} or at *ca.* 2089 cm^{-1}, depending on when the compound was isolated. If the complex was isolated within a few hours since precipitation, it would show the NCS band at *ca.* 2077 cm^{-1}. The complex which was isolated after being left as a suspension overnight shows the NCS band at *ca.* 2089 cm^{-1}. This probably represents a slow, kinetically controlled isomerisation of the complex.

The spectrum of complex **10** shows a striking sharp peak of medium intensity at 3641 cm^{-1}, assigned to a non-hydrogen-bonded OH. The microanalytical data for this complex and stoichiometry require that the OH group is a hydroxo ion. By comparison with the structure of complex **9**, the hydroxo ion probably acts as a bridging ligand in complex **10** (**Figure 3.2.10**). This is consistent with the absence of this peak in the spectrum of complex **9**, where the bridging ligand is an ethoxide ion. The fact that the OH stretch is sharp suggests that the OH^- occupies a well-protected site in complex **10** and that the macrocycle in **10** is probably folded as observed in the structure of **9**. If the

macrocycle were flat, the μ-OH^- would be able to form hydrogen bond to the furan oxygen, and would not give rise to the sharp OH stretch in the infrared spectrum.

The C-H absorption region of the infrared spectrum is also different in each case. Complex **10** shows the simplest pattern for the C-H stretches, with two absorptions at 2923 cm^{-1} (a doublet) and at 2865 cm^{-1}. The infrared spectra of complexes **8** and **9** each shows three C-H peaks, however, the positions and the appearance of these C-H peaks in the spectra of **8** and **9** are distinct. This may be interpreted as follows. The more simple pattern of C-H absorptions in the spectrum of **10** is consistent with it having a μ-OH^- bridge, as opposed to an ethoxide bridge in **9**. The more complex C-H absorptions pattern of **8** as compared with that of **10**, and the fact that the pattern is different from that of **9**, suggest that the bridging ligand in **8** is different from that in **9** or **10**, possibly a methoxide ion (see **Figure 3.2.11**).

The proposal that the bridging ligand in complex **8** is a methoxide ion is supported by the absence of a hydroxide stretch at *ca.* 3600 cm^{-1} in the spectrum of complex **8**. The microanalytical data for complex **8** also give good agreement with the formulation $Cu_2L^3(\mu\text{-}OCH_3)(NCS)_2(CH_3OH)(H_2O)$.

When the ring-closure reaction was carried out in ethanol, with exclusion of methanol, complex **9** was the product instead of complex **8**. This observation suggests that methanol is necessary for the formation of complex **8**, thus lending further support to the conclusion that complex **8** contains a methoxide bridge.

Therefore it may be concluded that the main structural difference among the complexes **8-10** lies in the nature of the non-macrocyclic-donor bridging species (**Figure 3.2.10**). Complex **8** contains a μ-OCH_3, complex **9** a μ-OCH_2CH_3, and complex **10** a μ-OH bridge as well as the phenoxo bridge of the macrocycle. In addition, the structures of complexes **8** and **10** are probably more symmetrical than that of **9**, with the macrocycle in **10** being folded as observed in complex **9**.

It is interesting to note that the μ-OCH_2CH_3 complex (**9**) crystallised from DMF only in the presence of ethanol, and the μ-OH complex (**10**) was obtained when ethanol was not present. This suggests that complex **9** was formed in preference to the other two complexes largely because of crystal packing effects.

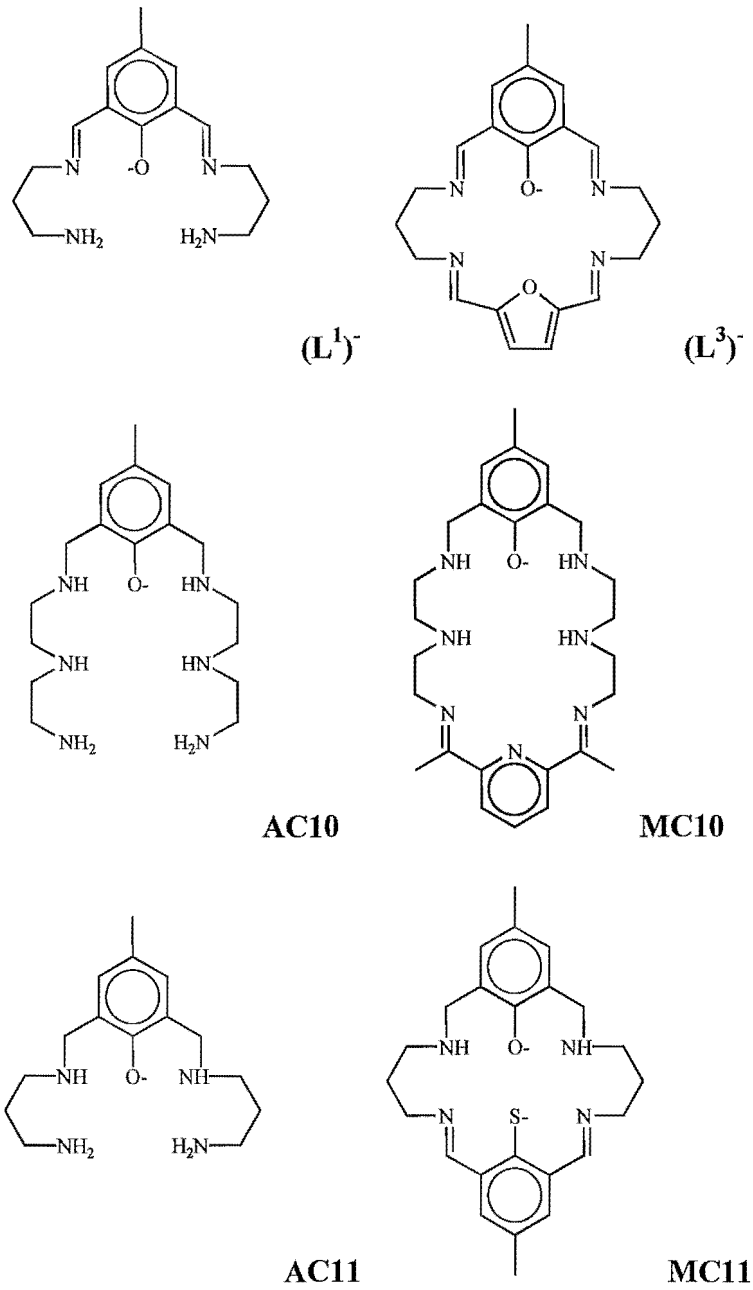

Figure 3.2.11. Chemical structures of the asymmetric macrocycles $(L^3)^-$, **MC10** and **MC11**, and of the corresponding acyclic precursor ligands $(L^1)^-$, **AC10** and **AC11**.

The basic structure of the macrocyclic Schiff-base ligand $(L^3)^-$ is similar to those of two asymmetric Schiff-base macrocycles, **MC10** and **MC11** (**Figure 3.2.11**), which were recently synthesised and structurally characterised.[62, 63] The aromatic moieties of each macrocycle consist of one phenol and one non-phenol fragments, while the two saturated side chains in each macrocycle are identical. In addition, the saturated chains in $(L^3)^-$ are the same as those in **MC11**, which are n-propyl groups.

However, the structures of the three macrocycles differ in details. Firstly, the non-phenolic fragments are different in each case; it is a furan in $(L^3)^-$, a pyridine in **MC10**, and a thiophenol in **MC11**. Secondly, the macrocycle $(L^3)^-$ contains four imine linkages, while **MC10** and **MC11** only have two imine linkages, belonging to the non-phenolic fragments of the macrocycles. Thirdly, the saturated side chains in **MC10** are derived from diethylenetriamine, while those in the other two macrocycles are derived from 1,3-diaminopropane.

The method of preparation of $(L^3)^-$ is similar to, but distinct from, those of **MC10** and **MC11**. All three macrocycles were prepared by stepwise methods and the macrocycles were generated from their respective acyclic precursors by metal template condensation.

The first main difference is the template metal ions employed in each case: Cu^{2+} for $(L^3)^-$, Pb^{2+} for **MC10**, and Ni^{2+} for **MC11**. The second is the nature of the acyclic precursors to the macrocycles. The acyclic precursor to $(L^3)^-$ is a dicopper(II) complex of a Schiff-base ligand, that is, $(L^1)^-$. The acyclic precursors to both **MC10** and **MC11** are metal-free ligands, which contain no imine linkages. **AC10** and **AC11** may be regarded as the reduced analogues of the acyclic Schiff-base ligands derived from the condensation of one molecule of 2,6-diformyl-4-methylphenol and two molecules of diethylenetriamine or 1,3-diaminopropane.

The macrocycle **MC10** was isolated as its dilead(II) perchlorate complex of formula $\{[Pb_2(\mathbf{MC10})Cl](ClO_4)_2\}_x$. The structure of this complex is polymeric, containing chains of macrocyclic units linked by a chloride ion (**Figure 3.2.12**). Each macrocyclic unit contains two lead(II) ions. In contrast to the dicopper(II) complex **9**, the metal ions are not bridged by ligands other than the macrocycle. The phenoxo oxygen and the pyridine nitrogen of the **MC10** bridge the two lead(II) ions in the complex. The interactions of the pyridine nitrogen with the lead ions are weak, however, with Pb...N distances of 2.90 and 3.09 Å. **MC10** adopts a twisted conformation (**Figure 3.2.12**), rather than folded as that of $(L^3)^-$ in complex **9**. The inclination between the phenol and the pyridine "head units" of **MC10** is 113°.

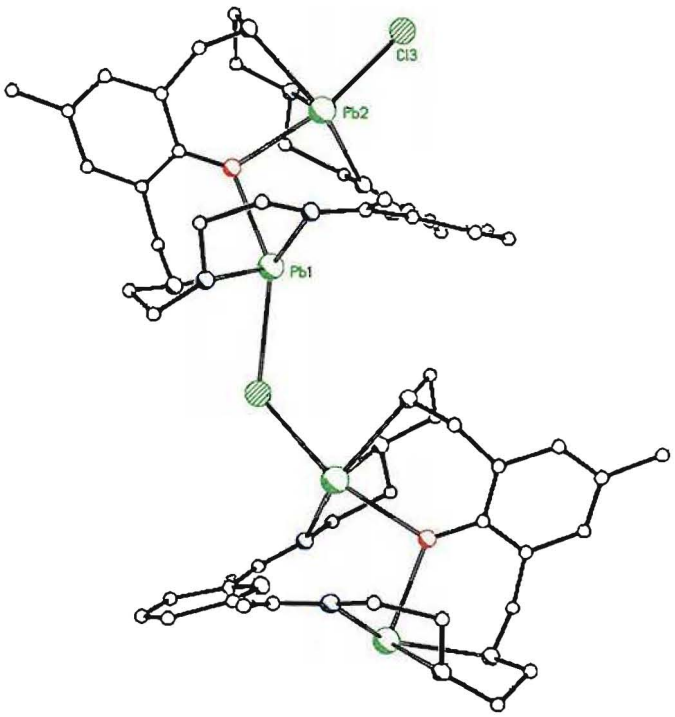

Figure 3.2.12. The polymeric structure of the complex $\{[Pb_2(\mathbf{MC10})Cl](ClO_4)_2\}_x$.[62]

Transmetallation of the dilead(II) complex of **MC10** with copper(II) salt was claimed to lead to the formation of a tricopper(II) complex of formulation $Cu_3(\mathbf{MC10})(OH)(ClO_4)_4(H_2O)$. However, this tricopper(II) complex has not been structurally characterised.

The macrocycle **MC11** was isolated as its dinickel(II) perchlorate complex, $[Ni_2(\mathbf{MC11})(CH_3CN)_2](ClO_4)_2$. The structure of the complex (**Figure 3.2.13**) shows two nickel(II) ions bound in the two N_2OS "compartments" of the macrocycle, having two distinct coordination geometries: square-planar and octahedral. The presence of two distinct coordination geometries of nickel(II) ions in the complex was proposed to be due to the macrocycle **MC11** providing a ligand field strength which is intermediate between those for square-planar and octahedral ligand field.[63]

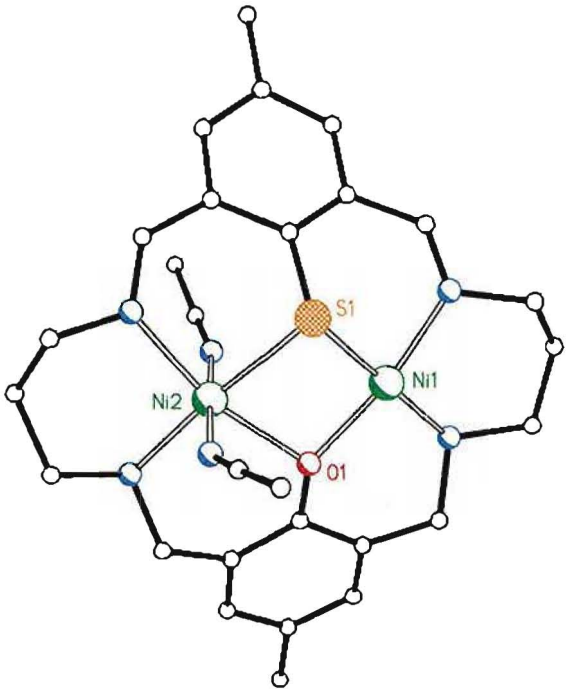

Figure 3.2.13. The structure of the complex $[Ni_2(\mathbf{MC11})(CH_3CN)_2](ClO_4)_2$.[63]

As implied above, the two nickel(II) ions are bridged by the two pendant donors of the macrocycle, the phenoxo oxygen and the thiolate sulfur. No other bridging ligands are present in the structure. The macrocycle adopts a slightly folded conformation, bending at the saturated side chains, as in the case of complex **9**. The extent of folding of **MC11** is less than that of $(L^3)^-$, however, with the two aromatic rings in **MC11** being inclined at 112.0(4)° (cf. 88.4° for $(L^3)^-$).

3.3 Condensation of 1,3-diamino-2-hydroxy-propane and 4-*t*-butyl-2,6-diformylphenol

Synthesis

Preparation of the copper(II) complex of the acyclic ligand $L^{4'}$ (**Figure 3.3.1**) was attempted by template methods, using 4-*t*-butyl-2,6-diformylphenol (TDFP), 1,3-diamino-2-hydroxypropane and copper(II) tetrafluoroborate in 1:3:2.5 molar ratio. TDFP was treated with an equivalent amount of NaOH prior to mixing with the other reactants in order to generate the phenolate and to encourage the chelation of two copper(II) ions by the diformylphenolate.

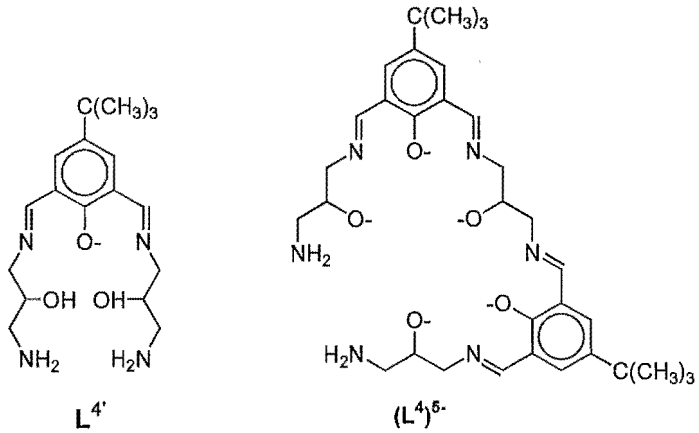

Figure 3.3.1

The product of this reaction is complex **11**, isolated as dark blue crystals. Treatment of a methanol solution of complex **11** with an aqueous solution of excess sodium nitrate, followed by slow evaporation, gave complex **12** as deep blue crystals with regular faces. When the same reaction was carried out by using copper(II) nitrate as the templating agent in place of copper(II) tetrafluoroborate, complex **12A** was obtained also as dark blue crystals.

The infrared spectra of these complexes (given in **Appendix B**) show the characteristic peaks of the imine and phenol C-O groups at *ca.* 1650 and 1555 cm^{-1}, respectively. The peaks at *ca.* 3570 and 3355 cm^{-1} present in the nujol spectrum of complex **11** suggest the presence of an OH group (presumably as hydroxo ion) and an NH_2 group, respectively. These peaks are not so evident in the KBr spectra of the

complexes, being obscured by the broad absorption at *ca.* 3400 cm^{-1}, which is probably due to water present in the KBr.

The broad peak at *ca.* 1053 cm^{-1} in the infrared spectrum of complex **11**, due to BF_4^- ion, is replaced by a broad peak at *ca.* 1370 cm^{-1}, assigned to NO_3^- ion, in the infrared spectrum of complex **12**. This indicates that anion exchange has taken place on treating complex **11** with $NaNO_3$. The infrared spectrum of complex **12A** is very similar to that of complex **12**, indicating that they probably have similar structures.

Preliminary X-ray crystallographic study

The structures of complexes **11** and **12** are severely disordered and have not yet been fully refined. However, the overall structure of the Schiff-base ligand and the manner in which the copper(II) ions are coordinated in each complex could be determined.

The ligand in these two complexes was revealed to be $(L^4)^{5-}$, which is the product of condensation of three molecules of 1,3-diamino-2-hydroxypropane and two molecules of 4-*t*-butyl-2,6-diformylphenol (a [3+2] Schiff-base ligand). In the complexes **11** and **12**, $(L^4)^{5-}$ takes a C-shape conformation, binding a non-planar hexagonal array of copper(II) ions in the ligand cavity. One hydroxo ion was found bridging two copper(II) ions at the open end of the "partly-formed" macrocyclic ligand (**Figure 3.3.2**).

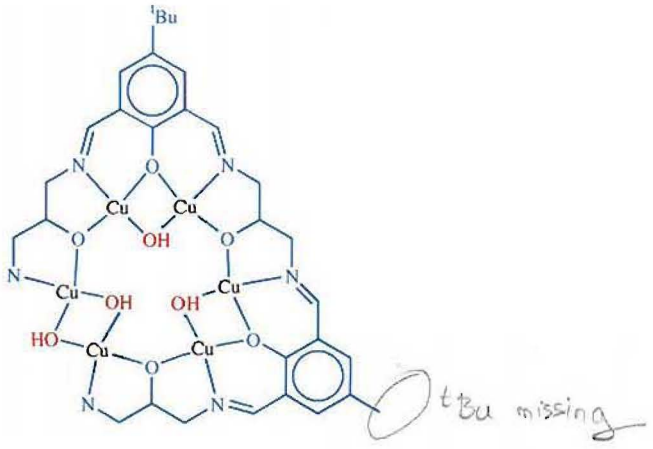

Figure 3.3.2. Schematic representation of the $[Cu_6L^4(\mu\text{-}OH)_4]^{3+}$ cation in the complexes **11** or **12** as revealed by X-ray crystallography .

In complexes **11** and **12**, $(L^4)^{5-}$ takes a C-shape conformation, appearing as a "partly-formed" macrocycle, binding a non-planar hexagonal array of copper(II) ions in the ligand cavity (**Figure 3.3.2**). A hydroxo ion bridges the two copper(II) ions which are chelated at the ends of the ligand.

In addition, three monoatomic bridges are found inside the Cu_6 ring. These donors refine as full-occupancy oxygen atoms, each bridges those copper(II) ions which are also bridged by a phenoxo oxygen of $(L^4)^{5-}$. However, the identity of these donors is still ambiguous, due to the disorder mentioned previously.

Fast-atom-bombardment mass spectrometry data

The fast-atom-bombardment (FAB) spectra of the complexes **11**, **12** and **12A** (given in **Figure 3.3.3**; the full spectra may be found in **Appendix C**) show a common intense peak in the region of interest at $^m/_e = 1051$, which corresponds to the species $[Cu_6L^4(OH)_4]^+$. The FAB mass spectra of the complexes also show a common peak at $^m/_e = 1017$ which corresponds to the species $[Cu_6L^4(OH)_2]^+$. These observations suggest that $[Cu_6L^4(OH)_4]^{3+}$ is a common cation for the three complexes.

This and the preliminary X-ray structure analysis suggest that the disordered structure of either **11** or **12** contains a major component having the cation $[Cu_6L^4(\mu\text{-}OH)_4]^{3+}$. The structure of this cation is discussed next.

(a)

(b)

(c)

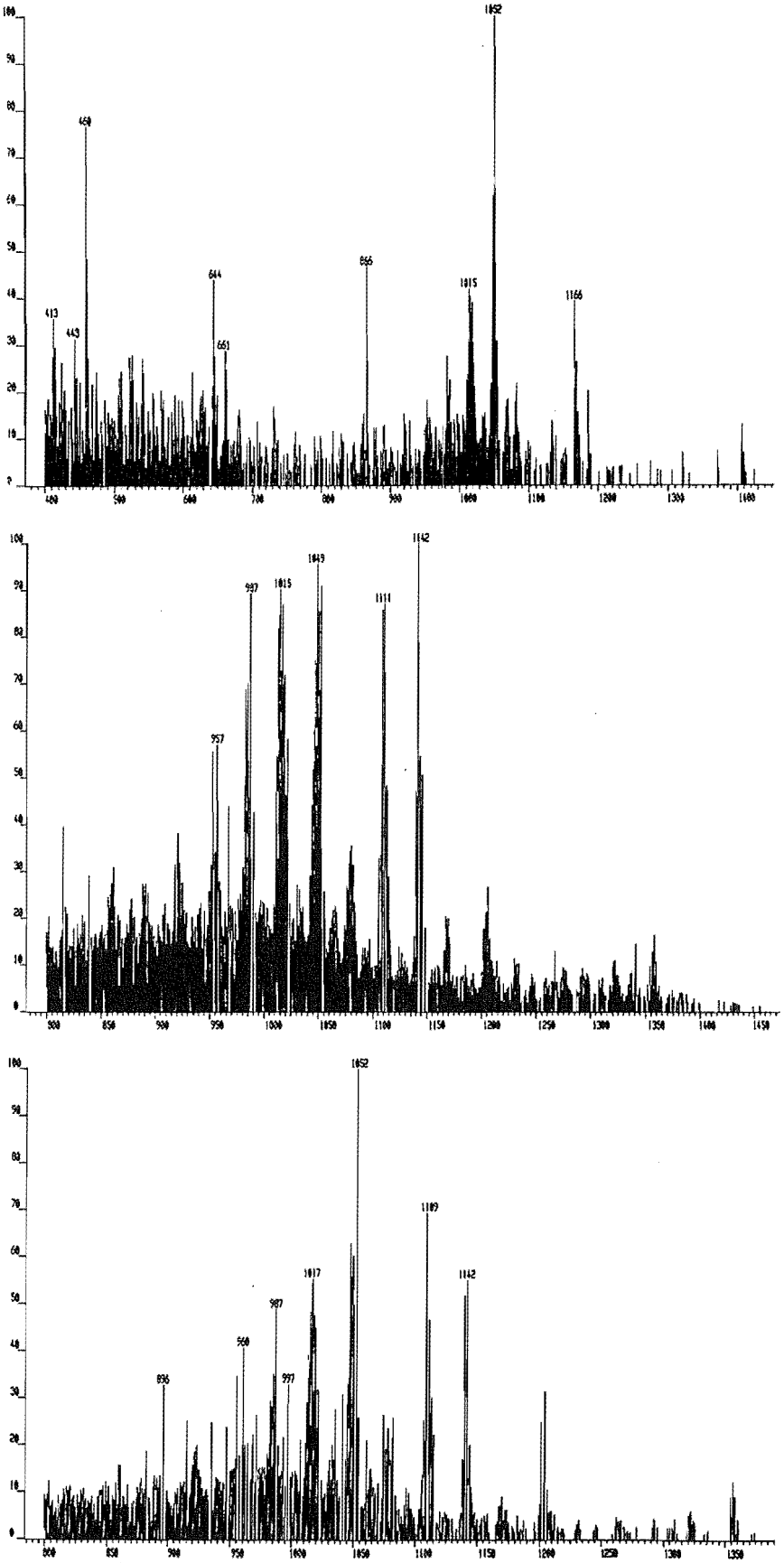

Figure 3.3.3. The FAB mass spectra of complexes **11** (a), **12** (b), and **12A** (c).

Structure of the hexacopper(II) complex $[Cu_6L^4(\mu\text{-}OH)_4]^{3+}$

The structure of the cations of complexes **11** and **12** are very similar. Since the structure of complex **12** has been further refined than that of **11**, the following discussion will be based on the structure of **12**.

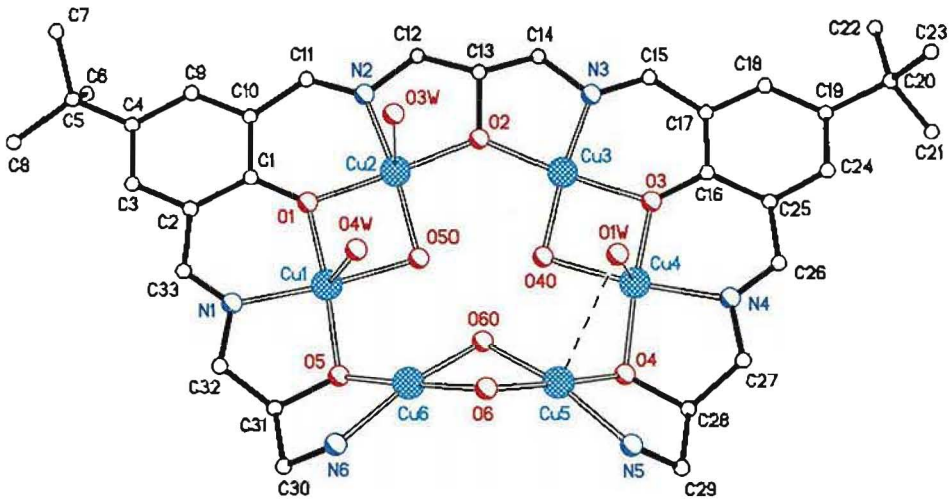

Figure 3.3.4. A perspective view of the hexacopper(II) cation $[Cu_6L^4(\mu\text{-}OH)_4]^{3+}$ of complex **12**, shown with the atom numbering system.

The structure of the hexacopper(II) cation $[Cu_6L^4(\mu\text{-}OH)_4]^{3+}$ is illustrated in **Figure 3.3.4.** The cation has a pseudo-mirror plane passing through one bridging alkoxo (O2) and the bridging hydroxo oxygen (O6) donor. The least-squares planes of the two phenyl rings of the ligand $(L^4)^{5-}$ are inclined at 2°, giving the cation a roughly planar conformation. All five pendant oxygen donors of $(L^4)^{5-}$ are deprotonated and each of these oxygen donors is bridging two copper atoms. The two NH_2 groups of $(L^4)^{5-}$ in complex **12** are 5.45 Å apart, comparable to the N(imine)···N(imine) distances of the phenoldiimine units [N1···N2 5.47 Å; N3···N4 5.48 Å] of $(L^4)^{5-}$, and to the NH_2···NH_2 separation of $(L^8)^-$ in complex **7*** (5.45 Å), but significantly smaller than the NH_2···NH_2 distances of $(L^1)^-$ in complexes **1** and **4** (5.60 Å and 5.67 Å, respectively).

* see Section 3.1. Complex **1**: $[Cu_2L^1(\mu\text{-}OH)(H_2O)](ClO_4)_2{\cdot}H_2O$; complex **4**: $[Cu_2L^1(\mu\text{-}OH)](BF_4)_2{\cdot}H_2O$; complex **7**:$[Cu_2L^8(\mu\text{-}OH)](BF_4)_2{\cdot}4H_2O$

The six-copper ions in **12** are bound within the "crescent" Schiff-base ligand in an approximately hexagonal array. The hexacopper(II) coordination environments are shown in **Figure 3.3.5**. The interatomic distances and bond angles which are relevant to the coordination spheres of the copper(II) ions in complex **12** are given in **Table 3.3.1**.

The Cu_6 ring may be regarded as being folded along the line passing through the copper atoms Cu1 and Cu4; the angle between the mean planes defined by Cu1-Cu4-Cu5-Cu6 and Cu1-Cu2-Cu3-Cu4 is 162.7°. The three central μ-OH^- donors form an equilateral triangle with O···O separations as follows, O40···O50 2.482(9), O40···O60 2.461(9), O50···O60 2.461(9) Å.

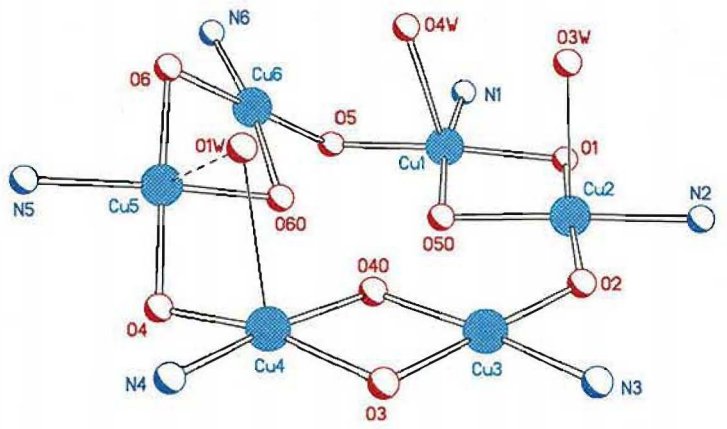

Figure 3.3.5. The coordination environments of the copper atoms in the hexacopper(II) cation $[Cu_6L^4(\mu\text{-}OH)_4]^{3+}$.

Around the hexacopper ring, the copper(II) ions are bridged alternately by single and double bridges. The single bridges are the three μ-alkoxo oxygen atoms of $(L^4)^{5-}$, with Cu-O-Cu bridge angles ranging from 111.0(4)° to 130.8(3)°. Two of the double bridges consist of a μ-phenoxo and a μ-OH^-, having Cu-O(phenoxo)-Cu angles of 99.0(3)° (O1) and 98.9(3)° (O3), and having Cu-O(H)-Cu angles of 96.4(3)° (O50) and 97.6(3)° (O40). The third double bridge consists of two μ-OH^- ions with Cu-O(H)-Cu angles of 93.8(4)° (O6) and 92.5(3)° (O60). As a consequence of this alternating single and double bridging, the Cu···Cu separations alternate between "long" and "short", respectively around the hexacopper ring [3.142(2)-3.405(2) Å for singly-bridged, 2.821(2)-2.926(2) Å for doubly-bridged].

Table 3.3.1. Selected intermolecular distances (Å) and bond angles (°) for $Cu_6L^4(\mu\text{-}OH)_4(NO_3)_3 \cdot nH_2O$ (complex **12**).

Cu1···Cu2	2.922(2)	Cu2···Cu3	3.405(2)	Cu3···Cu4	2.926(2)
Cu4···Cu5	3.142(2)	Cu5···Cu6	2.821(2)	Cu6···Cu1	3.176(2)
Cu1-O5	1.913(7)	Cu3-O2	1.874(6)	Cu5-O4	1.908(8)
Cu1-N1	1.91(1)	Cu3-O3	1.918(6)	Cu5-O6	1.933(8)
Cu1-O1	1.928(6)	Cu3-N3	1.920(7)	Cu5-O60	1.949(7)
Cu1-O50	1.967(7)	Cu3-O40	1.939(6)	Cu5-N5	1.984(9)
Cu1-O4W	2.40(1)	Cu3-O50A	3.034(7)	Cu6-O5	1.912(8)
Cu2-O2	1.871(6)	Cu4-O4	1.904(7)	Cu6-O6	1.932(8)
Cu2-O1	1.914(7)	Cu4-N4	1.907(8)	Cu6-O60	1.956(7)
Cu2-N2	1.924(7)	Cu4-O3	1.933(6)	Cu6-N6	2.02(1)
Cu2-O50	1.953(7)	Cu4-O40	1.949(6)	O40···O60	2.461(9)
Cu2-O40A	3.195(6)			O40···O50	2.482(9)
				O50···O60	2.461(9)
Cu2-Cu1-Cu6	118.38(5)	Cu1-Cu2-Cu3	117.54(5)	Cu2-Cu3-Cu4	117.40(5)
Cu3-Cu4-Cu5	119.35(5)	Cu6-Cu5-Cu4	121.73(6)	Cu5-Cu6-Cu1	120.89(6)
Cu1-O1-Cu2	99.0(3)	Cu3-O3-Cu4	98.9(3)	Cu6-O6-Cu5	93.8(4)
Cu2-O2-Cu3	130.8(3)	Cu4-O4-Cu5	111.0(4)	Cu1-O5-Cu6	112.3(4)
Cu3-O40-Cu4	97.6(3)	Cu2-O50-Cu1	96.4(3)	Cu5-O60-Cu6	92.5(3)
O5-Cu1-N1	85.0(4)	O2-Cu2-O40A	77.2(2)	O4-Cu4-N4	85.4(3)
N1-Cu1-O1	90.5(3)	O1-Cu2-O40A	100.6(3)	N4-Cu4-O3	91.0(3)
O5-Cu1-O50	102.3(3)	N2-Cu2-O40A	91.0(3)	O4-Cu4-O40	102.2(3)
O1-Cu1-O50	81.5(3)	O50-Cu2-O40A	85.0(2)	O3-Cu4-O40	81.2(3)
O5-Cu1-O4W	84.9(4)	O2-Cu3-N3	85.1(3)	O4-Cu5-O60	96.5(3)
N1-Cu1-O4W	101.3(4)	O3-Cu3-N3	92.0(3)	O6-Cu5-O60	82.5(3)
O1-Cu1-O4W	103.7(3)	O2-Cu3-O40	101.1(3)	O4-Cu5-N5	84.9(3)
O50-Cu1-O4W	84.6(3)	O3-Cu3-O40	81.8(3)	O6-Cu5-N5	96.5(4)
O2-Cu2-N2	85.3(3)	O2-Cu3-O50A	83.4(2)	O5-Cu6-O60	96.1(3)
O1-Cu2-N2	92.0(3)	O3-Cu3-O50A	98.7(2)	O6-Cu6-O60	82.3(3)
O2-Cu2-O50	100.4(3)	N3-Cu3-O50A	90.5(3)	O5-Cu6-N6	84.8(4)
O1-Cu2-O50	82.2(3)	O40-Cu3-O50A	89.9(2)	O6-Cu6-N6	97.0(4)

Transformation: -x, 1-y, -z

Each copper(II) ion in **12** has four equatorial donors (**Figure 3.3.5**). Those of Cu1, Cu2, Cu3 or Cu4 consist of an imine, a μ-phenoxo and a μ-alkoxo of $(L^4)^{5-}$, and an "inner" μ-OH^-. The donors to Cu5 or Cu6 comprise a primary amine and a μ-alkoxo of $(L^4)^{5-}$, and the two bridging μ-OH^- ions (O6 and O60). The distances from each copper(II) ion to its equatorial donors range from 1.87-2.02 Å, comparable to those observed in copper(II) complexes of related Schiff-base macrocycles.[49, 70-76]

Table 3.3.2. The r.m.s deviations of the donors and displacements of the copper atoms from the least-squares planes of the donors to each copper(II) ion in complex **12**.

	r.m.s deviation of the donors (Å)	Cu displacement (Å)
Cu1	0.028	0.105(5)
Cu2	0.061	0.033(5)
Cu3	0.020	0.013(4)
Cu4	0.092	0.109(4)
Cu5	0.108	0.078(4)
Cu6	0.086	0.065(5)

The two copper(II) ions Cu1 and Cu2 each have one monodentate axial oxygen donor (O4W and O3W, respectively), while the copper(II) ions Cu4 and Cu5 share one axial oxygen donor (O1W). These oxygen donors could possibly be water molecules or OH^- ions; the exact identity of these donors cannot be determined until the disorder in the structure is resolved.

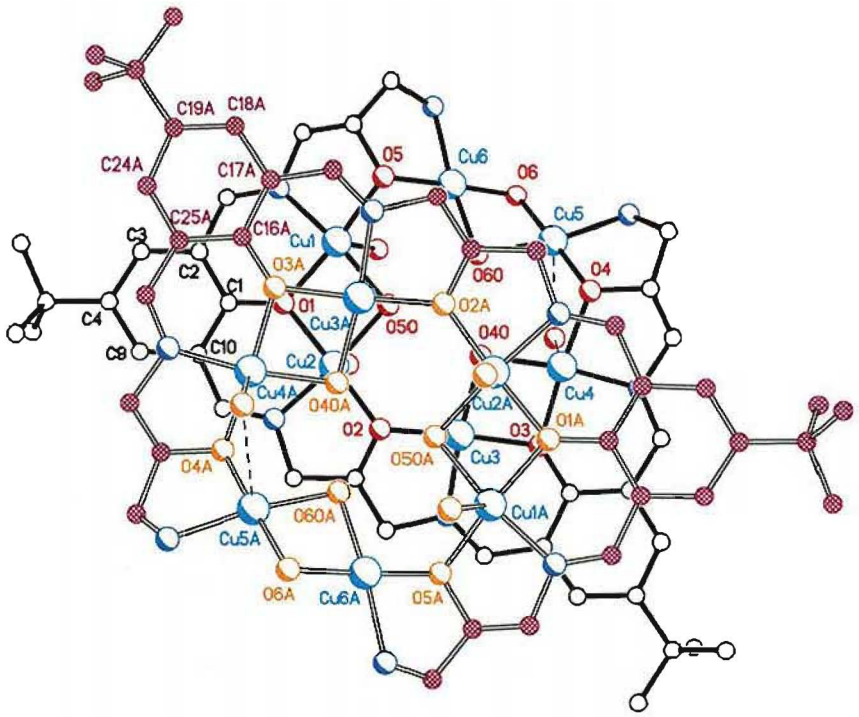

Figure 3.3.6. Arrangement of the two closest neighbouring hexacopper(II) cations $[Cu_6L^4(\mu\text{-}OH)_4]^{3+}$ in complex **12**, viewed perpendicular to the mean plane of the phenyl ring C1-C2-C3-C4-C9-C10.

In the crystal, the hexacopper(II) cations $[Cu_6L^4(\mu\text{-}OH)_4]^{3+}$ are arranged in pairs of two equivalent molecules. One of these pairs is shown in **Figure 3.3.6**. The two equivalent molecules are related by a centre of inversion and separated by *ca.* 3.4 Å. The Cu1-Cu2-Cu3-Cu4 mean planes of the two molecules are parallel to each other, while the adjacent phenyl rings are inclined at 2.0°.

The adjacent π systems (phenoldiimine moieties) of these two equivalent molecules are stacked "face-to-face", and have a laterally offset and rotated orientation with respect to each other. These observations are consistent with the presence of energetically favourable π-π interactions.[100]

Two long axial Cu···O intermolecular contacts and two symmetry-related links are present between the two adjacent hexacopper(II) cations. These links are Cu2···O40A [3.195(6) Å] and Cu3···O50A [3.034(7) Å], where O40 and O50 are two of the central μ-OH^- donors occupying the Cu6 cavity in one molecule (**Figure 3.3.7**).

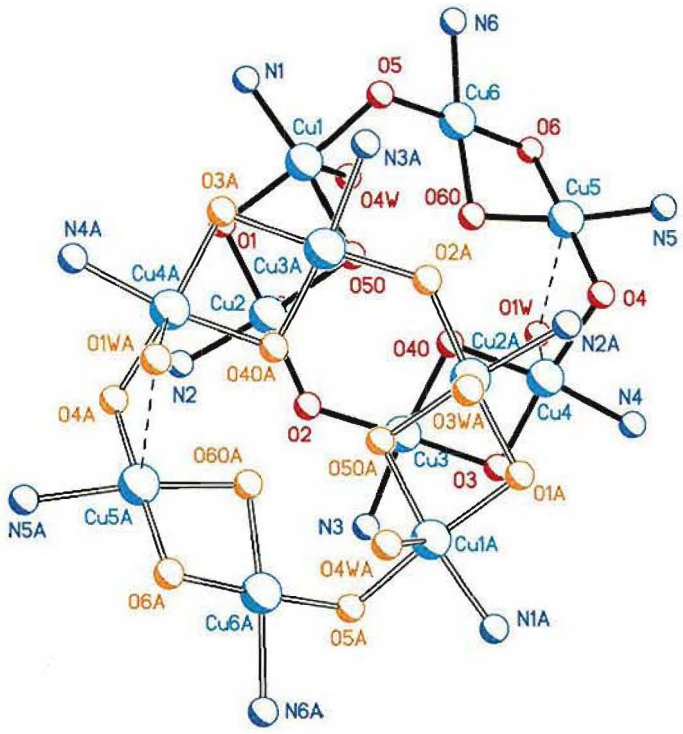

Figure 3.3.7. The coordination environments of the copper(II) ions of two adjacent cations $[Cu_6L^4(\mu\text{-}OH)_4]^{3+}$, viewed perpendicular to the least-squares plane defined by the copper atoms Cu1, Cu2 Cu3 and Cu4.

Modelling of the disorder in the structure of complex 12

The presence of a disorder in the structures of complex **11** and complex **12** mainly resulted in the appearance of an approximately tetrahedral array of residual electron density peaks in the centre of the Cu_6 core (**Figure 3.3.8**). X1, X2 and X3 coincide with O40, O50, O60; have approximately equal electron densities, and are 1.87-1.98 Å away from the nearest copper atoms. X4 lies in the centre of the tetrahedral array, while X7 is the "axial" component of the tetrahedral array. The distances and angles between the electron density peaks in this disordered region are listed in **Table 3.3.3**. In addition, two electron density peaks, X5 and X6, were also found to occupy the axial coordination sites of Cu2 and Cu1, respectively.

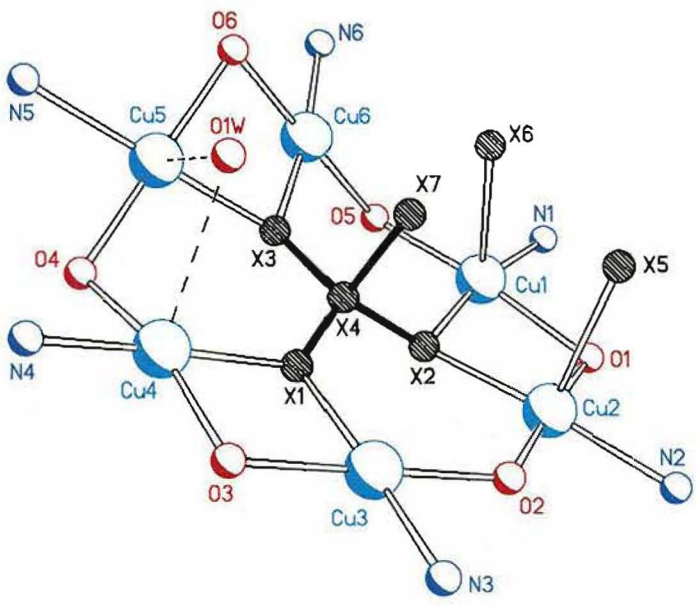

Figure 3.3.8. The copper(II) coordination environments in complex **12** showing the electron density peaks close to the copper atoms which are part of the disorder in the structure. These peaks (Xn) are numbered in order of decreasing electron density.

Table 3.3.3. Distances (Å) and bond angles (°) between the electron density peaks comprising the central bridge in the complex **12**.

X1-X4	1.45	X2-X4	1.51	X3-X4	1.45
X4-X7	1.61				
X1-X4-X2	113.8	X1-X4-X3	117.4	X2-X4-X3	117.4
X7-X4-X1	102.5	X7-X4-X2	101.8	X7-X4-X3	100.0

The main problem encountered in the refinement of the structures of complexes **11** and **12** is the modelling of the tetrahedrally-disposed electron density peaks in the centre of the Cu_6 ring of the two complexes. The structure of complex **11** is more severely disordered than that of complex **12**. Hence emphasis was placed on the structure of complex **12**, on the assumption that the tetrahedral species in complex **11** is the same as that in complex **12**, since **12** was derived from **11**.

It has been concluded (see previous discussion) that the cation $[Cu_6L^4(\mu\text{-}OH)_4]^{3+}$ is the major component of the cation of complex **12**. Since X1, X2 and X3 refine as full-occupancy oxygen atoms, these components of the tetrahedral species must not be very different from oxygen in terms of electron density. Hence the minor component of the cation would be expected to have a ligand which is tetrahedral and has three O atoms (or other atoms with similar electron density to oxygen). In addition, the three oxygen atoms of this central ligand are each capable of bridging two copper(II) ions.

The tetrahedral species cannot be a BF_4^- ion or a derivative/hydrolysis product of BF_4^- for the following reason. X4 has more electron density than X7, hence the X4-X7 peaks cannot be modelled as B-F or B-O.

On the other hand, the refinement of the structure of complex **12** converges when X4-X7 is refined as a partial-occupancy S-O or Cl-O. Thus it is possible that the tetrahedral species in the minor component of the cation is a $\mu_6\text{-}SO_4^{2-}$ or a $\mu_6\text{-}ClO_4^-$. However, the origin of these species is unclear. Neither anion was directly used in the synthesis of the complexes. One possible source of SO_4^{2-} is the 4-*t*-butyl-2,6-diformylphenol employed as the starting material.

In the current model, *ca.* 41% of the complex molecules in the crystal have a SO_4^{2-}, and *ca.* 59% have three OH^- ions in the centre of the Cu_6 ring.

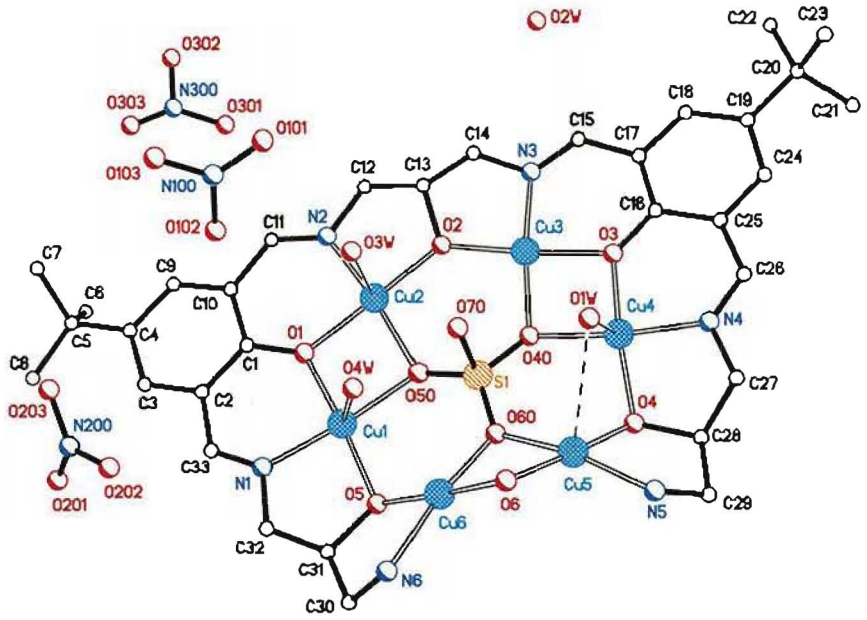

Figure 3.3.9. The current structural model used to refine complex **12**, where S1 and O70 have partial site occupancies.

Table 3.3.3. Bond lengths and angles relevant to the sulphate bridge in the minor component of the cation of complex **12**, $[Cu_6L^4(\mu\text{-}OH)(\mu_6\text{-}SO_4)]^{4+}$.

S1-O40	1.51(1)	S1-O50	1.49(1)	S1-O60	1.37(1)
		S1-O70	1.84(2)		
O40-S1-O50	111.6(6)	O50-S1-O60	118.5(7)	O60-S1-O40	116.9(6)
O40-S1-O70	104.0(9)	O50-S1-O70	103.7(9)	O60-S1-O70	98.9(9)

Complex **12A** was prepared using copper(II) nitrate as the templating agent in an attempt to obtain a hexacopper(II) complex of $(L^4)^{5-}$ which contains no tetrahedral ion. Unfortunately the yield of this preparation was quite low and the crystals recovered are too small for X-ray crystallographic data to be collected. Recrystallisation of the complexes may also yield crystalline products, each of which is composed of single component.

can use Rotating Anode to collect X-ray data if problem is size of crystal, as long as Xtal is single.

Structural comparison between the cation $[Cu_6L^4(\mu\text{-}OH)_4]^{3+}$ and the hexacopper(II) complexes of two [3+3] Schiff-base macrocycles

The Schiff-base macrocycles **MC19**, **MC20**[49] and **MC21**[103] (**Figure 3.3.10**) are able to bind six copper(II) ions inside each macrocyclic cavity in a manner similar to $(L^4)^{5-}$. The structure of $[\{Cu_6(\mathbf{MC19})(\mu\text{-}OH)_3(NO_3)\}_2]^{4+}$ [denoted $Cu_{12}(\mathbf{MC19})$][49] and of $[Cu_6(\mathbf{MC21})(\mu\text{-}OH)_2(\mu\text{-}OOCCH_3)_2(OCH_3)]^+$ [denoted $Cu_6(\mathbf{MC21})$][103] have been determined by X-ray crystallography.

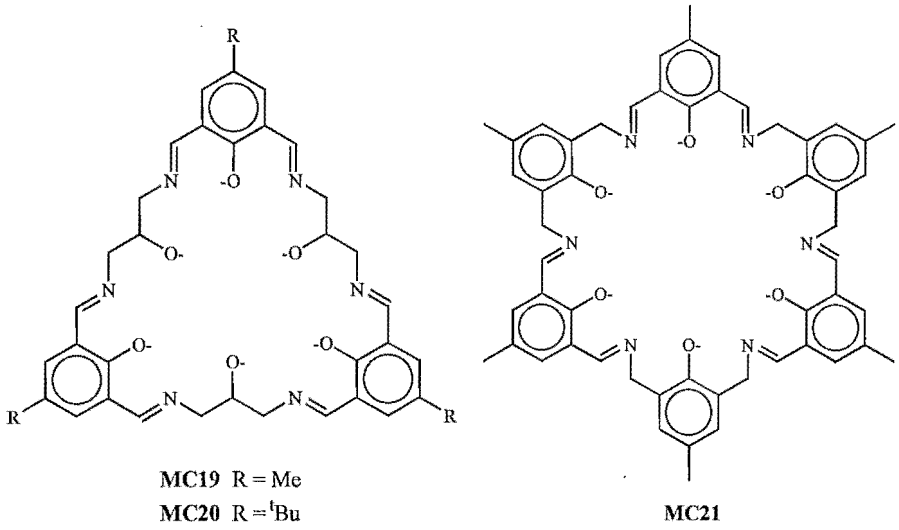

MC19 R = Me
MC20 R = ^{t}Bu

MC21

Figure 3.3.10.

The structure of $Cu_{12}(\mathbf{MC19})$ shows the complex to be dodecanuclear, and a centrosymmetric dimer of $[Cu_6(\mathbf{MC19})(\mu\text{-}OH)_3]^{6+}$ units (**Figure 3.3.11**). Some structural features of the hexacopper macrocyclic unit are similar to those of complex **12**. In the $[Cu_6(\mathbf{MC19})(\mu\text{-}OH)_3]^{6+}$ unit, the six copper(II) ions are organised into a ring-like array by the ligand. The copper atoms in $Cu_{12}(\mathbf{MC19})$ are bridged alternately by single and double bridges, resulting in an alternating "short" and "long" Cu···Cu separations, respectively. The double bridges in $Cu_{12}(\mathbf{MC19})$ involve the phenoxo groups of the ligand, while the single bridges involve the alkoxo groups.

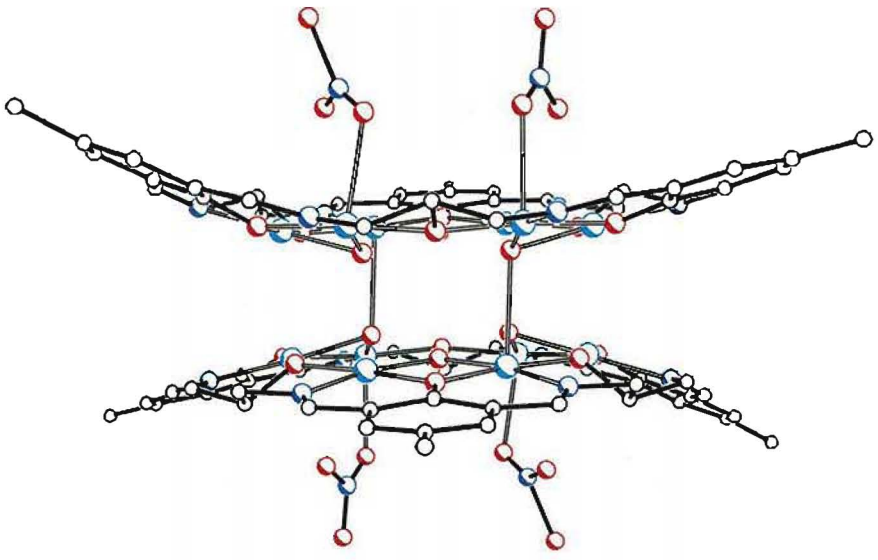

Figure 3.3.11. The structure of the dodecanuclear complex $[\{Cu_6(\mathbf{MC19})(\mu\text{-}OH)_3(NO_3)\}_2]^{4+}$ $[Cu_{12}(\mathbf{MC19})]$.

In $Cu_{12}(\mathbf{MC19})$, three hydroxo ions occupy the central cavity, each bridging a pair of copper atoms which is also bridged by a phenoxo oxygen atom. This is in contrast to the apparent tetrahedral species which occupy the Cu_6 cavity in complex **12**.

The marked difference between the structure of the macrocyclic complex and that of complex **12**, apart from the ligand structure, is the arrangement of the copper(II) ions. In the hexacopper macrocyclic unit of $Cu_{12}(\mathbf{MC19})$ the Cu_6 ring is close to being planar, in contrast to the folded arrangement of the Cu_6 core of **12**.

The planar arrangement of the copper ions in the macrocyclic complex $Cu_{12}(\mathbf{MC19})$ has been suggested[49b] to be due to the presence of alternating 6,6 and 5,5 chelate rings around the macrocyclic ring. The same chelate ring arrangement is observed in complex **12**, but the acyclic ligand $(L^4)^{5-}$ has two uncondensed "arms" which are relatively free to move. Hence this difference could be attributed to the higher degree of flexibility of the acyclic ligand $(L^4)^{5-}$ compared to the macrocyclic analogue **MC19**.

The structure of a hexacopper(II) complex of **MC21** is shown in **Figure 3.3.12**. In this complex, the macrocyclic ligand adopts a saddle-like conformation; a non-planar conformation is always observed for macrocycles which are derived from dicarbonylphenol and diaminophenol components. The six copper(II) ions are bound inside the macrocyclic ring in a boat-like arrangement, far from being planar. These features may be attributed to two factors. The first is the mismatch between the size of the macrocyclic ring (larger than that of **MC19**) and the size of a Cu6 hexagon. The second factor is the ability of the macrocycle to form twelve 6-membered chelate rings in a hexacopper complex. Another distinct structural feature of this macrocyclic complex is the presence of two, instead of three, μ-hydroxo ions in the central cavity of the Cu_6 ring.

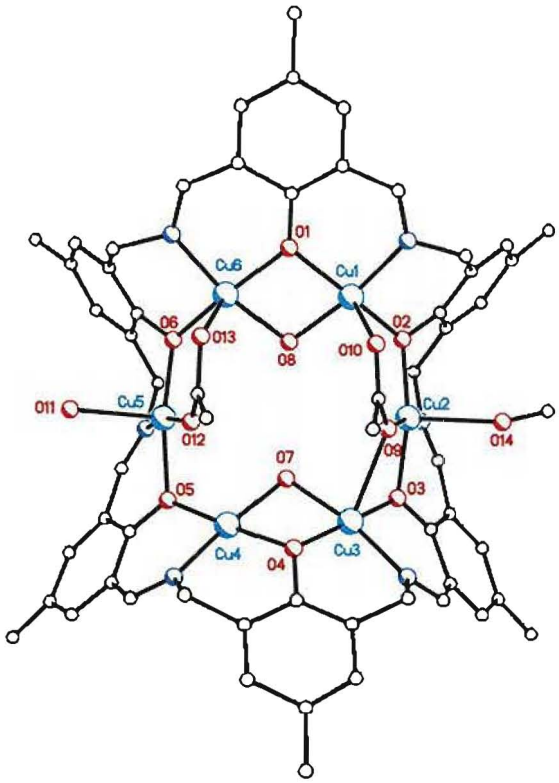

Figure 3.3.12. Structure of a hexacopper(II) complex of **MC21**,[103] showing the saddle-like conformation of the macrocyclic ligand.

3.4 Condensation of 1,5-diamino-3-hydroxypentane and 2,6-diformyl-4-methylphenol

Synthesis

In an attempt to prepare an acyclic Schiff-base ligand $L^{6'}$ (**Figure 3.4.1**), 2,6-diformyl-4-methylphenol (DFMP) was condensed with 1,5-diamino-3-hydroxypentane (1,5-DAHP) in the presence of copper(II) tetrafluoroborate template in a 1:3:3 molar ratio. Four complexes were obtained, listed in **Table 3.4.1**, three of which are complexes of the fully deprotonated macrocycle $(L^{6})^{4-}$ (**13**, **14**, **15**) and one is a dicopper complex (**16**) of the triply-deprotonated macrocycle $(HL^{6})^{3-}$ (**Figure 3.4.1**). The microanalytical data for the complexes **13** - **15** are given in **Table 3.4.1**, while selected infrared absorption bands of these complexes are given in **Table 3.4.2**. The structures of complexes **14** to **16** have been determined by single crystal X-ray structure analysis.

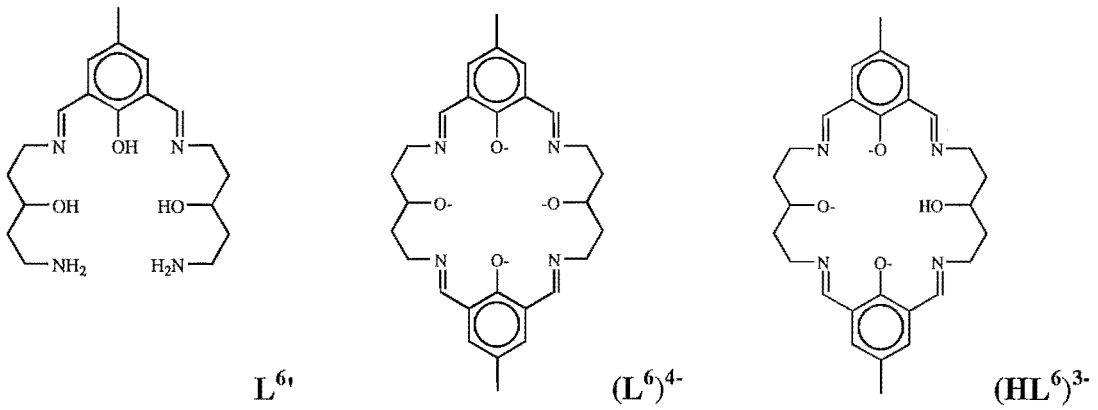

$L^{6'}$ $(L^{6})^{4-}$ $(HL^{6})^{3-}$

Figure 3.4.1.

The tetracopper complex **13** was obtained as a green precipitate directly from the reaction mixture. The infrared spectrum of this complex shows the C=N absorption at 1643 cm^{-1}, the phenol C-O at 1575 cm^{-1}, and the BF_4^- bands at 1059 and 522 cm^{-1}. No carbonyl C=O absorptions around 1700 cm^{-1} are observed. Overlapping with the broad envelope at *ca.* 3400 cm^{-1} (assigned to hydrogen bonded water molecules) are two weak bands around 3300 cm^{-1} and a broad shoulder around 3500 cm^{-1}. However, samples

from the subsequently repeated preparations (complex **13A**) did not show these latter features (see **Figure 3.4.2**; for full sized spectra see **Appendix B**).

Table 3.4.1. Complexes **13** - **16** and the microanalytical data for complexes **13** - **15**.

Complex	Formula	C	H	N
13	$Cu_4L^6(OH)(BF_4)_3(H_2O)_2$	31.99 (31.84)	3.39 (3.53)	5.67 (5.30)
14	$[\{Cu_4L^6(\mu_5\text{-}O)(BF_4)\}_2](BF_4)_2\cdot 2H_2O$	35.12 (35.39)	3.41 (3.61)	5.93 (5.90)
15·H_2O¶	$Cu_4L^6(\mu_4\text{-}OH)(HCOO)(OH)Cl\cdot 7H_2O$	35.60 (36.08)	4.32 (4.91)	6.06 (5.80)
16*	$[\{Cu_2(HL^6)(\mu_3\text{-}OH)\}_2]\cdot 4H_2O$	-	-	-

These weak bands around 3400 cm^{-1} are believed to be due to some impurity, possibly a copper(II) complex of the ligand $L^{6'}$ or some excess diamine. Complexes **13** and **13A** could be converted to the octacopper complex **14** by the same method (see below), indicating that the two complexes at least have a common macrocyclic cation. The infrared spectra show that these complexes also have BF_4^- as the counterion. In addition, the conversion to the octacopper dimer complex **14** is analogous to that of the tetracopper complex $[Cu_4(\mu_4\text{-}OH)L^6](ClO_4)_3$ to the octacopper dimer $[\{Cu_4(\mu_5\text{-}O)L^6(ClO_4)\}_2](ClO_4)_2$ (**14m**).[70] These observations and the microanalytical data suggest that complex **13** can be tentatively formulated as $Cu_4L^6(OH)(BF_4)_3(H_2O)_2$ with a proposed structure for the macrocyclic cation as illustrated in **Figure 3.4.3**.

The broad shoulder at *ca.* 3500 cm^{-1} in the infrared spectrum of **13** is probably due to the presence of non-hydrogen-bonded water molecules. Complex **13A** is believed to contain the $[Cu_4L^6(OH)(BF_4)_3]$ moiety probably along with water molecules which all form hydrogen bonds either to the other water molecules or to the BF_4^- ions. The difference between the structures of these complexes could be resolved by X-ray crystallography. However, this technique requires the complexes to be recrystallised.

¶ Crystal for X-ray structural analysis was found to have the formula containing six water molecules of crystallisation.

* The formula for complex **16** given in the table is derived from preliminary X-ray crystal structure analysis.

(a)

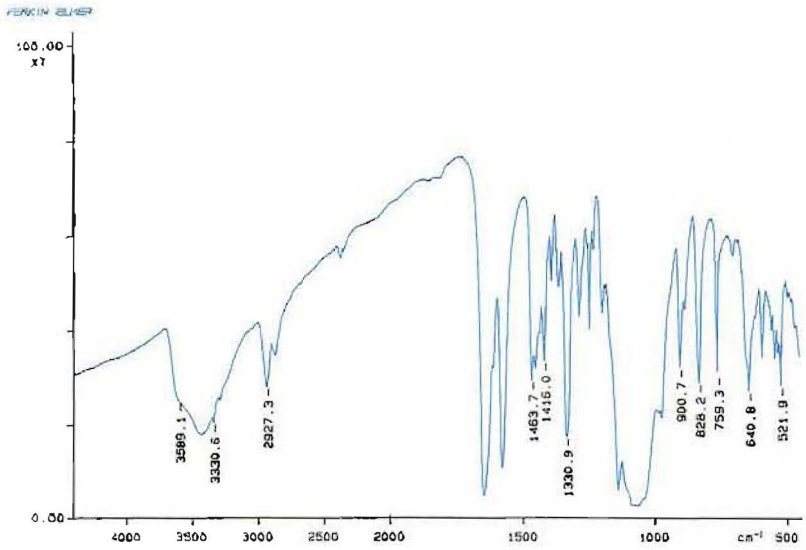

(b)

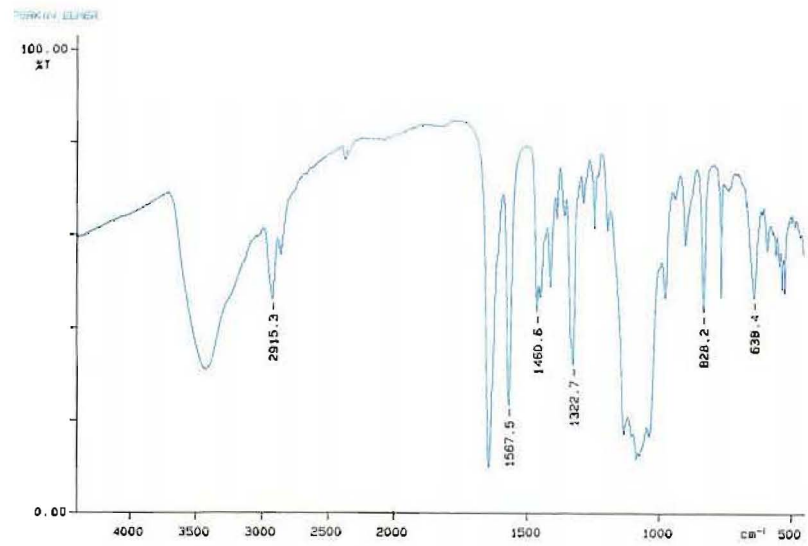

Figure 3.4.2. The infrared spectra of (a) complex **13**, and (b) complex **13A**.

Table 3.4.2. Infrared absorptions (cm^{-1}) of complexes **13** - **15** (s = sharp, b = broad; intensity: S = strong, M = medium).

Complex	aquo	ν(C=N)	ν(C=O)	ν(BF_4)
13	3423 M, b	1643 S, s	1575 S, s	1059 S, b
14	3439 M, b	1646 S, s	1576 S, s	1064 S, b
15	3482 M, b	1647 S, s 1632 S, s	1587 S, s 1570 S, s	none

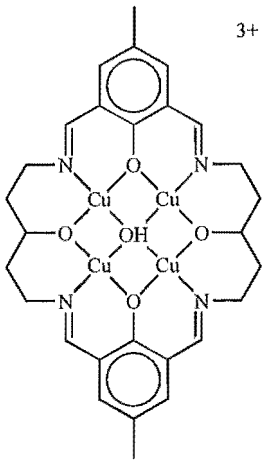

Figure 3.4.3. The proposed chemical structure of $Cu_4L^6(OH)(BF_4)_3(H_2O)_2$ (**13**).

Depending on the method of recrystallisation, the recrystallised complex could have quite a different structure from that of the original complex, as will be seen in the following discussion.

Recrystallisation of complex **13** gave $[\{Cu_4L^6(\mu_5\text{-}O)(BF_4)\}_2](BF_4)_2\cdot 2H_2O$ (**14**) or $[Cu_4L^6(\mu_4\text{-}OH)(\mu\text{-}HCOO)(OH)Cl]\cdot 6H_2O$ (**15**)*, depending on the conditions used. The octacopper dimer **14** was obtained from DMF by diethylether vapour diffusion, while the tetracopper complex **15** was obtained as hexagonal green crystals by slow evaporation of the DMF solution of **13**. The structures of complexes **14** and **15** have been determined by X-ray crystallographic studies and will be presented in the following discussion.

* The formula with six water molecules of crystallisation is obtained from X-ray crystal structure analysis.

Structure of $[\{Cu_4L^6(\mu_5\text{-}O)(BF_4)\}_2](BF_4)_2\cdot H_2O$ (14)

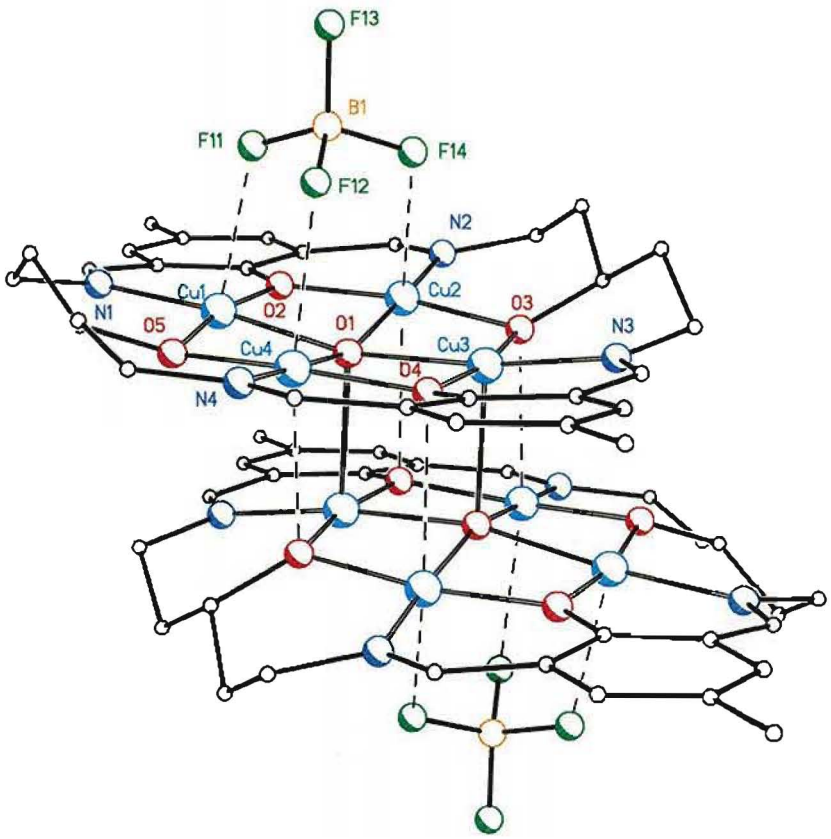

Figure 3.4.4. A perspective view of $[\{Cu_4L^6(\mu_5\text{-}O)(BF_4)\}_2]^{2+}$, the octacopper(II) dimeric cation of **14**.

X-ray crystallographic study revealed that complex **14** is a centrosymmetric octacopper dimer, consisting of two tetracopper(II) macrocyclic units (illustrated in **Figure 3.4.3**). The formula unit is completed by two uncoordinated BF_4^- anions and two half-occupancy water molecules. One symmetry-related pair of BF_4^- anions coordinates to the "open" faces of the octacopper dimer (**Figure 3.4.4**). The second tetrafluoroborate ion in the asymmetric unit shows a rotational disorder about one of its B-F bonds. Selected interatomic distances and bond angles are given in **Tables 3.4.3** and **3.4.4**, respectively. The coordination environment of the eight copper ions in the dimer is illustrated in **Figure 3.4.5**.

Four copper(II) ions are bound in an approximate square-planar array within each macrocyclic unit of complex **14** [deviations of the copper atoms from their mean

plane < 0.04 Å; 'diagonal' Cu···Cu = 4.016(2) Å and 4.072(2) Å; Cu-Cu-Cu angles are between 88.80(4)° and 91.07(4)°]. The Cu···Cu distances that form the 'sides' of the square are short but non-bonding [2.83-2.91 Å].[104] The oxygen donors of the macrocycle are all deprotonated; each of these oxygen donors bridges two copper ions with Cu-O-Cu bridge angle between 96.8° and 98.3°.

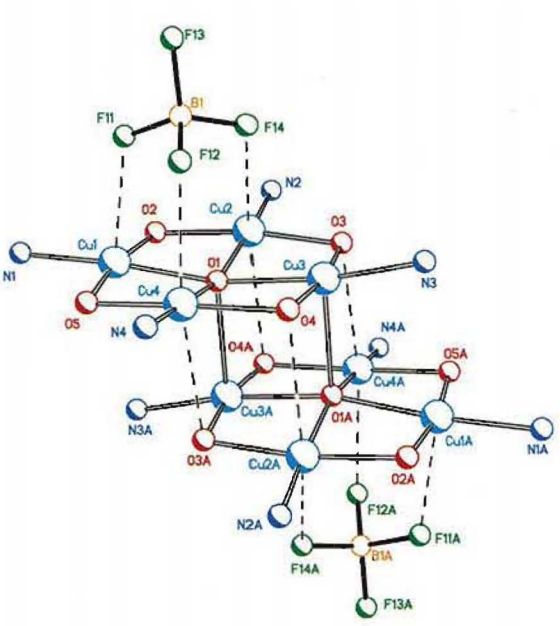

Figure 3.4.5. Coordination environments of the octacopper(II) core in $[\{Cu_4L^6(\mu_5\text{-}O)(BF_4)\}_2](BF_4)_2{\cdot}2H_2O$ (**14**).

Table 3.4.3. Intermolecular distances (Å) relevant to the copper(II) coordination environments in $[\{Cu_4L^6(\mu_5\text{-}O)(BF_4)\}_2](BF_4)_2{\cdot}2H_2O$ (**14**).

Cu1···Cu2	2.872(2)	Cu3···Cu4	2.905(1)
Cu1···Cu4	2.833(1)	Cu1···Cu3	4.072(2)
Cu2···Cu3	2.834(1)	Cu2···Cu4	4.016(2)
Cu3···Cu3A	3.224(2)	Cu3-O1	2.061(4)
Cu1-O1	2.034(4)	Cu3-O3	1.907(4)
Cu1-O2	1.900(4)	Cu3-O4	1.935(4)
Cu1-O5	1.867(4)	Cu3-N3	1.969(6)
Cu1-N1	1.966(5)	Cu3···O1A	2.363(4)
Cu1···F11	2.463(4)	Cu3···F14	3.164(4)
Cu2-O1	2.018(4)	Cu4-O1	2.045(4)
Cu2-O2	1.901(4)	Cu4-O4	1.923(4)
Cu2-O3	1.883(4)	Cu4-O5	1.878(4)
Cu2-N2	1.958(5)	Cu4-N4	1.971(6)
Cu2···F14	2.836(4)	Cu4···F12	2.528(4)
Cu2···O4A	2.795(4)	Cu4···O3A	2.702(4)

Transformation: A = 1-x, 1-y, -z

Table 3.4.4. Bond angles (°) relevant to the copper(II) coordination environments in $[\{Cu_4L^6(\mu_5\text{-}O)(BF_4)\}_2](BF_4)_2\cdot 2H_2O$ (**14**).

Cu1-O1-Cu2	90.3(2)	Cu3-O1-Cu4	90.0(2)
Cu1-O1-Cu4	88.0(2)	Cu2-O1-Cu3	87.9(2)
Cu1-O1-Cu3A	99.4(2)	Cu3-O1-Cu3A	93.3(2)
Cu2-O1-Cu3A	99.2(2)	Cu4-O1-Cu3A	98.4(2)
Cu1-O2-Cu2	98.2(2)	Cu3-O4-Cu4	97.7(2)
Cu2-O3-Cu3	96.8(2)	Cu4-O5-Cu1	98.3(2)
N1-Cu1-O2	92.4(2)	N3-Cu3-O3	96.6(2)
N1-Cu1-O5	96.6(2)	N3-Cu3-O4	91.0(2)
O1-Cu1-O2	84.7(2)	O1-Cu3-O3	86.1(2)
O1-Cu1-O5	85.9(2)	O1-Cu3-O4	85.5(2)
O5-Cu1-F11	95.8(2)	O1A-Cu3-O1	86.7(2)
N1-Cu1-F11	96.3(2)	O1A-Cu3-O3	91.0(2)
O2-Cu1-F11	87.9(2)	O1A-Cu3-O4	93.2(2)
O1-Cu1-F11	89.9(2)	O1A-Cu3-N3	102.5(2)
N2-Cu2-O2	90.6(2)	N4-Cu4-O4	92.1(2)
N2-Cu2-O3	96.0(2)	N4-Cu4-O5	96.4(2)
O1-Cu2-O2	85.1(2)	O1-Cu4-O4	86.3(2)
O1-Cu2-O3	88.0(2)	O1-Cu4-O5	85.3(2)
O3-Cu2-F14	83.0(2)	O5-Cu4-F12	92.2(2)
N2-Cu2-F14	110.8(2)	N4-Cu4-F12	93.1(2)
O2-Cu2-F14	100.0(2)	O4-Cu4-F12	91.0(2)
O1-Cu2-F14	73.0(1)	O1-Cu4-F12	85.8(2)
O4A-Cu2-O2	90.9(2)	O3A-Cu4-O4	84.6(2)
O4A-Cu2-O1	79.5(1)	O3A-Cu4-O1	79.0(1)
O4A-Cu2-N2	97.6(2)	O3A-Cu4-N4	102.1(2)
O4A-Cu2-O3	82.6(2)	O3A-Cu4-O5	90.1(2)

Transformation: A = 1-x, 1-y, -z

The equatorial coordination plane of each copper ion consists of a phenoxo oxygen, an alkoxo oxygen and an imine nitrogen from one macrocyclic ligand, and a μ_5-O^{2-} (O1) which is situated in the centre of the four copper atoms in one macrocyclic unit. The oxo ion also coordinates to a copper ion from the second macrocyclic unit [O1-Cu3A = 2.363(4) Å]. This coordination causes the O1 to be displaced by 0.269(4) Å from the mean plane of the four copper atoms in one macrocyclic unit, and Cu3 to be displaced from its equatorial O_3N plane, towards the second macrocyclic unit. The remaining copper ions in one macrocyclic unit are displaced from their O_3N coordination planes towards a weakly and axially coordinating tetrafluroborate ion, and away from the second macrocyclic unit. The O_3N coordination planes are all

approximately planar, with deviations from the O_3N plane of less than 0.043(2) Å. The displacements of the copper ions from their coordination planes are as follows: Cu1 0.275(5) Å, Cu2 0.389(4) Å, Cu3 0.317(6) Å, and Cu4 0.021(2) Å.

The O1-Cu3A bond, and its symmetry-related equivalent O1A-Cu3, form two strong links between the two macrocyclic units in the octacopper dimer. Two other Cu···O interactions [Cu2···O4A = 2.795(4) Å; Cu4···O3A = 2.702(4) Å] form weaker interactions. Centrosymmetric symmetry requires two other weaker linkages to be present between the tetracopper units of the dimer.

Oxo ions having five-coordinate and square-pyramidal geometry such as those observed in the octacopper(II) dimer **14**, are not common in transition metal complexes, but have been observed in the two other octacopper(II) macrocyclic complexes,[70] mentioned previously (**14m** and **14b**). The unusual coordination mode of O1 and the slight mismatch between the size of the Cu_4 cavity cause the copper-oxo bonds to be weaker than the other equatorial bonds of the copper. This is indicated by the significantly longer Cu-O1 bonds [2.02 - 2.06 Å] and by the more compressed Cu-O1-Cu angles [88.0 - 90.3°], compared to the bonds and angles involving the copper ions and the other macrocyclic donors.

Two symmetry-related tetrafluroborate ions weakly coordinate to the "open" faces of the octacopper macrocyclic dimer (see **Figures 3.4.3** and **3.4.4**) in a tripodal fashion (**Figure 3.4.5a**). Each of these BF_4^- ions interacts through three of its fluorine atoms with the four copper ions in one macrocyclic moiety. Two of these interactions are relatively strong [Cu1···F11 = 2.463(4) Å; Cu4···F12 = 2.528(4) Å] and two are relatively weak [Cu2···F14 = 2.836(4) Å; Cu3···F14 = 3.164(4) Å].

The shortest Cu-F interaction in complex **14** involves the copper ion which has no axial interaction on the opposite side of the macrocyclic plane (Cu1) while the longest Cu-F interaction involves the copper ion which has a strong axial bond to the oxo anion of the second tetracopper macrocyclic unit (Cu3). These observations suggest that distinct bonds are present between the tetrafluroborate ion and the copper ions, analogous to the observations and conclusion reported by M^{c}Kee[70] for perchlorate coordination to the two octacopper(II) macrocyclic dimers **14m** and **14b** (**Figure 3.4.6**).

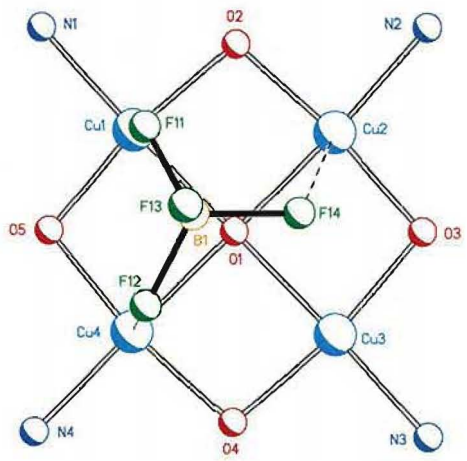

(a)

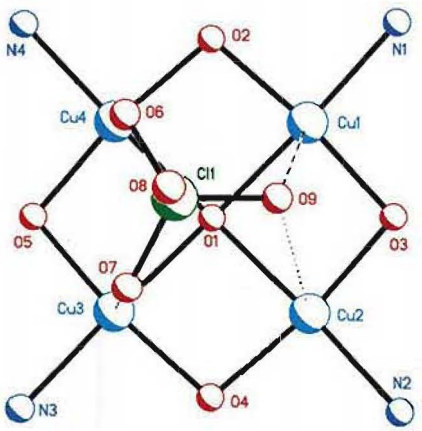

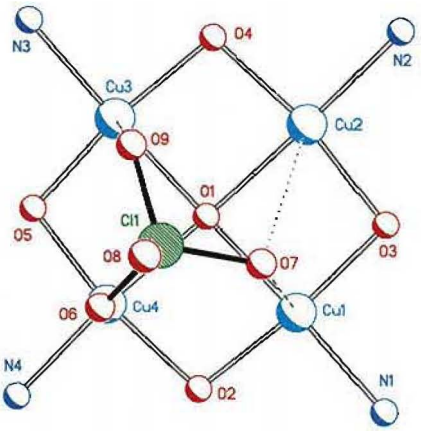

(b) (c)

Figure 3.4.6. View perpendicular to the least-squares plane of the four copper atoms in one macrocyclic unit of the dimer (a) $[\{Cu_4L^6(\mu_5\text{-}O)(BF_4)\}_2](BF_4)_2{\cdot}2H_2O$ (**14**), (b) $[\{Cu_4L^6(\mu_5\text{-}O)(ClO_4)\}_2](ClO_4)_2$ (**14m**); and (c) $[\{Cu_4(\mathbf{MC18})(\mu_5\text{-}O)(ClO_4)\}_2](ClO_4)_2$ (**14b**), showing two possible geometries of tripodal coordination of tetrafluoroborate or perchlorate ion to a Cu_4 surface.

The coordination geometry of the BF_4^- to the four copper(II) ions in complex **14** is the same as that of ClO_4^- to the four copper(II) ions in **14m** (**Figure 3.4.6b**). The anion in this coordination geometry has two relatively strong interactions with two of the copper(II) ions, and two weaker interactions with the other two copper(II) ions. Another tripodal coordination geometry is shown by the perchlorate ion in **14b** (**Figure 3.4.6c**), where the anion has three relatively strong interactions with three of the copper(II) ions and one weak interaction with the fourth copper(II) ion.

A recent survey of the Cambridge Structural Database shows that **14** is the first crystallographically characterised transition metal complex having a BF_4^- ion coordinated to four metal ions in a tripod-like fashion. In general, tetrafluoroborate ion does not coordinate to transition metal ions, although there are several structurally characterised transition metal complexes which have BF_4^- ions coordinating to the metal centres.[105] Most of these complexes contain BF_4^- ions coordinating to the metal ions through one of the F atoms. However, a few of the complexes[105a,b] have BF_4^- ions in a μ-1,3 bridging geometry, binding to two metal ions through two of the F atoms, and one complex[105c] has one BF_4^- ion coordinating to three rhenium ions through three of the F atoms.

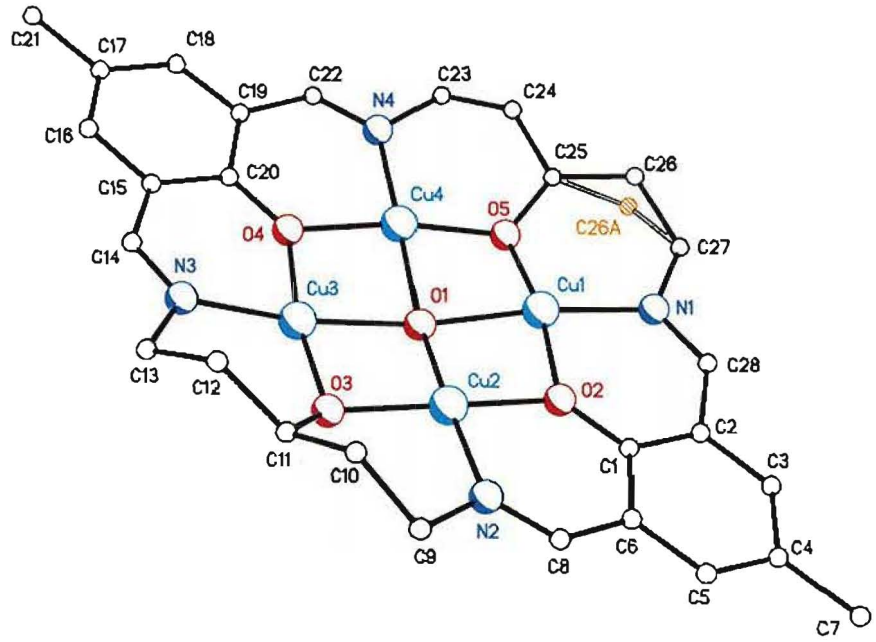

Figure 3.4.7. Perspective view of the tetracopper macrocyclic unit of $[\{Cu_4L^6(\mu_5\text{-}O)(BF_4)\}_2](BF_4)_2{\cdot}2H_2O$ (**14**).

The tetracopper macrocyclic unit (**Figure 3.4.7**) in the octacopper dimer **14** has a slightly dished conformation, with the two phenyl rings being inclined at174.5° away from the second macrocyclic unit. The second and fourth carbon atoms of the saturated, alkoxo containing, "side" of the [2+2] macrocycle show the most significant deviations from the macrocyclic plane. One of these carbon atoms is disordered between two positions (**Figure 3.4.7**) with occupancies of ca. 60% for the major site (C26) and ca.

40% for the minor site (C26A). These two sites lie on the opposite sides of the macrocyclic plane.

The geometries about the phenoxo oxygen atoms (O2 and O4) may be described as distorted trigonal planar (the sums of the angles at these O-atoms being 359.9(3)° and 357.6(3)°, respectively; the Cu-O-C angles are between 128° and 132°, while the Cu-O-Cu angles are less than 99°). This is expected for phenoxo oxygen that is bridging. The alkoxo oxygen atoms deviate from planarity more than the phenoxo oxgyen atoms, with the sums of the angles about O3 and O5 being 347.7(3)° and 351.0(3)°, respectively. However, the Cu-O-C angles at these alkoxo oxygens are between 124° and 127°. In contrast, the imine nitrogen atoms are all planar [sum of the angles at the nitrogen atom = 360.0(5)° for all imine nitrogen].

The ligand also has a slight "step" conformation. The least-squares plane of the C1-C6 ring is inclined at 8.1° "below", while the least-squares plane of the C15-C20 is inclined at 12.6° "above" the least-squares plane of the Cu_4-core (the second macrocyclic unit of the dimer is located "below" the least-squares plane of the Cu_4-core of the first unit).

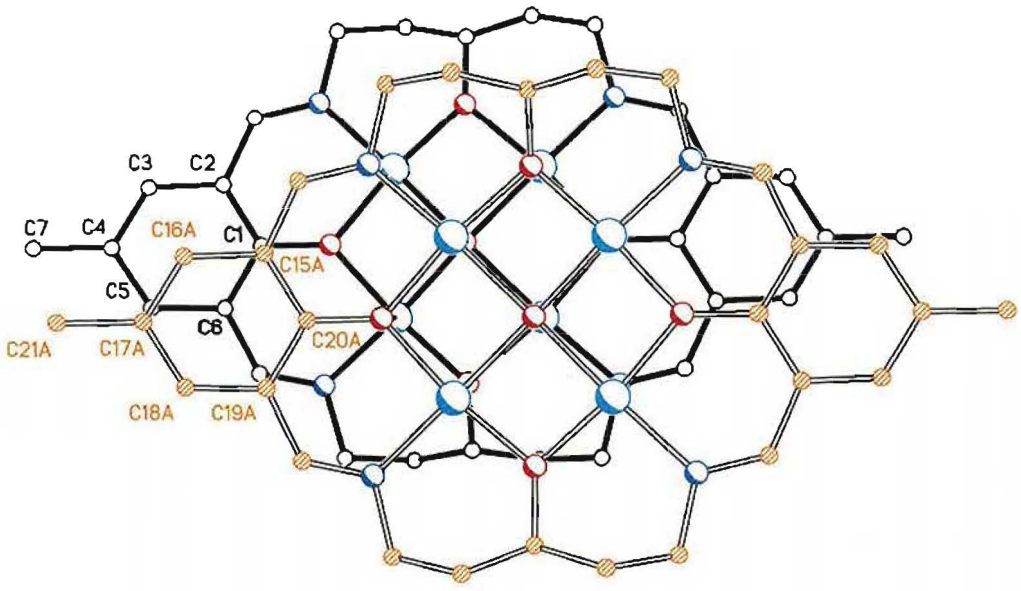

Figure 3.4.8. View perpendicular to the mean plane of C1-C6 of the octacopper(II) dimer $[\{Cu_4L^6(\mu_5\text{-}O)(BF_4)\}_2]^{2+}$ of **14**, showing the overlay between two adjacent π systems in the macrocyclic dimer. The coordinated tetrafluoroborate ions are omitted for clarity.

Intramolecular π-π interactions are present between the two adjacent macrocycles in one molecule, made possible by the parallel arrangement of the two macrocyclic units (**Figure 3.4.8**). The adjacent phenyl rings of the two macrocycles are separated by *ca.* 3.3 Å and almost parallel (the least-squares planes of the phenyl rings are inclined at 5.5°). The π systems of the two macrocyclic units are laterally offset but still show some overlap. These interactions are also responsible for holding the two macrocyclic halves of the octacopper dimer **14** as well as the Cu-O interactions described previously.

One of the phenyl rings (C15 to C20) of each macrocycle in the dimer is *ca.* 3.4 Å apart from an equivalent ring of an adjacent dimer (**Figure 3.4.9**). The two phenyl rings are stacked "face-to-face", however, they are more laterally offset than those within the dimer. These observations indicate the presence of attractive intermolecular π-π stacking interactions which lead to the packing of the dimers into layers. These layers extend approximately parallel to the *ab* plane of the unit cell (**Figure 3.4.10**).

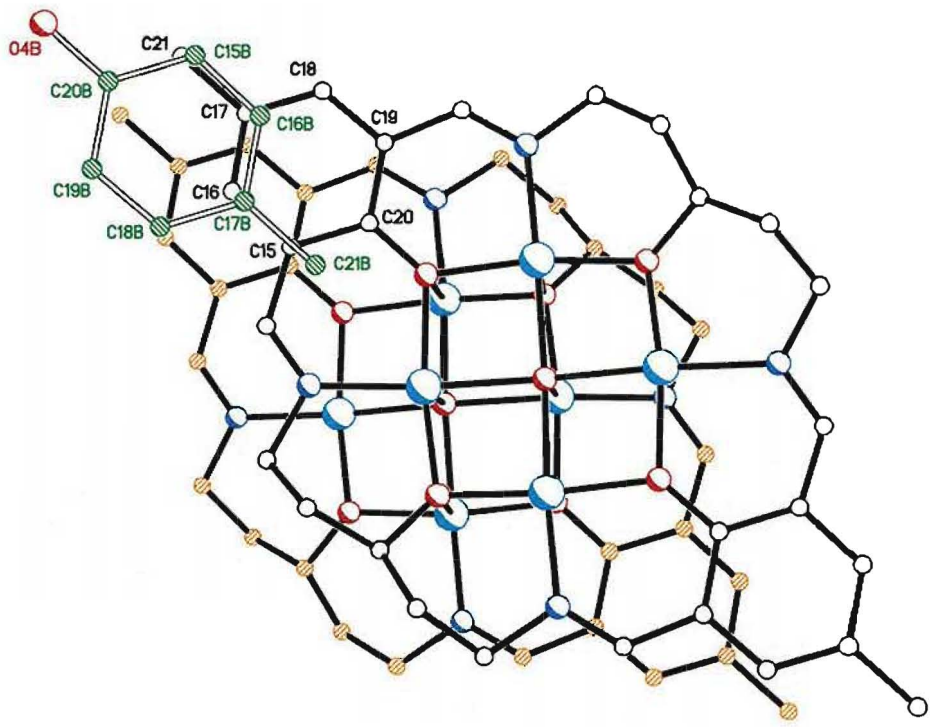

Figure 3.4.9. View perpendicular to the mean plane of the 6-membered ring C15B to C20B, showing the π-π interactions between two dimeric cations $[\{Cu_4L^6(\mu_5\text{-}O)(BF_4)\}_2]^{2+}$ in **14**. Only the 4-methylphenol fragment of the second dimer, which interacts with the first dimer, is shown for clarity (white bonds).

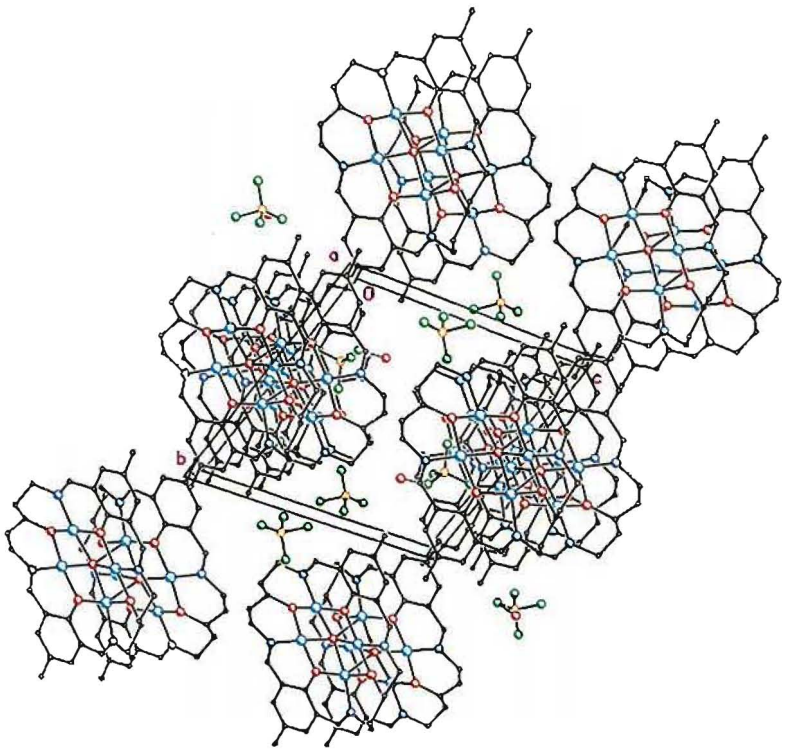

Figure 3.4.10. Molecular packing of $[\{Cu_4L^6(\mu_5\text{-}O)(BF_4)\}_2](BF_4)_2{\cdot}2H_2O$ (**14**), showing the π-π stacking of the molecules.

The space between the layers of macrocyclic units is filled with the BF_4^- ions which do not coordinate to the copper ions, that is, those BF_4^- involving B2, F21, F22, F23 and F24. This BF_4^- ion is disordered between two positions (**Figure 3.4.11**) with occupancies of 54% for one orientation [B2-F21-F22-F23-F24] and 46% for the second one [B2-F21-F22'-F23'-F24'], and forms two hydrogen bonds with the water molecule O1W from different unit cells (F23···O1WA = 2.66 Å; F22···O1WB = 2.85 Å; F22···O1WA = 3.08 Å).

The water molecule O1W also hydrogen bonds with the second water molecule O2W with O1W···O2W distance of 2.85 Å. Another hydrogen bond is present between the BF_4^- ion which is coordinated to the copper ions (the one involving B1), and O2W from a different unit cell (F13···O2WA = 2.61 Å). Two dimers in the crystal lattice, which are related by the transformation 2-x, 2-y, -1-z, are linked by hydrogen bonds in the manner shown in **Figure 3.4.12**.

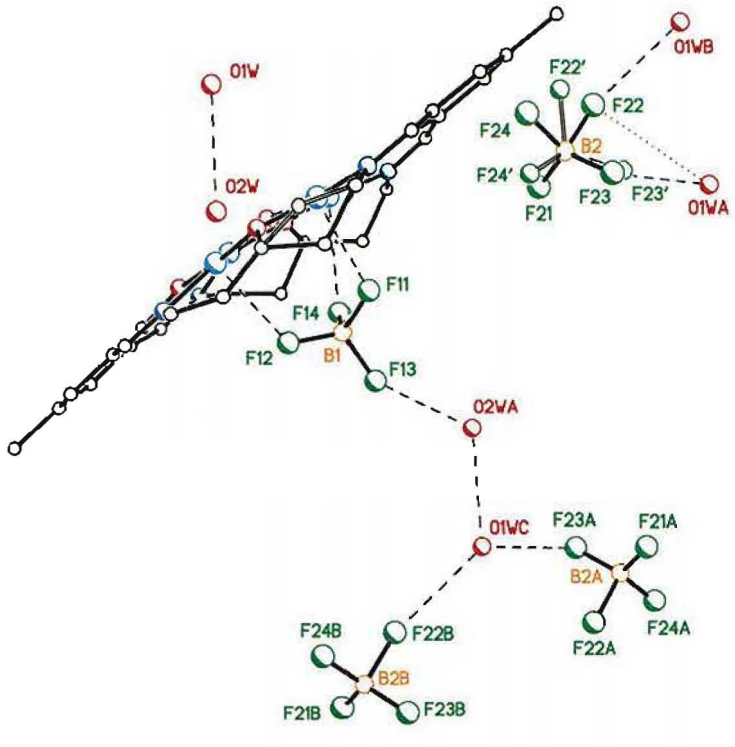

Figure 3.4.11. Details of hydrogen bonding interactions within the molecule of $[\{Cu_4L^6(\mu_5\text{-}O)(BF_4)\}_2](BF_4)_2{\cdot}2H_2O$ (**14**). Also shown is the disorder in one of the BF_4^- ions. The second half of the macrocyclic dimer is omitted for clarity.

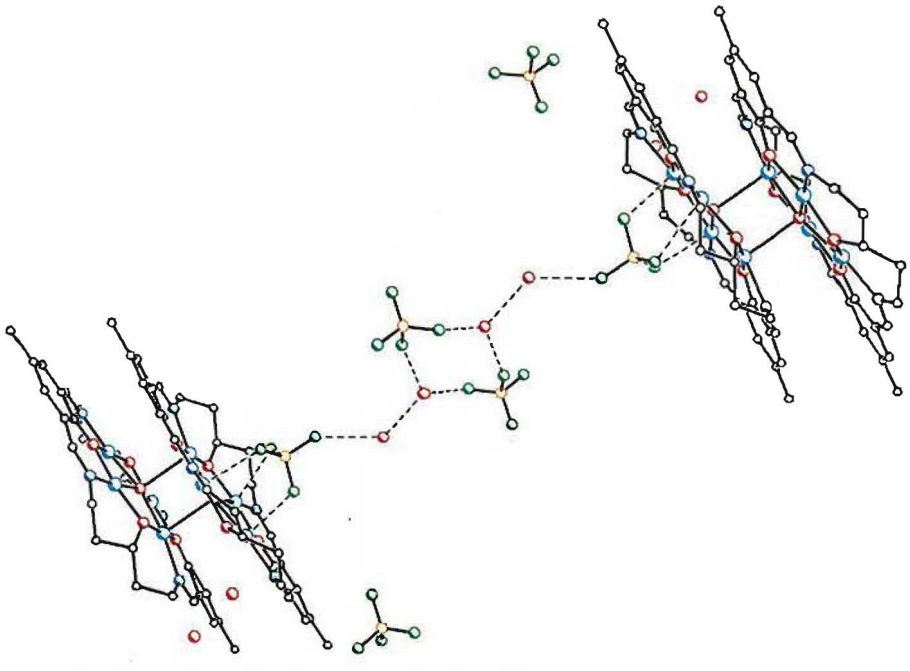

Figure 3.4.12. Hydrogen bonding interactions in $[\{Cu_4L^6(\mu_5\text{-}O)(BF_4)\}_2](BF_4)_2{\cdot}2H_2O$ (**14**).

Structural comparison with related macrocyclic dimers

Several macrocyclic complexes which form dimeric structures have been reported.[50, 70, 106] Closely related to the structure of $[\{Cu_4L^6(\mu_5\text{-}O)(BF_4)\}_2](BF_4)_2\cdot 2H_2O$ (**14**) are the structures of $[\{Cu_4L^6(\mu_5\text{-}O)(ClO_4)\}_2](ClO_4)_2\cdot 2H_2O$ (**14m**) and $[\{Cu_4(\mathbf{MC18})(\mu_5\text{-}O)(ClO_4)\}_2](ClO_4)_2$ (**14b**) (**Figure 3.4.13**), where **MC18** is the [2+2] macrocycle analogous to $(L^6)^{4-}$, having t-butyl substituents instead of methyl, on the phenyl rings of the macrocycle (**Figure 1.24a**).

The structures of **14m** and **14b** show ClO_4^- ions coordinated to the open face of the macrocyclic dimers in a tripodal manner. This is analogous to the BF_4^- ions coordination to the cation $[\{Cu_4L^6(\mu_5\text{-}O)\}_2]^{4+}$ in complex **14** (see previous discussion on BF_4^- coordination in complex **14**). The ability of the octacopper complexes to bind these substrates on their Cu_4O plane points to the possibility of carrying out metal-promoted reactions on the surface of the macrocyclic complex. The binding of various substrates is currently being investigated by McKee.[106a]

The complexes **14** and **14m** both contain the octacopper(II) cation $[Cu_4L^6(\mu_5\text{-}O)]_2^{4+}$. The structures of the cations in both complexes are almost identical, differing only in minor details. While the structure of the octacopper cation $[Cu_4(\mathbf{MC18})(\mu_5\text{-}O)]_2^{4+}$, present in **14b**, differs from the first cation mainly in the substituents on the macrocyclic phenyl rings. Complex **14m** was obtained by slow ether diffusion into DMF solution of its tetracopper analogue,[70] which is how complex **14** was obtained. These observations suggest that complexes **14** and **14m** were formed by the same mechanism.

The mechanism by which complexes **14m** and **14b** were formed from their respective tetracopper analogue has been established[70] by using electronic spectroscopy and is illustrated in **Figure 3.4.14**.

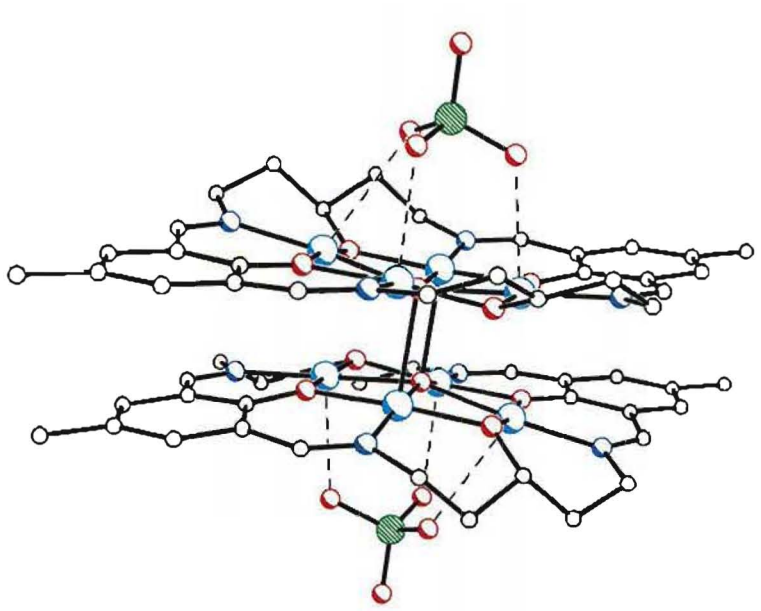

(a)

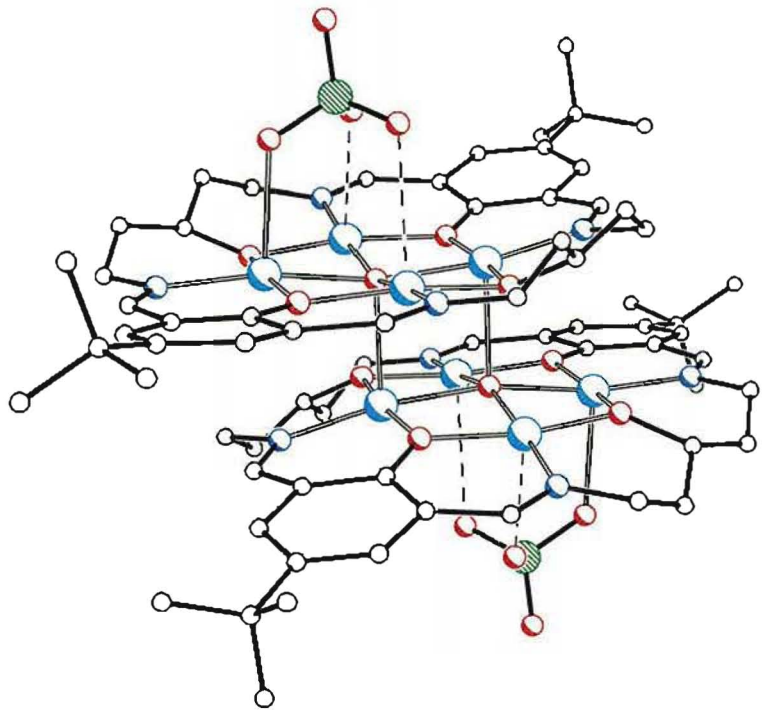

(b)

Figure 3.4.13. Structures of the cations of (a) $[\{Cu_4L^6(\mu_5\text{-}O)(ClO_4)\}_2](ClO_4)_2{\cdot}2H_2O$ (**14m**); (b) $[\{Cu_4(\mathbf{MC18})(\mu_5\text{-}O)(ClO_4)\}_2](ClO_4)_2$ (**14b**).[70]

The change with time of the d-d bands in the electronic spectra (DMF solution) of the tetracopper analogues, in the absence and presence of a base was monitored and showed the following results[70]. The spectra of the freshly prepared DMF solution of the tetracopper complexes correspond closely with the reflectance spectra of the respective complexes. In the absence of an added base, the solution spectra slowly changes to those of the respective octacopper complexes within a few days. In the presence of a base, the spectral change took place within seconds. It was also noted[70] that the conversion of the tetracopper complex to the octacopper complex was promoted by a base, and the reverse reaction is promoted by the addition of a small amount of acid.

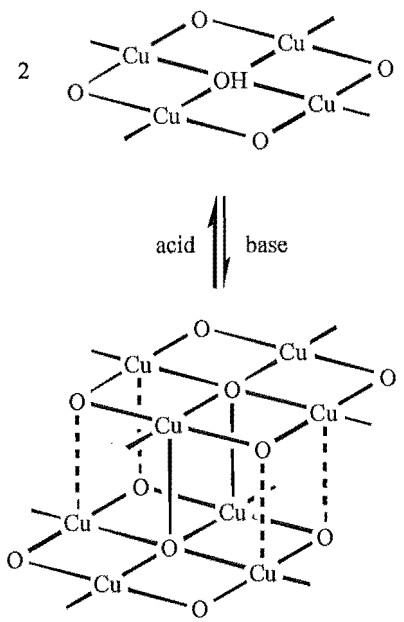

Figure 3.4.14. Dimerisation of a tetracopper complex $[Cu_4L(\mu_4\text{-}OH)]^{3+}$ into an octacopper complex $[\{Cu_4L(\mu_5\text{-}O)\}_2]^{4+}$, where L is the tetraimine Schiff-base macrocycles $(L^6)^{4-}$ or **MC18**.[70]

This behaviour is ascribed to a competition for the central oxygen ligand between protons and macrocycle-bound copper atoms. In protic solutions such as ethanol or methanol, the tetracopper complex with hydroxo in the centre is favoured. In less protic solution (DMF), the octacopper complex is preferred although the rate of conversion is slow. The addition of a base can assist deprotonation of the central hydroxo ion in the tetracopper complex, thereby increasing the rate of formation of the octacopper complex.

The relative orientation of the macrocycles in the octacopper dimer **14** is in contrast to that of the macrocycles in the tetranickel complex $[\{Ni_2L^2(MeCO_2)_2\}_2]^{2+}$ (**Figure 3.4.15**).[106b, 106c] The structure of the latter complex shows the two macrocycles oriented 90° relative to each other. Each macrocyclic dinickel unit in this dimer is bent away from the adjacent unit (the mean planes of the phenyl rings in a macrocyclic unit are inclined at 104°), in contrast to the near planar structure of the macrocyclic unit in **14**.

The complex also shows a Ni_4O_4 core with a cubane-type structure. It was suggested[106b, 106c] that the structure of this Ni_4O_4 core in the dimer is one of the reasons for the bending of the macrocyclic ligand. Another reason suggested is a that bending avoids steric interactions between the two macrocyclic units. Each nickel(II) ion is in an approximate octahedral environment. It was proposed that the requirement of the Ni(II) centres to have octahedral geometries is the driving force for the dimerisation.

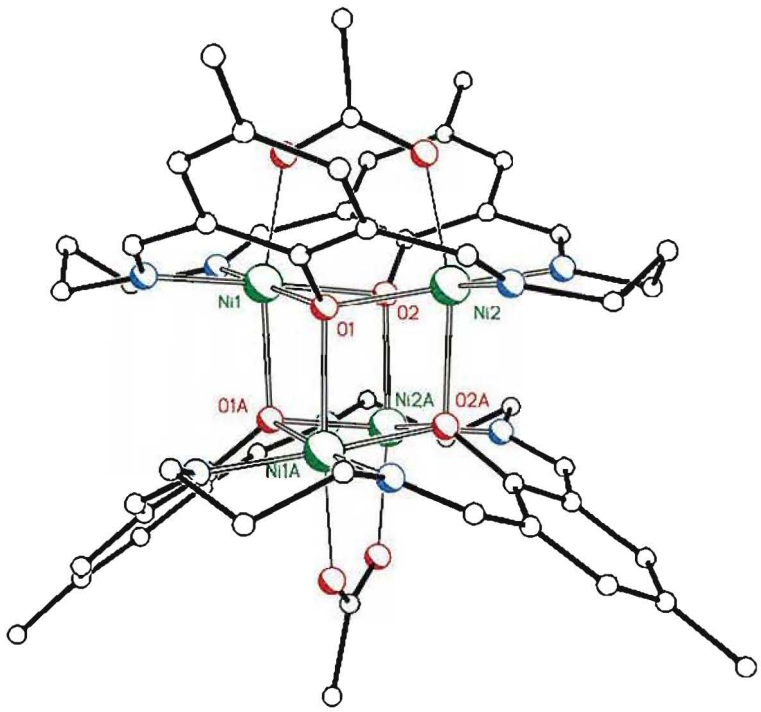

Figure 3.4.15. Structure of the tetranickel(II) dimer $[\{Ni_2L_2(MeCO_2)_2\}_2]^{2+}$.[106b, 106c]

Structure of $Cu_4L^6(\mu_4\text{-}OH)(\mu\text{-}HCOO)(OH)Cl\cdot 6H_2O$ (15)

X-ray crystal structure analysis of complex **15** revealed a disorder between four different orientations which are adopted by the molecules in the crystal (**Figure 3.4.16**). Each of these orientations is adopted by 25% of the molecules. Each shows one μ_2-formate, one monodentate hydroxo and one chloride ions bound to the surface of the approximately planar macrocyclic cation.

In each orientation, four copper ions are bound by the fully deprotonated macrocycle in a planar array that closely approximates a square [Cu...Cu "sides" = 2.884(1) Å and 2.957(1) Å; Cu...Cu "diagonal" = 4.131(1) Å]. A μ_4-OH^- ion is centrally bridging the four copper ions, and lying in the plane of the four copper ions. The macrocyclic donors provide the equatorial ligands for the copper ions. Each of the phenoxo and alkoxo oxygen atoms of the macrocycle $(L^6)^{4-}$ bridges a pair of copper ions with Cu-O-Cu bridge angles of 99.6(2)° (alkoxo) and 101.0(2)° (phenoxo).

The macrocycle $(L^6)^{4-}$ in this complex is essentially planar. The most significant deviations from the macrocyclic plane are shown by four of the carbon atoms of each saturated side chain (C7, C8 and the symmetry-related equivalent atoms). The phenoxo oxygen atoms lie on the plane of the four copper atoms, while the alkoxo oxygen atoms deviate from the Cu_4 plane by 0.470(6) Å.

The μ-$HCOO^-$ ion is axially bridging, in a μ-1,3 mode, the copper pair which is also bridged by an alkoxo oxygen (O2) of the macrocycle. The remaining pair of copper ions are each coordinated axially by a chloride ion (Cl7) and a monodentate hydroxide ion (O61) on the opposite side of the macrocyclic plane.

The four orientations differ in the positions of the bound chloride, hydroxo and formate relative to the other orientations. In orientations two, the μ-formate is bound "above", while the Cl^- and OH^- ions are "below" the macrocyclic plane. In the other two orientations (III and IV), the situation is reversed.

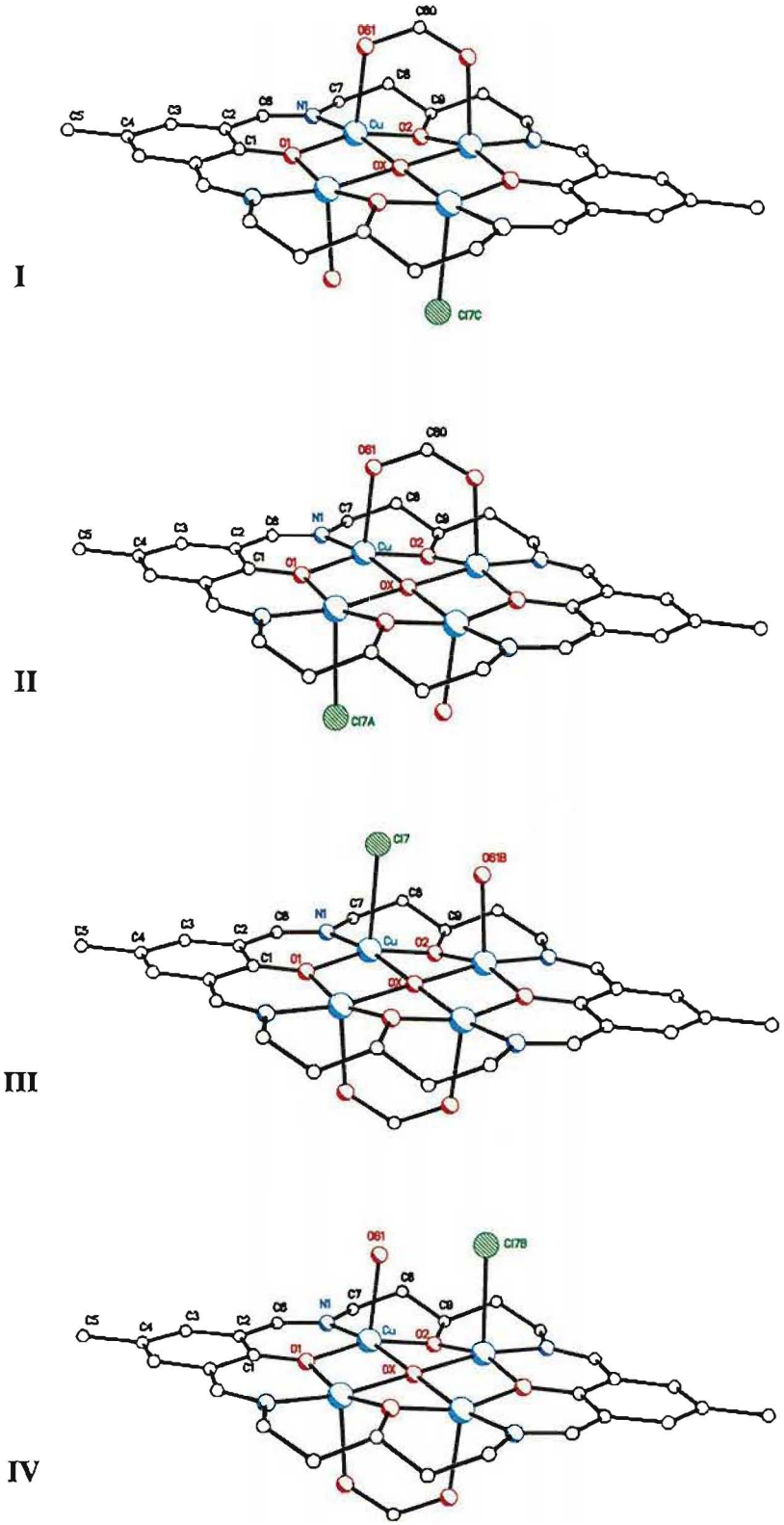

Figure 3.4.16. The four orientations of $Cu_4L^6(\mu_4\text{-}OH)(\mu\text{-}HCOO)(OH)Cl\cdot 6H_2O$ (**15**) in the crystal. The water molecules of crystalisation are not shown.

The presence of four orientations of the molecules in the crystal gives rise to an "average" or disordered structure (**Figure 3.4.17**) which has a 2/m point symmetry, such that the asymmetric unit contains only one quarter of the molecule. The C_2 axis coincides with the line dividing the molecule lengthwise, passing through the methyl substituent of the macrocycle (C5) and the phenoxo oxygen (O1). The mirror plane is perpendicular to the C_2 axis and to the plane of the macrocyclic cation, passing through the alkoxo oxygen O2. A hydroxo ion, Ox, lies in the centre of the four copper ions, and on the intersection of the two symmetry elements described previously.

In this "average" structure, each copper ion appears to be axially coordinated by a chloride ion (Cl7) having 0.25 site occupancy factor (s.o.f.) and an oxygen ligand (O61) with 0.75 s.o.f. The carbon atom (C60) of the μ-formate ion, lies on the mirror plane and has 0.25 s.o.f. Each formate oxygen atom and the monodentate hydroxo ion share the same site (O61) with s.o.f. of 0.50 and 0.25, respectively.

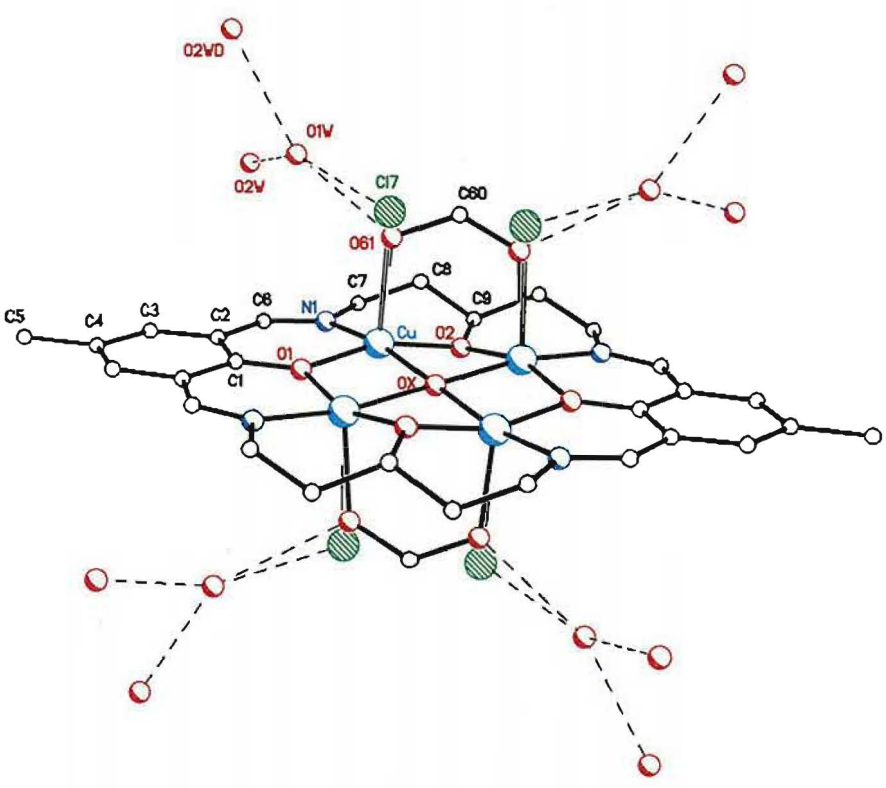

Figure 3.4.17. The "average" structure of $Cu_4L^6(\mu_4\text{-}OH)(\mu\text{-}HCOO)(OH)Cl\cdot 6H_2O$ (**15**).

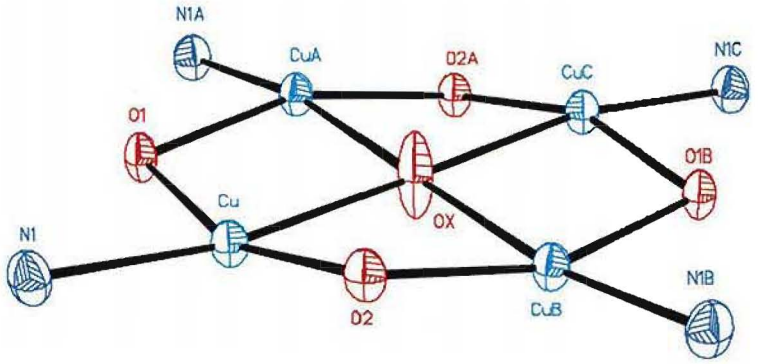

Figure 3.4.18. The Cu_4O core of $Cu_4L^6(\mu_4\text{-}OH)(\mu\text{-}HCOO)(OH)Cl\cdot 6H_2O$ (**15**), showing 30% probability thermal ellipsoids

Table 3.4.6. Selected intermolecular distances (Å) and bond angles (°) for the copper coordination environments in complex **15**.

Cu...CuA	2.884(1)	Cu...CuC	2.957(1)
Cu-O1	1.917(3)	Cu-Ox	2.065(1)
Cu-O2	1.889(3)	Cu-O61	2.263(10)
Cu-N1	1.951(5)	Cu-Cl7	2.734(10)
Cu-O1-CuC	101.0(2)	Cu-O2-CuA	99.6(2)
Cu-Ox-CuA	88.6(1)	Cu-Ox-CuC	91.4(1)
O1-Cu-N1	92.9(2)	O1-Cu-Ox	83.8(1)
O2-Cu-N1	96.8(2)	O2-Cu-Ox	83.9(1)
O2-Cu-O61	97.1(3)	O2-Cu-Cl7	97.6(2)
O1-Cu-O61	97.6(2)	O1-Cu-Cl7	97.7(2)
N1-Cu-O61	98.3(3)	N1-Cu-Cl7	95.1(2)
Ox-Cu-O61	91.2(2)	Ox-Cu-Cl7	94.4(2)

Transformations: A = 1-x, y, 1-z; B = x, 1-y, z; C = 1-x, 1-y, 1-z

Selected interatomic distances and bond angles relevant to the copper coordination environment in complex **15** are given in **Table 3.4.6**. The coordination environment of the tetracopper core is shown in **Figure 3.4.18**. Each copper ion is in an approximate square pyramidal geometry, bound equatorially to a μ-phenoxo oxygen (O1), a μ-alkoxo oxygen (O2) and an imine nitrogen (N1) donors of the macrocycle, and to the μ_4-hydroxo ion (Ox). Occupying the apical position of each copper ion is either a chloride ion (Cl7), a hydroxo ion (O61), or one formate oxygen atom (O61). Each

copper is displaced from its O_3N plane by 0.21 Å towards the axial ligand (Cl^-/OH^-/ formate). Each O_3N coordination plane of a copper(II) ion is only slightly distorted from planarity [deviations of the donor atoms from their mean plane each equals 0.04 Å].

The distances between the copper ions and the macrocyclic donors, and the bond angles are "normal" and comparable to those in related complexes.[70] However, the Cu-Ox bonds in **15** are significantly longer than the equatorial Cu-O bonds, and the Cu-Ox-Cu angles are significantly more compressed than the other Cu-O-Cu angles. These observations indicate that the Cu-Ox bonds are weaker than the other equatorial bonds. The weaker Cu-Ox bonds are probably a result of the unusual four-coordinate and planar coordination geometry of this oxygen, and to the mismatch between the Cu_4 cavity size and the normal Cu-O bond lengths.[70] This situation is similar to that of a related tetracopper complex of the macrocycle **MC18** (**Figure 3.4.19**), Cu_4(**MC18**), where a μ_4-OH^- is also found in the centre of a planar Cu_4 array.

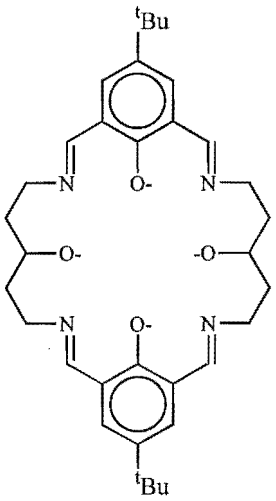

MC18

Figure 3.4.19.

The central oxygen ligand is believed to be an OH^- ion based on an examination of the thermal ellipsoids in the central part of the structure (**Figure 3.4.18**). The thermal ellipsoid of Ox is elongated in the direction perpendicular to the plane of the copper ion relative to the other atoms in the core. The same elongation is also observed for the

central hydroxo ligand of Cu_4(**MC18**)[70] which was suggested to be a consequence of a hydroxo ion at a centre of inversion being coordinated to four metal ions.

A hydroxo ion in such situation will be five-coordinate and have a square-pyramidal geometry. The oxygen atom of the μ_4-hydroxo ion is then expected to be slightly displaced from the plane of the four copper ions towards the hydrogen atom. Since the OH^- ion is lying on a centre of inversion, this displacement would lead to the oxygen being disordered between two positions, slightly above and below the Cu_4-plane, resulting in the elongation of the thermal ellipsoid of Ox. Moreover, the hydrogen atom will also be disordered above and below the plane of the macrocycle.

Two water molecules are also present in the asymmetric unit. One of these, O2W, lies on a C_2 axis which is different from the one passing through the macrocyclic moiety, and on the *ab* plane of the unit cell. The other water molecule, O1W, occupies a general position. O2W forms hydrogen bonds to O1W from two neighbouring asymmetric units [O1W...O2W = 2.849(8) Å]. Similarly, O1W forms hydrogen bonds to O2W from two symmetry-related positions, as well as to the coordinated chloride and hydroxo/formate oxygen [O1W...Cl7 = 2.63(1) Å; O1W...O61 = 2.89(1) Å]. These extensive hydrogen bonding interactions link the macrocyclic units in the crystals, as illustrated in **Figures 3.4.20** and **Figure 3.4.21**.

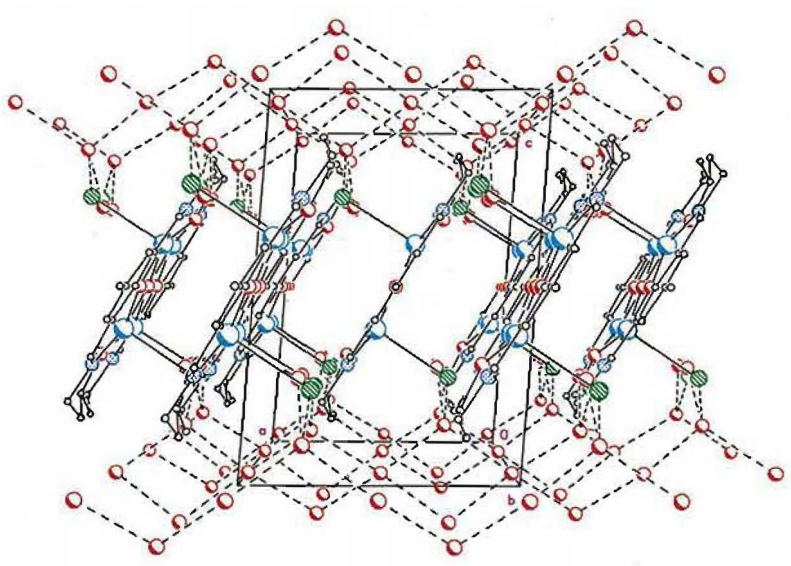

Figure 3.4.20. The hydrogen bonds which link individual macrocyclic units.

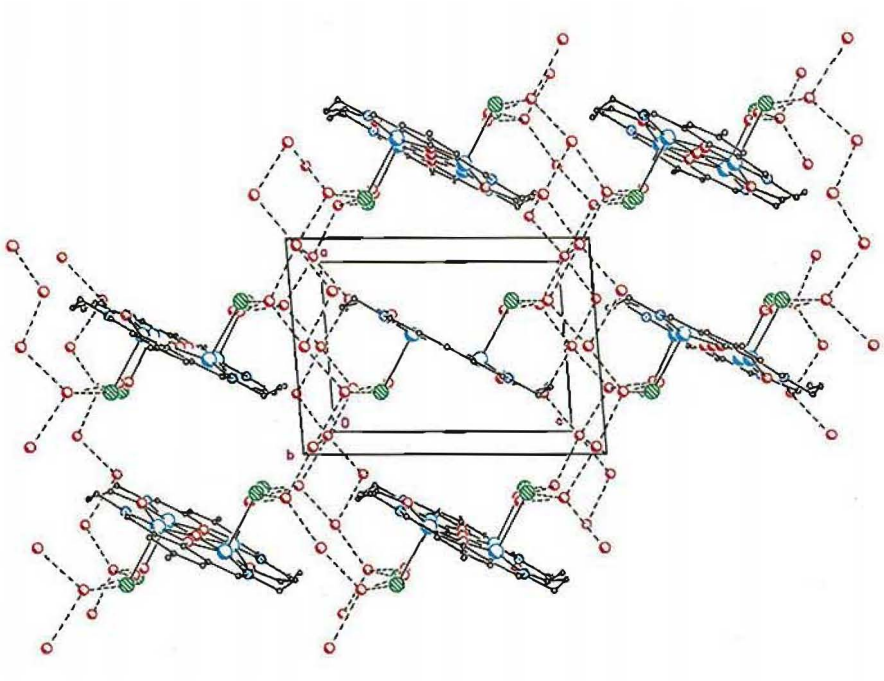

Figure 3.4.21. The hydrogen bonds in the crystal that link the "stacks" of macrocyclic units, viewed along the *b* axis.

Together with the hydrogen bonds present between the macrocyclic complexes, intermolecular π-π interactions hold the individual macrocyclic units in a very regular array in the crystal. The presence of π-π stacking interactions[100] are indicated by the following observations. The phenyl rings of two adjacent molecules are separated by 3.371(7) Å. Although these aromatic rings exhibit only a slight overlap (**Figure 3.4.22**), the π regions of the two molecules, that is, the phenol-diimine moieties, show significant overlap. In addition, the molecules are stacked face-to-face and oriented in the same direction, that is, the phenol "head" units are pointing along the *b* axis (**Figure 3.4.23**). The π-π interactions are partly responsible for holding the "stacks" of molecules in one "layer". The hydrogen bonds described previously then link the molecules in two adjacent "layers" (**Figures 3.4.23b**).

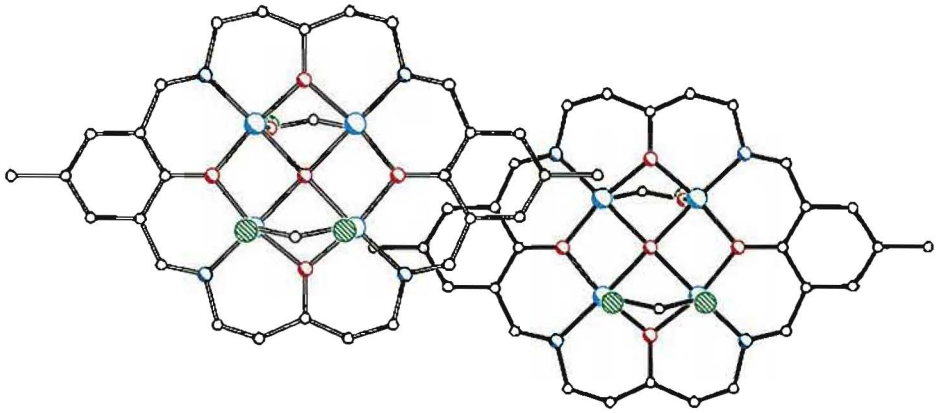

Figure 3.4.22. π-π interactions between two molecules of **15**, a view perpendicular to one of the phenyl rings of the molecule on the left (having white bonds).

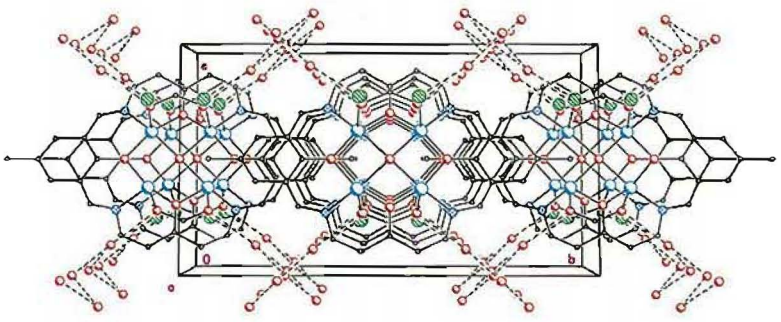

(a)

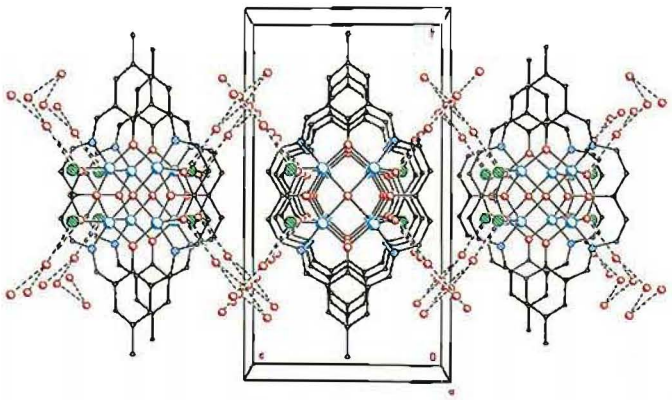

(b)

Figure 3.4.23. Molecular packing of complex **15**: (a) a view along the *a* axis, showing the face-to-face stacking of the molecules in one layer and the π-π overlaps of the phenol rings; (b) a view along the *b* axis, showing one "stack" of the molecules and the hydrogen bonds connecting them.

The planar structure of complex **15** is similar to that of Cu_4(**MC16**), but contrasts with the bowl-like structure of nickel(II) and zinc(II) tetranuclear complexes[80] of the macrocycle **MC18**. The tetracopper(II) and tetranickel(II) complexes each have a μ_4-hydroxo ion trapped in the centre of the M_4 core. The "trapping" of a hydroxo ion in the centre of the tetrametallic site may be a consequence of the organisation of the four metal ions by the macrocyclic ligands.[80] The "trapped" species, such as OH^- ion, in the centre of the tetranuclear macrocyclic complexes may be activated towards further reaction. For example, the μ-OH^- ion in Cu_4(**MC16**) could be replaced by azide ions relatively easily, to produce the corresponding di-μ-1,1-azide tetracopper(II) macrocyclic complex (**Figure 1.23**, Chapter 1).

Infrared spectroscopy

The infrared spectrum of complex **15** (illustrated in **Figure 3.4.24**; the full size spectrum may be found in **Appendix B**) does not show the characteristic peak of BF_4^- ions at *ca.* 1050 cm^{-1}. Two strong bands at *ca.* 1640 and 1570 cm^{-1} are assigned to the C=N and phenol C-O stretches, respectively. Combined with the absence of a carbonyl (*ca.* 1700 cm^{-1}) and the NH_2 stretches (*ca.* 3300 cm^{-1}), these observations indicate the formation of a macrocyclic complex containing no BF_4^- counterion, consistent with the X-ray crystallographic analysis results.

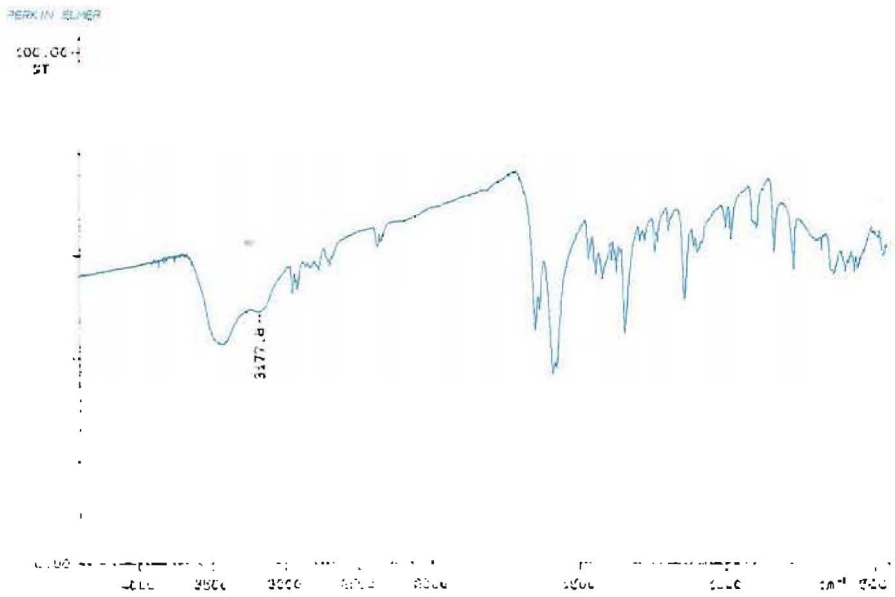

Figure 3.4.24. The infrared spectrum of $Cu_4L^6(\mu_4\text{-}OH)(\mu\text{-}HCOO)(OH)Cl\cdot 6H_2O$ (**15**).

The extensive hydrogen bonding interactions observed in the crystal structure of **15** possibly result in the lowering of the O-H stretches,[102] hence giving rise to the broad shoulder at *ca.* 3178 cm^{-1}. The weak absorptions around 2700 cm^{-1} in the spectrum of **15**, which are absent from the spectra of **13** and **14**, could be assigned to the C-H stretches of the formate ion. The peaks at *ca.* 2900 cm^{-1} in the spectrum of **15**, probably due to the methyl groups stretches, appear as two resolved peaks, as opposed to the methyl stretches normally observed in the spectra of related complexes as two overlapping peaks.

The C=N and phenol C-O bands in the infrared spectrum of **15** appear split (**Figure 3.4.24**). The C=N absorptions are observed at 1647 and 1632 cm^{-1}, while the phenol C-O absorptions occur at 1587 and 1570 cm^{-1}. There could be two reasons for this observations.

Firstly, the splitting could be caused by the imine and the phenol groups each having two different environments, resulting in the variation of the C=N or C-O bond strengths in the complex. The values of the C=N and $C\text{-}O_{(phenol)}$ bond lengths obtained from X-ray data cannot be used to verified this since the disorder in the structure gives rise to a symmetrical "averaged" structure. However, the individual ("non-averaged") structure of the complex ion itself is not symmetrical, with three distinct axial ligands to the copper ions. The difference in electronegativity of the Cl^- ligand and the axial oxygen donor (formate or OH^-) may cause the bond strengths of the imine groups (or phenol C-O groups) in the macrocycle to be unequal, due to more electron loss towards the copper from the chelate ring of the copper ion coordinated by Cl^-.

Secondly, the splitting of the peaks could be due to the formate C-O vibrations which overlaps with the imine or the $C\text{-}O_{(phenol)}$ bands. The crystal structure of complex **15** shows equivalent C-O bond lengths for the formate ion, indicating the presence of conjugation within the formate ion in the complex which means that the C-O bonds of the formate ion is neither a single nor a double bond. As a result of the conjugation, the formate C---O bond would absorb at a higher frequency region than C-O bond, but lower than a C=O bond, similar to the situation involving the phenol C-O bond (see **Introduction to Chapter 3**). Hence, the formate C-O would absorb in the same frequency region (1650 - 1570 cm^{-1}) as the C=N and phenol C-O functions.

Hydrolysis of DMF to formate

Slow evaporation of the DMF solution of complex $Cu_4L^6(OH)(BF_4)_3(H_2O)_2$ (**13**) gave complex **15** which contains a formate ion, found to be bridging two of the copper(II) ions. The incorporation of a formate ion into the macrocyclic complex cation $[Cu_4L^6(OH)]^{3+}$ to give the formate bridged complex (**15**) was rather perplexing, since a formate salt or formic acid was not added into the solution of complex **13**.

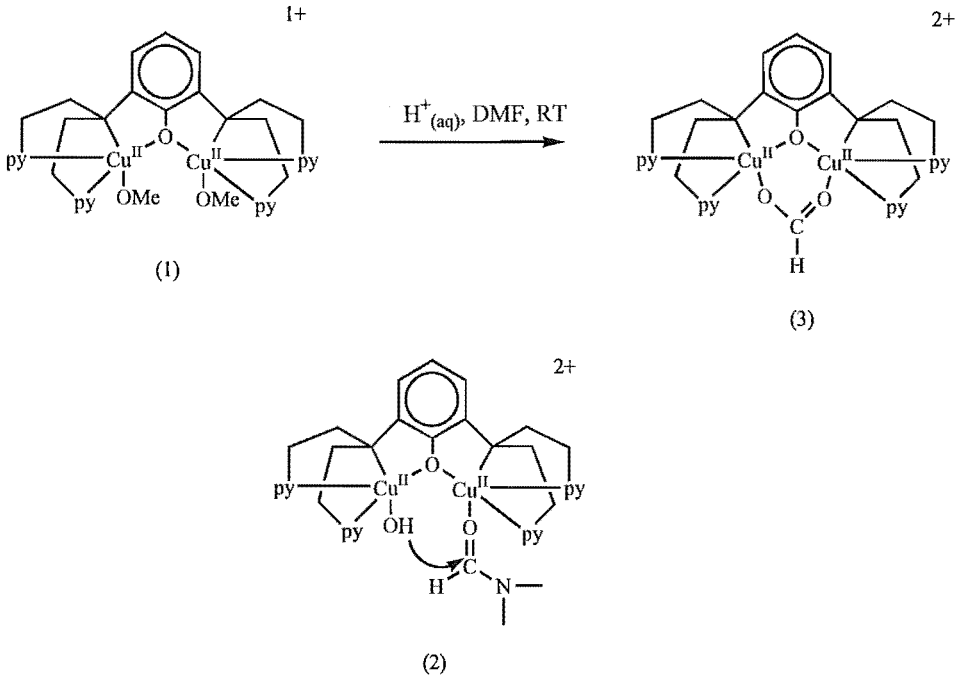

Figure 3.4.25. Hydrolysis of DMF by a dicopper(II) complex.[107]

However, Karlin et al. reported recently[107] the hydrolysis of DMF and other amides at 23 °C, promoted by a dicopper(II) complex of a "podal" ligand [**Figure 3.4.25** - complex (1)] and possibly by acid.* The crystal structures of complex (1) which promoted the hydrolysis reactions, and of the dicopper(II) complex which is the product of DMF hydrolysis, have been determined by X-ray crystallography. The structure of complex (1) shows one methoxo ligand coordinated to each of the copper(II) ions. The structure of complex (3) shows that the methoxo ligands have been replaced by a formate ion, found bridging in a μ-1,3 mode between the two copper(II) ions. On the basis of the structure of complex (1), the hydrolysis of DMF is proposed to proceed

* One equivalent of $HClO_4$ was added to the reaction mixture to optimise the formation of a (OH^-)-Cu...Cu-L (L = DMF or H_2O) species, that is, the acid functions as a co-catalyst. The hydrolysis of DMF in this case was found to have a pseudo-first-order rate with $k_{obs} = 0.3\ h^{-1}$.

through a key intermediate, complex (2) (**Figure 3.4.25**), which can bind a hydroxo ion and a DMF molecule at adjacent copper(II) sites. The proximity of the nucleophile (OH^-) and the substrate (DMF) in this intermediate will facilitate the nucleophilic attack at the substrate. In addition, the substrate would be activated towards nucleophilic attack by coordination to the metal ion (Lewis acid).

A μ-1,3 formate ion and a monodentate hydroxo ion coordinate axially to the surface of the planar Cu_4OH core in complex **15**. The μ-1,3 bridging mode of the $HCOO^-$ is the same as that of the formate ion in the dicopper(II) complex described previously [complex (3) - **Figure 3.4.25**]. The presence of the axial OH^- donor in **15** suggests that hydroxo ions might have coordinated to the Cu_4 surface of the cation $[Cu_4L^6(\mu_4\text{-}OH)]^{3+}$ of complex **13** (precursor for **15**) at some stage. The hydroxo ions possibly originated from water molecules present in complex **13** as water molecules of crystallisation or from water molecules in the atmosphere which came into contact during the evaporation period.

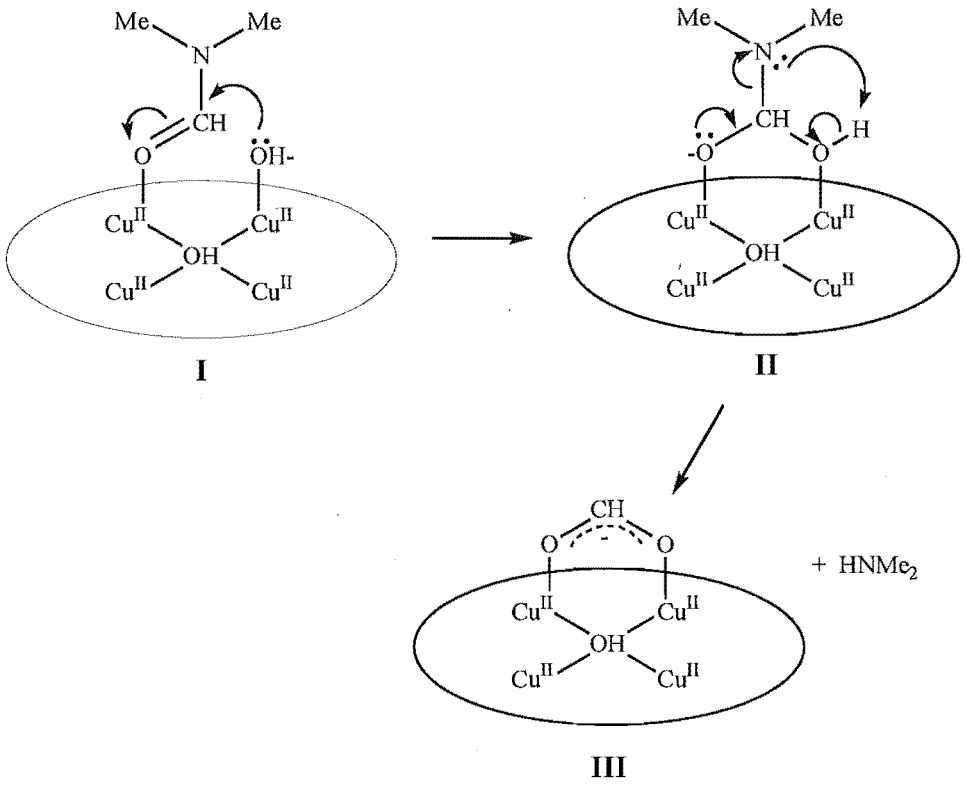

Figure 3.4.26. Possible mechanism for the copper(II) complex catalysed hydrolysis of DMF catalysed by a tetracopper(II) complex of $(L^6)^{4-}$.

DMF is a coordinating solvent, and there is a number of structurally characterised copper(II) complexes[108] in which a DMF molecule coordinates to the metal ion through the aldehyde oxygen. In addition, a tetracopper(II) complex of L^6 has been structurally characterised,[73] showing a roughly planar $[Cu_4L^6(\mu_4\text{-}OH)]^{3+}$ moiety on which three molecules of acetonitrile and one perchlorate ion coordinate to each copper(II) ion. This indicates that the cation $[Cu_4L^6(\mu_4\text{-}OH)]^{3+}$ is able to bind small molecules to its Cu_4 core. Hence it is quite likely that DMF, along with OH^- ion, are coordinated side-by-side to the cation $[Cu_4L^6(\mu_4\text{-}OH)]^{3+}$ of complex **13** as illustrated in structure **I** of **Figure 3.4.26**.

A subsequent nucleophilic attack by the hydroxo ion at the carbon atom of the coordinated DMF molecule would lead to the formation of a μ-1,3 $HCOO^-$ ion (structure **III - Figure 3.4.26**). That is, it is possible that the formate ion in complex **15** is the product of a slow hydrolysis of DMF solvent, catalysed by the tetracopper(II) complex cation $[Cu_4L^6(\mu_4\text{-}OH)]^{3+}$.

The complex **15** crystallised out of DMF in *ca.* 5 months at ambient temperature. This could mean that the hydrolysis of DMF, catalysed by complex **13**, is rather slow due to the absence of an acid co-catalyst (see footnote on p.173). Although the length of time taken for complex **15** to crystallise out of the solution is still much shorter than the normal half-life of amide hydrolysis (*ca.* 7 yrs at room temperature and pH~7),[107a] supporting the conclusion that the tetracopper complex promoted the hydrolysis. On the other hand, the above observation may also be due to the slow crystallisation of complex **15** from DMF, which in turn could be due to DMF being a rather involatile solvent at room temperature and/or the reasonably high solubility of the complex in DMF.

Further investigations are needed to elucidate the hydrolysis of DMF promoted by the macrocyclic tetracopper complex $[Cu_4L^6(\mu_4\text{-}OH)]^{3+}$ cation, in particular to study the kinetics of the catalysed hydrolysis.

Structure of $[\{Cu_2(HL^6)(\mu_3\text{-}OH)\}_2]$ (16)

The 'dimeric' complex $[\{Cu_2(HL^6)(\mu_3\text{-}OH)\}_2]$ (**16**) was obtained as a by-product of one of the preparations of complex **13**, isolated from methanol as a few dichroic crystals. Attempts to prepare this tetracopper di-μ_3-hydroxo dimer intentionally have not succeeded so far. Therefore no microanalytical or infrared data for this complex were obtained. However, crystals of **16** were obtained which were suitable for X-ray data collection, although only weakly diffracting.

This weakly diffracting crystal resulted in a poor diffraction data set, preventing a full refinement of the structure. However, the connectivity of the molecule could be determined as shown in **Figures 3.4.27** and **3.4.28**. Selected interatomic distances and bond angles are given in **Table 3.4.8**.

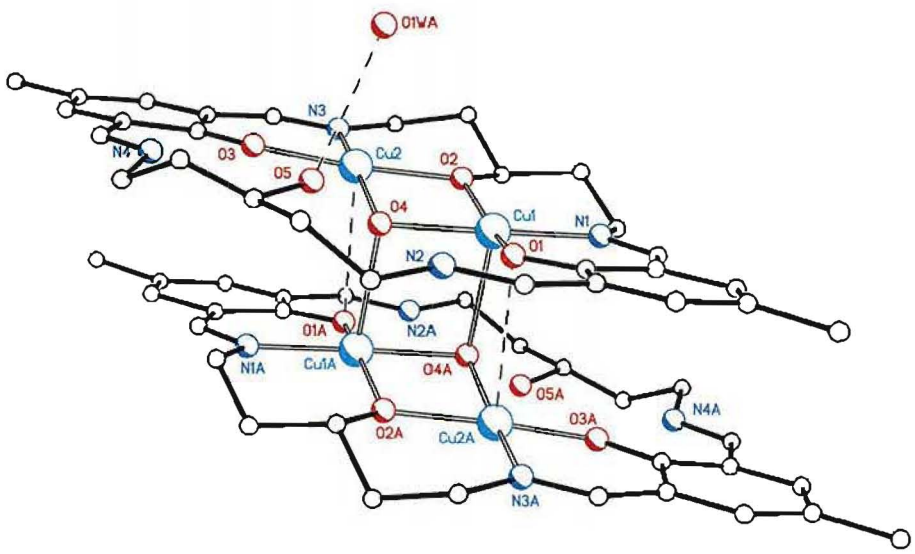

Figure 3.4.27 Structure of the 'dimeric' tetracopper complex **16**

Complex **16** is a centrosymmetric tetracopper(II) complex, having a dimer of two macrocyclic units, similar to complex **14**. In contrast to the case of the octacopper complex **14**, only two copper ions are bound in each macrocycle in **16**. These copper ions are held to one "side" of the macrocyclic ligand, at Cu...Cu separation of 2.985(4) Å, and bridged by an alkoxo oxygen (O2) of the macrocycle (**Figure 3.4.27**) [Cu1-O2-Cu2 = 102.5(9)°]

Four water molecules are present in the asymmetric unit, while no BF_4^- ions are detected. A hydroxo ion (O4) also bridges the copper ions in each macrocyclic unit [Cu1-O4-Cu2 = 99.9(8)°], and coordinates to a copper atom (Cu1A) from the second macrocyclic unit. The O4-Cu1A and the symmetry-related Cu1-O4A bonds link the two macrocyclic units in the dimer together, along with the weaker interactions Cu2...O1A and O1...Cu2A.

The macrocyclic ligand is probably the triply-deprotonated $(HL^6)^{3-}$ (**Figure 3.4.1**), having two μ-phenoxo and one μ-alkoxo donors. The coordination geometry about each copper atom in **16** is approximately square-pyramidal, suggesting that the copper atoms are in their +II oxidation states. O2 is bridging two copper ions, implying that this oxygen donor is an alkoxo instead of an alcohol group. On the other hand, O5 is not coordinated to any of the copper ions, but is hydrogen bonded to a water molecule (O1W) [O5...O1W = 2.8 Å], suggesting that it is a non-deprotonated alcohol group. The oxygen ligand O4 is three-coordinate, suggesting that it is a hydroxo ion. Stoichiometry then requires the two phenol groups of the macrocycle to be deprotonated.

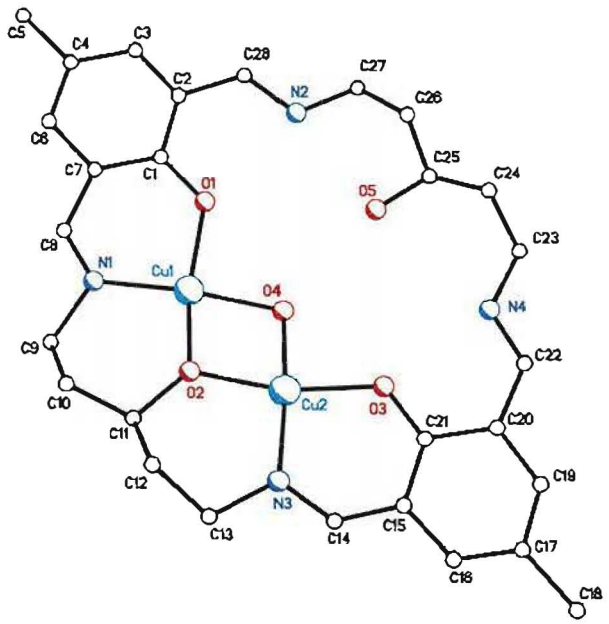

Figure 3.4.28. Structure of one macrocyclic unit of the dimer $[\{Cu_2(HL^6)(\mu_3\text{-}OH)\}_2]$ with the atom numbering system.

The equatorial coordination plane of each copper ion in **16** comprises a nitrogen donor from the macrocycle (presumed to be an imine nitrogen), a phenoxo oxygen and the shared alkoxo oxygen. The axial site of Cu1 is occupied by the μ_3-OH^- from the second macrocyclic unit, while one of the phenoxo oxygen from the second macrocyclic unit weakly and axially interacts with Cu2 [Cu2...O1A = 3.10 Å].

Table 3.4.8. Interatomic distances (Å) and bond angles (°) relevant to the copper coordination in complex **16**.

Cu1...Cu2	2.985(4)	Cu1...Cu1A	3.23
Cu1-O2	1.92(2)	Cu2-N3	1.91(2)
Cu1-O4	1.95(2)	Cu2-O4	1.95(2)
Cu1-O4A	2.42(2)	Cu2-O2	1.90(2)
Cu1-N1	1.94(2)	Cu2-O3	1.94(2)
Cu1-O1	1.96(2)	Cu2...O1A	3.10
Cu1-O2-Cu2	102.5(9)	Cu1-O4-Cu2	99.9(8)
Cu2-O4-Cu1A	98.3(7)	Cu1-O4-Cu1A	94.7(6)
O2-Cu1-O4	78.5(7)	O2-Cu2-O4	79.0(7)
O4-Cu1-O1	92.6(8)	O2-Cu2-N3	97.3(9)
N1-Cu1-O4A	92.9(7)	N3-Cu2-O3	94.0(9)
O1-Cu1-O4A	101.5(7)	O3-Cu2-O4	91.2(8)
N1-Cu1-O1	94.2(8)	N3-Cu2-O1A	89.4
O2-Cu1-O4A	95.3(7)	O2-Cu2-O1A	86.1
O4-Cu1-O4A	85.3(6)	O3-Cu2-O1A	103.0
O2-Cu1-N1	95.2(9)	O4-Cu2-O1A	81.1

Transformation: A = -x+1, -y, -z

The two adjacent, nearly-planar macrocycles in **16** are oriented parallel to each other and rotated laterally by 180° (**Figure 3.4.29**). The phenyl rings of the two macrocycles are separated by *ca.* 3.4 Å and adopt a laterally offset, "face-to-face" stacking arrangement. These observations indicate that π-π interactions[100] are present within the tetracopper dimer, similar to the octacopper complexes case (see discussion on the structure of **15**). The intramolecular π-π interactions are likely to be partly responsible for holding the two macrocyclic units together with the Cu-O interactions described before.

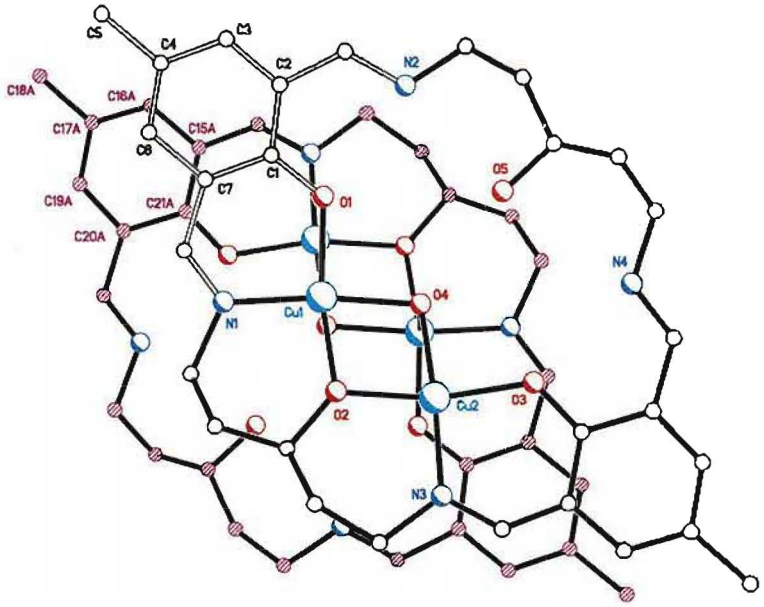

Figure 3.4.29. The tetracopper dimer [{$Cu_2(HL^6)(\mu_3\text{-}OH)\}_2$] (**16**) viewed perpendicular to the phenyl ring C1-C2-C3-C4-C6-C7..

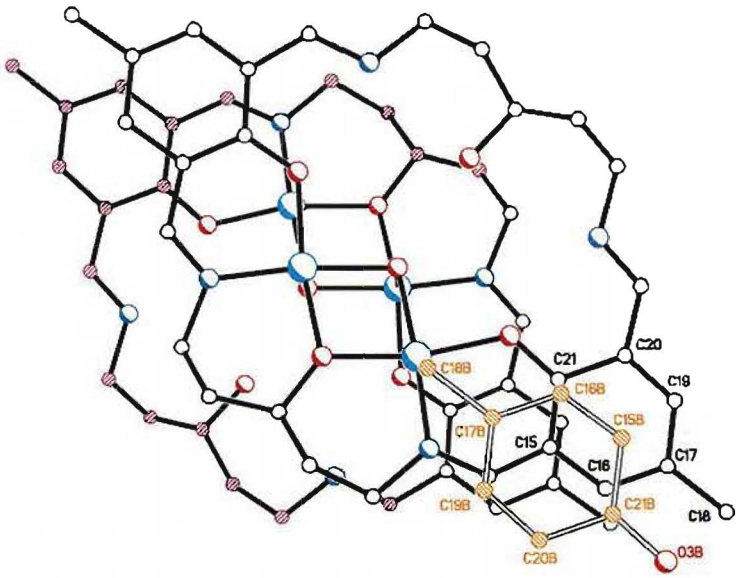

Figure 3.4.30. π-π interactions between adjacent dimer [{$Cu_2(HL^6)(\mu_3\text{-}OH)\}_2$] (**16**). Only the 4-methylphenol fragment of the second dimer is shown for clarity (orange C atoms with white bonds). The view is perpendicular to the least-squares plane of the phenyl ring of the second dimer.

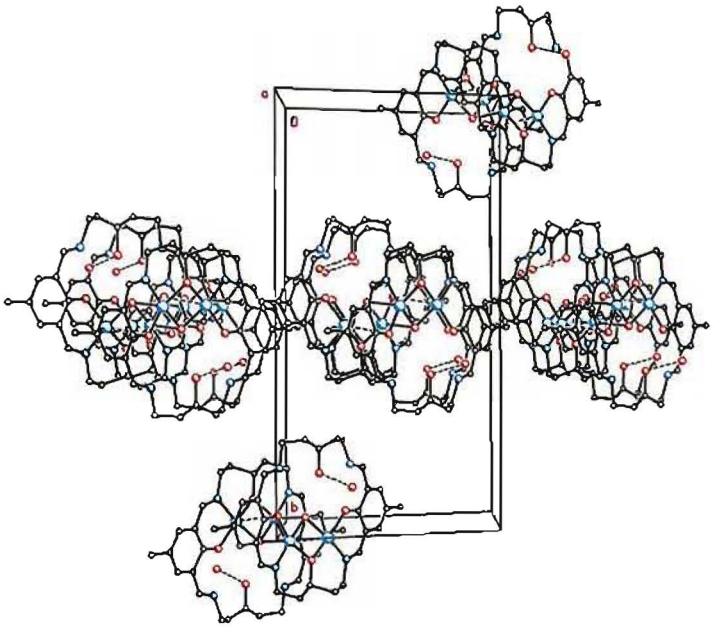

(a)

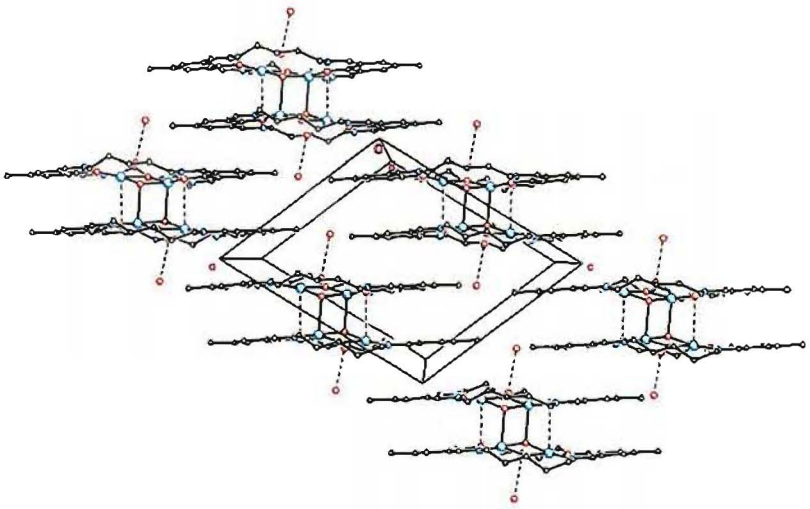

(b)

Figure 3.4.31. Molecular packing of complex **16** viewed along the crystallographic *a* axis.

Intermolecular π-π interactions are also present in complex **16** as shown by the arrangement of an aromatic phenyl ring of one dimer with respect to the symmetry-related equivalent ring of another dimer (**Figure 3.4.30**). The two rings are separated by *ca.* 3.4 Å, parallel to each other and adopt a laterally offset geometry. These

intermolecular π-π interactions lead to the parallel stacking of individual dimers to form layers of dimers (**Figure 3.4.31**).

Macrocyclic complexes which are similar to the dicopper(II) unit of complex **16** may be designated "lateral" dinuclear complexes. This type of complexes are potential precursors for hetero-tetranuclear macrocyclic complexes of the type illustrated in **Figure 3.4.32a**. This potential arises from the presence in the macrocyclic ligand of two vacant metal binding sites, which are available for binding of transition metal ions of appropriate size (probably comparable to the size of Cu^{2+}). The "lateral" dicopper(II) or dimetallic macrocyclic complexes are also potential precursors for trinuclear macrocyclic complexes, either homo-trinuclear or hetero-trinuclear (**Figure 3.4.32b**).

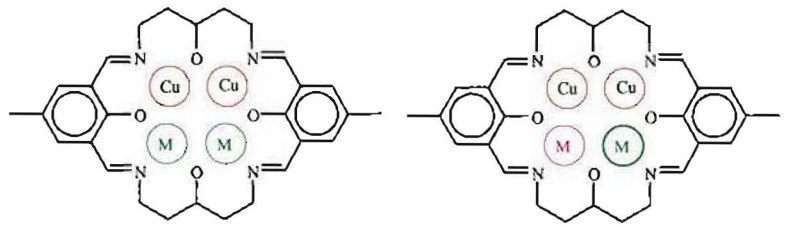

(a)

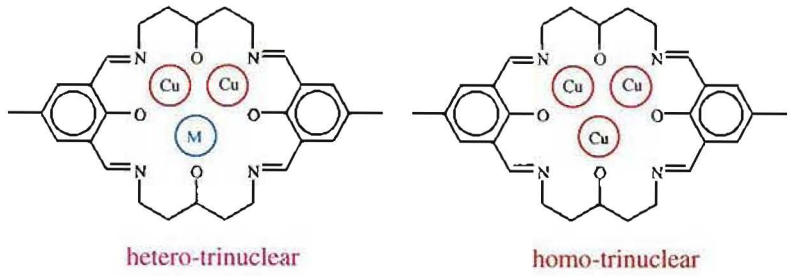

(b)

Figure 3.4.32. Schematic illustration of (a) hetero-tetranuclear macrocyclic complexes and (b) trinuclear macrocyclic complexes that could be formed from a "lateral" dicopper(II) macrocyclic complex of $(HL^6)^{3-}$.

One logical method to synthesise a dicopper(II) "lateral" complexes of $(HL^6)^{3-}$ is *via* the initial formation of an acyclic ligand containing two carbonyl and two imine functions. This method is illustrated in **Figure 3.4.33** and may be extended for other macrocyclic systems and for different transition metal ions.

The acyclic intermediate ligand could either be generated *in situ*, or be isolated possibly as its dicopper(II) complex. In any case, the chance of forming the acyclic Schiff-base ligand would be increased if the 1,5-diamino-3-hydroxypentane (1,5-DAHP) is templated onto the copper(II) ions, since 1,5-DAHP has been known to form dicopper(II) complexes.[109] Condensation of one such dicopper(II) complex with two equivalent amounts of 2,6-diformyl-4-methylphenol would be expected to generate the macrocyclic "lateral" dicopper(II) complex. This route to the "lateral" dicopper(II) complex of $(HL^6)^{3-}$ is currently being investigated by M^{c}Kee et al.[106a]

M^{c}Kee et al.[106a] are also investigating another approach to the preparation of a dicopper complex of the macrocycle $(HL^6)^{3-}$, namely by removing two copper(II) ions from an existing tetracopper complex of $(L^6)^{4-}$.

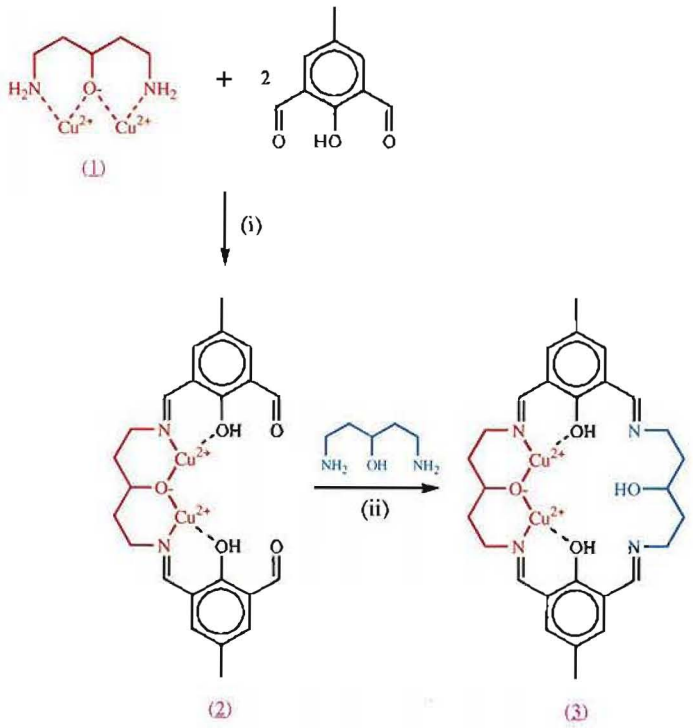

Figure 3.4.33. A possible synthetic route towards the formation of a dicopper "lateral" complex of $(HL^6)^{3-}$.

An *asymmetric* [2+2] Schiff-base macrocycle may be synthesised *via* an acyclic ligand such as that derived from the condensation of two molecules of 2,6-diformyl-4-methylphenol and one molecule of 1,5-diamino-3-hydroxypentane (complex (2) - **Figure 3.4.33**). Such a macrocyclic ligand could potentially be tetranucleating or

trinucleating, depending on the nature of the second diamine component employed in the second step of macrocyclisation.

3.5 Condensation of triethylenetetramine and 2,6-diformyl-4-methylphenol

Synthesis

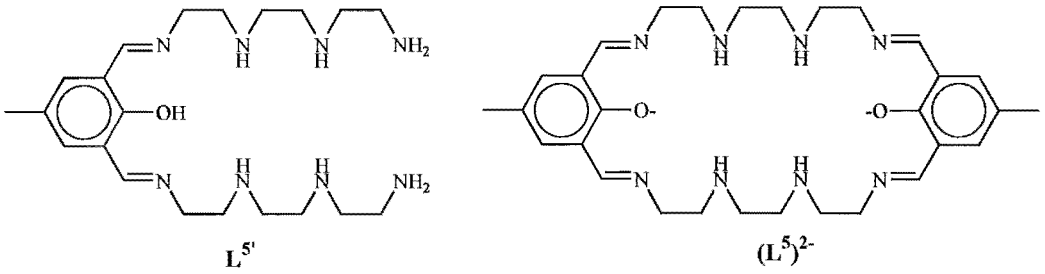

Figure 3.5.1.

Synthesis of the acyclic [1+2] Schiff-base ligand $L^{5'}$ (**Figure 3.5.1**) was attempted by the template condensation of 2,6-diformyl-4-methylphenol (1 eq) and triethylenetetramine (3.5 eq) using copper(II) tetrafluoroborate as the template. Initially, the reaction was carried out at room temperature (with the intention of preventing the formation of the macrocyclic analogue) using ethanol-methanol (1:1) mixture as the solvent. However, the product was the dicopper(II) complex $[Cu_2L^5](BF_4)_2{\cdot}2H_2O$¶ (complex **17**·$H_2O$), where $(L^5)^{2-}$ is the [2+2] Schiff-base macrocycle shown in **Figure 3.5.1**. When the preparation was carried out at reflux temperature, the complex $[Cu_2L^5](BF_4)_2{\cdot}H_2O$* (complex **17**) was obtained.

Complex **17** could also be obtained when the preparation was carried out in methanol at room temperature or at ~65 °C. However, when acetonitrile was employed as the solvent, neither complex **17** nor **17**·H_2O precipitated out of the solution, even when the solution was concentrated to a small volume. This was presumably due to the higher solubility of the complex in acetonitrile compared with ethanol or methanol.

The crystal structure of complex **17** has been determined by X-ray crystallography and is presented next.

¶ Microanalytical data: found C 40.45%; H 4.92%; N 12.95%; calculated C 40.79%; H 5.25%; N 12.68% ($[Cu_2L^5](BF_4)_2.2H_2O$ or $C_{30}H_{46}N_8O_4Cu_2B_2F_8$).

* Microanalytical data: found C 41.32%; H 4.92%; N 12.80%; calculated C 41.66%; H 5.12%; N 12.95% ($[Cu_2L^5](BF_4)_2.H_2O$ or $C_{30}H_{44}N_8O_3Cu_2B_2F_8$).

Crystal structure of $[Cu_2L^5](BF_4)_2 \cdot H_2O$ (17)

The asymmetric unit of **17** consists of a $[Cu_2L^5]^{2+}$ cation (**Figure 3.5.2**), two half-occupancy and one full-occupancy tetrafluoroborate ions and one lattice water molecule. One of the two half-occupancy BF_4^- ions lies on a C_2 axis while the second is disordered about a centre of symmetry; the full-occupancy BF_4^- ion is disordered about a B-F bond. The disorder in the BF_4^- ions will be discussed later.

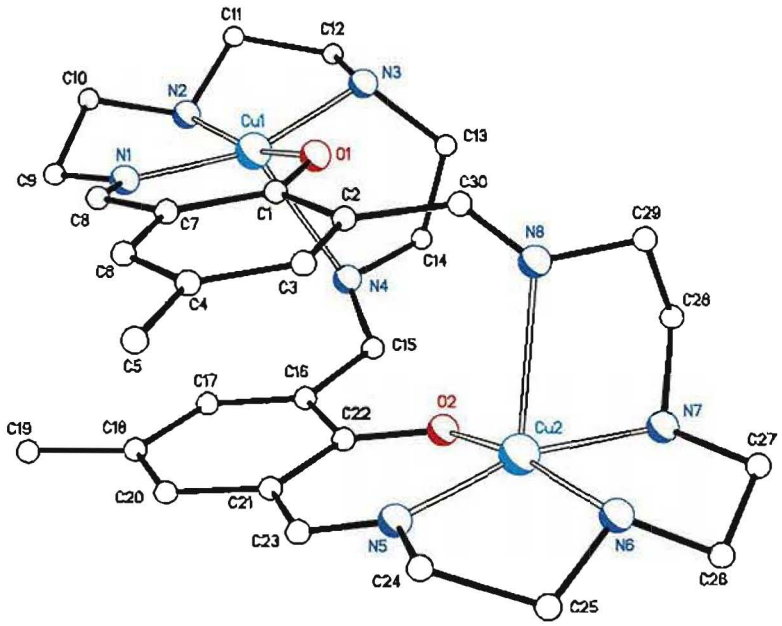

Figure 3.5.2. A perspective view of the cation of complex $[Cu_2L^5](BF_4)_2 \cdot H_2O$ (**17**) with the atom numbering scheme.

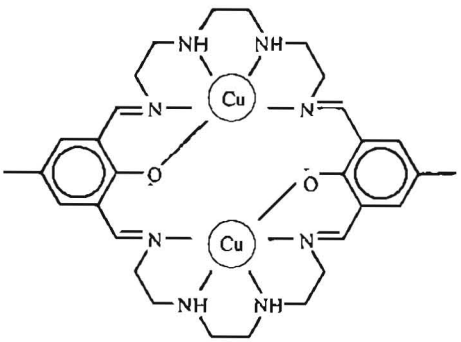

Figure 3.5.3. Schematic representation of the cation of the dinuclear complex $[Cu_2L^5](BF_4)_2 \cdot H_2O$ (**17**).

Interatomic distances and bond angles relevant to the copper coordination spheres are given in **Table 3.5.1**. The two copper(II) ions in complex **17** are bound at the sides of the fully-deprotonated macrocycle (**Figure 3.5.3**) at 6.581(1) Å apart, but are not bridged by the phenoxo oxygen donors. Each copper(II) ion in **17** is five-coordinate and in an approximately square-pyramidal geometry. One imine nitrogen donor is coordinated axially at *ca.* 2.4 Å away from the copper atom. The equatorial donors belong to the same side chain as the axial imine, consisting of two secondary amine nitrogen donors (at *ca.* 2.0 Å from the copper), an imine nitrogen and a phenoxo oxygen (each at *ca.* 1.9 Å from the copper).

Cu1 is displaced from its N_3O donor plane (N1-N2-N3-O1) by 0.252(2) Å, while Cu2 is displaced from its donor plane (N5-N6-N7-O2) by 0.252(2) Å. The donor atoms of Cu1 are almost coplanar [rms deviation = 0.008(2) Å], while those of Cu2 show a slight tetrahedral distortion from planarity with rms deviation of 0.011(2) Å. The interplanar angle of the two N_3O coordination planes is 6.8(1)°.

Table 3.5.1. Selected interatomic distances (Å) and bond angles (°) for the complex $[Cu_2L^5](BF_4)_2{\cdot}H_2O$ (**17**).

Cu1...Cu2	6.581(1)		
Cu1-O1	1.905 (3)	Cu2-O2	1.896 (4)
Cu1-N1	1.934 (4)	Cu2-N5	1.921 (4)
Cu1-N2	2.023 (5)	Cu2-N6	2.023 (5)
Cu1-N3	2.030 (4)	Cu2-N7	2.046 (5)
Cu1-N4	2.361 (5)	Cu2-N8	2.378 (5)
O1-Cu1-N1	94.1 (2)	O2-Cu2-N5	94.1 (2)
N1-Cu1-N2	84.3 (2)	N5-Cu2-N6	84.9 (2)
O1-Cu1-N3	93.3 (2)	O2-Cu2-N7	93.6 (2)
N2-Cu1-N3	84.6 (2)	N6-Cu2-N7	84.9 (2)
O1-Cu1-N4	88.2 (2)	O2-Cu2-N8	88.8 (2)
N1-Cu1-N4	116.8 (2)	N6-Cu2-N8	102.2 (2)
N2-Cu1-N4	105.2 (2)	N5-Cu2-N8	114.7 (2)
N3-Cu1-N4	79.7 (2)	N7-Cu2-N8	79.1 (2)

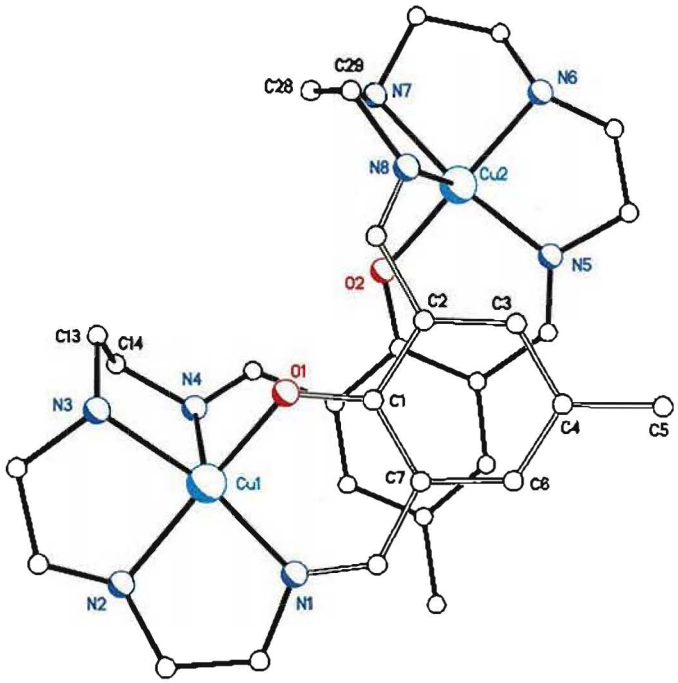

Figure 3.5.4. The complex $[Cu_2L^5](BF_4)_2 \cdot H_2O$ (**17**) viewed perpendicular to the phenyl ring C1-C2-C3-C4-C6-C7.

The macrocycle is folded so that the two planes defined by the aromatic phenyl rings are nearly parallel [being inclined at 3.1(2)°] and *ca.* 3.3 Å apart. These π regions of the macrocycle are also slightly offset laterally (**Figure 3.5.4**). These observations are consistent with the presence of an attractive π-π stacking interactions[100] which very likely contribute to the thermodynamic stability of the complex. The phenyl rings of the macrocycle are rotated laterally with respect to each other by *ca.* 90°. This is probably a consequence of the long, saturated moieties of the macrocycle which impart a considerable flexibility to the ligand.

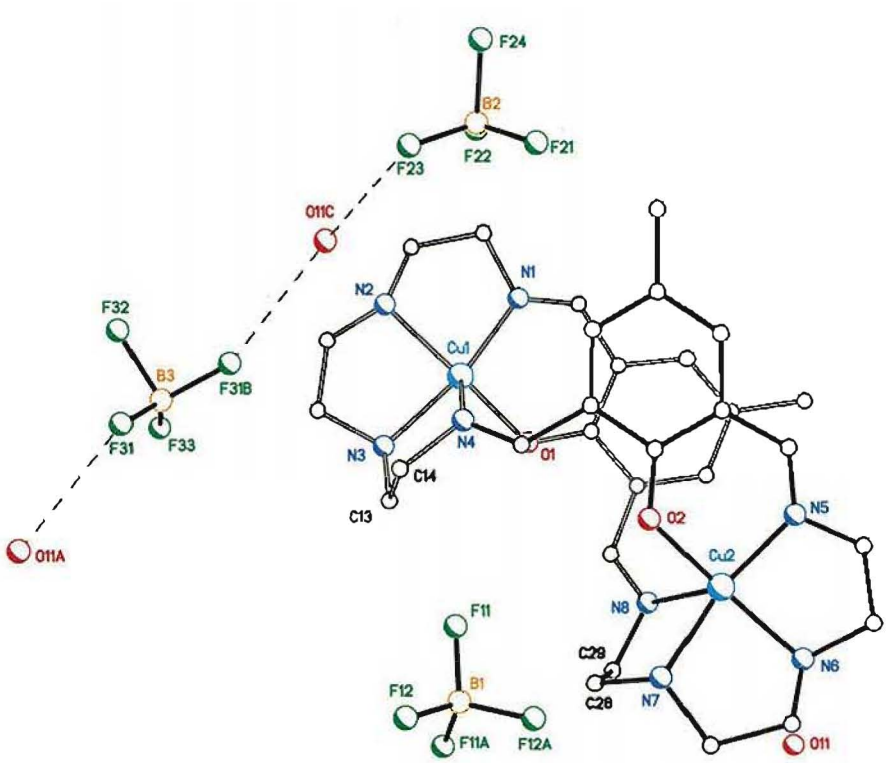

Figure 3.5.5. A perspective view of the complex $[Cu_2L^5](BF_4)_2{\cdot}H_2O$ (**17**) showing the three BF_4^- ions associated with the macrocyclic cation in the solid state. Two of the BF_4^- ions form hydrogen bonds (dashed lines) with the water molecules of crystallisation.

The half-occupancy BF_4^- ion (B1-F11-F12-F11A-F12A) which lies on a C_2 axis has the C_2 axis running through the boron atom B1 and the midpoint of the F11-F11A vector. The full-occupancy BF_4^- ion (that involving B2 - **Figure 3.5.6**) is disordered between two positions related by rotation about one B-F bond, with orientation 1 (B2-F21-F22-F23-F24) having a 60.7% occupancy, and orientation 2 (B2-F21-F25-F26-F27) a 39.3% occupancy. The second half-occupancy BF_4^- ion (that involving B3) is disordered between two positions (**Figure 3.5.7**), with 50% occupancy for each orientation, related by a centre of symmetry which lies on the midpoint of the B3-B3A vector.

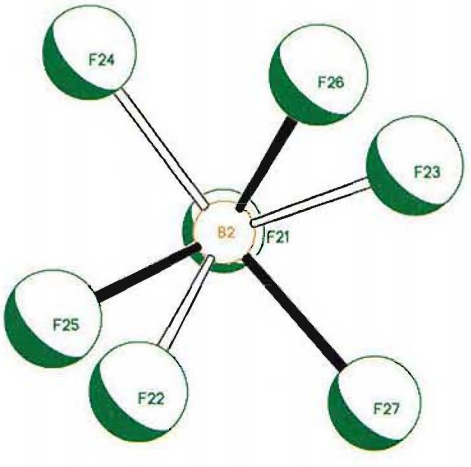

Figure 3.5.6. The BF_4^- ion which is disordered about a B-F bond (B2-F21), viewed approximately along the B2-F21 bond. Orientation 1 is shown in white bonds, orientation 2 in black bonds.

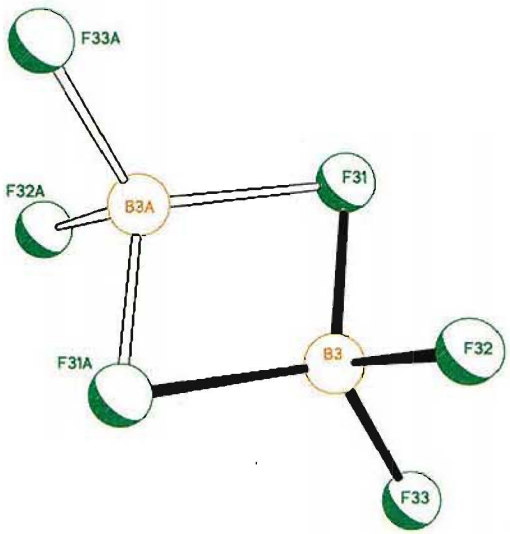

Figure 3.5.7. The BF_4^- ion that is disordered about a centre of symmetry.

The disordered BF_4^- ions form hydrogen bonds with two of the water molecules of crystallisation from two different unit cells (**Figure 3.5.5**), with equal hydrogen bond distances of 2.86 Å. These hydrogen bonds link three BF_4^- ions and two water molecules, but do not link individual macrocyclic units in the crystal (**Figure 3.5.8**). π-π interactions seem to be the major interactions that contribute to the packing of individual macrocyclic cations in the crystal. This is shown by the face-to-face stacking of the folded macrocyclic cations, where the adjacent phenyl rings of two molecules are separated by *ca.* 3.2 Å and almost parallel, being inclined at just 3.1°.

The macrocyclic cations are arranged in the same orientation in each stack. Since the folded macrocycle has a C-shape, each stack forms a hollow extending approximately parallel to the b axis. In the crystal, each stack has an equivalent stack related by a C_2 axis, resulting in the formation of some kind of a "tunnel" between the two stacks of macrocyclic cations. This cavity is filled by the BF_4^- ions that lie along the same C_2 axis. Each of these BF_4^- ions does not exactly lie in the hollow of the individual macrocyclic cations, but is slightly shifted "down" the stack, along the *b* axis with respect to the cations (**Figure 3.5.9**). Between these cation - BF_4^- - cation stacks lie the other BF_4^- ions and the water molecules of crystallisation which are linked by hydrogen bonds into anion-water-anion-water-anion chains.

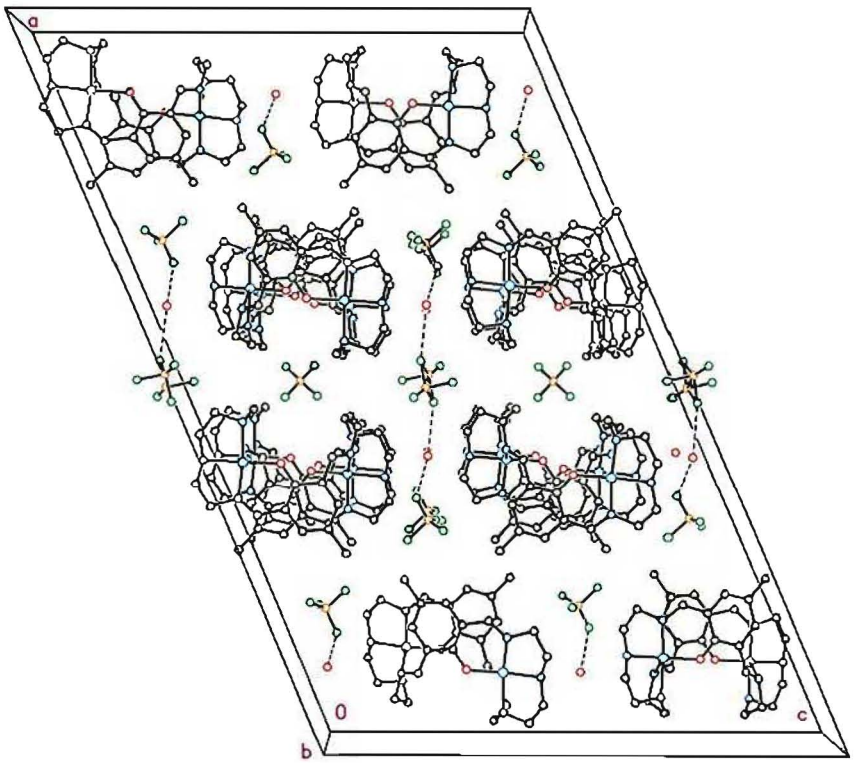

Figure 3.5.8. Crystal packing of the complex $[Cu_2L^5](BF_4)_2{\cdot}H_2O$ **17**, viewed along the crystallographic *b* axis, showing the parallel stacking of the cations and the hydrogen bonds.

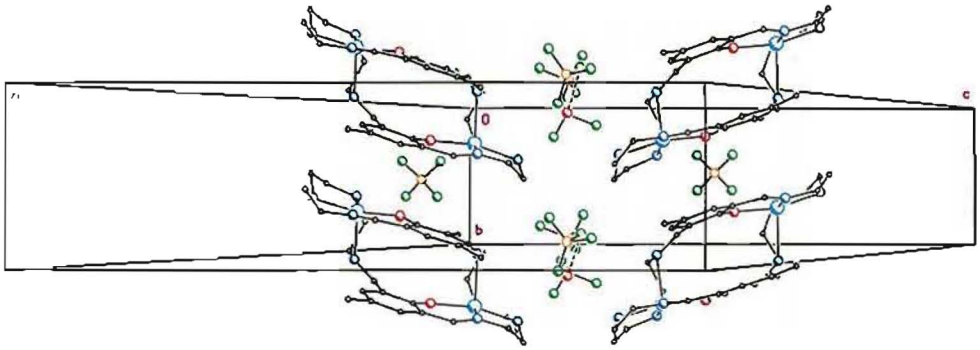

Figure 3.5.9. Crystal packing of the complex $[Cu_2L^5](BF_4)_2 \cdot H_2O$ **17**, viewed along the *ac* plane and perpendicular to the crystallographic *b* axis.

Infrared spectroscopy

The infrared spectra of **17**·H_2O and of **17** are basically the same and consistent with the structure of the macrocyclic complex as determined by X-ray crystallography. The spectra both show a strong and sharp peak at *ca.* 1641 cm^{-1}, characteristic of an imine group, a sharp peak with medium intensity at *ca.* 1545 cm^{-1}, assigned to the phenol C-O stretch, three sharp peaks of medium intensities in the 3300 - 3200 cm^{-1} region, assigned to secondary amine stretches and a split BF_4^- band at 1084 and 1041 cm^{-1}. No carbonyl absorption at *ca.* 1700 cm^{-1} is present in either spectrum. The split tetrafluoroborate band is probably due to those BF_4^- ions which are involved in hydrogen bonding interactions described previously. The hydrogen bonds are likely to distort the tetrafluoroborate ions from being a regular tetrahedron.

There is one noticable difference between the two spectra in the O-H stretching region, 3600 - 3500 cm^{-1} (**Figure 3.5.10**). In the spectrum of **17** only a single, broad envelope centred at 3440 cm^{-1} is present, but the spectrum of complex **17**·H_2O shows a broad band at *ca.* 3440 cm^{-1}, and two sharper shoulders.

These observations suggest that the only difference in the two complexes is the presence of a water molecule in **17**·H_2O which probably occupies an isolated site, preventing it from forming any hydrogen bonds, hence giving rise to the sharp O-H stretches in the infrared spectrum.

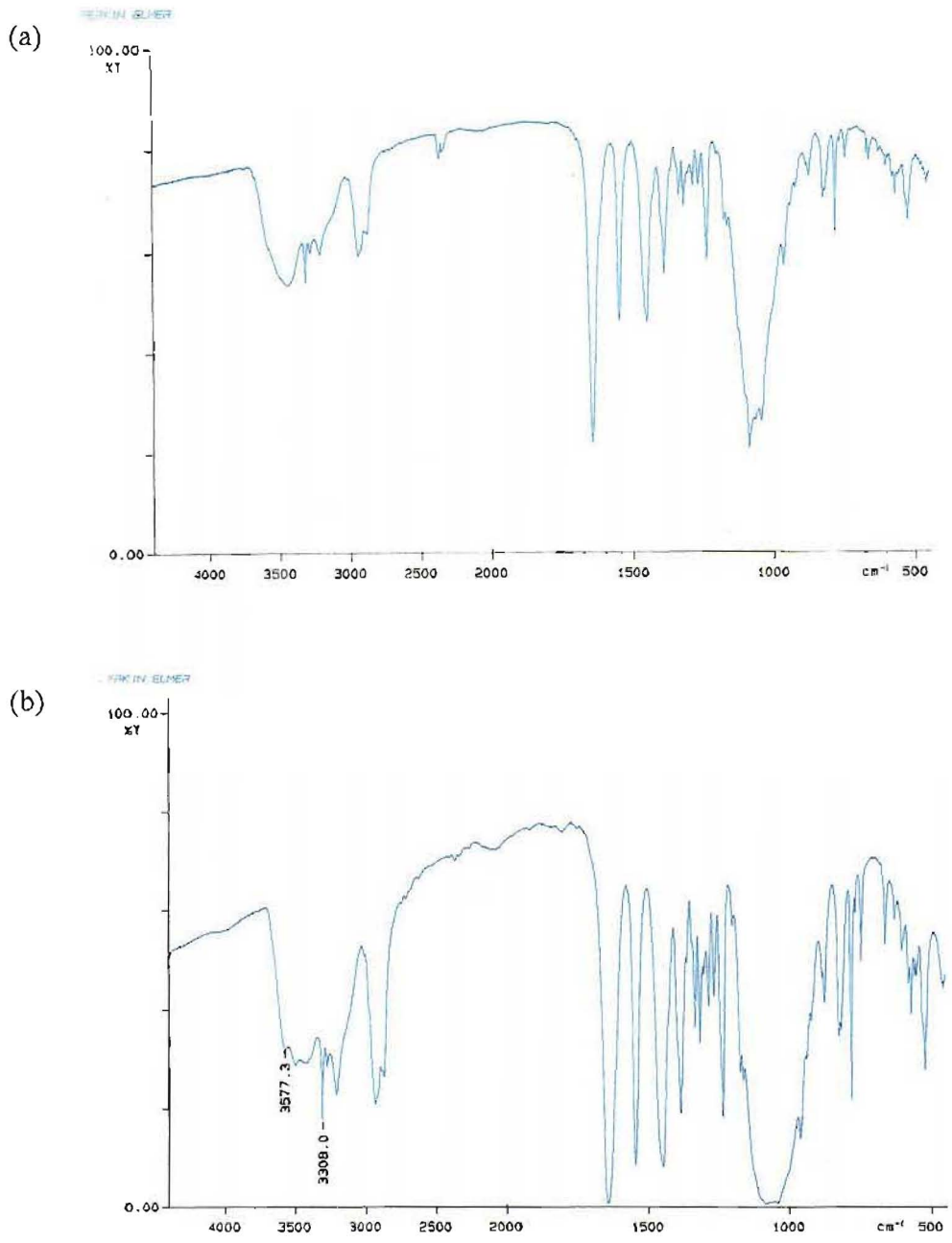

Figure 3.5.10. Infrared spectra of (a) $[Cu_2L^5](BF_4)_2 \cdot H_2O$ (**17**) and (b) $[Cu_2L^5](BF_4)_2 \cdot 2H_2O$ (**17**$\cdot H_2O$).

Magnetic measurements

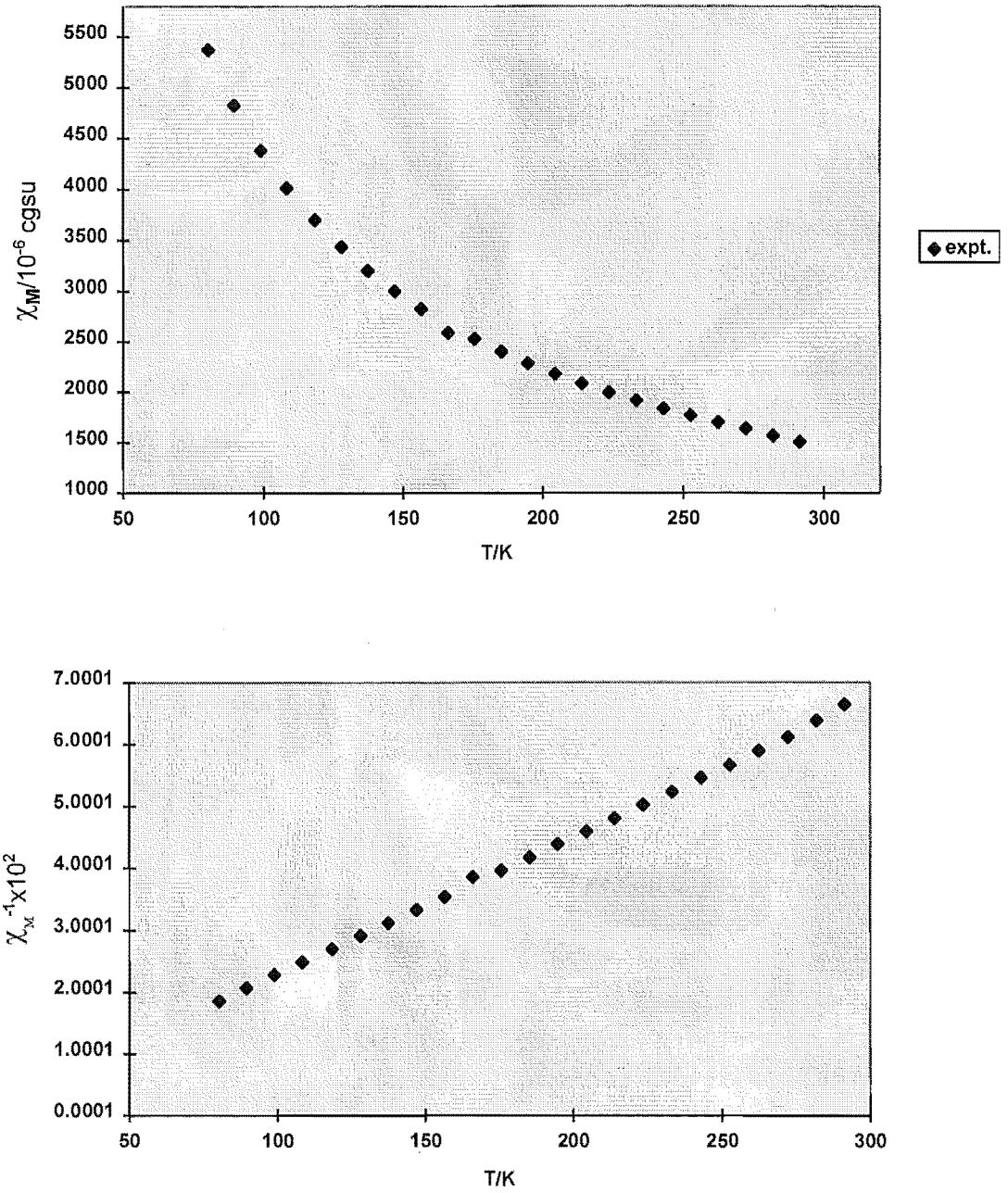

Figure 3.5.11. Temperature dependence of the molar magnetic susceptibility (χ_M) of $[Cu_2L^5](BF_4)_2 \cdot H_2O$.

The temperature variation of the magnetic susceptibility of the dicopper(II) complex **17** follows the Curie law within the temperature range of 80-300 K (**Figure 3.5.11**), with a magnetic moment of 1.88 B.M. per copper ion. The EPR spectrum of the complex (**Figure 3.5.12**), obtained as frozen DMF glass, shows some hyperfine

splitting with $A_{\|} = 52$ G. The magnetic measurements do not indicate significant magnetic interactions between the copper(II) ions, but the EPR shows that some weak

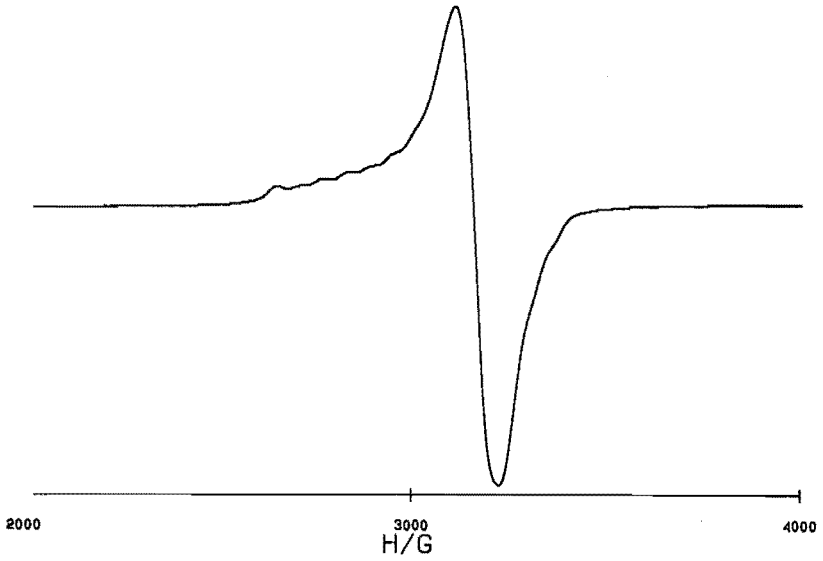

Figure 3.5.12. The EPR spectrum of $[Cu_2L^5](BF_4)_2 \cdot H_2O$ (**17**) as a frozen dimethylformamide glass.

coupling still exists, which probably is a through-space coupling. These observations are consistent with the X-ray structure which shows a significantly large separation between the copper(II) ions (*ca.* 6.5 Å).

Structural comparison with related complexes

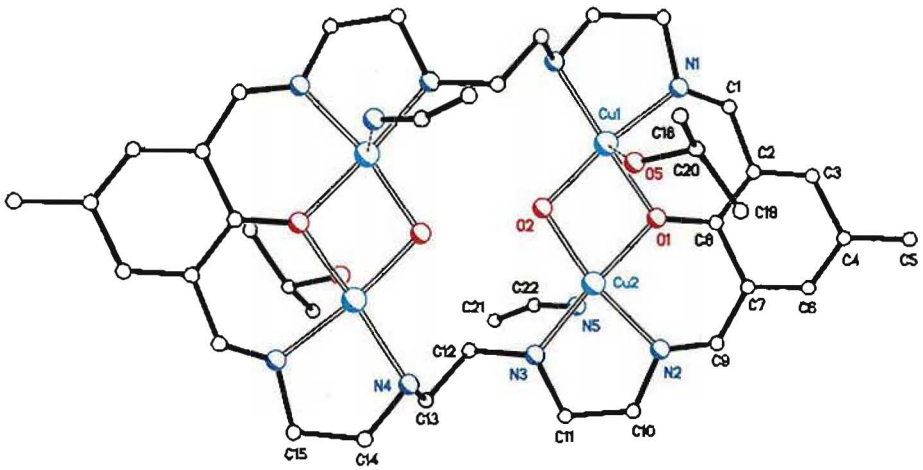

Figure 3.5.13. The structure of $[Cu_4L^5(OH)_2(^iPrOH)_2(CH_3CN)_2]^{4+}$ (**17T**), showing the open conformation of the macrocycle $(L^5)^{2-}$.

The macrocyclic ligand $(L^5)^{2-}$ has been shown[67] to be able to form an approximately planar copper(II) complex, as well as the folded complex **17**, when the 30-membered macrocycle adopts an open cavity conformation. In the open cavity conformation the macrocycle has a suitable ring size, and a proper number and arrangement of donor atoms to accomodate four copper(II) ions inside the macrocyclic cavity. The structure of the tetracopper(II) complex of $(L^5)^{2-}$ is illustrated in **Figure 3.5.13**.

The tetracopper(II) complex, $[Cu_4L^5(OH)_2(^iPrOH)_2(CH_3CN)_2]^{4+}$ (**17T**) is centrosymmetric with the phenol groups of the macrocycle being fully-deprotonated. In contrast to complex **17**, the phenoxo oxygen atoms in **17T** are each bridging a pair of copper(II) ions, so that the tetranuclear complex may be regarded as being composed of two dicopper(II) units, being a "dimer-of-dimers".[67] The "diagonally-related" copper(II) ions are also symmetry-related and separated by 6.510(5) Å [Cu1...Cu1'] and 5.821(4) Å [Cu2...Cu2'], where Cu1' and Cu2' are the symmetry equivalent atoms.

Two hydroxo ions occupy the central cavity of the Cu_4 core; each bridging two copper atoms and completing the coordination spheres of the copper(II) ions. Several "external" ligands are also present in this complex, occupying the axial coordination

sites of the copper(II) ions. The presence of these non-macrocyclic donors is in contrast to the case of complex **17**, where the donors for the copper(II) ions come from the macrocyclic ligand alone.

The fact that the macrocycle $(L^5)^{2-}$ is able to accomodate two or four Cu(II) ions within its cavity demonstrates the flexibility of the ligand, allowing it to adopt different conformations, to suit the synthetic conditions and to conform to the metal ion stereochemical preference.

The structural differences between complexes **17** and **17T** could partly be a consequence of the different methods of preparation, particularly the mixing order of the three reactants (diformylphenol, diamine and copper(II) template).

Complex **17** was prepared by mixing triethylenetetramine (trien) with copper(II) tetrafluoroborate, followed by mixing with 2,6-diformyl-4-methylphenol (DFMP). Upon mixing the copper(II) tetrafluoroborate and trien, a violet blue solution was obtained, suggesting complexation of Cu(II) by trien. Examination of the crystal structure of complex **17** suggests that presumably at this stage one trien molecule complexed one copper ion using all four of the nitrogen donors, giving the 1:1 Cu(II):amine complex illustrated in **Figure 3.5.11**, Scheme A. On addition of DFMP, two such "templated" trien molecules would condense with two molecules of DFMP to form the macrocycle $(L^5)^{2-}$ as the dicopper(II) complex **17**.

On the other hand, complex **17T** was prepared by mixing DFMP, triethylamine and copper(II) perchlorate, followed by addition of trien. The triethylamine would very likely deprotonate the diformylphenol. Since it has long been recognised that a phenoxo oxygen can bind two transition metal ions simultaneously, acting as a bridge between the metal ions, it is thus likely that the 2,6-diformyl-4-methylphenolate would chelate two copper(II) ions per molecule of DFMP. Possibly the 1:2 complex[67] or 2:2 complex[98] of DFMP and copper(II) (**Figure 3.5.12** - structures **I** and **II**, respectively) was formed at this stage. Subsequent condensation of two molecules of the templated 2,6-diformyl-4-methylphenolate with two molecules of trien would intuitively be expected to lead to the formation of complex **17T** (Scheme B - **Figure 3.5.11**).

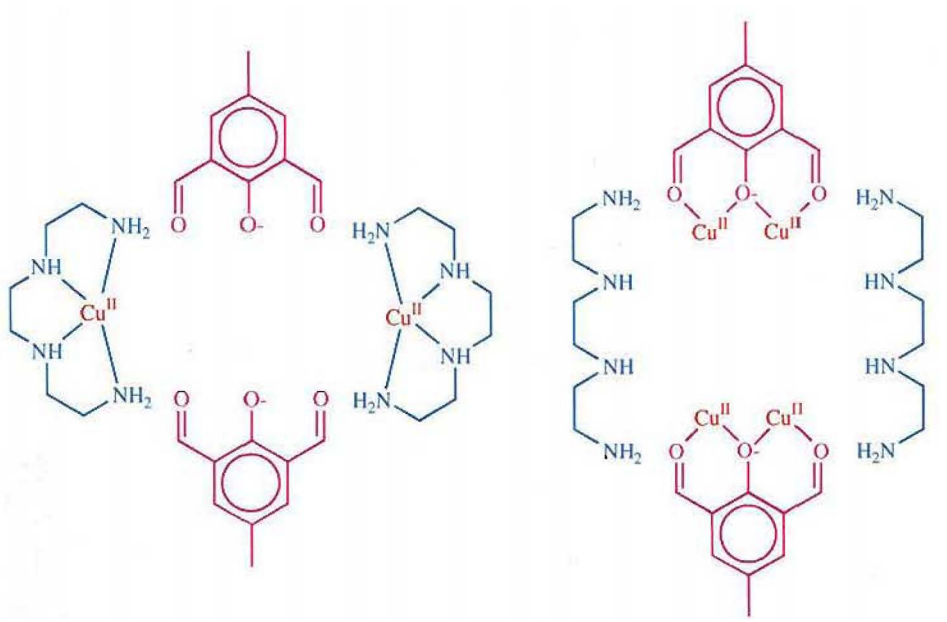

Scheme A Scheme B

Figure 3.5.11. Proposed mechanism of formation of complex **17** (Scheme A). Proposed mechanism of formation of complex **17T** (Scheme B).

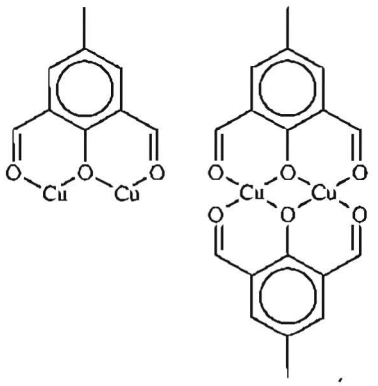

I **II**

Figure 3.5.12. 1:2 complex (**I**) and 2:2 complex (**I**) of DFMP and copper(II).

Several other phenol-containing Schiff-base macrocycles which have folded conformations have been structurally characterised.[76, 106c, 110, 111] These macrocycles (**Figure 3.5.13**) show different degrees of folding, measured by the angles between the planes defined by the phenyl rings in each macrocycle (14° for **MC22**; 25° for **MC23**; 7° for **MC24**; 2° for **MC25**). The macrocycles **MC22**, **MC23**[106c, 110] and H_2(**MC24**)[76]

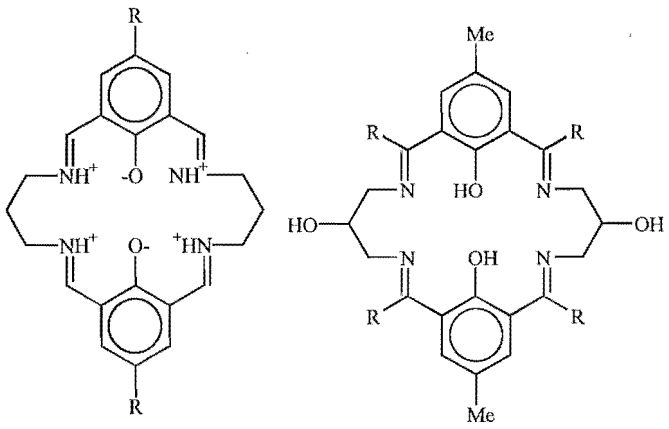

MC22 R = Me
MC23 R = ^{t}Bu

MC24 R = H
MC25 R = Me

Figure 3.5.13.

were isolated free of metal ions. Hydrogen bonds involving the protonated macrocyclic donors may stabilise the ligands in the absence of metal ions. On the other hand, the macrocycle **MC25** was isolated as its mononuclear barium(II) complex.[111]

The difference in the degree of folding of the macrocycles **MC22** and **MC23** was ascribed to the steric bulk of the *p*-substituents of the phenol rings.[106c] The structure of complex **17** supports this conclusion, with the methyl subtituents of $(L^5)^{2-}$ being rotated away from each other by *ca.* 90°. This mutually-rotated orientation would be expected to reduce the steric repulsion between the methyl substituents and hence increase the folding of the macrocycle. It was also suggested[106c] that the degree of folding of macrocycles of this type might be controlled by adjusting the length of the macrocyclic saturated chains.

The structure of the macrocycle H_2(**MC24**)[76] shows that the molecular cleft formed by the folded macrocycle is occupied by water molecules which are intramolecularly hydrogen bonded to the macrocyclic donors. Whereas in the barium complex of **MC25** the barium(II) ion sits above the folded macrocycle (**Figure 3.5.14**). These observations, and the facts that the macrocycle $(L^5)^{2-}$ can fold to quite a different extent depending on the number of copper(II) ions coordinated, suggest that the degree of folding of a macrocycle may also be influenced by the coordination of metal ion(s) to the macrocycle, by the type and number of metal ion(s) coordinated, or by intramolecular hydrogen bonds.

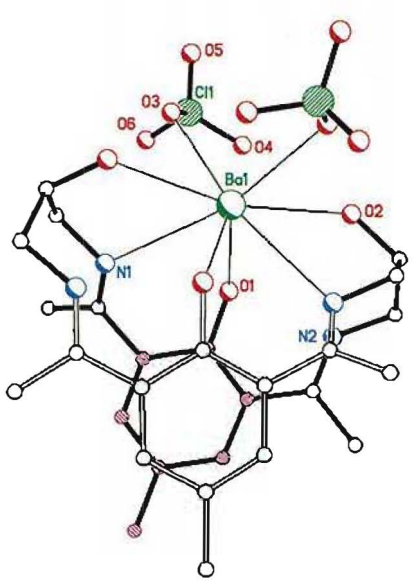

Figure 3.5.14. The structure of a barium(II) complex of H_2(**MC25**)[111] viewed perpendicular to the mean plane of the phenyl ring that is coloured in purple.

If the macrocycle $(L^5)^{2-}$ had an open conformation in complex **17**, the two copper(II) ions could be regarded as being coordinated diagonally (**Figure 3.5.15**) within the potentially tetranucleating macrocycle, leaving two vacant metal binding sites, also diagonally-related. The copper(II) arrangement here is different from that found in complex **16** (**Section 3.4**), where the two copper(II) ions are bound by the tetranucleating macrocycle $(L^6)^{4-}$ laterally (**Figure 3.5.15**).

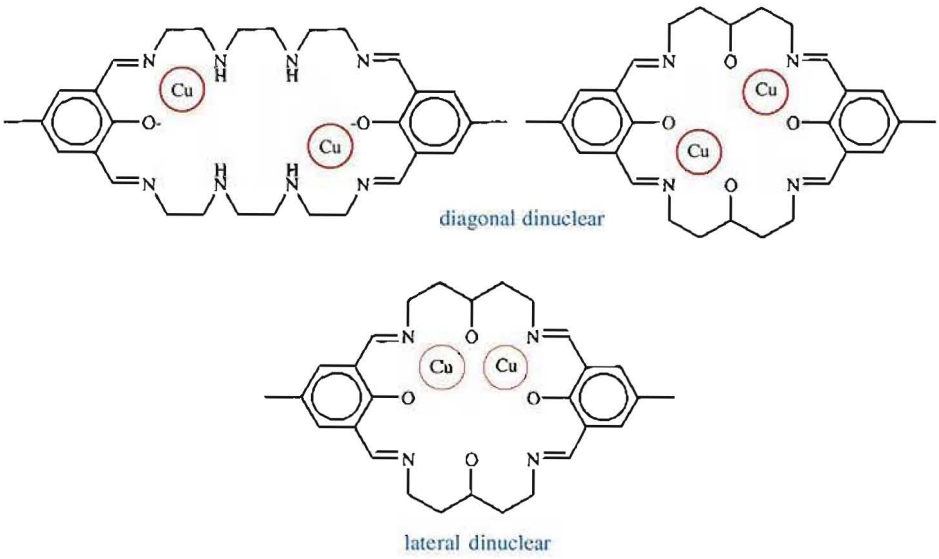

Figure 3.5.15.

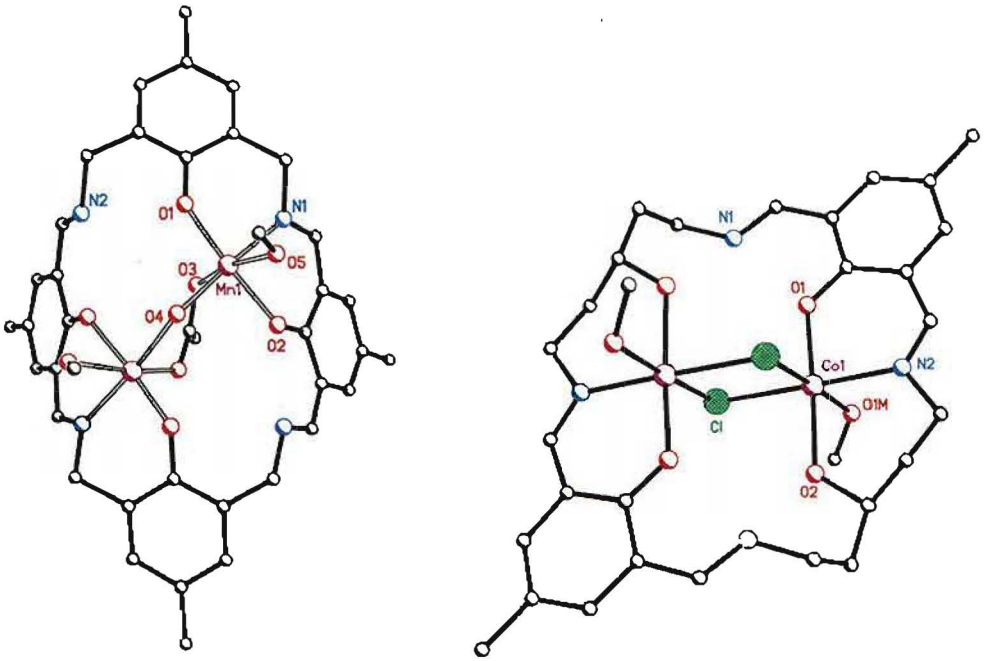

(a) (b)

Figure 3.5.16. The crystal structures of
(a) $[Mn_2H_2(\mathbf{MC17})(\mu\text{-OOCMe})(\mu\text{-OH})(MeOH)_2]^{2+}$ $[Mn_2(\mathbf{MC17})]$[112]; and
(b) $[Co_2(H_4L^6)Cl_2(CH_3OH)_2]^{2+}$.[73]

Other structurally characterised dinuclear transition metal complexes, where the two metal centres are related diagonally, include the dimanganese(III) complex of $H_2(\mathbf{MC17})^{2-}$, $[Mn_2H_2(\mathbf{MC17})(\mu\text{-OOCMe})(\mu\text{-OH})(MeOH)_2]^{2+}$ [denoted $Mn_2(\mathbf{MC17})$ hereafter][112] and the dicobalt(II) complex of $(H_2L^6)^{2-}$ $[Co_2(H_4L^6)Cl_2(CH_3OH)_2]^{2+}$,[73] the structures of which are shown in **Figure 3.5.16**.

In these two complexes, the two metal ions are doubly-bridged; the manganese(III) ions in $Mn_2(\mathbf{MC17})$ by a OH^- ion and an acetate ion, the cobalt(II) ions in $[Co_2(H_4L^6)Cl_2(CH_3OH)_2]^{2+}$ by two chloride ions. This is in contrast to the copper(II) ions in **17** which are not bridged by any non-macrocyclic donors.

In both the manganese(III) and cobalt(II) diagonal complexes, intramolecular proton transfer from the phenol to the imine group, analogous to that observed in a phenol-based cryptate system,[113] is either presumed or verified (see discussion below). In contrast, the macrocycle in complex **17** is not protonated either at its phenol or imine donors.

The two hydrogen atoms of the macrocyclic ligand in the dimanganese(III) complex could not be located on the basis of the diffraction data.[112] However, these hydrogen atoms are believed to have been transferred to the uncoordinated nitrogen donors and hydrogen bonded to the deprotonated phenol group, as observed in the structure of the dihydrochloride salt of **MC17**.[112] On the other hand, the hydrogen atoms originating from the phenol groups of the macrocycle in the complex $[Co_2(H_4L^6)Cl_2(CH_3OH)_2]^{2+}$ could be located from X-ray diffraction data, shown to be attached to the uncoordinated imine nitrogen donors of the macrocyclic ligand.[73]

These diagonal complexes have a potential to form heterotetranuclear complexes of a different type from that of the heterotetranuclear complexes that could be generated from the lateral complexes such as complex **16** (**Section 3.4**). Some of the possible types of heterotetranuclear macrocyclic complex that may be generated from the diagonal and lateral dicopper(II) complexes are illustrated schematically in **Figure 3.5.17**.

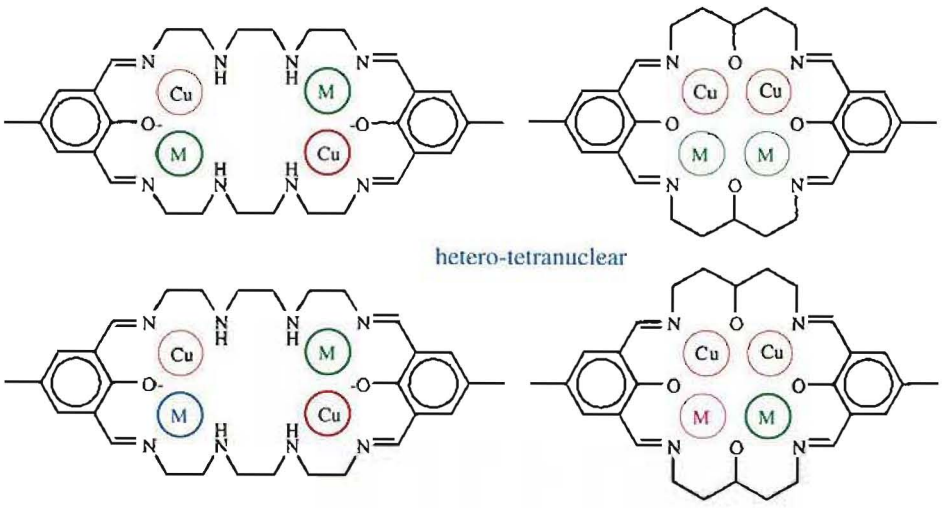

Figure 3.5.17. Some possible heterotetranuclear complexes of the macrocycles L^5 and L^6 that may be generated from the corresponding dicopper(II) complexes.

CONCLUSIONS AND SUGGESTIONS FOR FUTURE WORK

The present work has demonstrated some results concerning the applicability of a stepwise template condensation strategy to prepare asymmetric Schiff-base macrocycles. These results are summarised below.

Isolation of acyclic intermediate ligands

The first step of the stepwise method, ie. the isolation of an acyclic ("partly-formed" macrocyclic) ligand as its copper(II) complex, gave positive results when 1,3-diaminopropane was employed as the diamine component. Two diimine-diamine ligands were successfully prepared from the [2+1] condensation of 1,3-diaminopropane and 2,6-diformyl-4-R-phenol [R = Me, $(L^1)^-$; R = ^{t}Bu, $(L^8)^-$] as their dicopper(II) hydroxo-bridged complexes. X-ray crystallography has revealed the structures of these complexes and showed that the two ligands have very similar conformations in their copper(II) complexes.

The formation of an acyclic or a macrocyclic product from the template condensation of 1,3-diaminopropane and 2,6-diformyl-4-methylphenol appeared to depend on the pH of the reaction mixture. The macrocyclic copper(II) complex was preferentially formed when the mixture was basic, such as in the presence of a high excess of diamine or an added base.

An acyclic Schiff-base ligand, $(L^4)^{5-}$, was isolated as a copper(II) complex from the template condensation of 4-*t*-butyl-2,6-diformylphenol (TDFP) with 1,3-diamino-2-hydroxypropane. However, preliminary X-ray crystal structure analysis of this complex (and of a derivative of this complex) showed that the ligand was derived from the condensation of three molecules of 1,3-diamino-2-hydroxypropane and two molecules of TDFP (a [3+2] condensation product). The ligand was also shown to be templated onto a Cu_6 ring and to have its two NH_2 groups of $(L^4)^{5-}$ in a similar spatial arrangement to those of the NH_2 acyclic ligands $(L^1)^-$ and $(L^8)^-$.

The structures of the hexacopper(II) complexes of $(L^4)^{5-}$ showed severe disorder involving the ligands that occupy the centre of the Cu_6 ring. The major component of the hexacopper(II) complex contains three μ-hydroxo ions in the central cavity of the Cu_6 ring. Fast-atom-bombardment mass spectrometry supported this assignment. The minor component was indicated by X-ray crystallography to contain a tetrahedral species (possibly SO_4^{2-} or ClO_4^-) which bind centrally to the Cu_6 ring. The possible source of ClO_4^- is uncertain; however, the source of SO_4^{2-} is suspected to be the 4-*t*-butyl-2,6-diformylphenol whose preparation[73] involved the use of sulfuric acid at one stage.

Towards the end of this work, a method for the preparation of 4-*t*-butyl-2,6-diformylphenol was acquired (see Experimental) which does not involve the use of sulfuric acid. Hence the synthesis of $(L^4)^{5-}$ will be able to be carried out in the exclusion of SO_4^{2-} to obtain a hexacopper(II) complex which may not be a combination of some species and consequently may be able to be fully characterised structurally.

Those systems which involved the use of 1,5-diamino-3-hydroxypentane (1,5-DAHP), or triethylenetetramine (trien), as the diamine component and 2,6-diformyl-4-methylphenol as the diformylphenol component, did not yield acyclic intermediate ligands under the experimental conditions employed. Instead, the copper(II) complexes of the [2+2] Schiff-base macrocycles [diamine = 1,5-DAHP, $(L^6)^{4-}$ or $(HL^6)^{3-}$; trien, $(L^5)^{2-}$] were obtained as the main products.

For the system involving 1,5-DAHP, the preferential formation of the macrocyclic complexes over the acyclic analogue could be due to kinetic as well as thermodynamic factors (see **Section 3.4**). The formation of the acyclic ligand may be promoted, and the formation of the macrocyclic product hindered, by the use of some coordinating anions or small ligands in the synthesis. These ligands may coordinate to the copper(II) ions, thus completing the coordination spheres of the copper(II) ions and preventing further template condensation with a second molecule of 2,6-diformyl-4-methylphenol.

In these cases, a metal template other than Cu(II) may be more effective in generating the acyclic Schiff-base ligands. This could be combined with a modification of the method introduced by Brooker and Croucher[62, 91] to prepare a derivative of 1,5-DAHP or triethylenetetramine one of whose NH_2 groups is protected. This approach is outlined in **Scheme 1** below.

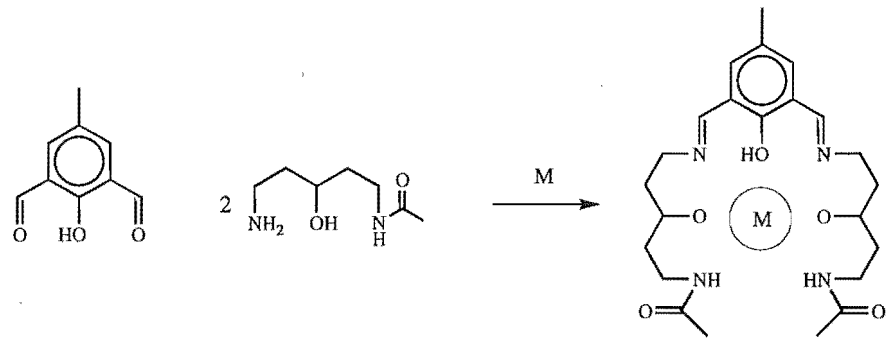

Scheme 1.

Ring-closure condensation

The acyclic ligand $(L^1)^-$ which was templated on two copper(II) ions underwent a ring-closure cyclocondensation with 2,5-diformylfuran (DFF) to generate an asymmetric tetraimine macrocycle, $(L^3)^-$. The ring-closure condensation of the copper(II) complexes of $(L^4)^{5-}$ and $(L^8)^-$ with DFF would also be expected to give a macrocyclic product, since the structures of these copper(II) complexes indicate that the spatial arrangement of the NH_2 groups of these ligands is very similar to that of $(L^1)^-$ in its dicopper(II) complex.

The ring-closure condensation reaction of the hexacopper(II) complex of $(L^4)^{5-}$ with DFF or other dicarbonyl compounds could possibly lead to the isolation of a new

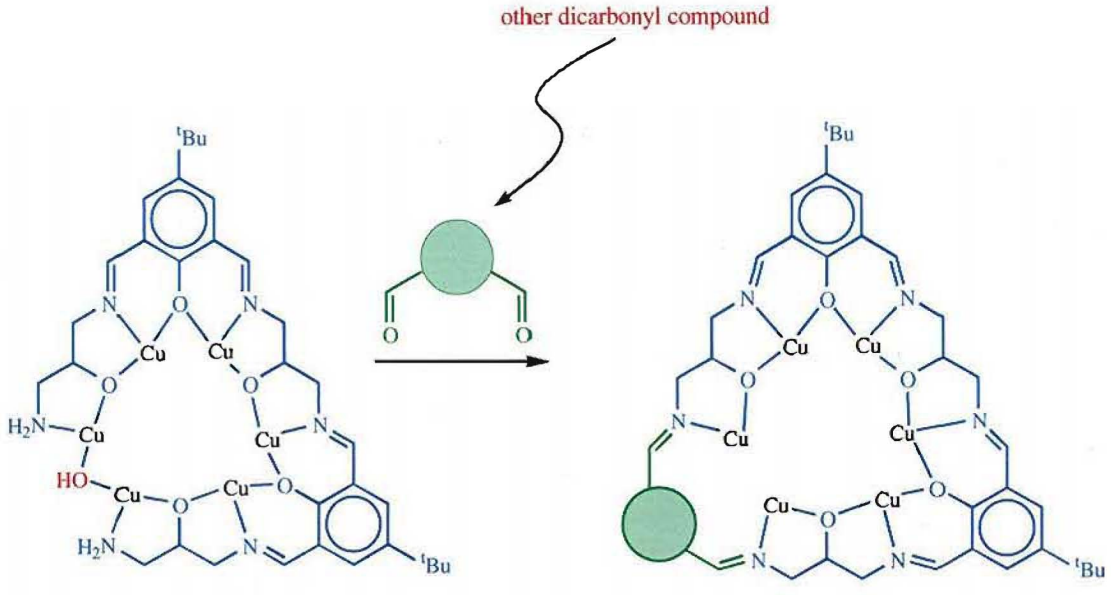

Scheme 2.

[3+3] asymmetric Schiff-base macrocycle (**Scheme 2**). This macrocycle would have a potential to bind a mixture of transtition metal ions, giving polynuclear complexes with interesting properties.

A methoxo-bridged or an ethoxo-bridged complex was obtained when the solvent was methanol or ethanol, repectively. This indicates that the nature of the dicopper(II) complex of the asymmetric macrocycle $(L^3)^{\cdot}$ depends on the solvent employed in the ring-closure condensation of $(L^1)^{\cdot}$. In addition, the methoxo ligand in the methoxo-bridged dicopper(II) complex of $(L^3)^{\cdot}$ seemed to be readily replaced by either a hydroxo or an ethoxo ion, in N,N-dimethylformamide at room temperature.

Additional results

The tetracopper(II) complex cation of the [2+2] Schiff-base macrocycle $(L^6)^{4\cdot}$, derived from 2,6-diformyl-4-methylphenol and 1,5-diamino-3-hydroxypentane, is able to promote the hydrolysis of N,N-dimethylformamide at room temperature. Further investigations on the kinetic of this catalytic reaction may be carried out.

GLOSSARY

1,5-DAHP	1,5-diamino-3-hydroxypentane
DAP	2,6-diacetylpyridine
DFF	2,5-diformylfuran
DFMP	2,6-diformyl-4-methylphenol
DMF	*N,N*-dimethylformamide
EPR	electron paramagnetic resonance
TDFP	4-*t*-butyl-2,6-diformylphenol

REFERENCES

1. M.J. Baldwin, M.D. Lowery, E.I. Solomon. *Chem. Rev.*, 1992, **92**, 521.
2. E.I. Solomon, K.W. Penfield, D.E. Wilcox. *Struct. Bonding*, 1983, **53**, 1.
3. N. Kitajima. *Adv. Inorg. Chem.*, 1992, **39**, 1.
4. T.G. Spiro, B. Kincaid, J.A. Larrabee, J.M. Brown, M. Powers. *J. Am. Chem. Soc.*, 1980, **102**, 4210.
5. K.O. Hodgson, R. Lontie, T.K. Eccles. *J. Am. Chem. Soc.*, 1981, **103**, 984.
6. J.E. Carpenter, K.A. Magnus, Hoa Ton-That. *Chem. Rev.*, 1994, **94**, 727.
7. D.E. Root, E.I. Solomon, B.L. Hemming, in *Bioinorganic Chemistry of Copper*, (K.D. Karlin, Z. Tyeklar, editors), Chapman & Hall, New York-London, 1993, 3.
8. T.B. Freedman, T.M. Loehr, J.S. Loehr. *J. Am. Chem. Soc.*, 1976, **98**, 2809.
9. T.G. Spiro, J.A. Larrabee. *J. Am. Chem. Soc.*, 1980, **102**, 4217.
10. K.A. Magnus, H. Ton-That, J.E. Carpenter, in *Bioinorganic Chemistry of Copper*, (K.D. Karlin, Z. Tyeklar, editors), Chapman & Hall, New York, 1993, 143.
11. S. Iwata, C. Ostermeier, B. Ludwig, H. Michel. *Nature*, 1995, **376**, 660.
12. T. Tsukihara, H. Aoyama, E. Yamashita, T. Tomizaki, H. Yamaguchi, K. Shinzawa-Itoh, R. Nakashima, R. Yaono, S. Yoshikawa. *Science*, 1995, **269**, 1069.
13. A. Messerschmidt. *Adv. Inorg. Chem.*, 1994, **40**, 121.
14. J.A. Fee. *Structure and Bonding (Berlin)*, Springer-Verlag Berlin Heidelberg, Germany, 1975, **23**, 1.

15. D.J. Spira-Solomon, M. Allendorf, E.I. Solomon. *J. Am. Chem. Soc.*, 1986, **108**, 5318.

16. J.L. Cole, P.A. Clark, E.I. Solomon. *J. Am. Chem. Soc.*, 1990, **112**, 9534.

17. J.L. Cole, E.I. Solomon, L. Avigliano, L. Morpurgo. *J. Am. Chem. Soc.*, 1991, **113**, 9080.

18. K.O. Hodgson, E.I. Solomon, T.J. Thamann, C.D. LuBien, M.E. Winkler, R.A. Scott, M.S. Co. *J. Am. Chem. Soc.*, 1981, **103**, 7014.

19. K.O. Hodgson, E.I. Solomon, D.J. Spira-Solomon, Kau Lung-Shan, J.E. Penner-Hahn. *J. Am. Chem. Soc.*, 1987, **109**, 6433.

20. J.L. Cole, E.I. Solomon, G.O. Tan, E.K. Yang, K.O. Hodgson. *J. Am. Chem. Soc.*, 1990, **112**, 2243.

21. J.L. Cole, D.P. Ballou, E.I. Solomon. *J. Am. Chem. Soc.*, 1991, **113**, 8544.

22. E.I. Solomon, P.A. Clark. *J. Am. Chem. Soc.*, 1992, **114**, 1108.

23. (a) A. Messerschmidt, R. Ladenstein, R. Huber, M. Bolognesi, L. Avigliano, R. Petruzzelli, A. Rossi, A. Finazzi-Agro. *J. Mol. Biol.*, 1992, **224**, 179.

(b) V.N. Zaitsev, I. Zaitseva, B. Bax, G. Card, A. Ralph, P. Lindley, *Diagnostic & Therapeutic Aspects of Metals in Biology, Meeting of the Inorganic Biochemistry Discussion Group,* University of North London, 19 & 20 December 1994.

24. A. Messerschmidt, R. Huber. *Eur. J. Biochem.*, 1990, **187**, 341.

25. L. Calabrese, M. Carbonaro, G. Musci. *J. Biol. Chem.*, 1989, **264**, 6183.

26. V. M^{c}Kee. *Adv. Inorg. Chem.*, 1994, **40**, 323.

27. K.D. Karlin, J. Zubieta, Q. Gan, A. Farooq, S. Liu. *Inorg. Chim. Acta*, 1989, **165**, 37.

28. S. Meenakumari, A.R. Chakravarty. *J. Chem. Soc., Dalton Trans.*, 1992, 2749.

29. F.B. Hulsbergen, R.W.M. ten Hoedt, G.C. Verschoor, J. Reedijk, A.L. Spek. *J. Chem. Soc., Dalton Trans.*, 1983, 539.

30. D. Datta, A. Chakravorty. *Inorg. Chem.*, 1983, **22**, 1611.

31. R.J. Butcher, C.J. O'Connor, E. Sinn. *Inorg. Chem.*, 1981, **20**, 537.

32. A.R. Chakravarty, S. Meenakumari, S.K. Tiwari. *Inorg. Chem.*, 1994, **33**, 2085.

33. S. Meenakumari, S.K. Tiwary, A.R. Chakravarty. *Inorg. Chem.*, 1994, **33**, 2085.

34. Y. Agnus, R. Louis, C. Boudon, B. Metz, J.P. Gisselbrecht, M. Gross. *Inorg. Chem.*, 1991, **30**, 3155.

35. M. Angaroni, G.A. Ardizzoia, T. Beringhelli, G. La Monica, D. Gatteschi, N. Masciocchi, M. Moret. *J. Chem. Soc., Dalton Trans.*, 1990, 3305.

36. D. Luneau, H. Oshio, H. Okawa, S. Kida. *J. Chem. Soc., Dalton Trans.*, 1990, 2283.

37. P. Chaudhuri, I. Karpenstein, M. Winter, C. Butzlaff, E. Bill, A.X. Trautwein, U. Florke, H. Haupt. *J. Chem. Soc., Chem. Commun.*, 1992, 321-322.

38. A. Bencini, A. Bianchi, E. Garcia-Espana, M. Micheloni, P. Paoletti. *Inorg. Chem.*, 1988, **27**, 176.

39. a) H. Adams, N.A. Bailey, M.J.S. Dwyer, D.E. Fenton, P.C. Hellier, P.D. Hempstead. *J. Chem. Soc., Chem. Commun.*, 1991, 1297.

b) D.E. Fenton, H. Adams, N.A. Bailey, M.J.S. Dwyer, P.C. Hellier, P.D. Hempstead, J.M. Latour. *J. Chem. Soc., Dalton Trans.*, 1993, 1207.

40. L.F. Lindoy. *The Chemistry of Macrocyclic Ligand Complexes*, Cambridge University Press, Cambridge-New York-New Rochelle-Melbourne-Sydney, 1990.

41. P. Guerriero, P.A. Vigato, D.E. Fenton, P.C. Hellier. *Acta Chem. Scand.*, review. 1992, **46**, 1025.

42. S.M. Nelson, in *Copper Coordination Chemistry: Biochemical and Inorganic Perspectives*, (K.D. Karlin, J. Zubieta, editors), Adenine Press, New York, 1983, 331.

43. S.M. Nelson, C.V. Knox, M. M^{c}Cann, M.G.B. Drew. *J. Chem. Soc., Dalton Trans.*, 1981, 1669.

44. D.E. Fenton, D.H. Cook. *J. Chem. Soc., Dalton Trans.*, 1979, 266.

45. D.H. Cook, D.E. Fenton. *J. Chem. Soc., Dalton Trans.*, 1979, 810.

46. M.G.B. Drew, D.E. Fenton, M. M^{c}Cann, S.M. Nelson, D.H. Cook. *J. Chem. Soc., Dalton Trans.*, 1979, 414.

47. D.E. Fenton, P.A. Vigato, S.J. Kitchen, C.M. Spencer, S. Tamburini. *J. Chem. Soc., Dalton Trans.*, 1988, 685.

48. H.C. Aspinall, J. Black, I. Dodd, M. Harding, S.J. Winkley. *J. Chem. Soc., Dalton Trans.*, 1993, 709.

49. (a) S.S. Tandon, L.K. Thompson, J.N. Bridson. *J. Chem. Soc., Chem. Commun.*, 1992, 911.

(b) J.N. Bridson, S.S. Tandon, L.K. Thompson, C. Benelli. *Inorg. Chem.*, 1995, 34, 5507.

50. S.A. Brooker, V. M^{c}Kee, W.B. Shepard, L.K. Pannell. *J. Chem. Soc., Dalton Trans.*, 1987, 2555.

51. S.A. Brooker, R.J. Kelly, G.M. Sheldrick. *J. Chem. Soc., Chem. Commun.*, 1994, 487.

52. S. Kida, H. Okawa. *Inorg. Nucl. Chem. Letters*, 1971, **7**, 751.

53. S. Kida, H. Okawa. *Bull. Chem. Soc. Jpn.*, 1972, **45**, 1759.

54. D.N. Hendrickson, R.C. Long. *J. Am. Chem. Soc.*, 1983, **105**, 1513.

55. S. Kida, N. Matsumoto, H. Okawa, H. Sakiyama, M. Tadokoro, M. Kodera. *J. Chem. Soc., Dalton Trans.*, 1992, 313.

56. H. Okawa, J. Nishio, M. Ohba, M. Tadokoro, N. Matsumoto, M. Koikawa, S. Kida, D.E. Fenton. *Inorg. Chem.*, 1993, **32**, 2949.

57. Y. Aratake, N. Matsumoto, M. Ohba, H. Okawa, H. Sakiyama, M. Tadokoro. *Inorg. Chim. Acta*, 1993, **212**, 183.

58. S. Kida, M. Koikawa, N. Matsumoto, H. Okawa, M. Tadokoro. *J. Chem. Soc., Dalton Trans.*, 1991, 1657.

59. M.G.B. Drew, J. Nelson, S.M. Nelson. *J. Chem. Soc., Dalton Trans.*, 1981, 1678.

60. S.M. Nelson, M.G.B. Drew, F.S. Esho. *J. Chem. Soc., Dalton Trans.*, 1982, 407.

61. S.K. Mandal, K. Nag. *J. Chem. Soc., Dalton Trans.*, 1984, 2141.

62. S.A. Brooker, P.D. Croucher. *J. Chem. Soc., Chem. Commun.*, 1993, 1278.

63. S.A. Brooker, P.D. Croucher. *J. Chem. Soc., Chem. Commun.*, 1995, 2075.

64. N.H. Pilkington, R. Robson. *Aust. J. Chem.*, 1970, **23**, 2225.

65. H. Sakiyama, K. Motoda, H. Okawa, S. Kida. *Chemistry Letters*, 1991, 1133.

66. D.E. Fenton, N. Matsumoto, K. Motoda, H. Okawa, H. Sakiyama. *J. Chem. Soc., Dalton Trans.*, 1995, 3419.

67. H. Okawa. *Bull. Chem. Soc. Jpn.*, 1970, **43**, 3019.

68. V. M^{c}Kee, J. Smith. *J. Chem. Soc., Chem. Commun.*, 1983, 1465.

69. N.A. Bailey, D.E. Fenton, R. Moody, C.O. Rodriguez de Barbarin, I.N. Sciambarella, J. Latour, D. Limosin, V. M^{c}Kee. *J. Chem. Soc., Dalton Trans.*, 1987, 2519.

70. (a) V. M^{c}Kee, S.S. Tandon. *J. Chem. Soc., Dalton Trans.*, 1991, 221.
(b) V. M^{c}Kee, S.S. Tandon. *Inorg. Chem.*, 1989, **28**, 2901.

71. V. M^{c}Kee, S.S. Tandon. *J. Chem. Soc., Chem. Commun.*, 1988, 385.

72. V. M^{c}Kee, S.S. Tandon. *J. Chem. Soc., Chem. Commun.*, 1988, 1334.

73. J. Wikaira. unpublished results.

74. A.J. Downard, V. M^{c}Kee, S.S. Tandon. *Inorg. Chim. Acta*, 1990, **173**, 181.

75. L.K. Thompson, S.S. Tandon, J.N. Bridson, V. M^{c}Kee, A.J. Downard. *Inorg. Chem.*, 1992, **31**, 4635.

76. V. M^{c}Kee, S.S. Tandon. *J. Chem. Soc., Dalton Trans.*, 1989, 19.

77. M. Bell, A.J. Edwards, B.F. Hoskins, E.H. Kachab, R. Robson. *J. Chem. Soc., Chem. Commun.*, 1987, 1852.

78. M.J. Grannas, B.F. Hoskins, R. Robson. *J. Chem. Soc., Chem. Commun.*, 1990, 1644.

79. M.J. Grannas, B.F. Hoskins, R. Robson. *Inorg. Chem.*, 1994, **33**, 1071.

80. M. Bell, A.J. Edwards, B.F. Hoskins, E.H. Kachabs, R. Robson. *J. Am. Chem. Soc.*, 1989, **111**, 3603.

81. A.J. Edwards, B.F. Hoskins, E.H. Kachab, A. Markiewicz, K.S. Murray, R. Robson. *Inorg. Chem.*, 1992, **31**, 3585.

82. R.R. Gagne, C.L. Spiro, T.J. Smith, C.A. Hamann, W.R. Thies, A.K. Shiemke. *J. Am. Chem. Soc.*, 1981, **103**, 4073.

83. D.E. Fenton, Shaohua Gou. *Inorg. Chim. Acta*, 1994, 169.

84. R.S. Drago, M.J. Desmond, B.B. Corden, K.A. Miller. *J. Am. Chem. Soc.*, 1983, **105**, 2287.

85. S. Taniguchi. *Bull. Chem. Soc. Jpn.*, 1984, **57**, 2683.

86. S.A. Brooker. *Ph.D. thesis*, University of Canterbury, Christchurch, New Zealand, 1989.

87. E.P. Papadopoulos, A. Jarrar, C.H. Issidorides. *J. Org. Chem.*, 1966, 615.

88. O. Mancera, G. Rosenkranz, F. Sondheimer. *J. Chem. Soc.*, 1953, 2189.

89. G.R. Owen, C.B. Reese. *J. Chem. Soc. (C)*, 1970, 2401.

90. I. Murase, M. Hatano, M. Tanaka, S. Ueno, S. Kida, H. Okawa. *Bull. Chem. Soc. Jpn.*, 1982, **55**, 2402.

91. S.A. Brooker. personal communication.

92. S. Aspinall. *J. Am. Chem. Soc.*, 1941, **63**, 852.

93. A.R. Jacobson, A.N. Makris, L.M. Sayre. *J. Org. Chem.*, 1987, **52**, 2592.

94. J.A. Ibers, W.C. Hamilton. *International Tables for Crystallography Vol. C*, Kynoch Press, Birmingham, 1992

95. (a) G.M. Sheldrick, *SHELXS-86, A Program for Crystal Structure Solution*, Göttingen University, 1986.

(b) G.M. Sheldrick, *SHELXL-92*, Göttingen University, 1992.

(c) G.M. Sheldrick, *SHELXL-93*, Göttingen University, 1993.

(d) Siemens *SHELXTL* version 4.2, Göttingen University.

96. N.A. Bailey, D.E. Fenton, J. Lay, P.B. Roberts, J. Latour, D. Limosin. *J. Chem. Soc., Dalton Trans.*, 1986, 2681.

97. H. Okawa, T. Tokii, Y. Nonaka, Y. Muto, S. Kida. *Bull. Chem. Soc. Jpn.*, 1973, **46**, 1462.

98. S.K. Mandal, K. Nag. *Inorg. Chem.*, 1983, **22**, 2567.

99. K. Nakamoto. *Infrared Spectra of Inorganic and Coordination Compounds (2nd ed.)*, Wiley Interscience, New York, 1970.

100. C.A. Hunter, J.K.M. Sanders. *J. Am. Chem. Soc.*, 1990, **112**, 5525.

101. (a) B.F. Hoskins, N.J. M^{c}Leod, H.A. Schaap. *Aust. J. Chem.*, 1976, 29, 515.

(b) H. Adams, N.A. Bailey, P. Bertrand, C.O. Rodriguez de Barbarin, D.E. Fenton, Shaohua Gou. *J. Chem. Soc., Dalton Trans.*, 1995, 275.

102. R.M. Silverstein, G.C. Bassler, T.C. Morrill. *Spectrometric identification of organic compounds 4th edition.*, John Wiley & Sons, Singapore, 1981, Ch 3.

103. B.F. Hoskins, R. Robson, P. Smith. *J. Chem. Soc., Chem. Commun.*, 1990, 488.

104. A.F. Wells. *Structural inorganic chemistry, 5th edition*, Oxford University Press, Oxford, 1984.

105. See for example : (a) J. Foley, D. Kennefick, D. Phelan, S. Tyagi, B.J. Hathaway. *J. Chem. Soc., Dalton Trans.*, 1983, 2333; (b) E. Horn, M.R. Snow, E.R.T. Tiekink. *Aust. J. Chem.*, 1987, **40**, 761; (c) Chan-Cheng Su, Chen-Bor Li. *Polyhedron*, 1994, **13**, 825; (d) Liang-Ping Wu, M.E. Keniry, B.J. Hathaway. *Acta Cryst.*, 1992, **C48**, 35; (e) L.S. van der Sluys, K.A. Kubat-Martin, G.J. Kubas, K.G. Caulton. *Inorg. Chem.*, 1991, **30**, 306; (f) R.R. Burch, J.C. Calabrese, S.D. Ittel. *Organometallics*, 1988, **7**, 1642; (g) C.S. Yang, H.C. Horng, F.L. Liao, C.P. Cheng. *J. Chem. Soc., Chem. Commun.*, 1994, 1637; (h) W.C. Velthuizen, J.G. Haasnoot, A.J. Kinneging, F.J. Rietmeijer, J. Reedijk. *J. Chem. Soc., Chem. Commun.*, 1983, 1366.

106. (a) P.E. Kruger, V. M^{c}Kee, J. Wikaira. unpublished results.

(b) A.J. Atkins, A.J. Blake, M. Schroder. *J. Chem.Soc. Chem. Commun.*, 1993, 1662.

(c) A.J. Atkins, A.J. Blake, S. Parsons, M. Schroder, L. Ruiz-Ramirez, D. Black, A. Marin-Becerra. *J. Chem. Soc., Chem. Commun.*, 1996, 457.

107. K.D. Karlin, N.M. Murthy, M. Mahroof-Tahir. *J. Am. Chem. Soc.*, 1993, **115**, 10404.

108. See for example: (a) N.A. Bailey, D.E. Fenton, R. Moody, P.J. Scrimshire, J.-M. Latour. *Inorg. Chim. Acta*, 1986, **124**, L1; (b) N.A. Bailey, D.E. Fenton, R. Moody, P.J. Scrimshire, E. Beloritzky, P.H. Fries, J.-M. Latour, *J. Chem. Soc.,*

Dalton Trans., 1988, 2817; (c) P. Betz, A. Bino, *Inorg. Chim. Acta*, 1988, **145**, 11; (d) N. Kitajima, K. Fujisawa, Y. Moro-oka. *J. Am. Chem. Soc.*, **112**, 3210, 1990.

109. (a) Y. Nishida, S. Kida. *Memoirs of the Faculty of Science, Kyushu University Series C*, 1981, **13**, 35.

(b) I. Murase, M. Hatano, M. Tanaka, S. Ueno, S. Kida, H. Okawa. *Bull. Chem. Soc. Jpn.*, 1982, **55**, 2402.

110. M. Schroder, A.J. Atkins, A.J. Blake. *J. Chem. Soc., Chem. Commun.*, 1993, 353.

111. N.A. Bailey, D.E. Fenton, P.B. Roberts, A.M. Walford. *J. Chem. Soc., Dalton Trans.*, 1987, 1865.

112. A.J. Edwards, B.F. Hoskins, B. Moubaraki, K.S. Murray, R. Robson, J.C. Wilson. *J. Chem. Soc., Dalton Trans.*, 1994, 1837-42.

113. M.G.B. Drew, G. Morgan, J. Nelson, O.W. Howarth. *J. Chem. Soc., Dalton Trans.*, 1994, 3149.

Appendix A

Atomic coordinates

Table A1. Atomic coordinates (x 10^4) and equivalent isotropic displacement parameters ($Å^2$ x 10^3) for $[Cu_2L^1(\mu\text{-}OH)(H_2O)](ClO_4)_2 \cdot H_2O$ (complex **1**). (U(eq) is defined as one third of the trace of the orthogonalized Uij tensor.

Atom	x	y	z	U(eq)
Cu1	-512(1)	5500(1)	875(1)	24(1)
Cu2	1752(1)	4494(1)	1289(1)	22(1)
O1	723(4)	5447(2)	1426(1)	22(1)
C1	447(6)	5727(3)	1843(2)	19(1)
C2	1183(6)	5471(3)	2238(2)	21(1)
C3	844(6)	5768(3)	2672(2)	23(1)
C4	-180(6)	6322(3)	2736(2)	24(1)
C5	-566(8)	6618(4)	3209(2)	39(2)
C6	-865(7)	6584(3)	2341(2)	26(1)
C7	-600(6)	6293(3)	1903(2)	20(1)
C8	-1402(7)	6630(3)	1524(2)	26(1)
N1	-1449(6)	6401(3)	1107(2)	29(1)
C9	-2323(8)	6864(4)	785(2)	37(2)
C10	-3408(8)	6397(4)	525(2)	40(2)
C11	-2709(9)	5941(5)	141(2)	48(2)
N2	-1759(6)	5339(4)	326(2)	39(2)
N3	2143(6)	3392(3)	1170(2)	29(1)
C12	3432(8)	3019(4)	1372(2)	36(2)
C13	3669(8)	3235(4)	1872(2)	35(2)
C14	4028(7)	4054(3)	1944(2)	29(1)
N4	2748(5)	4541(3)	1876(2)	23(1)
C15	2359(6)	4940(3)	2222(2)	23(1)
O2	559(5)	4605(2)	746(1)	27(1)
O3	3658(5)	5091(3)	942(2)	41(1)
O4	-4003(6)	4198(4)	660(2)	68(2)
Cl1	-1736(2)	3802(1)	1667(1)	36(1)
O11	-1558(10)	3401(4)	1249(2)	101(3)
O12	-2647(6)	3417(3)	1983(2)	59(2)
O13	-2272(6)	4541(3)	1577(2)	58(2)
O14	-351(5)	3879(3)	1868(2)	57(2)
Cl2	1838(2)	6729(1)	212(1)	46(1)
O21	3198(8)	6816(6)	76(3)	121(3)
O22	1372(12)	7411(4)	387(2)	121(4)
O23	1544(10)	6187(6)	508(4)	151(5)
O24	1011(8)	6615(5)	-205(3)	94(3)

Table A2. Atomic coordinates (x 10^4) and equivalent isotropic displacement parameters ($Å^2$ x 10^3) for $[Cu_2L^1(\mu\text{-}OH)](BF_4)_2 \cdot H_2O$ (complex **4**). U(eq) is defined as one third of the trace of the orthogonalized Uij tensor.

Atom	x	y	z	U(eq)
Cu1	289(1)	1390(1)	1064(1)	15(1)
Cu2	2019(1)	421(1)	2451(1)	15(1)
O1	2602(5)	1213(2)	1822(2)	16(1)
O2	-269(5)	679(2)	1792(2)	16(1)
O11	-2679(5)	248(2)	-1095(3)	23(1)
N1	-2052(6)	1361(2)	255(3)	19(1)
N2	1194(6)	2181(2)	620(3)	17(1)
N3	4552(6)	308(2)	2981(3)	16(1)
N4	915(6)	-269(2)	3143(3)	19(1)
C1	-2616(7)	1838(3)	-481(4)	22(1)
C2	-1002(8)	2184(3)	-827(4)	24(1)
C3	1(8)	2563(3)	-61(4)	27(1)
C4	2773(7)	2404(3)	888(4)	18(1)
C5	4203(7)	2150(2)	1555(3)	16(1)
C6	5749(7)	2518(2)	1755(4)	19(1)
C7	7247(7)	2328(3)	2358(3)	17(1)
C8	8888(8)	2744(3)	2599(4)	26(1)
C9	7151(7)	1740(3)	2753(4)	19(1)
C10	5617(7)	1353(2)	2584(3)	16(1)
C11	4089(7)	1559(2)	1986(3)	17(1)
C12	5764(7)	733(3)	3000(3)	18(1)
C13	5193(8)	-298(2)	3379(4)	24(1)
C14	3805(8)	-610(3)	3979(4)	26(1)
C15	2081(8)	-812(3)	3419(4)	25(1)
B1	-2556(9)	-710(3)	896(5)	23(1)
F11	-1783(5)	-939(2)	1758(2)	35(1)
F12	-3354(5)	-126(2)	1066(2)	32(1)
F13	-3847(5)	-1102(2)	478(3)	36(1)
F14	-1176(4)	-611(2)	278(2)	28(1)
B2	1040(9)	1190(3)	4703(5)	23(1)
F21	42(6)	1729(2)	4621(2)	47(1)
F22	-145(6)	688(2)	4571(3)	51(1)
F23	1931(5)	1169(2)	5600(3)	40(1)
F24	2254(6)	1176(2)	4016(3)	57(1)

Table A3. Atomic coordinates (x 10^4) and equivalent isotropic displacement parameters ($Å^2$ x 10^3) for $[Cu_2L^2(H_2O)_2](BF_4)_2$ (complex **5**). U(eq) is defined as one third of the trace of the orthogonalized Uij tensor.

Atom	x	y	z	U(eq)
Cu1	396(1)	6158(1)	177(1)	20(1)
N1	1562(2)	6627(2)	730(2)	22(1)
N2	-140(2)	7610(2)	123(2)	23(1)
O1	705(1)	4589(2)	279(1)	22(1)
O11	606(1)	6114(2)	-1346(2)	29(1)
C1	1552(2)	3002(2)	808(2)	21(1)
C2	2342(2)	2546(3)	1282(2)	25(1)
C3	3046(2)	3185(3)	1686(2)	25(1)
C4	3887(2)	2689(3)	2191(2)	30(1)
C5	2942(2)	4306(3)	1583(2)	24(1)
C6	2167(2)	4801(3)	1119(2)	22(1)
C7	1447(2)	4146(2)	727(2)	22(1)
C8	2184(2)	5981(2)	1075(2)	24(1)
C9	1763(2)	7807(2)	775(2)	25(1)
C10	1166(2)	8422(3)	1236(2)	27(1)
C11	312(2)	8625(2)	534(2)	27(1)
C12	-904(2)	7779(2)	-355(2)	24(1)
Cu2	4355(1)	5936(1)	-372(1)	22(1)
N3	4533(2)	7479(2)	-641(2)	25(1)
N4	3127(2)	5911(2)	-952(2)	26(1)
O2	5588(1)	5650(2)	120(2)	24(1)
O21	4343(1)	6283(2)	1247(2)	28(1)
C13	7029(2)	6090(2)	924(2)	25(1)
C14	7658(2)	6901(3)	1242(2)	27(1)
C15	7499(2)	7999(3)	1083(2)	26(1)
C16	8166(2)	8858(3)	1444(3)	33(1)
C17	6690(2)	8284(3)	567(2)	26(1)
C18	6037(2)	7522(2)	242(2)	23(1)
C19	6200(2)	6391(2)	424(2)	22(1)
C20	5243(2)	7978(2)	-293(2)	24(1)
C21	3841(2)	8190(3)	-1181(2)	30(1)
C22	3040(2)	7965(3)	-900(3)	35(1)
C23	2625(2)	6908(3)	-1307(3)	36(1)
C24	2688(2)	5025(3)	-1131(2)	27(1)
B1	173(2)	6243(3)	2732(3)	28(1)
F11	-415(1)	5644(2)	3042(2)	46(1)
F12	891(1)	6426(2)	3479(1)	44(1)
F13	-181(1)	7256(2)	2387(2)	40(1)
F14	398(1)	5695(2)	1993(1)	39(1)
B2	5975(3)	4419(3)	3194(3)	34(1)
F21	6761(2)	4900(2)	3514(2)	77(1)
F22	5487(2)	4620(2)	3810(2)	78(1)
F23	6070(1)	3292(2)	3120(2)	38(1)
F24	5575(1)	4824(2)	2281(2)	50(1)

Table A4. Atomic coordinates (x 10^4) and equivalent isotropic displacement parameters ($Å^2$ x 10^3) for $[Cu_2L^8(\mu\text{-}OH)](BF_4)_2 \cdot 4H_2O$ (complex **7**). U(eq) is defined as one third of the trace of the orthogonalized Uij tensor.

Atom	x	y	z	U(eq)
Cu1	4951(1)	2425(1)	292(1)	24(1)
Cu2	4049(1)	1514(1)	-77(1)	32(1)
O1	4282(2)	2606(4)	370(5)	25(1)
O2	4725(8)	1326(19)	6(54)	28(9)
O2'	4705(5)	1420(12)	-331(34)	29(5)
N1	5084(2)	3559(4)	699(6)	23(2)
N2	5593(3)	1978(5)	175(7)	30(2)
N3	3406(2)	1811(4)	235(6)	27(2)
N4	3971(3)	304(5)	-281(7)	38(2)
O11	3993(3)	1860(6)	-2108(9)	72(3)
C1	4057(3)	3221(5)	851(8)	25(2)
C2	4286(3)	3938(5)	1213(7)	22(2)
C3	4035(3)	4570(5)	1710(7)	25(2)
C4	3554(3)	4540(5)	1897(8)	28(2)
C5	3289(3)	5255(6)	2406(8)	30(2)
C6	3180(5)	5864(8)	1488(11)	59(3)
C7	3541(5)	5643(10)	3337(13)	82(5)
C8	2814(5)	4970(9)	2868(13)	69(4)
C9	3339(3)	3829(5)	1531(8)	25(2)
C10	3565(3)	3175(5)	1024(8)	28(2)
C11	3282(3)	2486(5)	691(8)	28(2)
C12	3027(3)	1234(6)	-58(9)	38(2)
C13	3136(4)	338(7)	211(10)	43(3)
C14	3504(4)	-40(7)	-532(11)	49(3)
C15	5989(3)	2566(6)	108(8)	32(2)
C16	5931(3)	3273(6)	927(8)	30(2)
C17	5563(3)	3883(6)	577(8)	28(2)
C18	4783(3)	4069(5)	1079(7)	21(2)
O22	5000	2020(8)	2500	62(3)
O33	4050(3)	1305(5)	2508(8)	58(2)
O44	3137(3)	1754(5)	-3039(7)	58(2)
B1	2192(4)	2853(7)	-1223(10)	33(2)
F11	2630(2)	2810(4)	-1708(6)	60(2)
F12	2222(2)	3306(4)	-245(5)	53(2)
F13	2039(2)	2080(4)	-986(6)	55(2)
F14	1890(2)	3245(4)	-1965(5)	56(2)
B2	5000	3426(10)	-2500	32(3)
F21	4692(4)	3015(7)	-3097(10)	116(4)
F22	4827(4)	4022(7)	-1797(11)	128(4)
B3	4364(10)	-321(17)	1889(25)	43(6)
F31	5117(4)	258(7)	1502(10)	123(4)
F32	5000	-933(13)	2500	157(7)
F33	4123(7)	-377(12)	1911(18)	91(6)

Table A5. Atomic coordinates (x 10^4) and equivalent isotropic displacement parameters ($Å^2$ x 10^3) for $[Cu_2L^3(\mu\text{-}OCH_2CH_3)(NCS)_2]$ (complex **9**). U(eq) is defined as one third of the trace of the orthogonalized Uij tensor.

Atom	x	y	z	U(eq)
Cu1	-135(1)	6154(1)	3875(1)	21(1)
Cu2	-404(1)	5037(1)	2502(1)	21(1)
N1	-898(4)	6270(2)	5170(3)	21(1)
N2	-1460(4)	4234(2)	2631(3)	21(1)
N3	-1624(4)	5118(2)	1118(3)	20(1)
N4	-1715(4)	7083(2)	3564(3)	23(1)
C5	-5025(5)	4123(2)	6310(3)	25(1)
C4	-3982(5)	4437(2)	5640(3)	21(1)
C3	-3626(5)	4174(2)	4771(3)	20(1)
C2	-2652(5)	4452(2)	4142(3)	18(1)
C1	-2003(4)	5029(2)	4367(3)	16(1)
O1	-1153(3)	5328(2)	3760(2)	19(1)
C7	-2314(5)	5297(2)	5261(3)	18(1)
C6	-3295(5)	4989(2)	5867(3)	20(1)
C8	-1750(5)	5888(2)	5592(3)	23(1)
C9	-630(6)	6868(2)	5662(4)	28(1)
C10	-1649(6)	7377(3)	5273(4)	30(1)
C11	-1364(6)	7578(3)	4261(4)	30(1)
C12	-2785(5)	7206(2)	2999(3)	22(1)
C13	-3301(5)	6804(2)	2241(3)	22(1)
C14	-4415(6)	6890(3)	1606(4)	29(1)
C15	-4378(6)	6391(3)	962(4)	32(1)
C16	-3237(5)	6019(2)	1251(3)	24(1)
O2	-2566(3)	6266(2)	2047(2)	21(1)
C17	-2683(5)	5460(2)	820(3)	24(1)
C18	-1309(5)	4572(2)	525(3)	24(1)
C19	-1973(5)	3978(2)	931(3)	27(1)
C20	-1298(6)	3764(2)	1871(4)	28(1)
C21	-2334(5)	4095(2)	3302(3)	21(1)
N41	1501(4)	6746(2)	4014(3)	24(1)
C42	2488(5)	7070(2)	4134(4)	23(1)
S43	3911(2)	7523(1)	4328(1)	39(1)
N51	1428(5)	4639(2)	1970(3)	28(1)
C52	2536(5)	4383(3)	1884(3)	24(1)
S53	4086(2)	4008(1)	1782(1)	41(1)
O31	462(3)	5838(2)	2675(2)	25(1)
C32	1584(7)	6096(3)	2102(4)	45(2)
C33	973(8)	6637(3)	1545(5)	58(2)

Table A6. Atomic coordinates (x 10^4) and equivalent isotropic displacement parameters ($Å^2$ x 10^3) for $\{[Cu_6L^4(\mu\text{-}OH)_4](BF_4)_2\}^+$ (complex **11**). U(eq) is defined as one third of the trace of the orthogonalized Uij tensor.

Atom	x	y	z	U(eq)
Cu1	3681(2)	8162(2)	4084(1)	92(1)
Cu2	2889(1)	6225(2)	4180(1)	79(1)
Cu3	3621(1)	5109(1)	5375(1)	68(1)
Cu4	5589(1)	5481(1)	6160(1)	66(1)
Cu5	6383(1)	7005(1)	5700(1)	70(1)
Cu6	5304(2)	8519(2)	4723(1)	88(1)
S1	4523(5)	6830(6)	5163(4)	82(3)
O15	4255(12)	7238(12)	5857(10)	71(5)
O1	3103(8)	7214(9)	3657(7)	98(5)
O2	2655(7)	5210(7)	4685(6)	78(3)
O3	4607(7)	4879(8)	5974(6)	75(3)
O4	6611(8)	6044(8)	6354(6)	84(4)
O5	6258(8)	7906(11)	5011(8)	118(6)
O11	3907(7)	6096(7)	4843(6)	74(3)
O12	5370(7)	6381(8)	5447(6)	75(3)
O13	4557(7)	7514(9)	4640(6)	79(3)
O14	4322(8)	9129(10)	4396(9)	111(5)
N1	2737(17)	8837(23)	3637(15)	174(10)
N2	1870(10)	6149(11)	3522(8)	87(5)
N3	3224(8)	4110(9)	5781(6)	66(3)
N4	5960(8)	4664(9)	6893(7)	68(3)
N5	7476(10)	7417(12)	5997(8)	92(5)
N6	6018(10)	9503(11)	4591(10)	94(5)
C1	1986(19)	8026(25)	3471(16)	82(9)
C1'	2313(33)	8389(45)	2864(30)	109(17)
C2	2401(15)	7509(20)	3141(13)	118(8)
C3	1780(12)	6764(16)	2914(11)	109(9)
C4	1291(13)	5629(14)	3524(10)	89(6)
C5	1284(11)	4947(12)	4067(10)	80(5)
C6	604(11)	4490(13)	3996(9)	78(5)
C7	503(11)	3794(12)	4450(10)	78(5)
C8	-307(12)	3295(13)	4369(12)	91(6)
C9	-335(17)	2683(25)	4934(19)	204(21)
C10	-497(18)	2916(26)	3562(18)	229(25)
C11	-1030(14)	3874(21)	4382(21)	172(15)
C12	1127(10)	3644(12)	4972(9)	72(4)
C13	1867(10)	4090(11)	5096(8)	65(4)
C14	1918(11)	4775(11)	4622(9)	74(5)
C15	2506(11)	3822(11)	5657(8)	69(4)
C16	3870(11)	3654(13)	6329(10)	86(6)
C17	4484(12)	4352(15)	6578(11)	106(8)
C18	5354(11)	3955(14)	6921(12)	93(6)
C19	6551(10)	4662(12)	7374(9)	72(5)
C20	7243(12)	5284(12)	7395(9)	80(5)
C21	7921(10)	5195(13)	7938(9)	78(5)
C22	8603(11)	5684(13)	8034(9)	76(5)
C23	9310(12)	5544(14)	8639(11)	88(6)
C24	9560(13)	4573(15)	8650(12)	103(7)
C25	9054(12)	5706(16)	9363(10)	96(6)
C26	10045(13)	6102(18)	8571(11)	111(8)
C27	8553(13)	6322(13)	7522(10)	86(5)
C28	7918(10)	6487(13)	6986(9)	77(5)
C29	7246(10)	5945(13)	6889(9)	75(5)

*Table **A6** continued*

*Table **A6** continued*

C30	8000(12)	7172(14)	6495(11)	98(7)
C31	7598(15)	8182(19)	5535(13)	121(8)
C32	6921(18)	8546(25)	5228(17)	146(10)
C33	6814(14)	9175(15)	4640(14)	114(8)
B1	2643(12)	8325(13)	5630(10)	109(8)
F11	2079(10)	8820(13)	5240(9)	181(7)
F12	2684(8)	7571(11)	5304(7)	142(5)
F13	2399(10)	8154(12)	6255(8)	165(6)
F14	3370(11)	8688(15)	5830(12)	232(10)
B2	4959(13)	8615(15)	2787(11)	170(16)
F21	5016(8)	8608(11)	2056(7)	139(5)
F22	4193(10)	8359(14)	2879(10)	194(8)
F23	5562(12)	8061(15)	3175(11)	235(10)
F24	5140(10)	9465(11)	3059(8)	156(6)
O21	3215(8)	6085(8)	6293(7)	88(4)
O22	524(14)	1654(19)	2455(13)	85(7)
O23	5077(12)	8897(16)	5990(11)	154(7)
O24	2476(20)	5220(28)	7384(18)	263(15)
O25	971(17)	501(23)	2084(15)	225(12)
O26	1527(21)	1672(29)	1989(20)	277(16)

Table A7. Atomic coordinates (x 10^4) and equivalent isotropic displacement parameters ($Å^2$ x 10^3) for $[Cu_6L^4(\mu\text{-}OH)_4](NO_3)_3 \cdot nH_2O$ (complex **12**). U(eq) is defined as one third of the trace of the orthogonalized Uij tensor.

Atom	x	y	z	U(eq)
Cu1	89(1)	4300(1)	-2503(1)	25(1)
Cu2	1739(1)	4724(1)	-801(1)	23(1)
Cu3	909(1)	5654(1)	-87(1)	22(1)
Cu4	-1324(1)	5990(1)	-1326(1)	22(1)
Cu5	-2526(1)	5587(1)	-3520(1)	38(1)
Cu6	-1863(1)	4811(1)	-4094(1)	38(1)
O1	1606(6)	4217(2)	-1532(6)	31(2)
O2	1912(5)	5202(2)	-8(5)	22(2)
O3	-31(6)	6136(2)	-151(5)	26(2)
O4	-2801(6)	5846(2)	-2244(6)	37(2)
O5	-1496(7)	4309(2)	-3368(7)	49(2)
O6	-2183(7)	5327(2)	-4793(7)	46(2)
N1	226(9)	3787(3)	-3156(9)	52(3)
N2	3283(7)	4584(2)	49(6)	21(2)
N3	2161(7)	5877(2)	998(6)	21(2)
N4	-2011(7)	6513(3)	-1319(7)	30(2)
N5	-3763(9)	5963(3)	-4285(8)	44(3)
N6	-2437(10)	4469(3)	-5411(8)	53(3)
C1	2355(9)	3903(3)	-1417(8)	28(2)
C2	2073(9)	3554(3)	-2028(8)	28(2)
C3	2819(9)	3215(3)	-1837(9)	34(3)
C4	3892(9)	3210(3)	-1051(9)	32(3)
C5	4688(10)	2847(3)	-818(10)	39(3)
C6	4838(12)	2729(4)	390(10)	53(3)
C7	5907(11)	2944(4)	-1027(13)	59(4)
C8	4169(13)	2488(4)	-1450(13)	63(4)
C9	4187(9)	3572(3)	-500(9)	28(2)
C10	3456(8)	3916(3)	-658(8)	24(2)
C11	3855(9)	4257(3)	16(8)	23(2)
C12	3738(9)	4895(3)	863(8)	28(2)
C13	3108(9)	5282(3)	487(9)	32(3)
C14	3129(10)	5590(3)	1363(9)	33(3)
C15	2191(8)	6229(3)	1417(8)	25(2)
C16	224(9)	6483(3)	364(8)	25(2)
C17	1278(9)	6527(3)	1159(8)	24(2)
C18	1467(9)	6890(3)	1735(8)	29(2)
C19	685(9)	7213(3)	1554(9)	30(3)
C20	938(10)	7614(3)	2167(9)	35(3)
C21	-193(12)	7757(4)	2543(12)	58(4)
C22	1967(13)	7577(4)	3109(12)	67(4)
C23	1235(13)	7929(4)	1381(12)	59(4)
C24	-319(9)	7168(3)	739(9)	29(2)
C25	-590(9)	6812(3)	144(8)	25(2)
C26	-1643(9)	6811(3)	-689(9)	28(2)
C27	-3035(11)	6549(4)	-2232(11)	48(3)
C28	-3641(11)	6163(4)	-2398(11)	48(3)
C29	-4447(10)	6122(4)	-3512(9)	42(3)
C30	-2625(16)	4056(5)	-5000(12)	77(5)
C31	-1710(15)	3967(4)	-4053(15)	88(6)
C32	-737(15)	3741(6)	-4099(15)	117(9)
C33	1027(11)	3520(4)	-2882(10)	49(3)
N100	5049(9)	4824(3)	-3655(8)	45(3)
O102	4262(8)	4583(3)	-3454(8)	60(2)

Table A7 continued

*Table **A7** continued*

O103	5800(10)	4673(3)	-4121(9)	75(3)
O101	5054(10)	5174(3)	-3433(9)	78(3)
N200	2487(11)	3140(4)	-4678(10)	59(3)
O201	2108(7)	2836(3)	-4321(7)	49(2)
O202	1765(14)	3388(5)	-5202(13)	120(5)
O203	3551(12)	3233(4)	-4478(11)	101(4)
N300	7298(17)	3959(6)	1783(16)	106(5)
O301	6436(9)	4181(3)	1887(8)	66(3)
O302	8244(21)	4064(7)	2460(19)	189(8)
O303	7440(19)	3713(7)	1255(18)	169(7)
O1W	-653(9)	6112(3)	-3070(8)	66(3)
O2W	4654(10)	6267(3)	3287(9)	86(4)
O3W	2667(8)	5022(3)	-2267(7)	52(2)
O4W	583(9)	4746(3)	-3845(8)	65(3)
S1	-509(7)	5170(2)	-2049(6)	47(3)
O40	-455(6)	5481(2)	-1167(5)	24(2)
O50	107(6)	4790(2)	-1630(5)	26(2)
O60	-1563(6)	5145(2)	-2796(5)	30(2)
O70	460(20)	5378(7)	-2918(19)	62(7)

Table A8. Atomic coordinates (x 10^4) and equivalent isotropic displacement parameters ($Å^2$ x 10^3) for $[\{Cu_4L^6(\mu_5\text{-}O)(BF_4)\}_2](BF_4)_2 \cdot 2H_2O$ (complex **14**). U(eq) is defined as one third of the trace of the orthogonalized Uij tensor.

Atom	x	y	z	U(eq)
Cu1	5314(1)	3841(1)	-2388(1)	18(1)
Cu2	7260(1)	4668(1)	6(1)	17(1)
Cu3	5943(1)	6301(1)	505(1)	16(1)
Cu4	4081(1)	5560(1)	-1941(1)	18(1)
O1	5491(4)	4936(3)	-919(3)	16(1)
O2	6802(4)	3473(3)	-1368(3)	18(1)
O3	7433(4)	5785(3)	1307(3)	18(1)
O4	4467(4)	6714(3)	-536(3)	18(1)
O5	3802(4)	4293(4)	-3160(3)	20(1)
N1	5085(6)	2633(5)	-3738(4)	26(1)
N2	8897(5)	4259(5)	825(4)	23(1)
N3	6476(5)	7761(4)	1731(4)	21(1)
N4	2761(6)	6215(5)	-2893(5)	27(1)
C1	7311(6)	2611(5)	-1565(5)	17(2)
C2	6764(6)	1798(5)	-2662(5)	19(2)
C3	7309(7)	889(5)	-2824(6)	23(2)
C4	8375(7)	749(5)	-1960(6)	24(2)
C5	8934(6)	1587(5)	-883(6)	23(2)
C6	8438(6)	2506(5)	-673(5)	19(2)
C7	8930(8)	-236(6)	-2170(7)	37(2)
C8	9165(7)	3354(6)	456(5)	23(2)
C9	9884(7)	5021(6)	2002(6)	35(2)
C10	9874(7)	6211(6)	2148(6)	37(2)
C11	8706(6)	6488(5)	2280(5)	20(2)
C12	8803(7)	7728(6)	2538(6)	36(2)
C13	7736(7)	8054(6)	2801(6)	34(2)
C14	5848(7)	8519(6)	1658(5)	23(2)
C15	4695(6)	8523(5)	687(5)	19(2)
C16	4235(6)	9484(5)	823(6)	22(2)
C17	3202(7)	9648(5)	-52(6)	23(2)
C18	2657(7)	8827(5)	-1123(6)	22(2)
C19	3086(6)	7853(5)	-1329(5)	19(2)
C20	4088(6)	7665(5)	-403(5)	18(2)
C21	2706(7)	10677(6)	135(6)	28(2)
C22	2502(6)	7123(5)	-2499(6)	22(2)
C23	2068(9)	5692(7)	-4156(6)	56(3)
C24	2620(16)	5027(12)	-4625(8)	149(8)
C25	3185(7)	4156(6)	-4371(5)	26(2)
C26	3942(21)	3654(16)	-4952(10)	30(5)
C26'	3100(38)	3036(29)	-5087(16)	39(10)
C27	4142(9)	2568(7)	-4901(6)	52(2)
C28	5728(7)	1882(6)	-3673(6)	26(2)
B1	7221(7)	6471(7)	-1835(7)	23(2)
F11	6951(4)	5341(3)	-2476(4)	37(1)
F12	6016(4)	6735(3)	-2097(3)	35(1)
F13	8059(4)	7170(3)	-2095(3)	35(1)
F14	7876(4)	6594(4)	-666(3)	48(1)
B2	7348(11)	1074(8)	-5590(8)	62(3)
F21	7797(6)	2065(4)	-4742(4)	76(2)
F22	8158(20)	449(14)	-4865(12)	73(5)
F23	7728(25)	1013(16)	-6404(15)	79(10)
F24	6088(13)	479(15)	-5933(16)	83(9)
F22'	6932(28)	126(9)	-5449(16)	108(11)
F23'	8117(23)	1022(18)	-6156(18)	84(8)
F24'	6162(13)	1287(16)	-6431(11)	110(7)
O1W	333(36)	1138(29)	-5634(24)	280(17)
O2W	436(50)	2729(41)	-6839(37)	413(25)

Table A9. Atomic coordinates (x 10^4) and equivalent isotropic displacement parameters ($Å^2$ x 10^3) for $[Cu_4L^6(\mu_4\text{-OH})(\mu\text{-HCOO})Cl(OH)]$ (complex **15**). U(eq) is defined as one third of the trace of the orthogonalized Uij tensor.

Atom	x	y	z	U(eq)
Cu	5654(1)	4289(1)	3803(1)	24(1)
O1	5000	3688(2)	5000	26(1)
O2	6708(7)	5000	3070(4)	25(1)
OX	5000	5000	5000	57(3)
N1	6596(7)	3589(2)	2866(4)	32(1)
C1	5000	3031(3)	5000	21(2)
C2	5694(7)	2677(3)	4081(5)	24(1)
C3	5687(7)	1981(3)	4113(5)	28(1)
C4	5000	1627(4)	5000	29(2)
C5	5000	881(4)	5000	37(2)
C6	6485(7)	2973(3)	3099(5)	26(1)
C7	7484(13)	3762(3)	1803(7)	66(3)
C8	7099(23)	4376(5)	1289(9)	35(4)
C9	7374(13)	5000	1934(7)	36(2)
C7'	7484(13)	3762(3)	1803(7)	66(3)
C8'	8096(34)	4381(9)	1632(19)	23(6)
C9'	7374(13)	5000	1934(7)	36(2)
O2W	5000	2463(3)	0	40(2)
O1W	2690(8)	3238(3)	1221(5)	81(2)
C60	2685(25)	5000	2314(18)	46(5)
O61	3107(12)	4378(4)	2759(8)	68(3)
Cl7	2630(12)	4339(4)	2461(8)	51(2)

Table A10. Atomic coordinates (x 10^4) and equivalent isotropic displacement parameters (Å^2 x 10^3) for [{Cu_2HL^6(μ-OH)}$_2$] (complex **16**). U(eq) is defined as one third of the trace of the orthogonalized Uij tensor.

Atom	x	y	z	U(eq)
Cu1	6481(3)	204(1)	396(3)	44(1)
Cu2	5294(3)	227(2)	2076(3)	48(1)
N1	7263(20)	764(9)	-216(16)	44(6)
N2	7609(24)	-1516(11)	20(19)	65(7)
N3	4778(21)	789(10)	2852(18)	52(6)
N4	4877(26)	-1476(13)	3058(21)	75(8)
O1	7244(16)	-418(8)	-104(13)	49(5)
O2	6080(16)	704(8)	1356(14)	48(5)
O3	4852(16)	-380(8)	2838(13)	49(5)
O4	5594(15)	-287(8)	1061(12)	43(4)
O5	6613(19)	-1342(10)	1753(16)	68(6)
C1	8030(24)	-389(11)	-646(20)	43(7)
C2	8568(23)	-859(11)	-893(20)	41(7)
C3	9348(29)	-848(15)	-1489(23)	66(9)
C4	9654(26)	-351(12)	-1850(21)	50(7)
C5	10417(33)	-329(17)	-2596(27)	90(12)
C6	9161(24)	135(13)	-1620(20)	51(7)
C7	8369(22)	118(11)	-971(18)	36(6)
C8	7946(25)	658(12)	-786(21)	48(7)
C9	6906(30)	1368(14)	-150(23)	63(9)
C10	6938(33)	1546(16)	867(27)	83(11)
C11	6005(29)	1302(13)	1285(24)	59(8)
C12	6085(32)	1487(16)	2371(26)	80(10)
C13	4969(29)	1391(14)	2709(25)	66(9)
C14	4096(27)	668(14)	3447(22)	58(8)
C15	3776(24)	165(13)	3760(20)	49(7)
C16	2998(26)	161(14)	4377(21)	58(8)
C17	2650(24)	-303(12)	4747(20)	48(7)
C18	1820(31)	-297(16)	5425(25)	81(10)
C19	3046(28)	-783(14)	4451(23)	63(9)
C20	3846(27)	-831(13)	3877(22)	55(8)
C21	4140(22)	-338(11)	3426(18)	36(6)
C22	4182(29)	-1376(14)	3625(24)	64(9)
C23	5047(40)	-2064(19)	2696(33)	106(14)
C24	6215(32)	-2134(16)	2551(27)	79(10)
C25	6444(38)	-1917(18)	1735(32)	92(12)
C26	7158(50)	-2156(23)	1160(40)	150(19)
C27	7345(40)	-2102(18)	145(31)	100(13)
C28	8325(28)	-1416(14)	-594(23)	64(9)
O1W	941(26)	1082(13)	6781(22)	115(9)
O2W	4852(35)	-3326(17)	1601(29)	163(13)
O3W	3875(29)	-2853(14)	252(23)	129(11)
O4W	1299(30)	1281(15)	4929(24)	134(11)

Table A11. Atomic coordinates (x 10^4) and equivalent isotropic displacement parameters ($Å^2$ x 10^3) for $[Cu_2L^5](BF_4)_2 \cdot H_2O$ (complex **17**). U(eq) is defined as one third of the trace of the orthogonalized Uij tensor.

Atom	x	y	z	U(eq)
Cu1	1053(1)	8055(1)	4087(1)	22(1)
Cu2	1254(1)	2175(1)	2309(1)	24(1)
O1	1076(1)	7821(6)	3392(1)	22(1)
O2	1223(1)	2436(5)	2995(1)	23(1)
N1	1543(1)	8667(7)	4455(2)	23(1)
N2	1018(1)	9003(7)	4778(2)	30(1)
N3	524(1)	8257(7)	3769(2)	26(1)
N4	901(1)	4791(7)	4030(2)	23(1)
N5	1755(1)	2346(7)	2603(2)	24(1)
N6	1304(1)	1329(7)	1619(2)	27(1)
N7	749(1)	1275(7)	1932(2)	27(1)
N8	959(1)	5147(7)	2047(2)	24(1)
C1	1360(1)	7732(7)	3298(2)	20(1)
C2	1339(1)	7046(8)	2789(2)	18(1)
C3	1635(1)	6915(8)	2670(2)	24(1)
C4	1963(1)	7429(8)	3041(2)	25(1)
C5	2284(2)	7244(10)	2909(3)	36(2)
C6	1985(1)	8086(8)	3535(2)	24(1)
C7	1698(1)	8224(8)	3680(2)	19(1)
C8	1761(1)	8761(8)	4228(2)	22(1)
C9	1641(2)	9177(9)	5022(2)	31(2)
C10	1329(2)	10150(10)	5070(2)	35(2)
C11	683(2)	10034(10)	4616(3)	38(2)
C12	405(2)	8866(10)	4196(3)	34(2)
C13	367(1)	6445(9)	3507(2)	30(2)
C14	520(1)	4744(9)	3868(2)	28(1)
C15	1024(1)	3567(8)	3803(2)	20(1)
C16	1393(1)	3488(8)	3891(2)	19(1)
C17	1649(1)	4049(8)	4381(2)	22(1)
C18	2001(1)	4081(8)	4465(2)	24(1)
C19	2274(1)	4760(10)	4990(2)	35(2)
C20	2084(1)	3539(8)	4035(2)	25(1)
C21	1836(1)	2987(8)	3529(2)	22(1)
C22	1476(1)	2925(8)	3447(2)	20(1)
C23	1952(1)	2594(8)	3102(2)	23(1)
C24	1903(2)	2100(10)	2193(2)	31(1)
C25	1670(2)	776(10)	1761(3)	37(2)
C26	1045(2)	-180(9)	1392(2)	34(2)
C27	699(2)	468(10)	1391(2)	34(2)
C28	498(1)	2824(9)	1894(2)	31(2)
C29	601(1)	4641(9)	1698(2)	28(1)
C30	998(1)	6435(8)	2403(2)	22(1)
B1	0	225(15)	2500	30(2)
F11	218(1)	1342(5)	2919(1)	38(1)
F12	-203(1)	-921(5)	2687(2)	43(1)
B2	1862(3)	3898(14)	6106(4)	78(4)
F21	1977(2)	2492(10)	5896(3)	145(3)
F22	1878(4)	5679(14)	5973(5)	111(6)
F23	1553(3)	3489(20)	6144(6)	103(5)
F24	2118(3)	3694(14)	6651(3)	98(4)
F25	2041(7)	5506(28)	6182(11)	198(21)
F26	1710(5)	3658(35)	6454(6)	108(9)
F27	1563(4)	4270(23)	5594(5)	124(8)
B3	-90(6)	6081(48)	4931(16)	124(13)
F31	-274(2)	4667(13)	4959(4)	163(3)
F32	-11(3)	6809(24)	5475(4)	122(6)
F33	-209(4)	7531(28)	4619(6)	162(7)
O11	1002(2)	3888(8)	592(2)	74(2)

Appendix B

Infrared spectra of complexes

PERKIN ELMER

cm-1	%	cm-1	%	cm-1	%	cm-1	%
3491.7	29.06	3317.9	21.06	3264.7	33.36	2953.9	47.30
2359.5	62.72	2341.3	64.88	2020.1	71.62	1700.1	77.13
1638.5	8.56	1621.7	22.39	1605.2	42.65	1563.7	15.30
1465.1	51.67	1444.3	37.05	1416.1	39.88	1396.3	61.17
1363.4	65.71	1343.1	32.81	1335.8	37.64	1275.9	58.00
1242.7	47.48	1196.4	47.71	1092.2	2.07	1035.5	16.58
988.6	44.93	978.9	45.50	925.0	42.12	890.2	59.03
847.8	65.73	827.7	43.81	768.1	42.04	668.0	53.63
623.2	12.97	569.8	56.96	556.0	51.89	496.0	53.58

36 peaks found

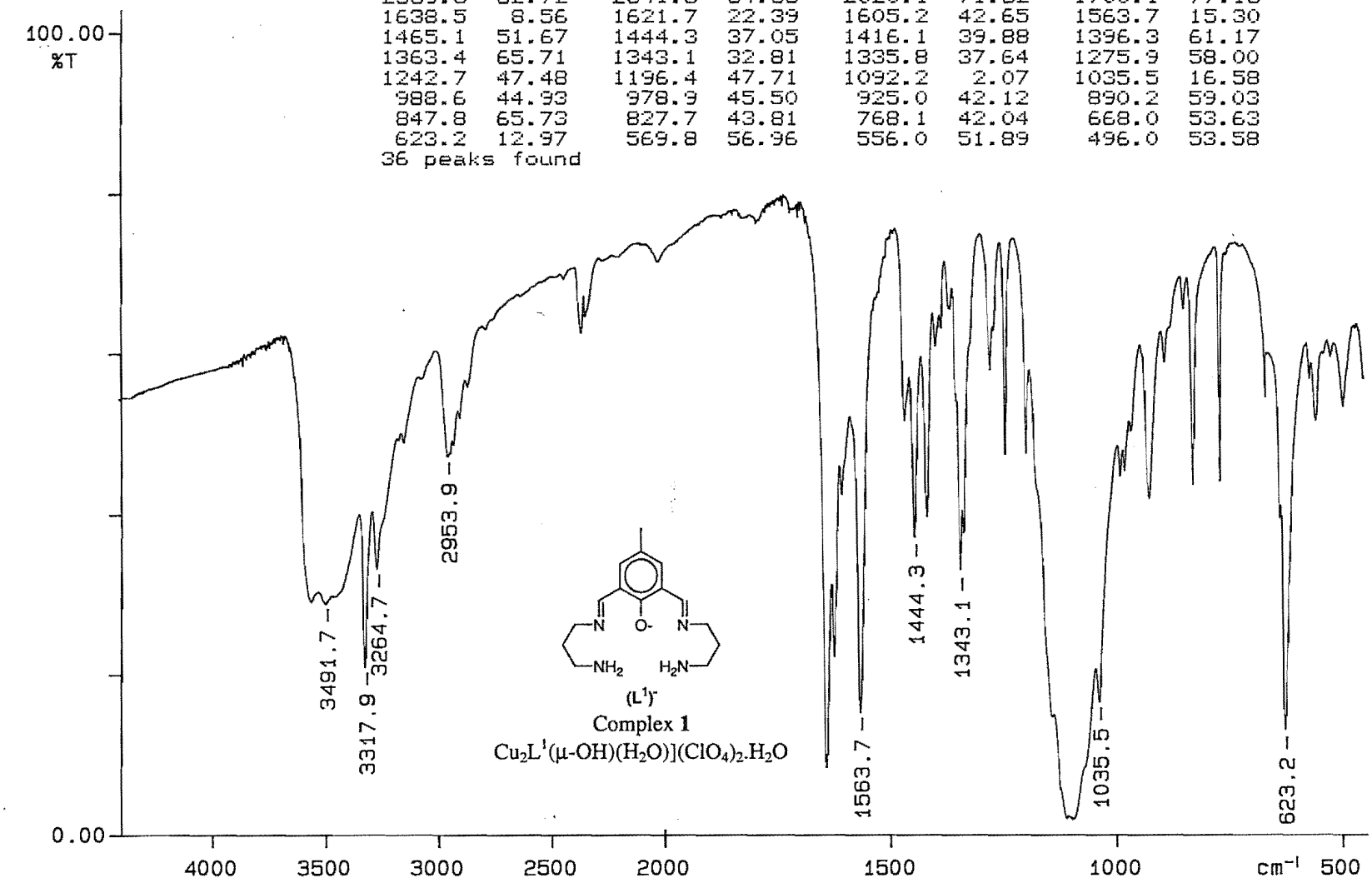

$(L^1)^-$

Complex **1**

$Cu_2L^1(\mu\text{-}OH)(H_2O)](ClO_4)_2.H_2O$

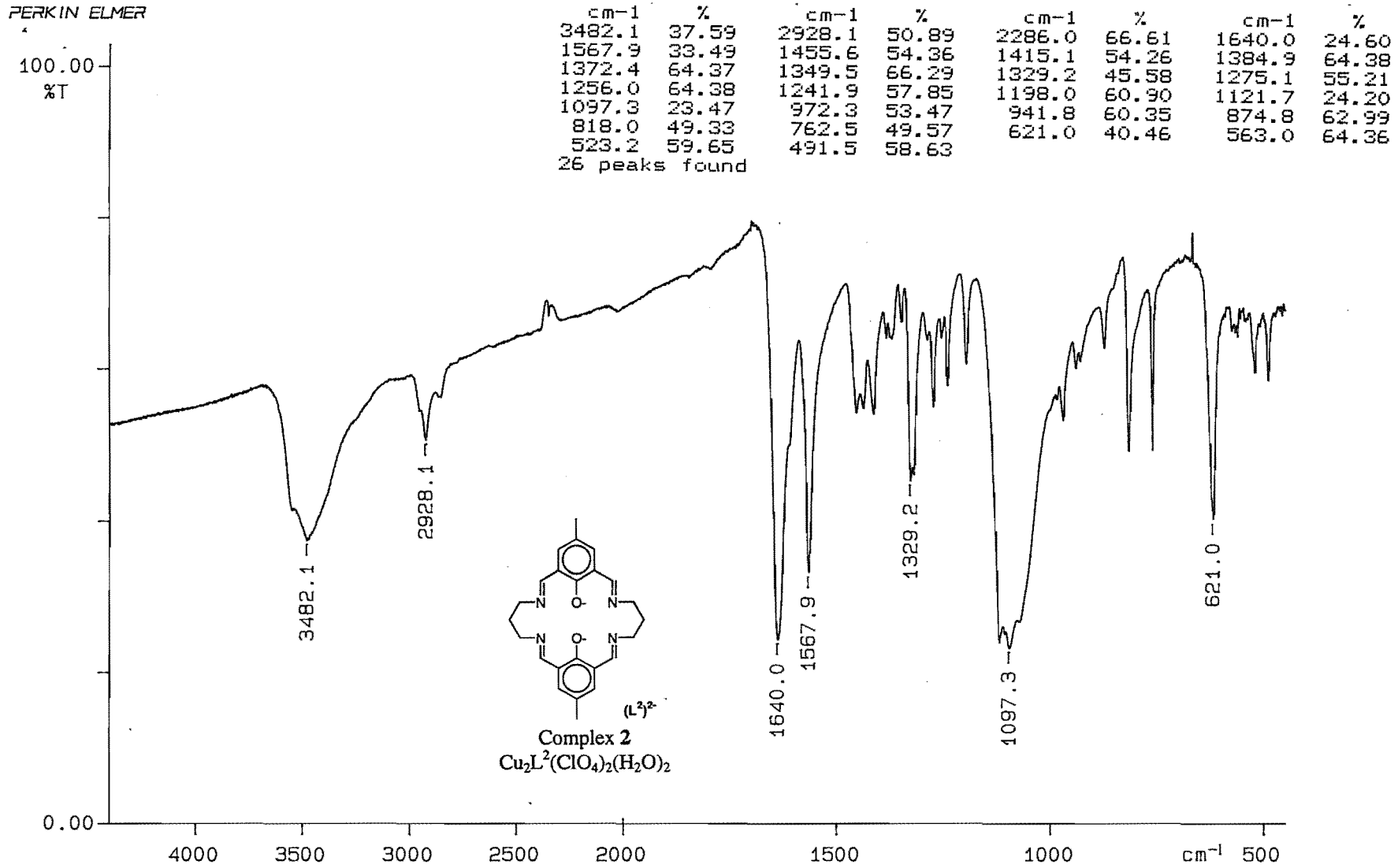

cm-1	%	cm-1	%	cm-1	%	cm-1	%
3482.1	37.59	2928.1	50.89	2286.0	66.61	1640.0	24.60
1567.9	33.49	1455.6	54.36	1415.1	54.26	1384.9	64.38
1372.4	64.37	1349.5	66.29	1329.2	45.58	1275.1	55.21
1256.0	64.38	1241.9	57.85	1198.0	60.90	1121.7	24.20
1097.3	23.47	972.3	53.47	941.8	60.35	874.8	62.99
818.0	49.33	762.5	49.57	621.0	40.46	563.0	64.36
523.2	59.65	491.5	58.63				

26 peaks found

PERKIN ELMER

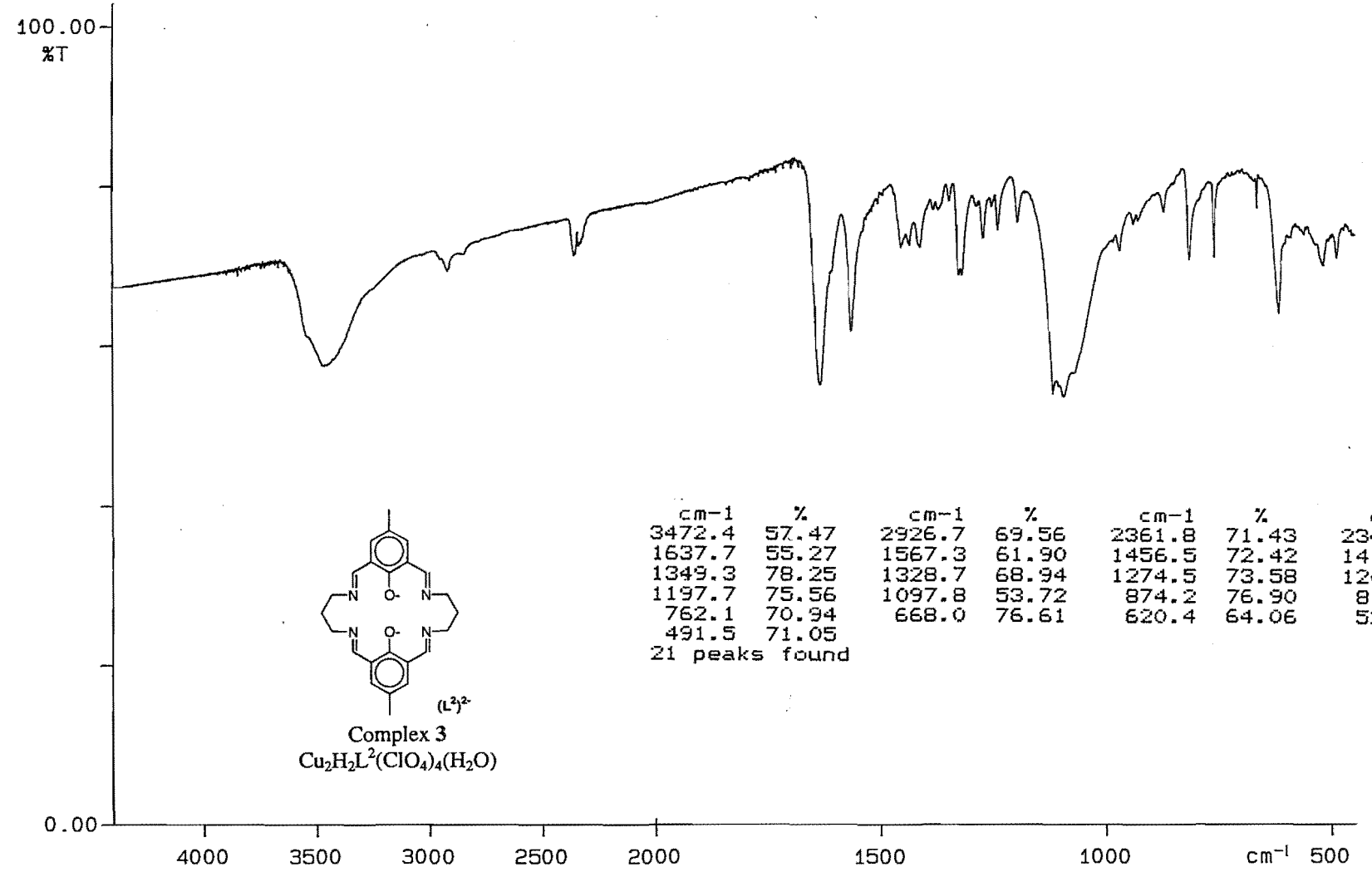

Complex 3

$Cu_2H_2L^2(ClO_4)_4(H_2O)$

cm-1	%	cm-1	%	cm-1	%	cm-1	%
3472.4	57.47	2926.7	69.56	2361.8	71.43	2341.5	72.63
1637.7	55.27	1567.3	61.90	1456.5	72.42	1414.6	72.42
1349.3	78.25	1328.7	68.94	1274.5	73.58	1241.3	74.69
1197.7	75.56	1097.8	53.72	874.2	76.90	817.5	70.92
762.1	70.94	668.0	76.61	620.4	64.06	522.5	70.18
491.5	71.05						

21 peaks found

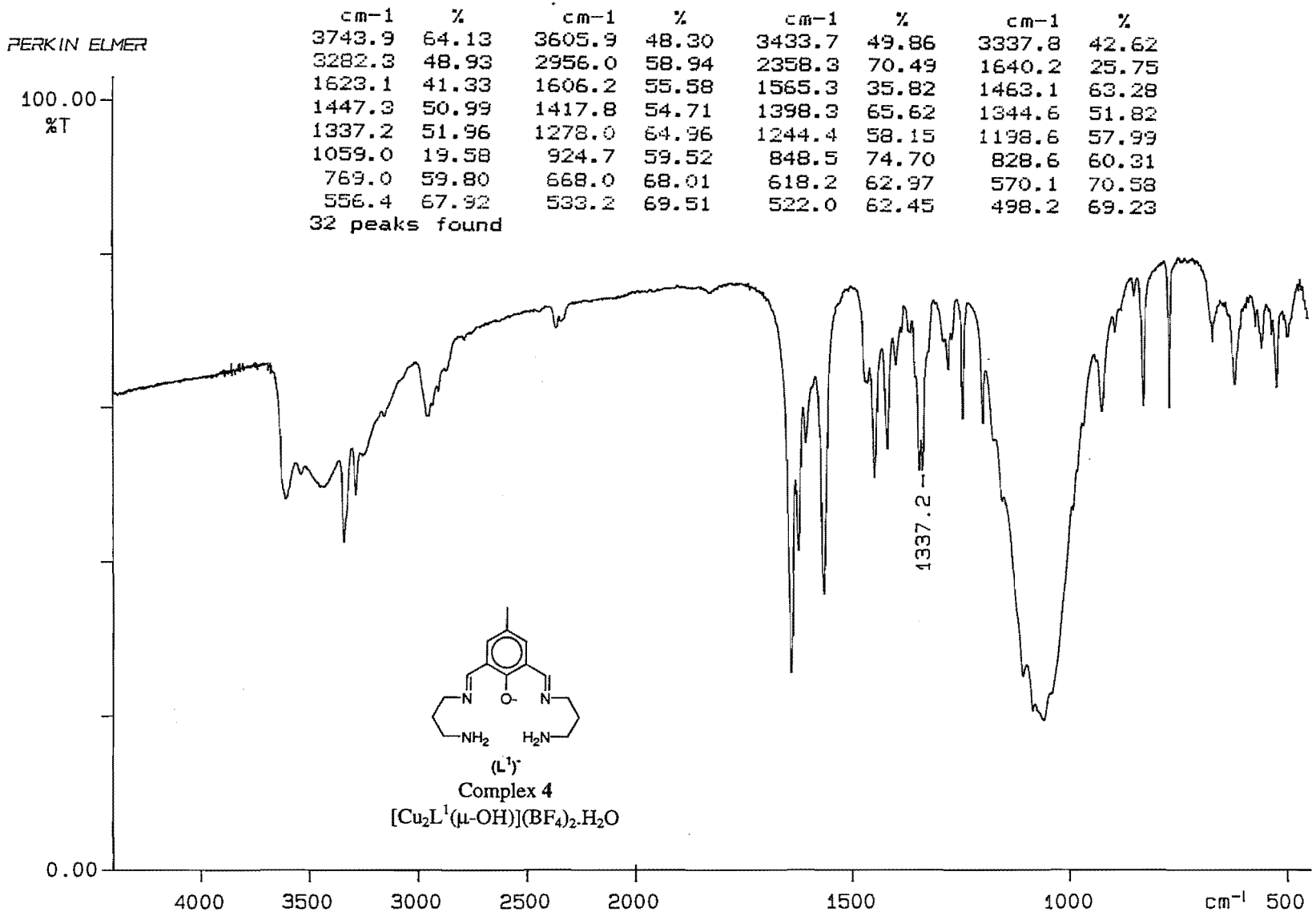

cm-1	%	cm-1	%	cm-1	%	cm-1	%
3743.9	64.13	3605.9	48.30	3433.7	49.86	3337.8	42.62
3282.3	48.93	2956.0	58.94	2358.3	70.49	1640.2	25.75
1623.1	41.33	1606.2	55.58	1565.3	35.82	1463.1	63.28
1447.3	50.99	1417.8	54.71	1398.3	65.62	1344.6	51.82
1337.2	51.96	1278.0	64.96	1244.4	58.15	1198.6	57.99
1059.0	19.58	924.7	59.52	848.5	74.70	828.6	60.31
769.0	59.80	668.0	68.01	618.2	62.97	570.1	70.58
556.4	67.92	533.2	69.51	522.0	62.45	498.2	69.23

32 peaks found

$(L^1)^-$

Complex 4

$[Cu_2L^1(\mu\text{-}OH)](BF_4)_2.H_2O$

PERKIN ELMER

cm-1	%	cm-1	%	cm-1	%	cm-1	%
3578.8	23.26	3508.3	21.64	2931.1	38.21	1637.5	4.06
1568.1	8.66	1456.3	31.92	1440.0	32.87	1415.6	31.41
1374.8	49.08	1350.1	50.44	1329.9	18.49	1276.3	32.50
1256.3	50.67	1242.3	37.52	1198.4	41.47	1120.7	12.05
1075.8	5.53	973.7	28.54	943.6	41.39	875.8	48.57
818.1	22.90	762.9	26.22	623.7	44.03	574.0	50.80
563.9	49.92	522.8	34.43	491.9	39.82		

27 peaks found

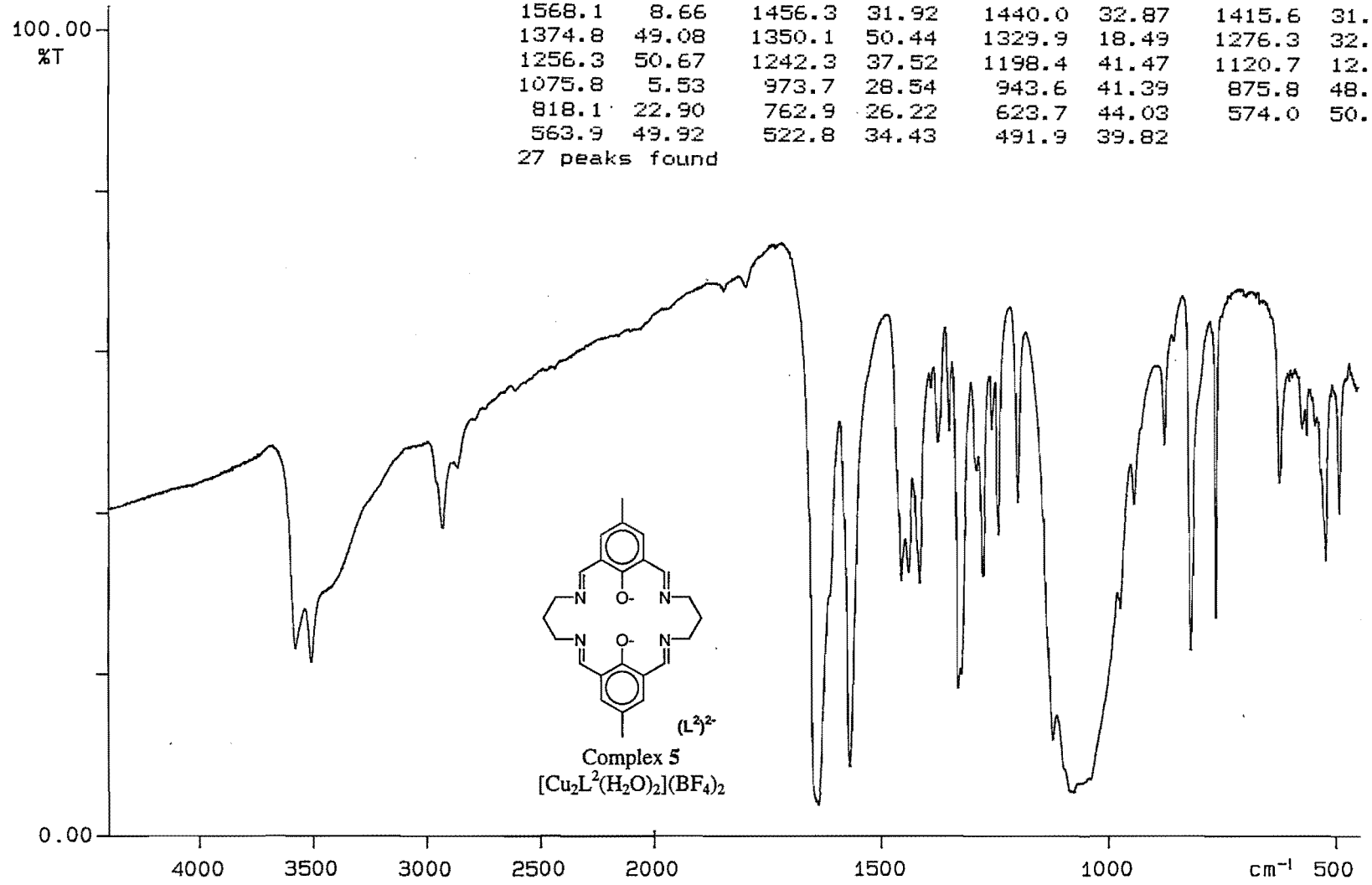

$(L^3)^{2-}$

Complex 5

$[Cu_2L^2(H_2O)_2](BF_4)_2$

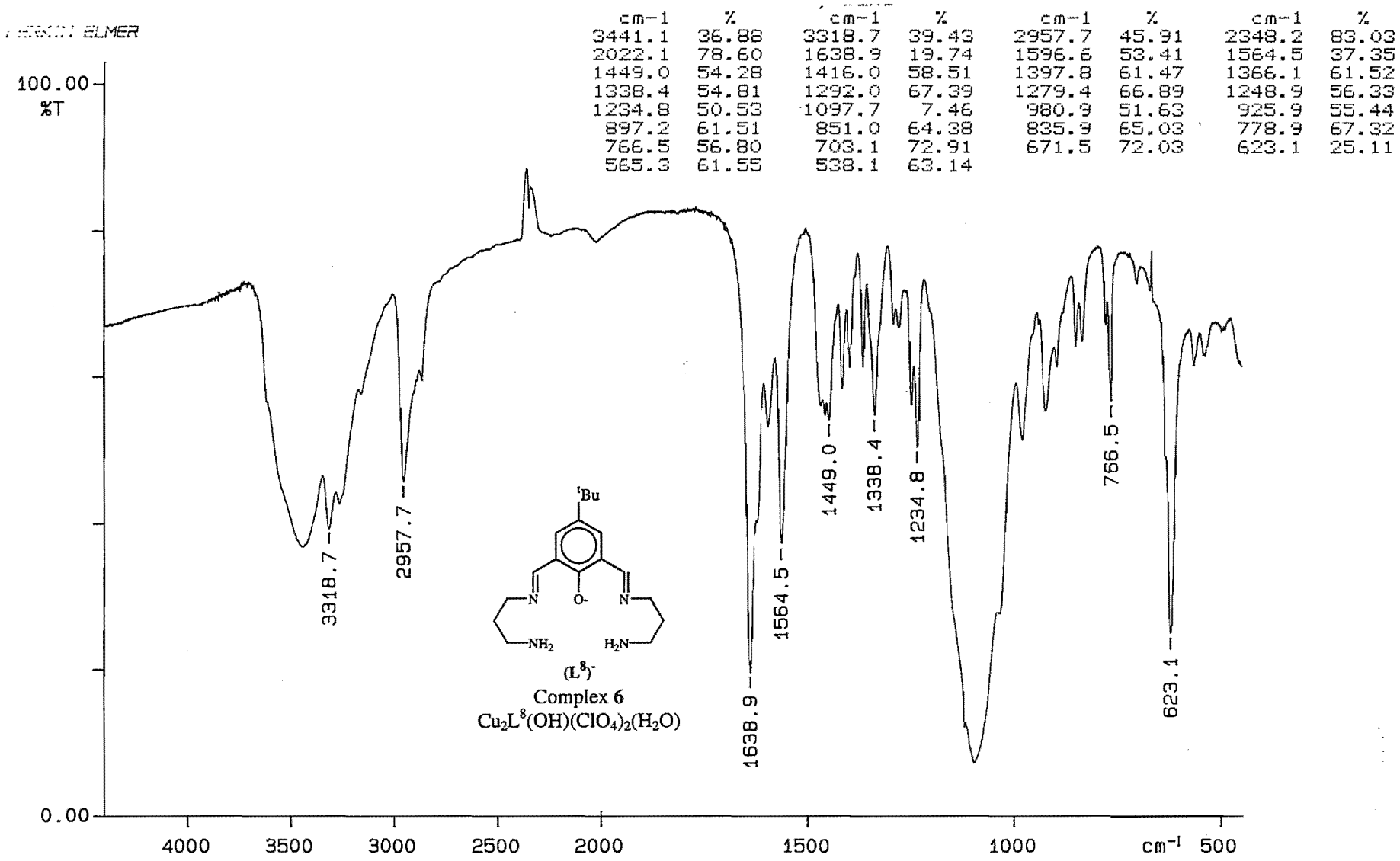

cm-1	%	cm-1	%	cm-1	%	cm-1	%
3441.1	36.88	3318.7	39.43	2957.7	45.91	2348.2	83.03
2022.1	78.60	1638.9	19.74	1596.6	53.41	1564.5	37.35
1449.0	54.28	1416.0	58.51	1397.8	61.47	1366.1	61.52
1338.4	54.81	1292.0	67.39	1279.4	66.89	1248.9	56.33
1234.8	50.53	1097.7	7.46	980.9	51.63	925.9	55.44
897.2	61.51	851.0	64.38	835.9	65.03	778.9	67.32
766.5	56.80	703.1	72.91	671.5	72.03	623.1	25.11
565.3	61.55	538.1	63.14				

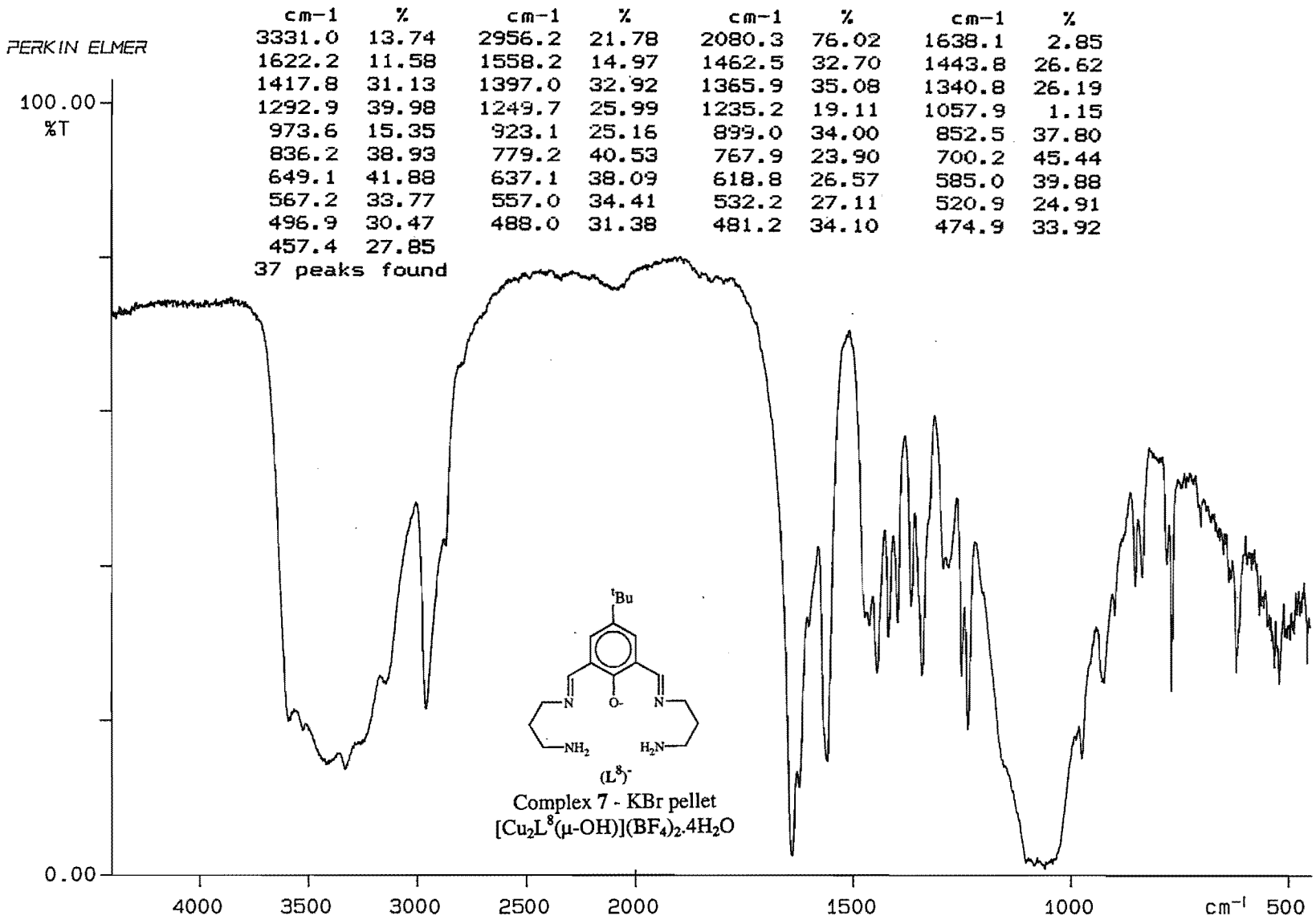
PERKIN ELMER
100.00
%T
0.00
4000
3500
3000
2500
2000
1500
1000
cm-1
500
cm-1 % cm-1 % cm-1 % cm-1 %
3331.0 13.74 2956.2 21.78 2080.3 76.02 1638.1 2.85
1622.2 11.58 1558.2 14.97 1462.5 32.70 1443.8 26.62
1417.8 31.13 1397.0 32.92 1365.9 35.08 1340.8 26.19
1292.9 39.98 1249.7 25.99 1235.2 19.11 1057.9 1.15
973.6 15.35 923.1 25.16 899.0 34.00 852.5 37.80
836.2 38.93 779.2 40.53 767.9 23.90 700.2 45.44
649.1 41.88 637.1 38.09 618.8 26.57 585.0 39.88
567.2 33.77 557.0 34.41 532.2 27.11 520.9 24.91
496.9 30.47 488.0 31.38 481.2 34.10 474.9 33.92
457.4 27.85
37 peaks found
tBu
N
O-
N
NH2
H2N
(L8)-
Complex 7 - KBr pellet
[Cu2L8(μ-OH)](BF4)2.4H2O

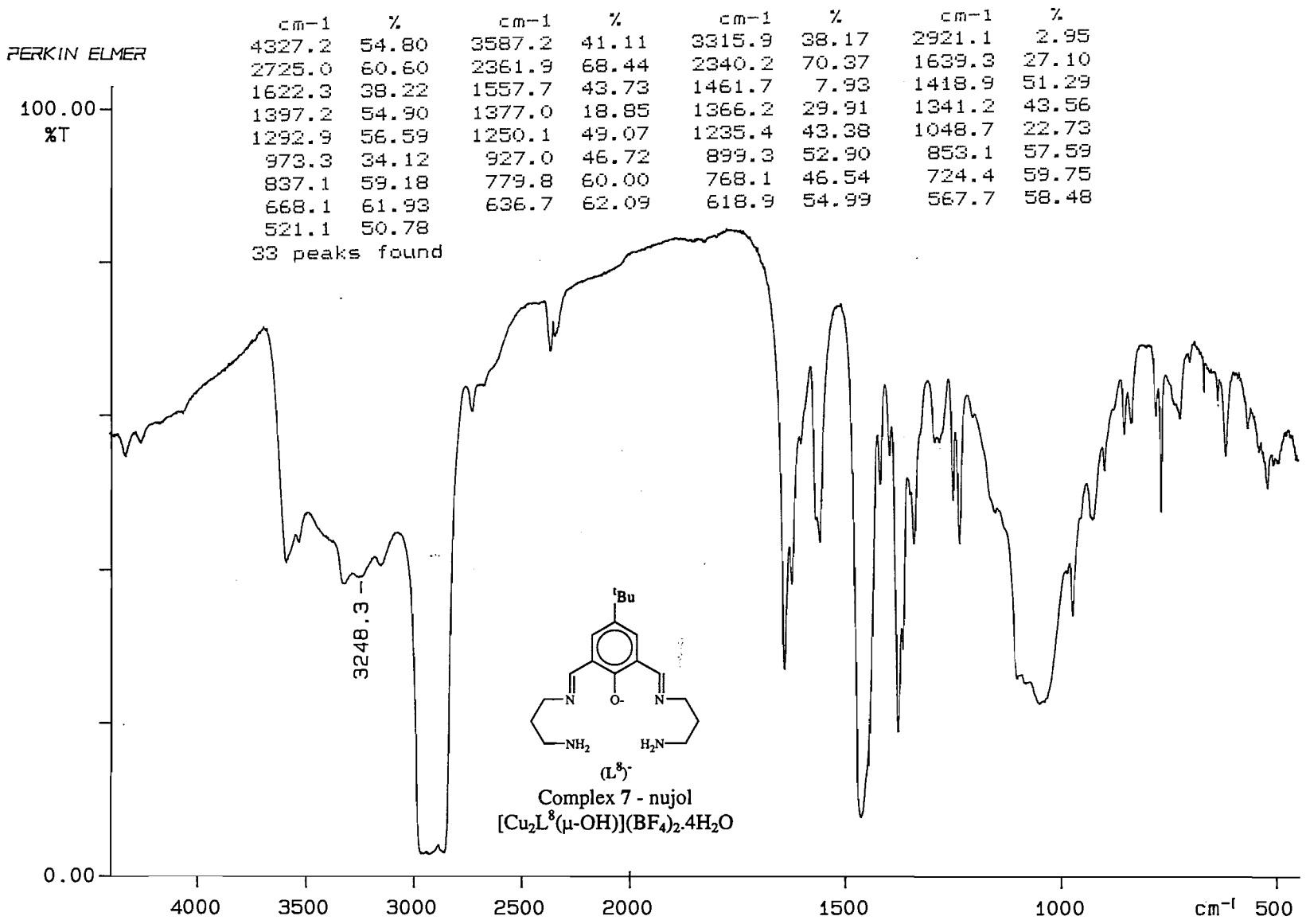

cm-1	%	cm-1	%	cm-1	%	cm-1	%
4327.2	54.80	3587.2	41.11	3315.9	38.17	2921.1	2.95
2725.0	60.60	2361.9	68.44	2340.2	70.37	1639.3	27.10
1622.3	38.22	1557.7	43.73	1461.7	7.93	1418.9	51.29
1397.2	54.90	1377.0	18.85	1366.2	29.91	1341.2	43.56
1292.9	56.59	1250.1	49.07	1235.4	43.38	1048.7	22.73
973.3	34.12	927.0	46.72	899.3	52.90	853.1	57.59
837.1	59.18	779.8	60.00	768.1	46.54	724.4	59.75
668.1	61.93	636.7	62.09	618.9	54.99	567.7	58.48
521.1	50.78						

33 peaks found

$(L^8)^-$

Complex 7 - nujol

$[Cu_2L^8(\mu\text{-}OH)](BF_4)_2.4H_2O$

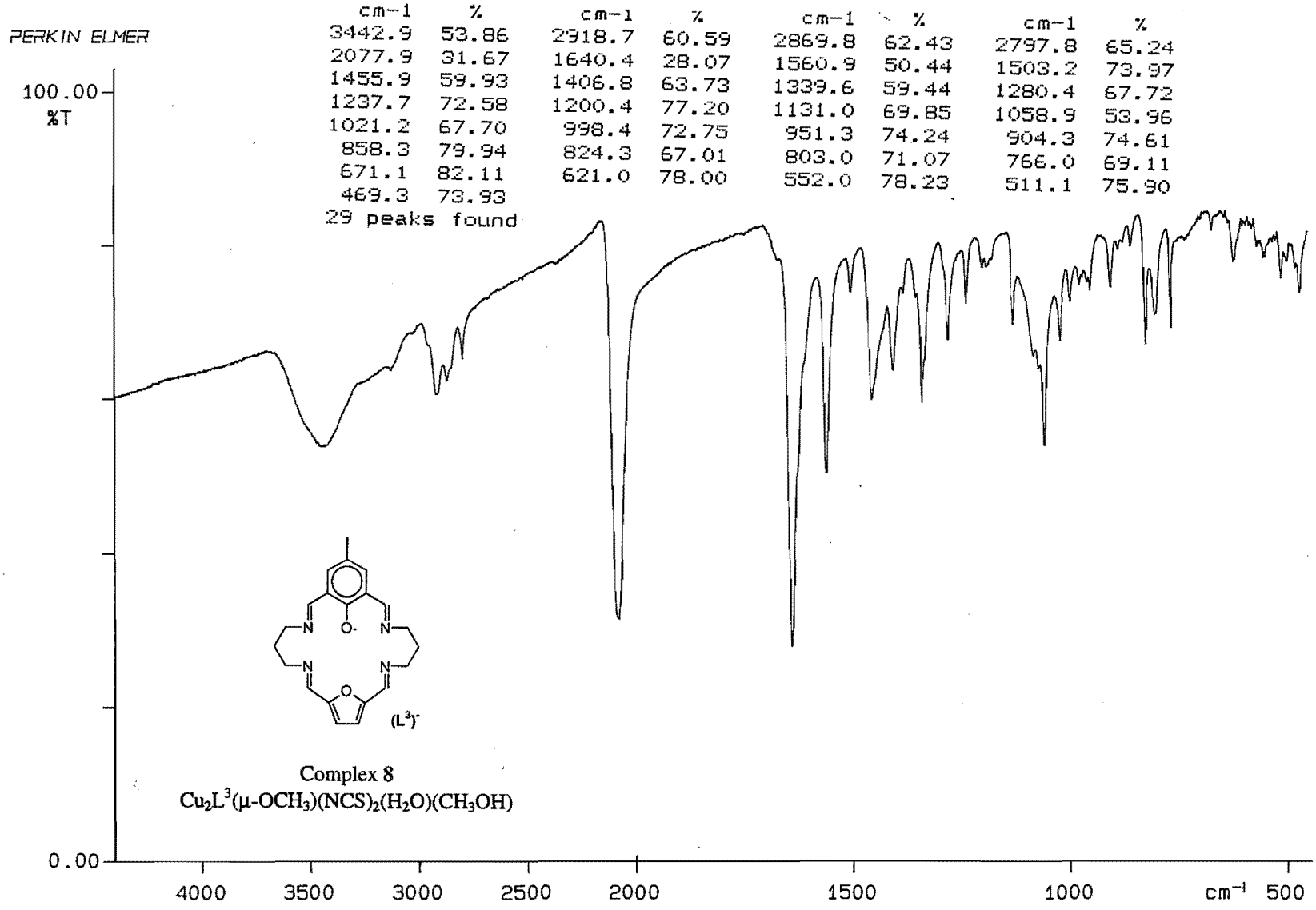
PERKIN ELMER
100.00
%T
0.00
4000
3500
3000
2500
2000
1500
1000
cm-1
500
cm-1 % cm-1 % cm-1 % cm-1 %
3442.9 53.86 2918.7 60.59 2869.8 62.43 2797.8 65.24
2077.9 31.67 1640.4 28.07 1560.9 50.44 1503.2 73.97
1455.9 59.93 1406.8 63.73 1339.6 59.44 1280.4 67.72
1237.7 72.58 1200.4 77.20 1131.0 69.85 1058.9 53.96
1021.2 67.70 998.4 72.75 951.3 74.24 904.3 74.61
858.3 79.94 824.3 67.01 803.0 71.07 766.0 69.11
671.1 82.11 621.0 78.00 552.0 78.23 511.1 75.90
469.3 73.93
29 peaks found
N
O-
N
N
N
O
(L3)-
Complex 8
Cu2L3(μ-OCH3)(NCS)2(H2O)(CH3OH)

PERKIN ELMER

cm-1	%	cm-1	%	cm-1	%	cm-1	%
3445.9	35.40	2915.9	41.54	2868.2	43.81	2796.9	47.79
2359.3	59.18	2340.3	61.43	2088.9	11.21	1639.5	8.86
1560.1	26.45	1502.1	60.07	1455.9	39.54	1406.4	46.75
1383.8	50.45	1339.1	38.81	1280.1	49.91	1237.2	56.79
1190.8	63.64	1130.7	53.38	1083.7	42.25	1058.8	31.67
1020.4	51.03	997.9	57.08	951.3	59.45	904.0	60.15
858.0	68.63	824.2	48.79	804.3	54.26	765.8	50.88
668.0	65.44	619.9	65.62	549.9	66.41	510.9	61.79
468.8	59.43						

33 peaks found

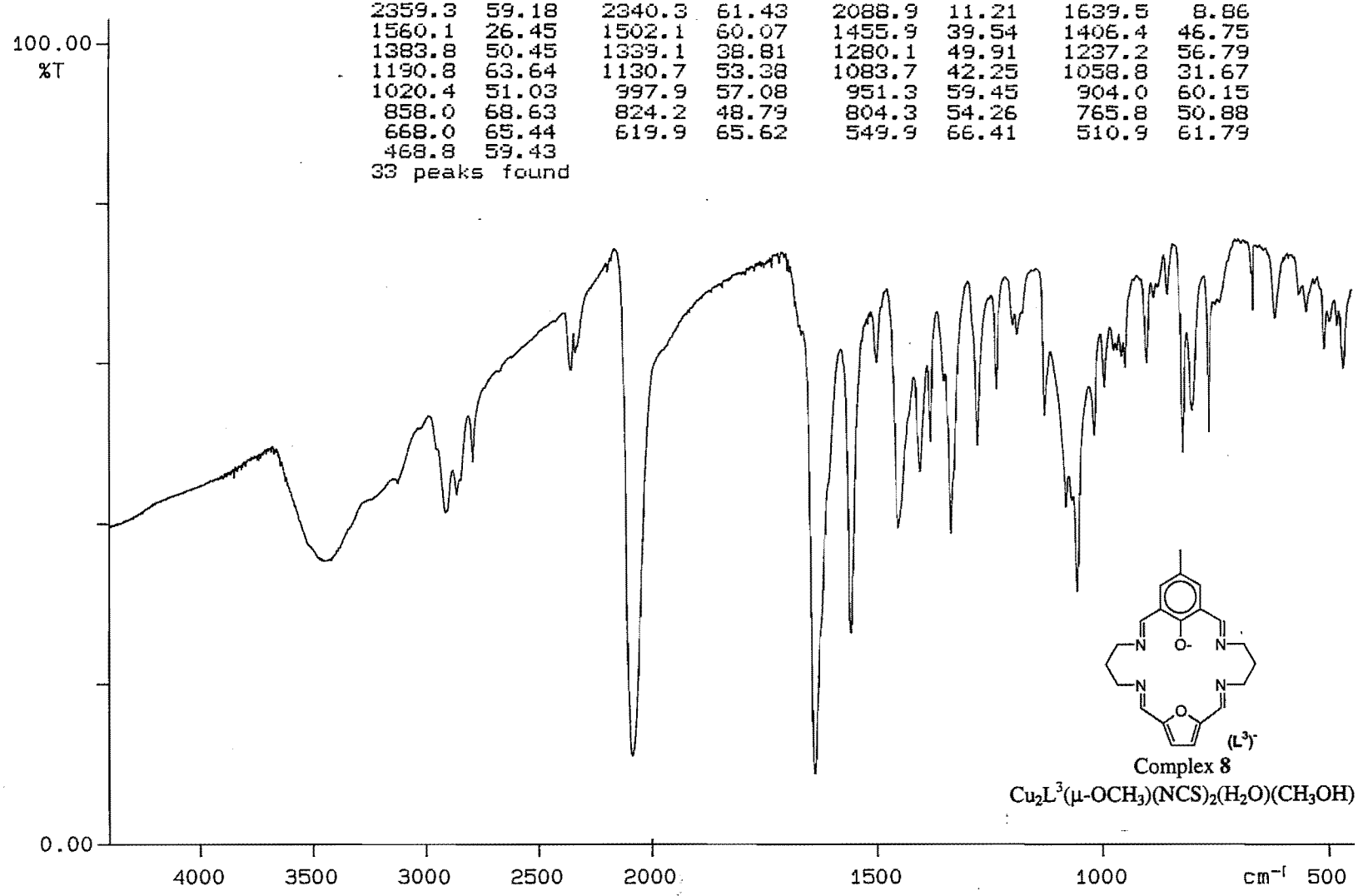

Complex **8**

$Cu_2L^3(\mu\text{-}OCH_3)(NCS)_2(H_2O)(CH_3OH)$

cm-1	%	cm-1	%	cm-1	%	cm-1	%
3444.8	46.75	2964.4	50.04	2919.9	46.30	2867.9	43.20
2095.6	12.84	2076.4	9.06	1640.8	11.17	1564.0	31.62
1502.6	59.48	1456.0	39.00	1429.7	58.73	1406.2	51.42
1385.4	61.27	1372.8	60.16	1352.0	57.79	1338.0	41.23
1278.0	49.06	1238.6	56.92	1203.8	66.34	1178.9	67.69
1132.1	55.90	1106.2	56.44	1057.6	32.23	1020.0	47.99
998.0	60.58	975.9	61.20	958.3	56.78	906.2	57.73
857.9	69.57	823.1	50.97	801.3	52.92	765.4	55.58
673.1	75.72	621.4	70.39	595.3	78.59	565.7	72.95
550.6	72.93	532.3	77.73	498.9	69.03	468.1	65.84

40 peaks found

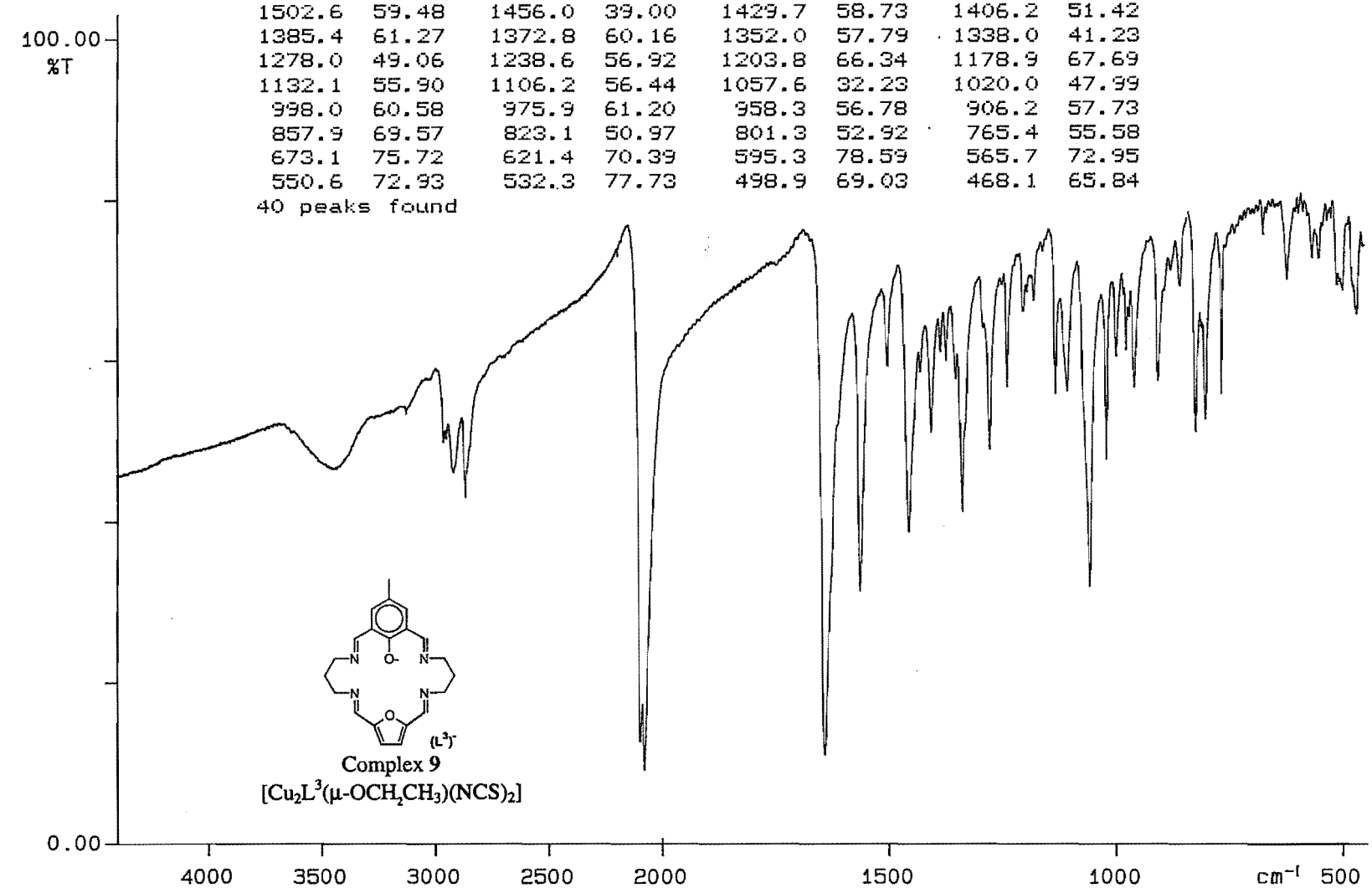

Complex **9**

$[Cu_2L^3(\mu\text{-}OCH_2CH_3)(NCS)_2]$

PERKIN ELMER

cm-1	%	cm-1	%	cm-1	%	cm-1	%
3640.7	33.78	3449.5	41.77	2922.8	43.20	2864.2	43.64
2349.0	65.36	2081.4	5.68	1641.1	8.73	1558.8	28.17
1501.2	55.96	1457.7	33.79	1409.4	41.57	1384.7	54.71
1353.4	54.26	1340.1	38.67	1281.3	46.08	1233.1	55.11
1198.9	64.31	1183.0	60.53	1130.9	50.21	1059.5	30.94
1023.2	48.76	998.5	61.16	969.6	49.70	904.6	54.48
871.0	63.22	825.5	46.53	808.6	57.86	768.3	50.08
696.0	73.81	670.5	73.72	661.8	74.02	614.2	67.30
567.9	69.04	554.0	71.39	526.8	68.76	505.8	54.33
473.1	57.83						

37 peaks found

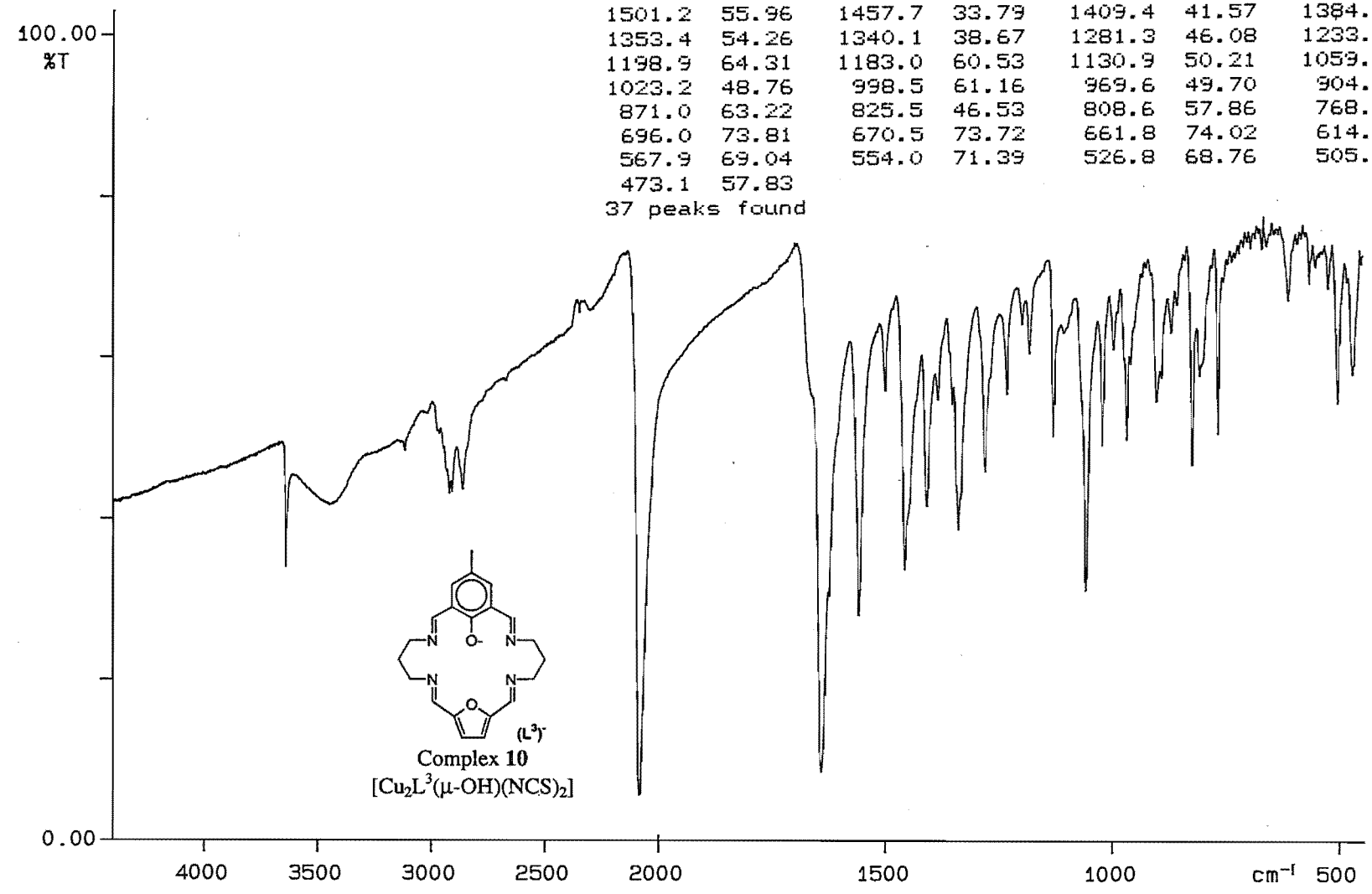

Complex **10**

$[Cu_2L^3(\mu\text{-}OH)(NCS)_2]$

PERKIN ELMER

cm-1	%	cm-1	%	cm-1	%	cm-1	%
3423.7	27.52	2959.9	41.76	2871.3	56.00	2117.9	80.48
1652.3	14.01	1555.5	33.29	1456.2	47.83	1397.5	53.01
1366.6	55.09	1326.6	49.31	1233.3	19.94	1053.3	6.25
896.8	56.01	846.1	45.62	780.7	53.72	764.8	46.36
705.0	49.54	633.8	47.72	575.1	50.94	533.6	41.73
521.8	39.43	485.1	47.20				

22 peaks found

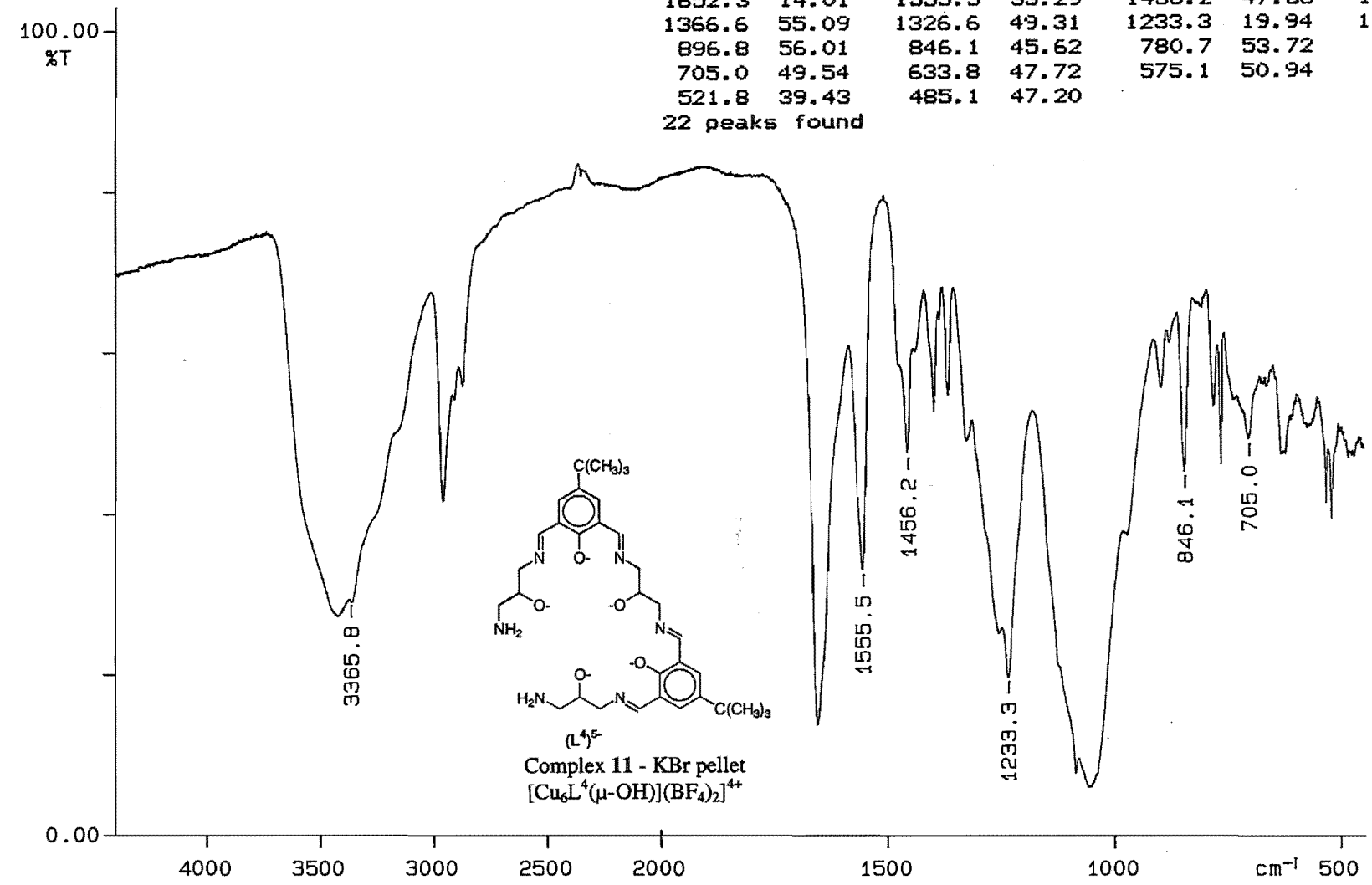

Complex 11 - KBr pellet

$[Cu_6L^4(\mu\text{-}OH)](BF_4)_2]^{4+}$

PERKIN ELMER

cm-1	%	cm-1	%	cm-1	%	cm-1	%
3573.0	39.63	3354.9	38.24	2926.8	1.01	2870.9	8.59
2360.0	71.50	1652.0	23.65	1556.4	43.99	1458.0	24.67
1397.7	61.14	1376.8	45.28	1366.6	48.67	1326.9	57.96
1234.7	27.89	1053.1	12.56	898.2	61.52	847.0	56.18
781.5	60.87	764.5	52.66	722.1	57.34	668.0	59.79
627.9	55.04	609.2	57.80	570.0	57.30	520.2	46.56

24 peaks found

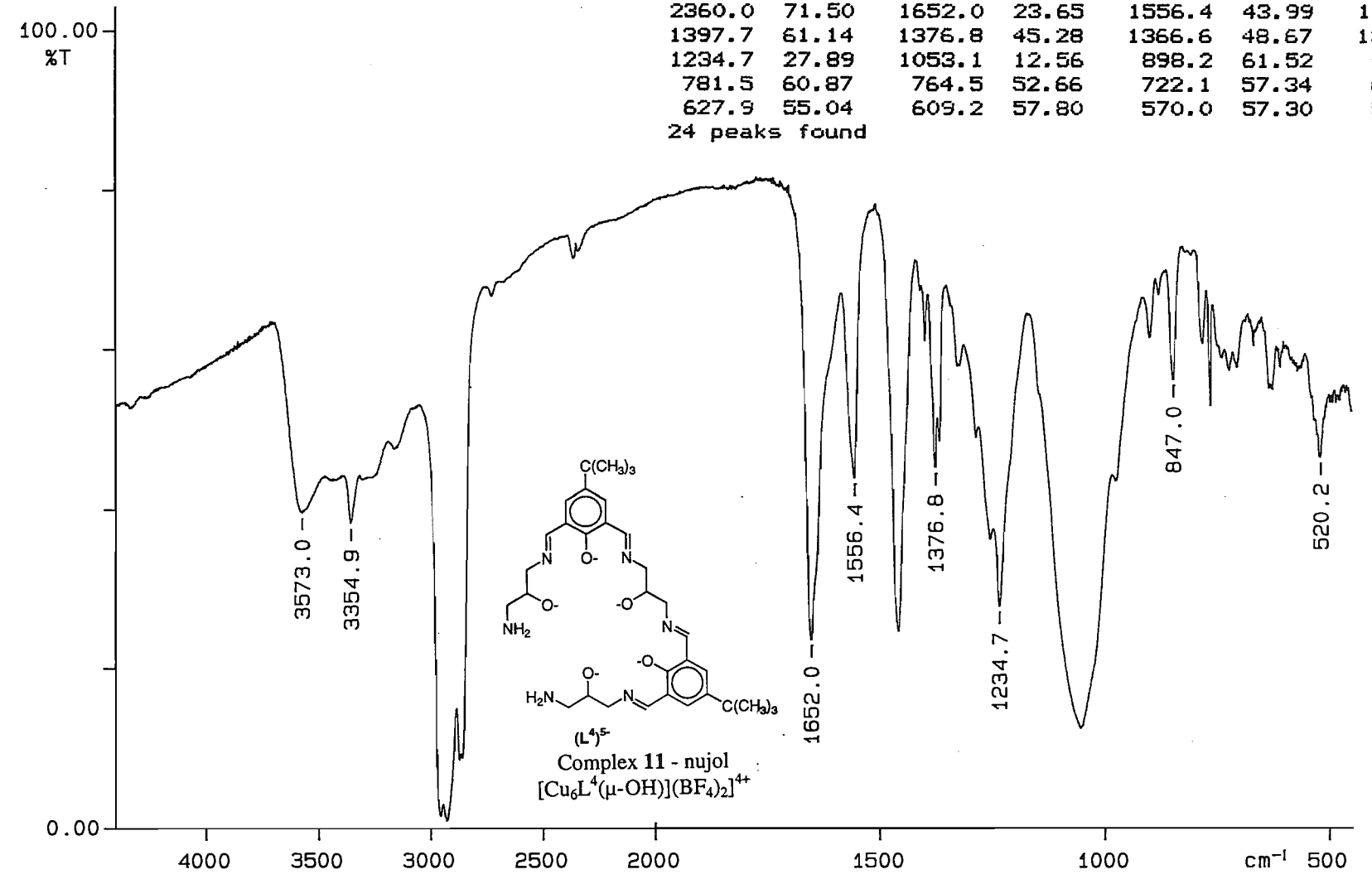

Complex 11 - nujol

$[Cu_6L^4(\mu\text{-}OH)](BF_4)_2]^{4+}$

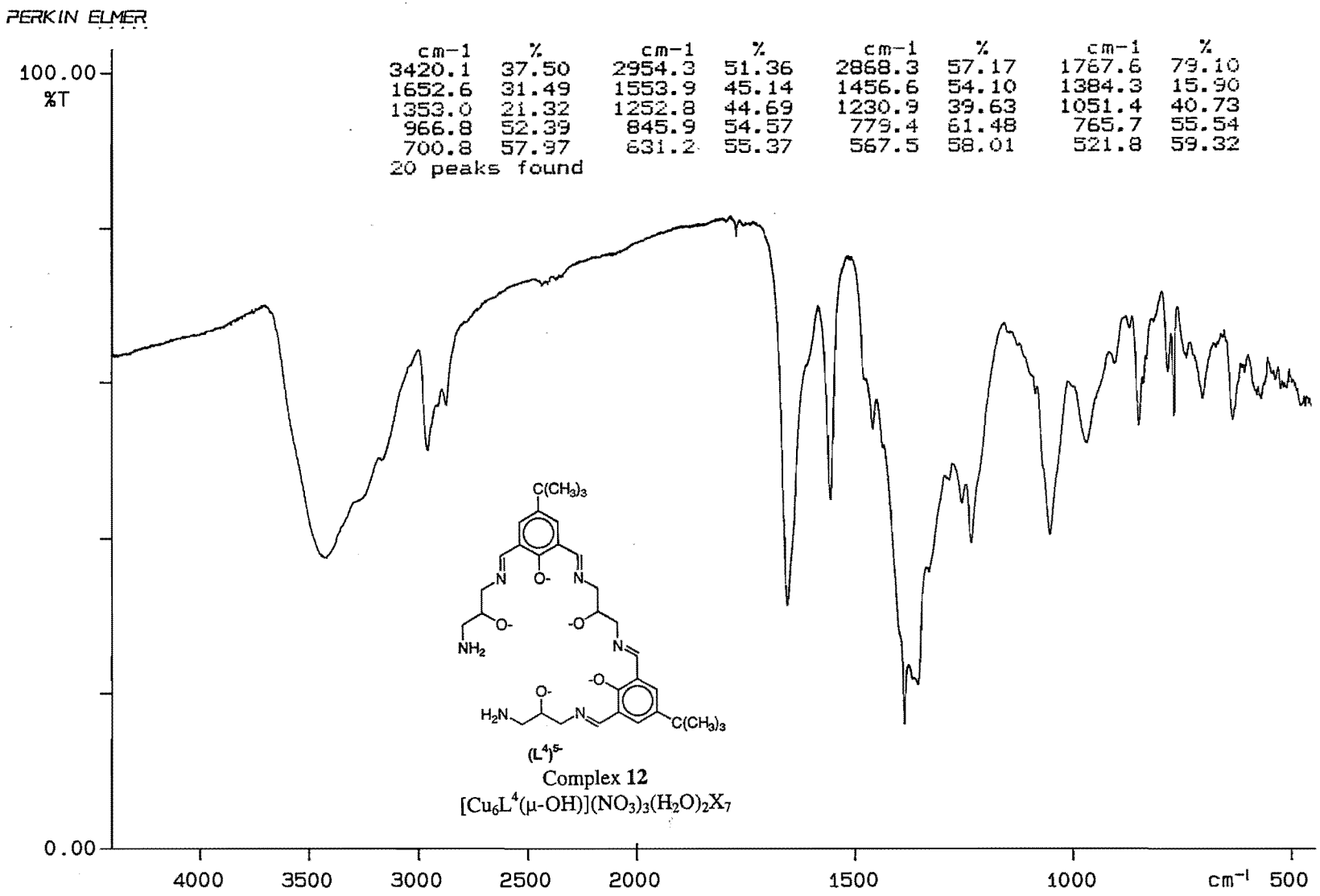

Complex **12**

$[Cu_6L^4(\mu\text{-}OH)](NO_3)_3(H_2O)_2X_7$

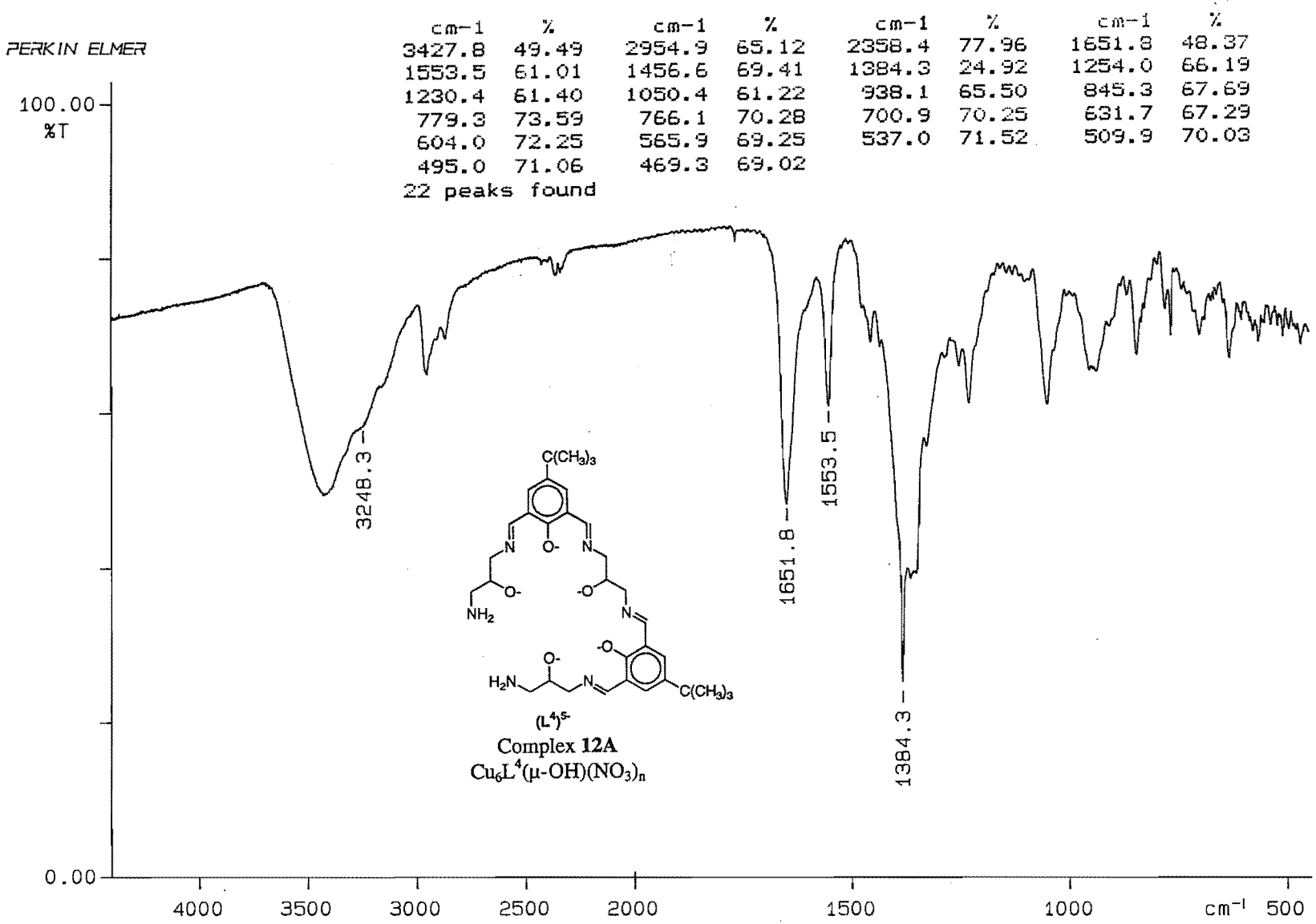

Complex **12A**

$Cu_6L^4(\mu\text{-}OH)(NO_3)_n$

PERKIN ELMER

cm-1	%	cm-1	%	cm-1	%	cm-1	%
3422.8	18.33	2927.3	28.39	2862.0	35.09	2363.1	55.59
1643.4	5.03	1574.9	10.96	1463.7	29.65	1449.9	32.45
1416.0	33.75	1387.9	50.83	1360.9	49.63	1330.9	17.81
1282.3	43.38	1244.4	40.35	1228.3	57.34	1195.0	43.98
1132.7	6.40	1059.2	2.87	900.7	32.39	828.2	29.16
759.3	30.70	700.2	56.17	640.8	27.28	591.5	34.77
556.3	40.21	544.5	34.16	533.0	35.39	521.9	28.49

28 peaks found

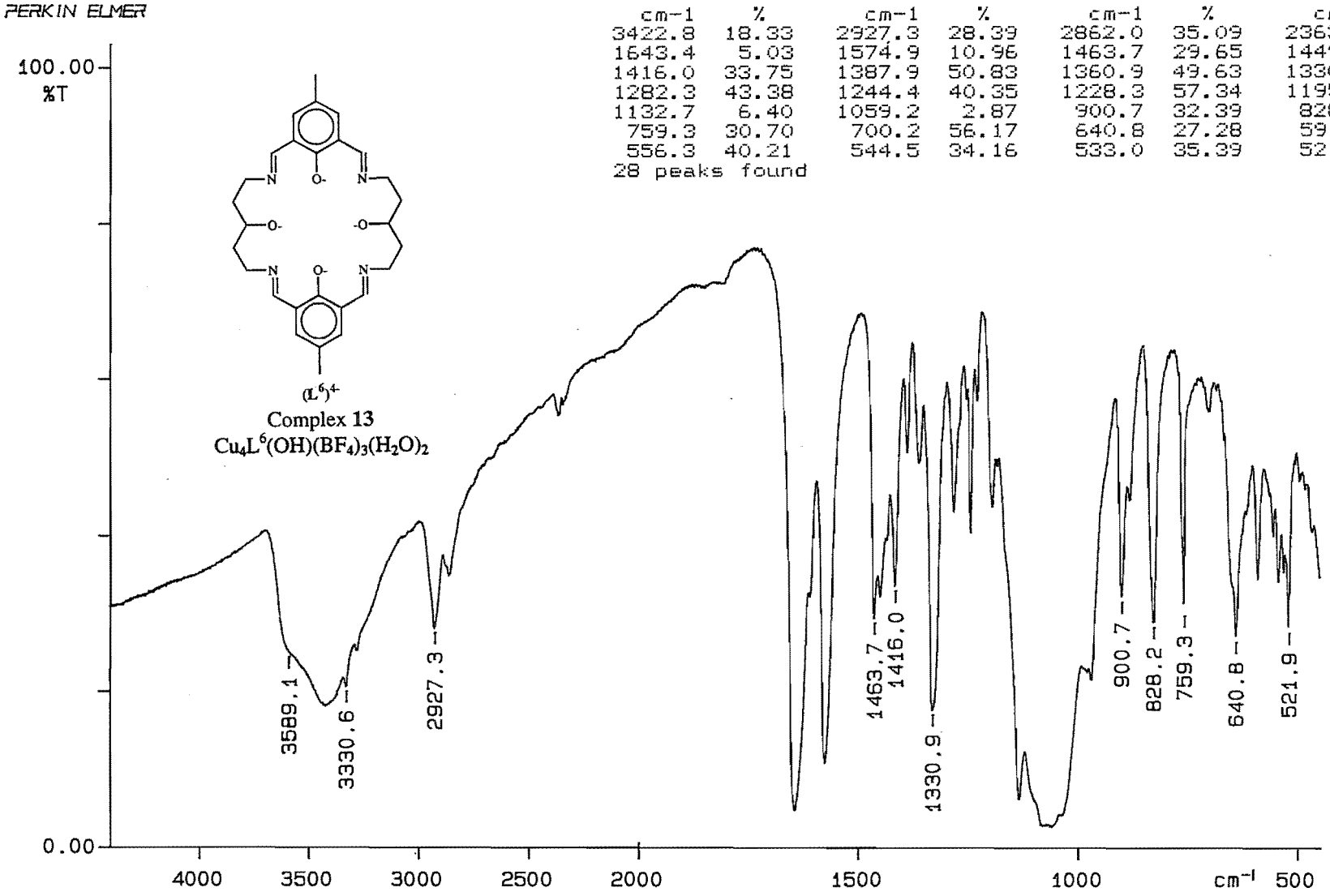

$(L^6)^{4+}$

Complex 13

$Cu_4L^6(OH)(BF_4)_3(H_2O)_2$

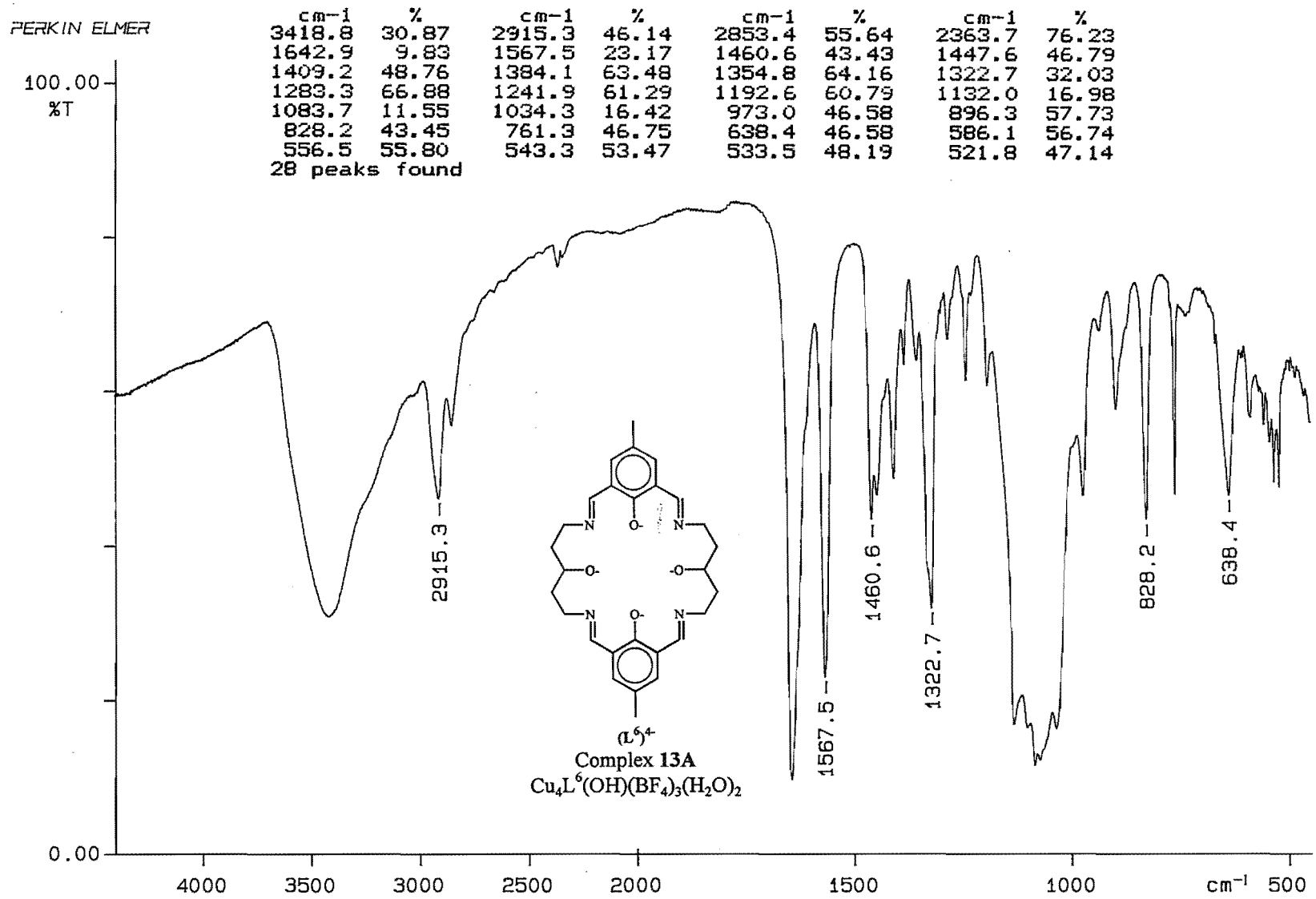
PERKIN ELMER
cm-1 % cm-1 % cm-1 % cm-1 %
3418.8 30.87 2915.3 46.14 2853.4 55.64 2363.7 76.23
1642.9 9.83 1567.5 23.17 1460.6 43.43 1447.6 46.79
1409.2 48.76 1384.1 63.48 1354.8 64.16 1322.7 32.03
1283.3 66.88 1241.9 61.29 1192.6 60.79 1132.0 16.98
1083.7 11.55 1034.3 16.42 973.0 46.58 896.3 57.73
828.2 43.45 761.3 46.75 638.4 46.58 586.1 56.74
556.5 55.80 543.3 53.47 533.5 48.19 521.8 47.14
28 peaks found
100.00
%T
0.00
2915.3
1567.5
1460.6
1322.7
828.2
638.4
4000
3500
3000
2500
2000
1500
1000
cm-1
500
(L6)4-
Complex 13A
Cu4L6(OH)(BF4)3(H2O)2

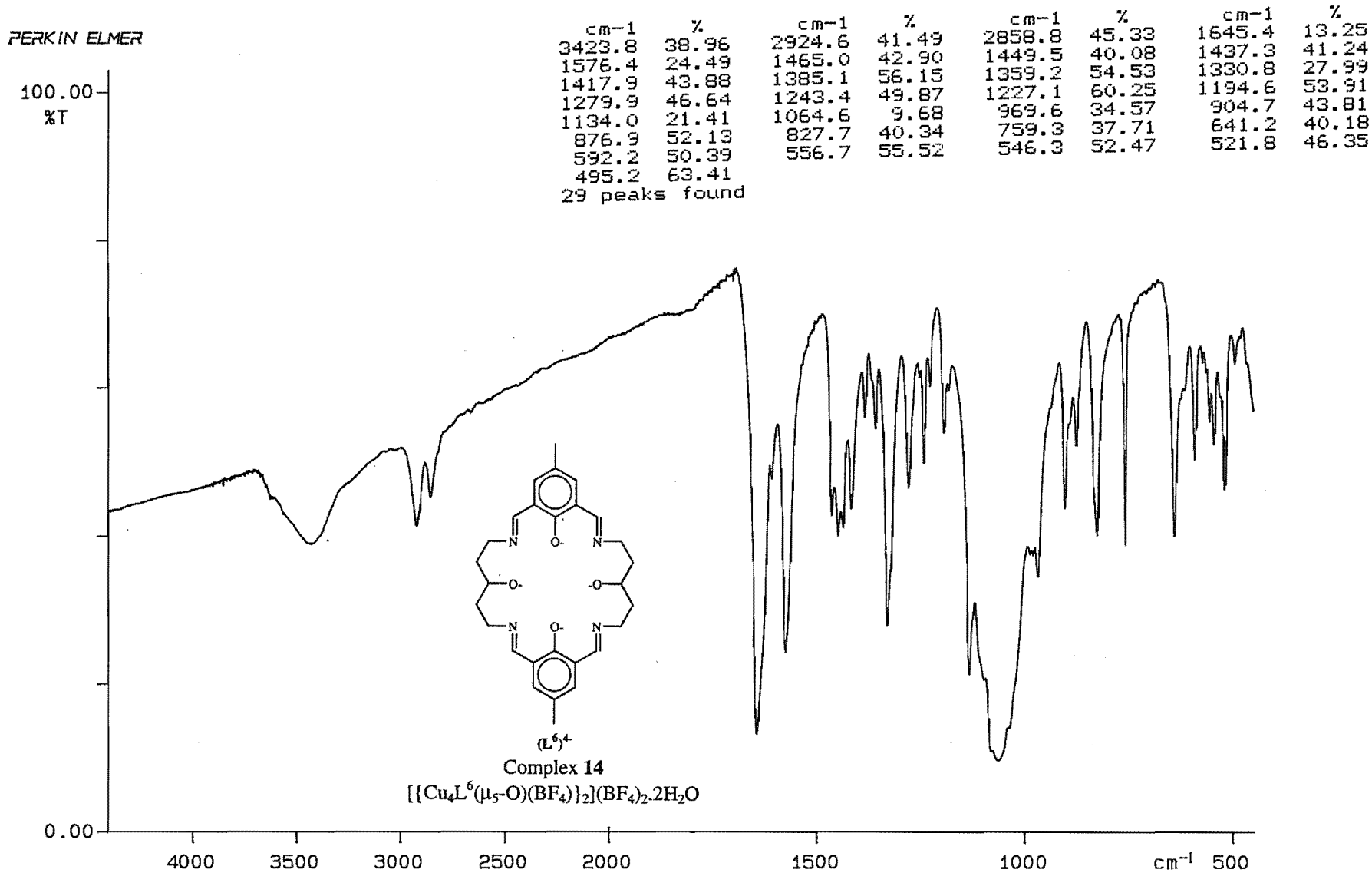

$(L^6)^{4-}$

Complex **14**

$[\{Cu_4L^6(\mu_5\text{-}O)(BF_4)\}_2](BF_4)_2.2H_2O$

PERKIN ELMER

cm-1	%	cm-1	%	cm-1	%	cm-1	%
3424.7	42.69	2945.9	52.54	2909.8	53.40	2760.9	57.00
2687.5	57.93	2361.9	61.56	1646.9	45.30	1631.5	49.63
1587.2	36.91	1465.1	59.31	1439.8	56.28	1417.3	55.48
1385.0	58.92	1367.8	56.48	1340.6	44.93	1287.6	62.87
1237.3	60.60	1227.7	62.82	1189.6	64.79	1136.4	51.67
1090.6	60.58	994.2	65.42	975.6	63.16	888.1	65.37
830.2	60.77	763.2	56.91	668.0	60.37	626.8	56.39
587.2	56.83	557.0	56.73	545.9	57.39	465.0	59.96

32 peaks found

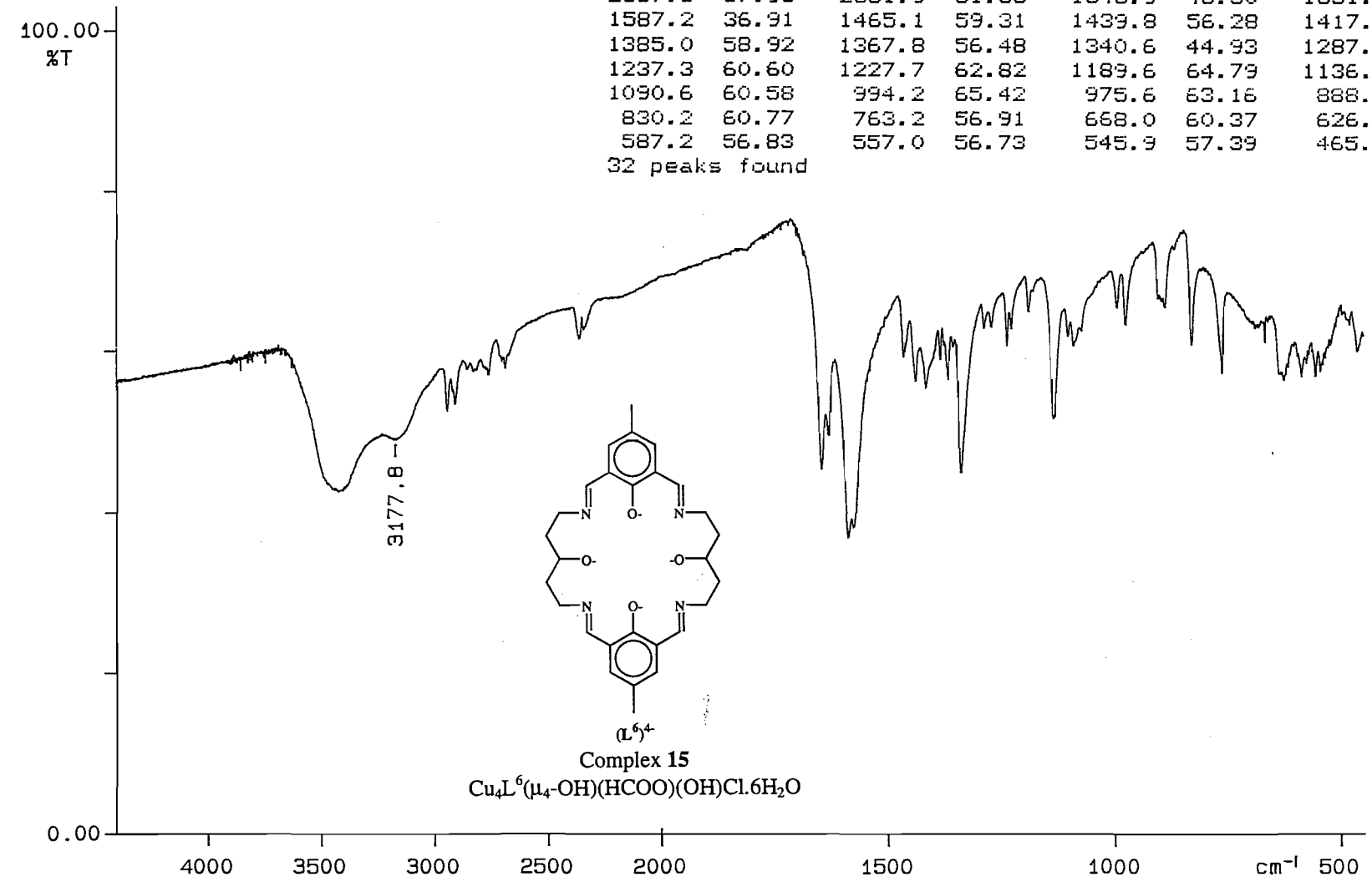

$(L^6)^{4-}$

Complex **15**

$Cu_4L^6(\mu_4\text{-}OH)(HCOO)(OH)Cl.6H_2O$

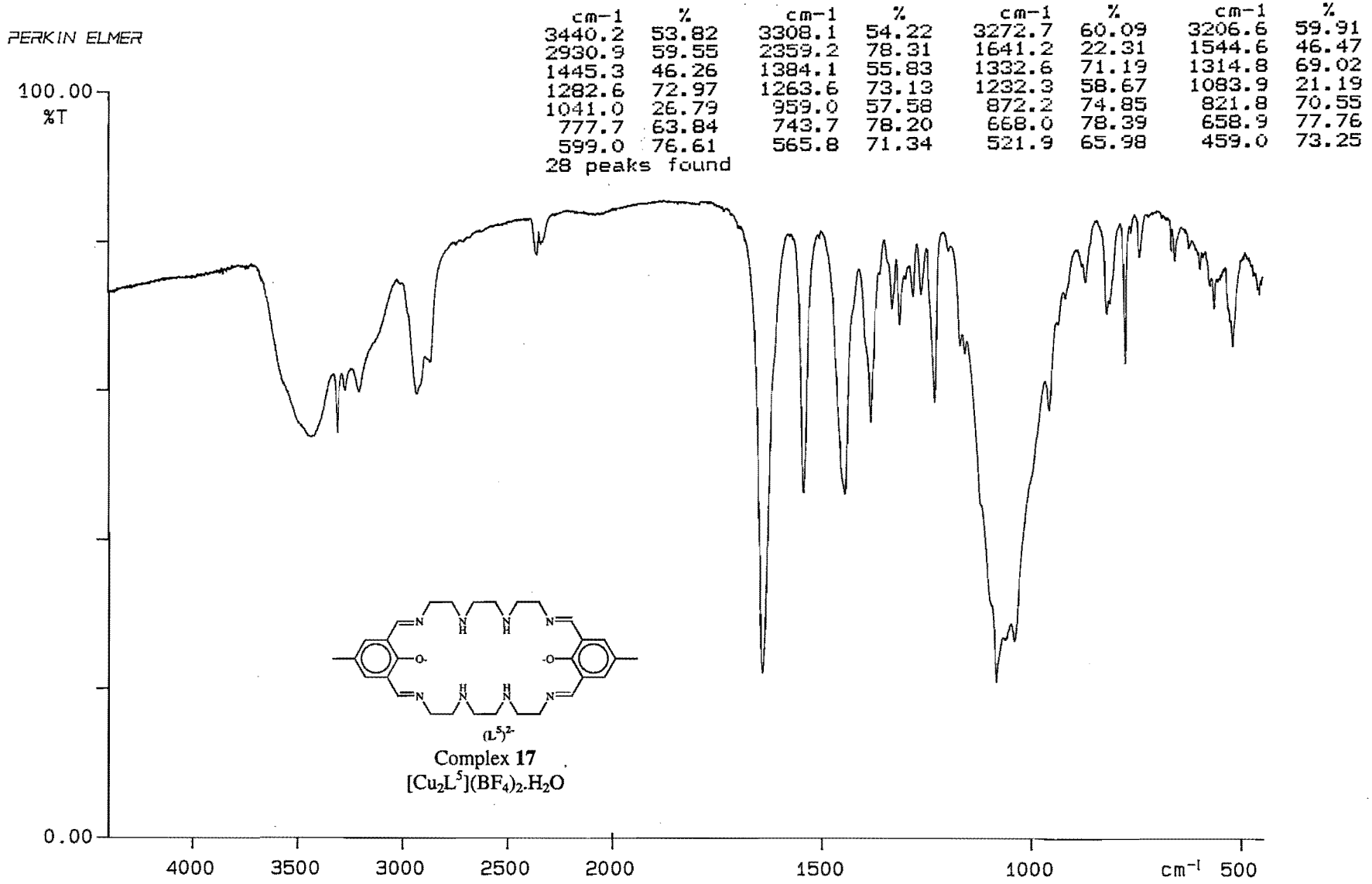

$(L^5)^{2-}$

Complex **17**

$[Cu_2L^5](BF_4)_2.H_2O$

cm-1	%	cm-1	%	cm-1	%	cm-1	%
3497.5	28.92	3308.0	17.94	3272.0	28.69	3206.5	23.10
2930.6	21.11	2866.1	26.60	1642.1	0.96	1545.0	8.61
1445.0	8.21	1383.9	18.97	1332.6	36.68	1314.7	33.25
1282.5	40.84	1264.2	42.86	1232.7	18.27	1199.2	57.15
1172.1	27.51	1160.4	25.70	1081.9	0.89	959.2	13.98
872.4	41.56	821.9	34.71	777.5	22.14	763.9	59.68
743.9	49.95	658.9	53.33	625.2	58.22	598.4	52.07
575.2	45.47	566.2	39.42	552.2	47.00	521.8	27.70
458.3	44.65						

33 peaks found

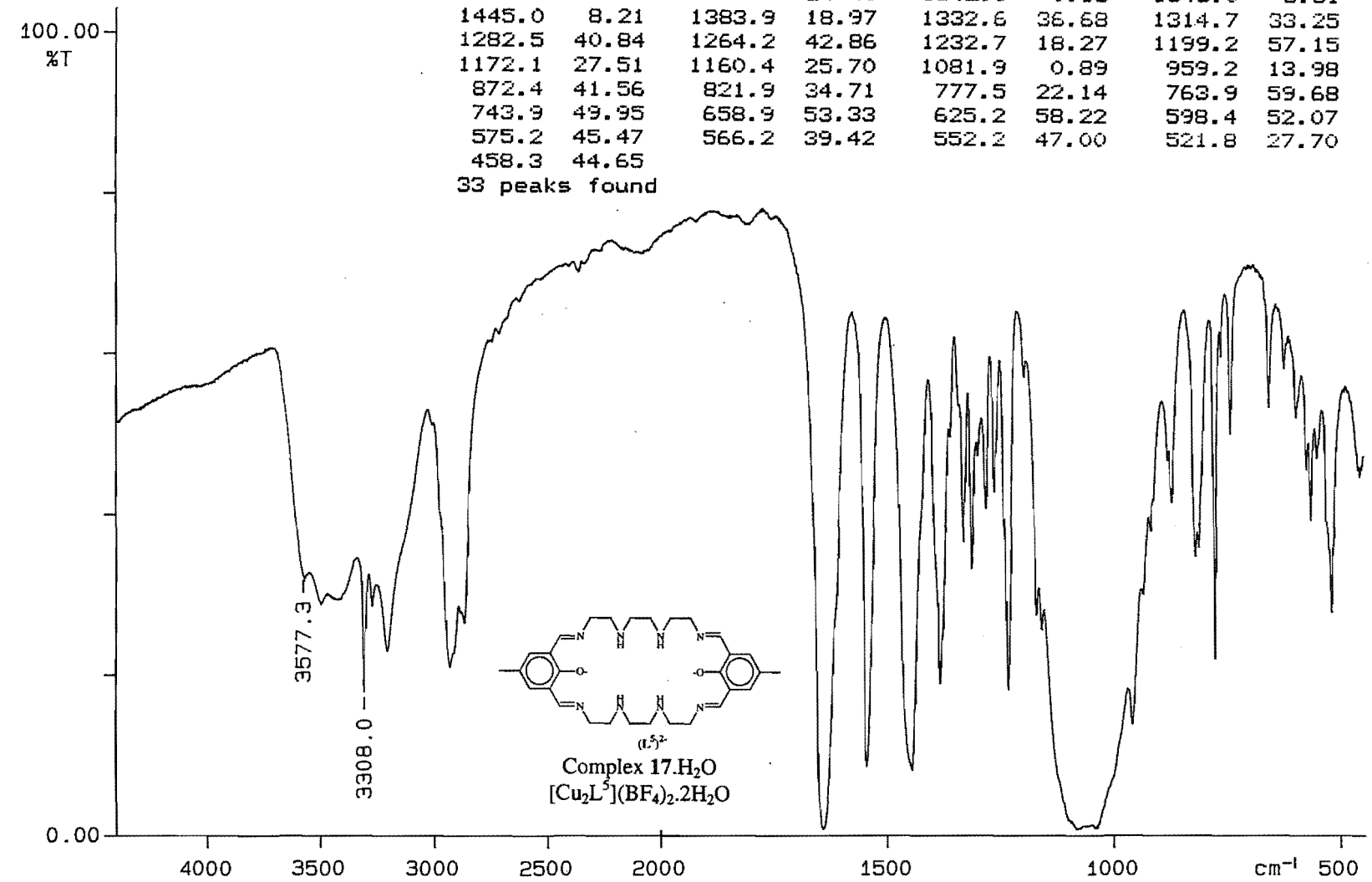

$(L^5)^{2-}$

Complex **17**.H_2O

$[Cu_2L^5](BF_4)_2.2H_2O$

Appendix C

Fast-atom-bombardment mass spectra

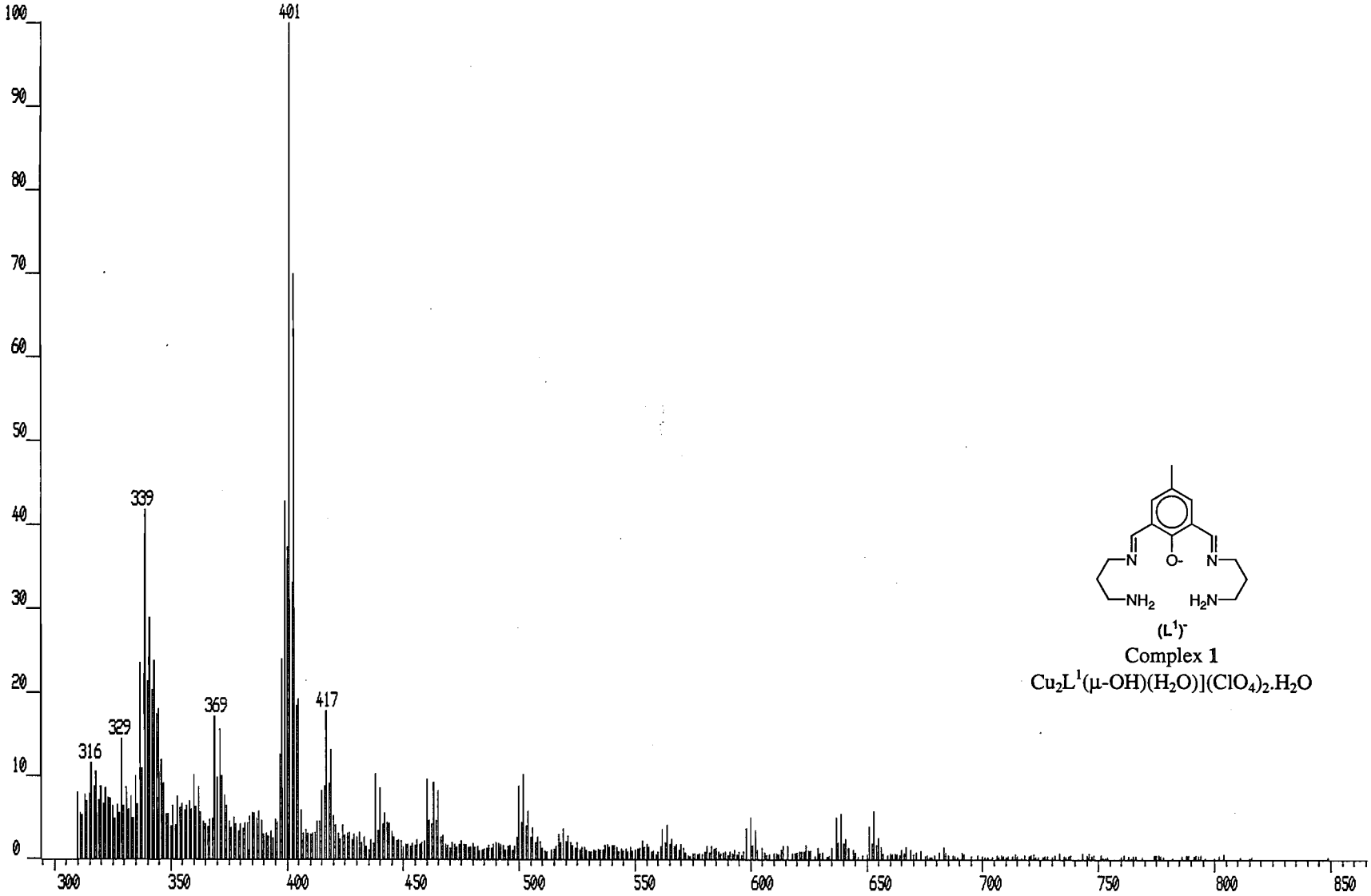

$(L^1)^-$

Complex **1**

$Cu_2L^1(\mu\text{-}OH)(H_2O)](ClO_4)_2.H_2O$

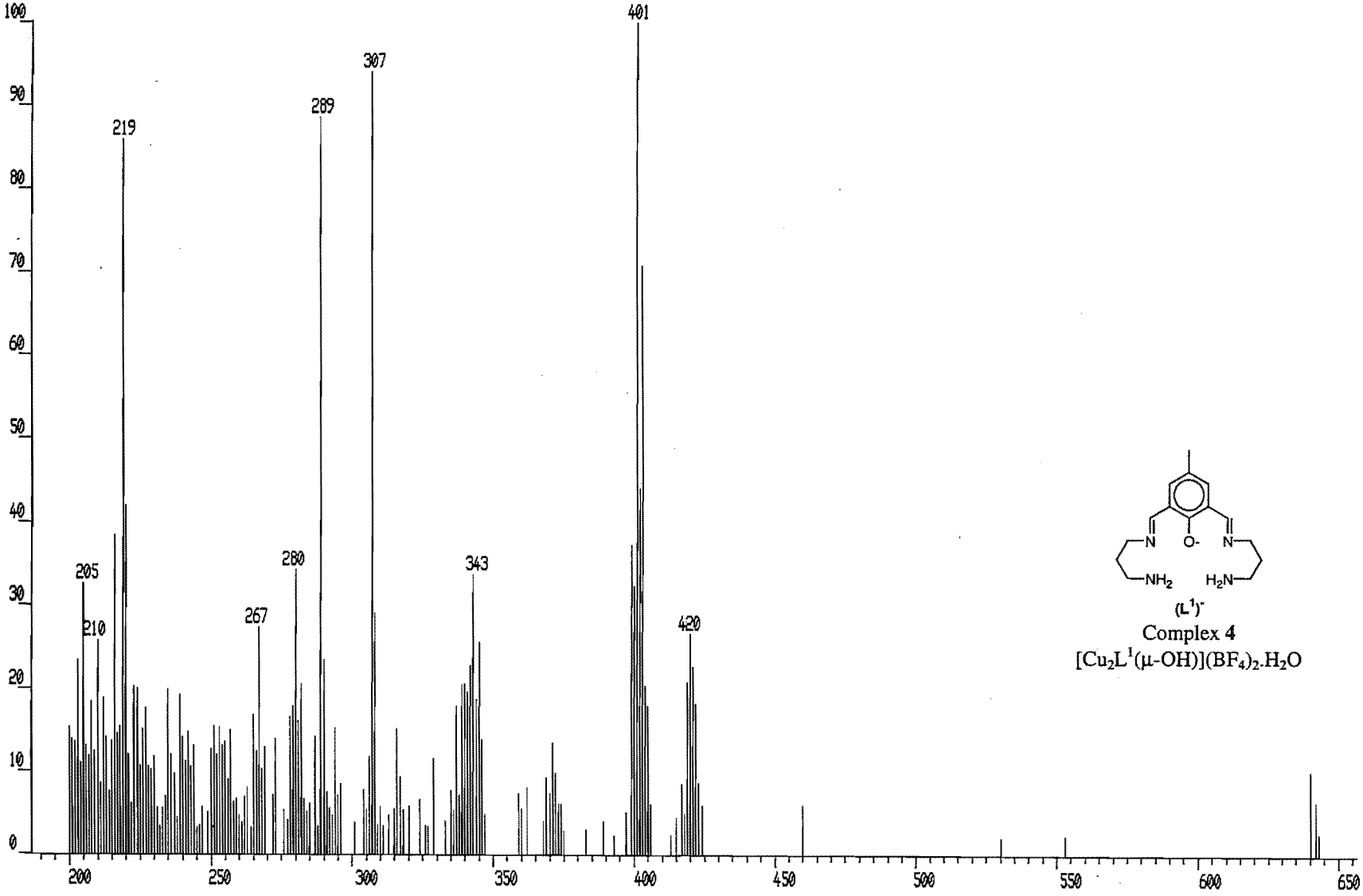

$(L^1)^-$

Complex **4**

$[Cu_2L^1(\mu\text{-}OH)](BF_4)_2.H_2O$

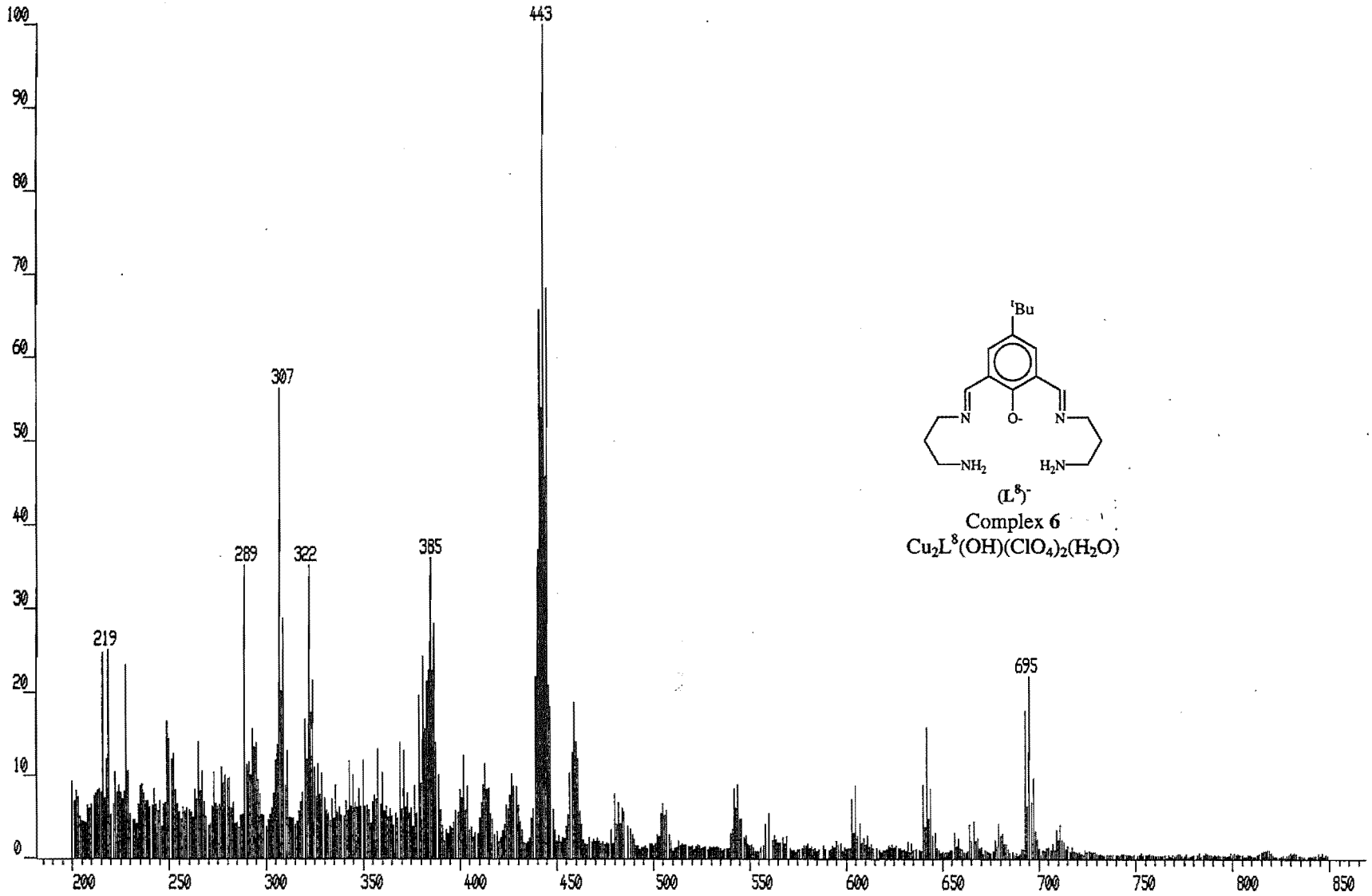

$(L^8)^-$

Complex **6**

$Cu_2L^8(OH)(ClO_4)_2(H_2O)$

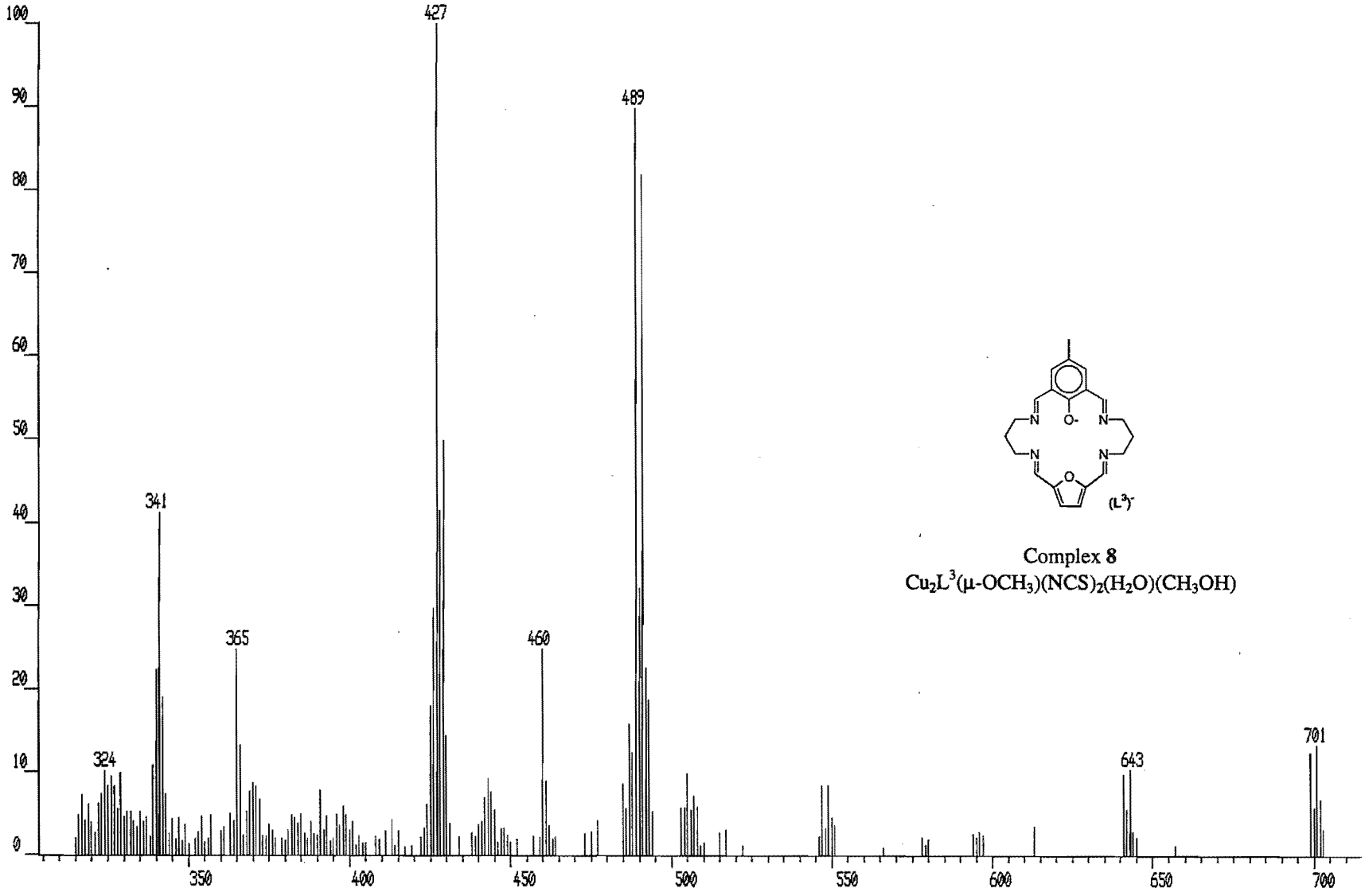

Complex **8**

$Cu_2L^3(\mu\text{-}OCH_3)(NCS)_2(H_2O)(CH_3OH)$

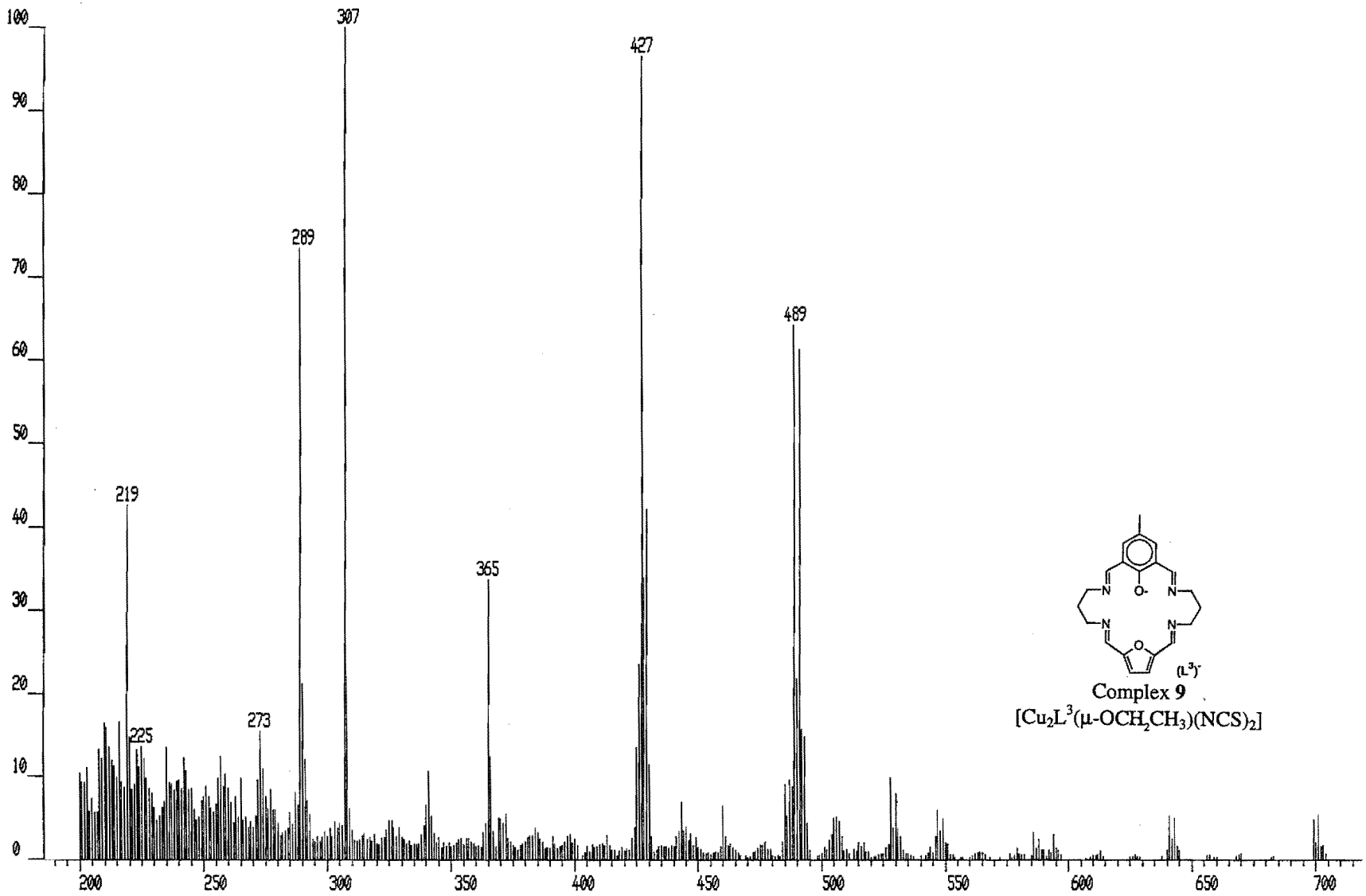

Complex **9**

$[Cu_2L^3(\mu\text{-}OCH_2CH_3)(NCS)_2]$

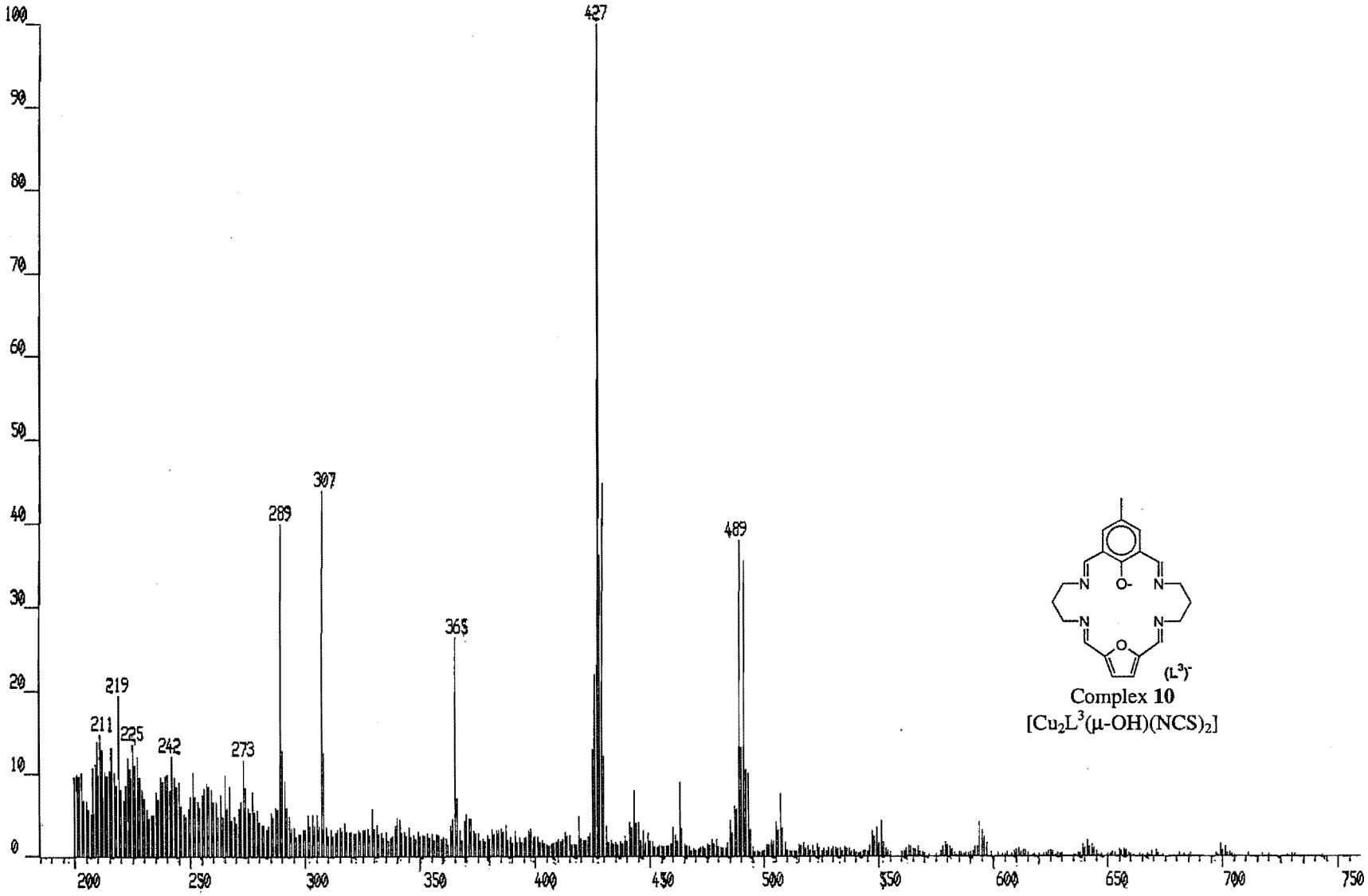

Complex **10**
$[Cu_2L^3(\mu\text{-}OH)(NCS)_2]$

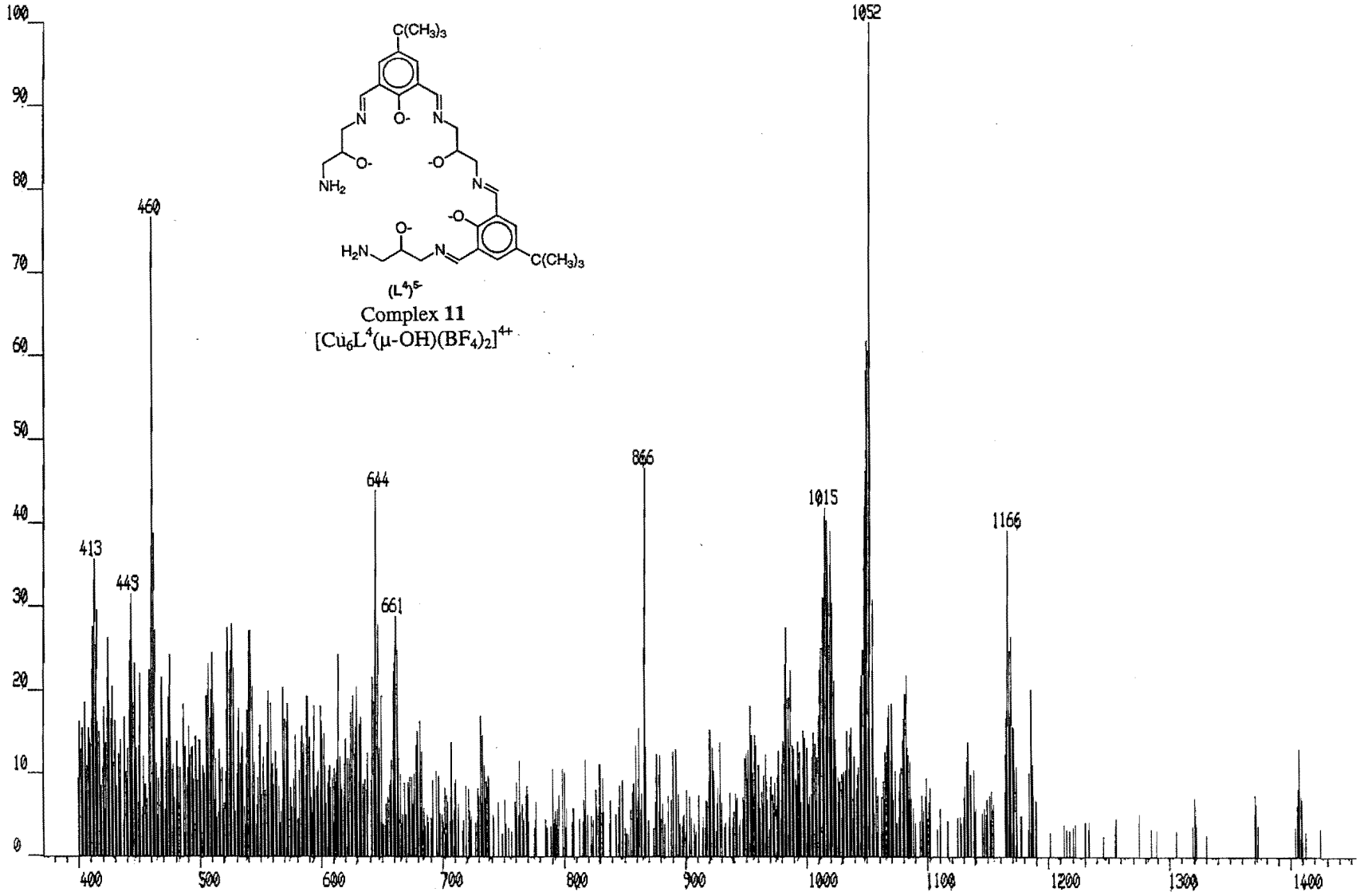
C(CH3)3
N
O-
N
O-
-O
NH2
N
-O
O-
H2N
N
C(CH3)3
(L4)5-
Complex 11
[Cu6L4(μ-OH)(BF4)2]4+
100
90
80
70
60
50
40
30
20
10
0
400
500
600
700
800
900
1000
1100
1200
1300
1400
460
413
443
644
661
866
1015
1052
1166

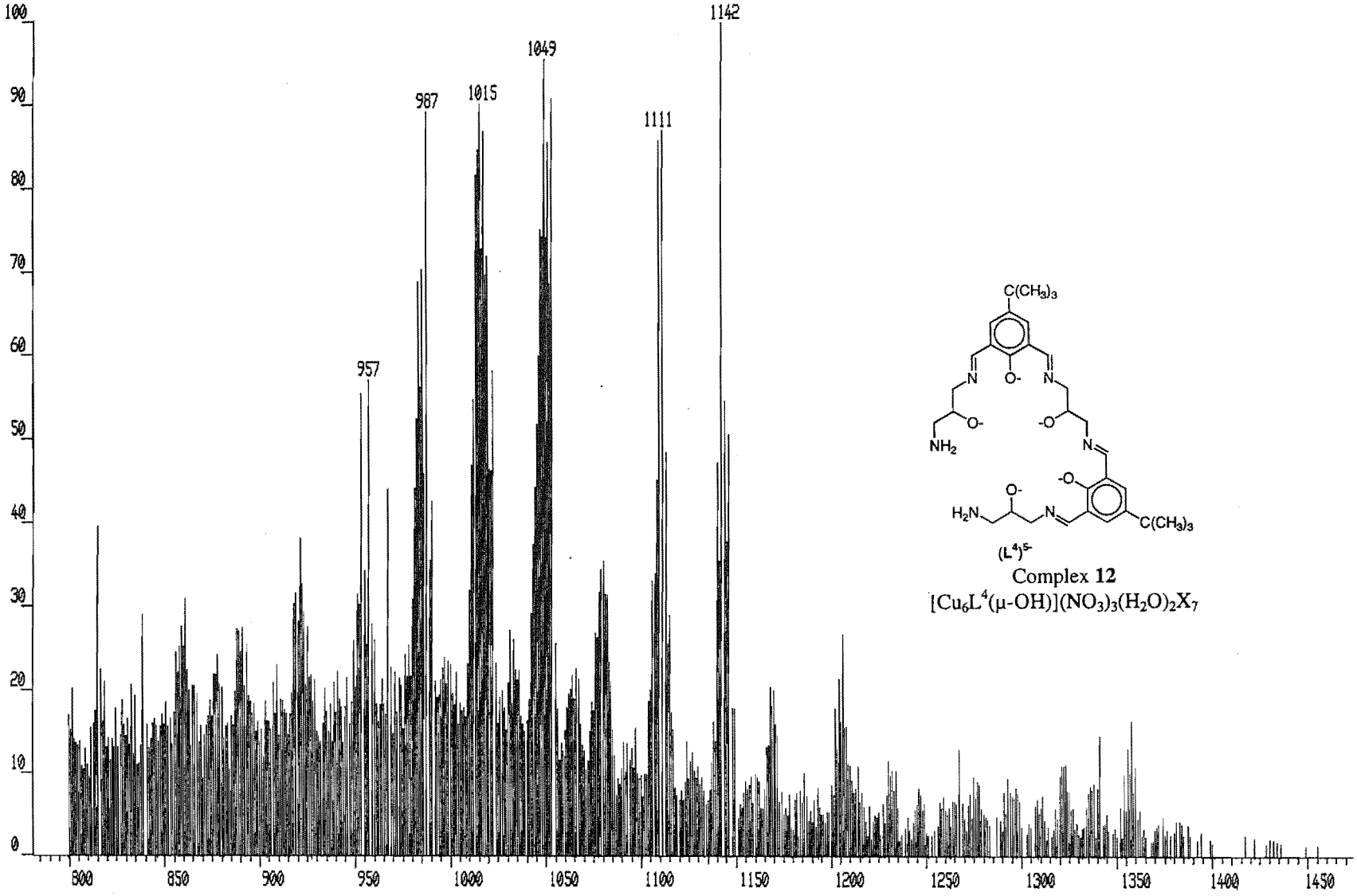

$(L^4)^{5-}$

Complex **12**

$[Cu_6L^4(\mu\text{-}OH)](NO_3)_3(H_2O)_2X_7$

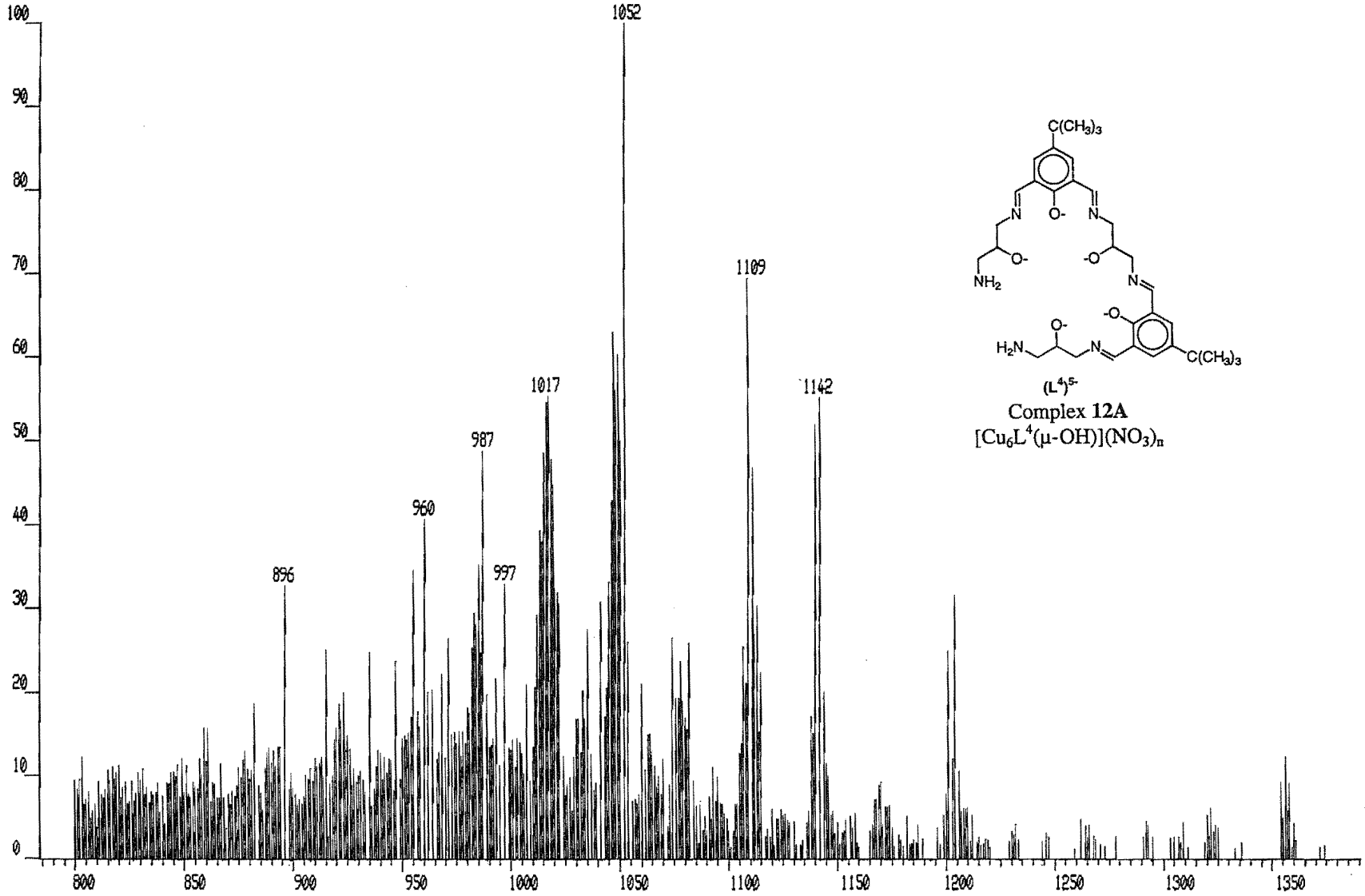

$(L^4)^{5-}$

Complex **12A**

$[Cu_6L^4(\mu\text{-}OH)](NO_3)_n$

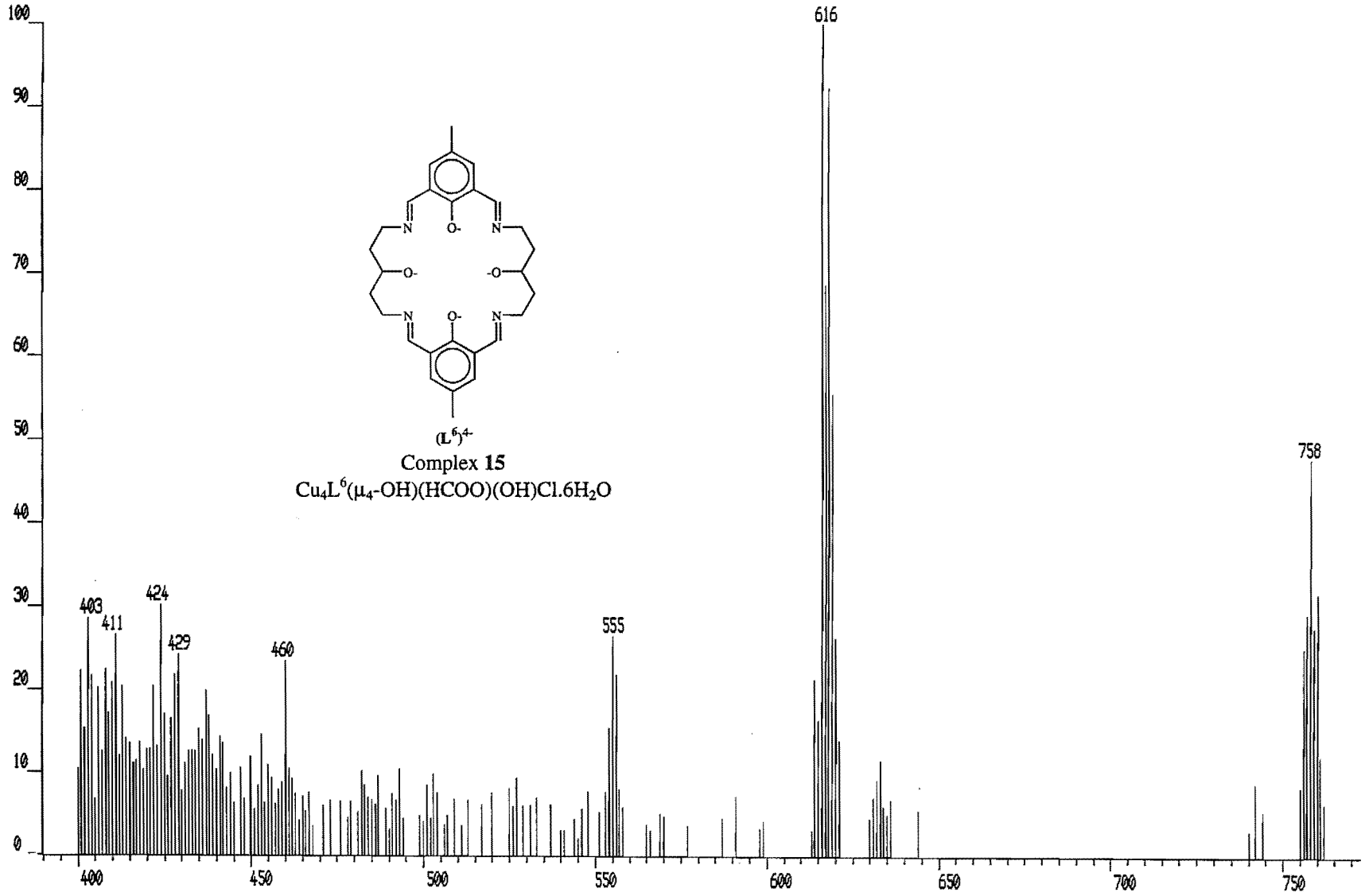

$(L^6)^{4-}$

Complex **15**

$Cu_4L^6(\mu_4\text{-}OH)(HCOO)(OH)Cl.6H_2O$

Appendix D

List of Schiff-base complexes and ligands prepared in this work

Complex **1** - $[Cu_2L^1(\mu\text{-}OH)(H_2O)](ClO_4)_2\cdot H_2O$

Complex **2** -$Cu_2L^2(ClO_4)_2(H_2O)_2$

Complex **3**- $Cu_2H_2L^2(ClO_4)_4(H_2O)$

Complex **4** - $[Cu_2L^1(\mu\text{-}OH)](BF_4)_2\cdot H_2O$

Complex **5** - $[Cu_2L^2(H_2O)_2](BF_4)_2$

Complex **6** - $[Cu_2L^8(\mu\text{-}OH)](ClO_4)_2\cdot H_2O$

Complex **7** - $[Cu_2L^8(\mu\text{-}OH)](BF_4)_2\cdot 4H_2O$

Complex **8** - $Cu_2L^3(\mu\text{-}OCH_3)(NCS)_2(CH_3OH)(H_2O)$

Complex **9** - $Cu_2L^3(\mu\text{-}OCH_2CH_3)(NCS)_2$

Complex **10** - $Cu_2L^3(\mu\text{-}OH)(NCS)_2$

Complex **11** - $\{[Cu_6L^4(\mu\text{-}OH)_4](BF_4)_2\}^+$

Complex **12** - $[Cu_6L^4(\mu\text{-}OH)_4](NO_3)_3\cdot nH_2O$

Complex **12A** - $[Cu_6L^4(\mu\text{-}OH)_4](NO_3)_n$

Complex **13** - $Cu_4L^6(OH)(BF_4)_3(H_2O)_2$

Complex **14** - $[\{Cu_4L^6(\mu_5\text{-}O)(BF_4)\}_2](BF_4)_2\cdot 2H_2O$

Complex **15** - $[Cu_4L^6(\mu_4\text{-}OH)(\mu\text{-}HCOO)(OH)Cl]$

Complex **17** - $[Cu_2L^5](BF_4)_2\cdot H_2O$

Complex **17**$\cdot H_2O$ - $[Cu_2L^5](BF_4)_2\cdot 2H_2O$

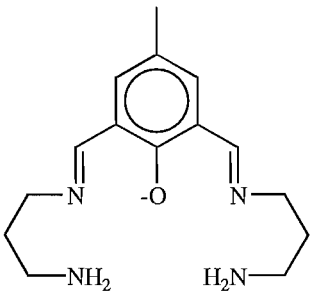

$(L^1)^-$

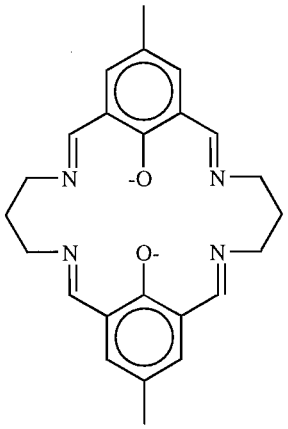

$(L^2)^{2-}$

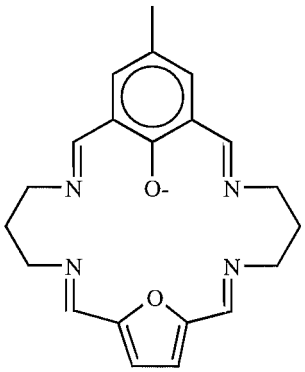

$(L^3)^-$

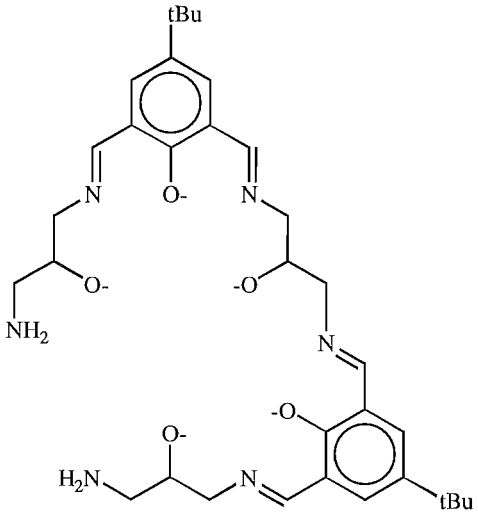

$(L^4)^{5-}$

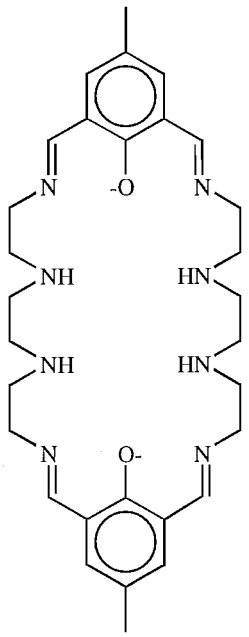

$(L^5)^{2-}$

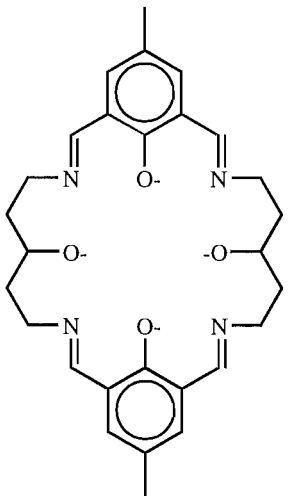

$(L^6)^{4-}$

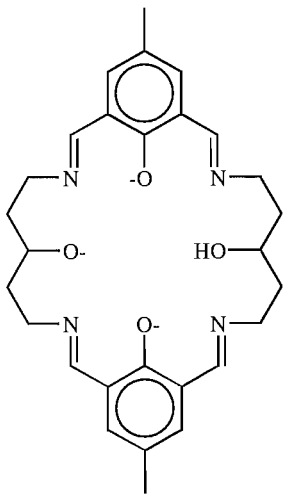

$(HL^6)^{3-}$

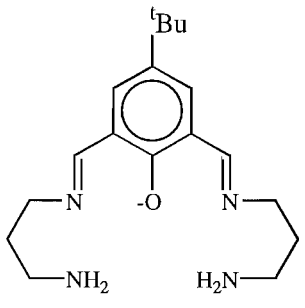

$(L^8)^-$

Appendix E

List of other Schiff-base ligands

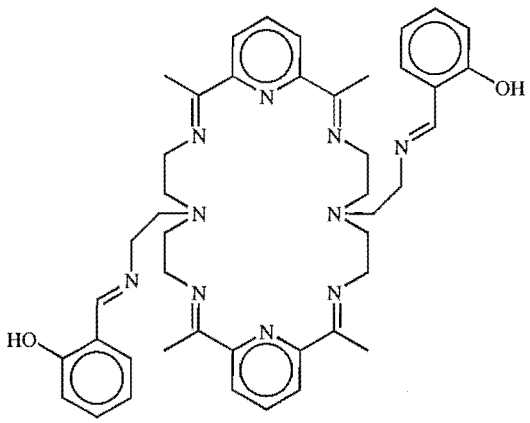

MC1

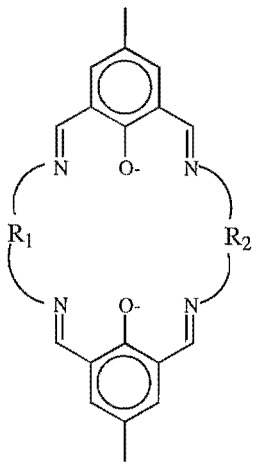

MC2

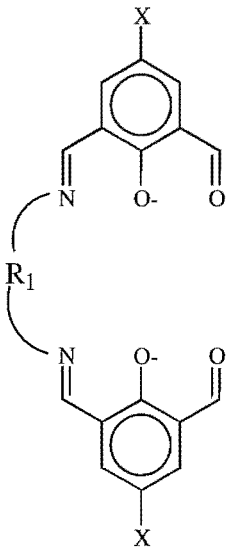

	R_1	X
AC2a		Me
AC2b		Me
AC2c	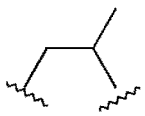	Me
AC2d	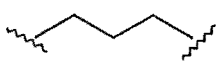	^{t}Bu

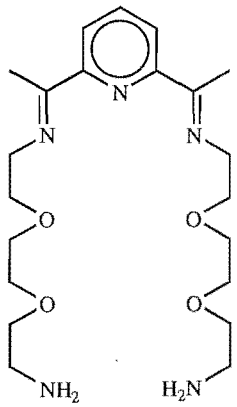

AC3

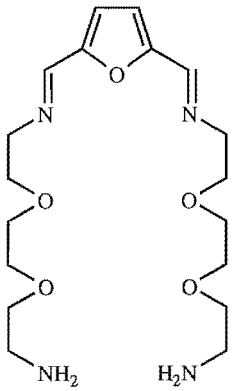

AC4

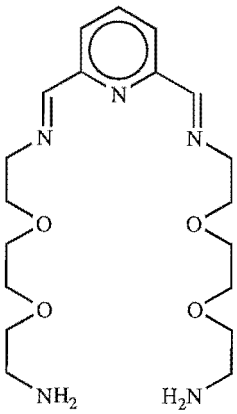

AC5

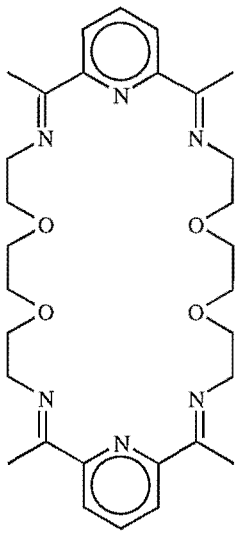

MC3

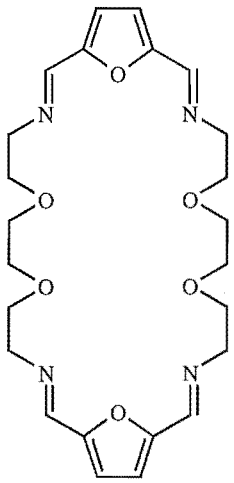

MC4

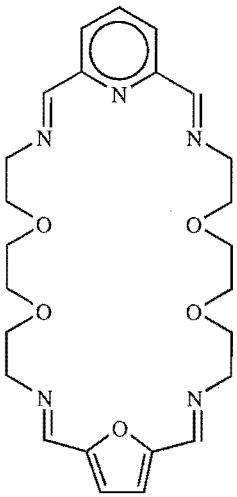

MC5

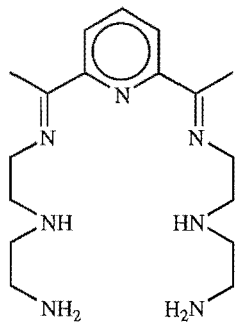

AC6

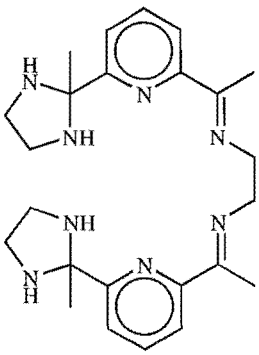

AC7

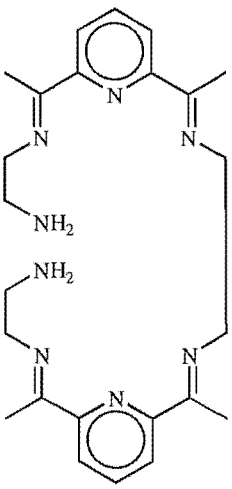

AC8

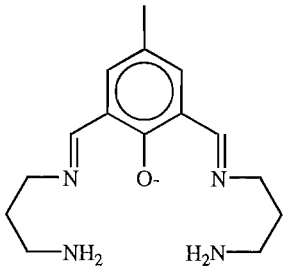

AC9

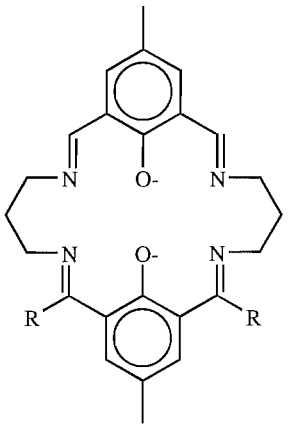

MC9

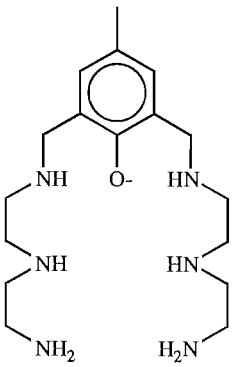

AC10

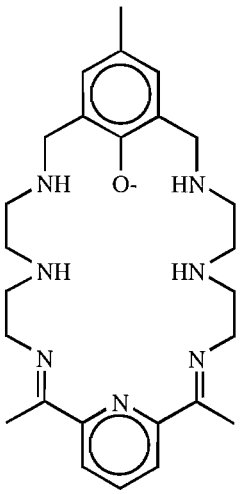

MC10

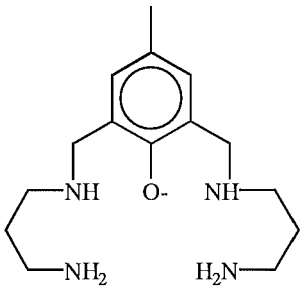

AC11

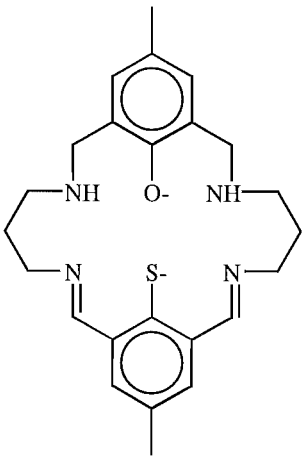

MC11

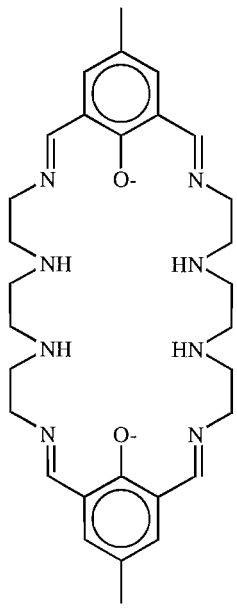

MC12

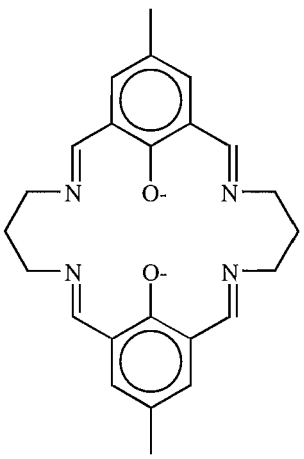

MC13

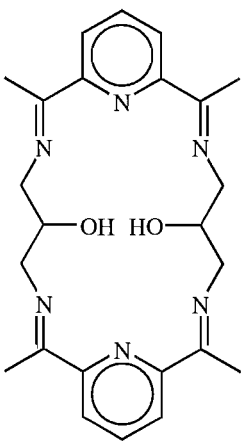

MC14

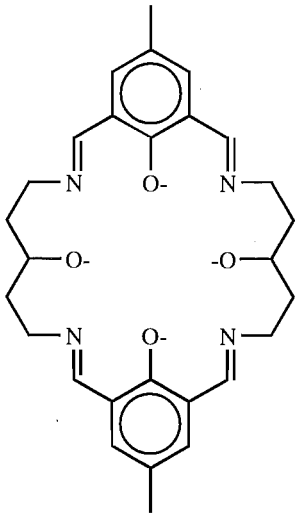

MC15

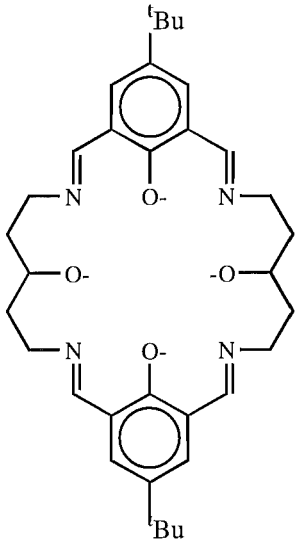

MC16

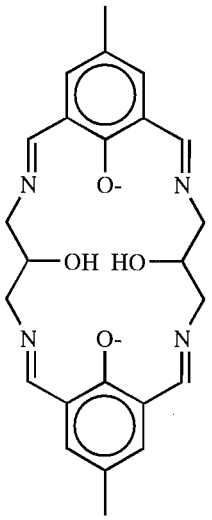

MC17

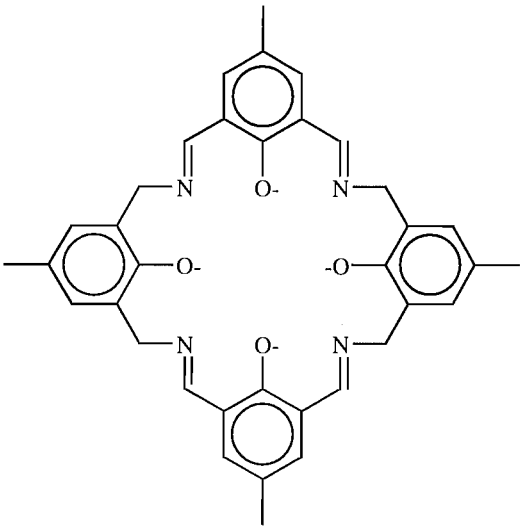

MC18

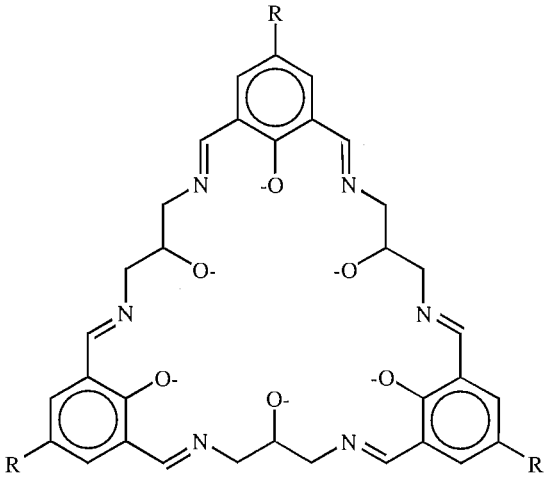

MC19 R = Me

MC20 R = ^{t}Bu

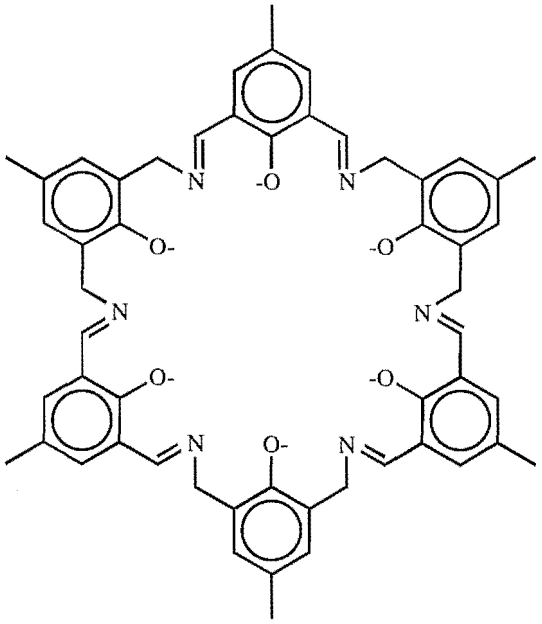

MC21

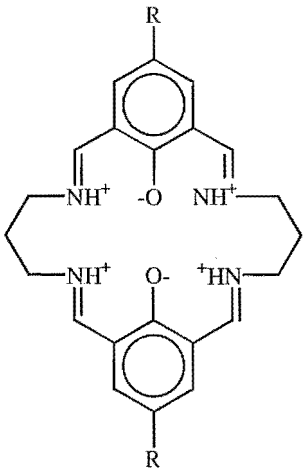

MC22 R = Me

MC23 R = ^{t}Bu

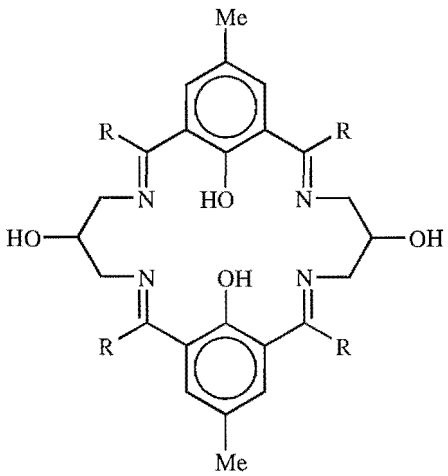

MC24 R = H

MC25 R = Me